Representing Battery Energy Storage in Electric Power Systems Studies

Claudio Ricardo Vergara Ramírez

Dissertation submitted to the Faculty of Engineering
of University of Porto
in partial fulfilment of the requirements for the
degree of Doctor of Philosophy

Dissertation Supervisor: Prof. Professor João A. Peças-Lopes
Full Professor at the Department of Electrical and Computer Engineering, Faculty of Engineering, University of Porto.

Dissertation Co-Supervisor: Prof. Ignacio J. Pérez-Arriaga
Professor & Director of the BP Chair on Energy & Sustainability
Instituto de Investigacion Tecnologica (IIT) Universidad Pontificia Comillas.

Sustainable Energy Systems
PhD Program

February 2015

FACULDADE DE ENGENHARIA DA UNIVERSIDADE DO PORTO

Abstract

Faculdade de Engenharia
PhD Program

Doctor of Philosophy

Representing Battery Energy Storage in Electric Power Systems Studies

by Claudio Ricardo Vergara Ramírez

An increasing penetration of variable energy resources motivated by the need to reduce carbon dioxide emissions, growing concerns about grid resilience in the face of recent weather events and technological progress driven by the demand for portable electronics in the last three decades are expanding the application space for grid-connected battery energy storage systems (BESS). At the same time, the technical differences between electrochemical devices and traditional storage means, like pumped-hydro, and new applications being enabled by the modularity inherent to batteries are challenging existing models and methodologies to assess their ability to create and capture value streams. A generic model is presented in this Thesis which unifies the physical and control aspects of a BESS. By adapting parts of it and using novel methodologies applied to concrete case studies, it is shown that significant insight on this matter can be gained, which is useful to guide operation, investment and policy decisions.

Acknowledgements

If the last four years have exceeded by far the expectations I had in 2010 about the experience of following a doctoral program is mostly because I have come across great people. Starting with my supervisor, Professor João Peças Lopes encouraged me from the beginning to pursue challenging paths, and then effectively helped funnel my enthusiasm towards a consistent research topic. I found in Porto University, and in particular in the Power Systems Unit of INESC-TEC, a community of free-thinkers and doers from which I learned things that changed my perception about how to do research in general, and in particular about energy systems beyond electricity. This wouldn't have been possible without a remarkable groups of professors and administrative staff.

The 18 moths spent at MIT was a sequence of unexpected events that will likely have lifelong implications for me. Steve Connors walked me through the doors of an organization marked by an high likelihood to be surprised on a daily basis. I'm thankful to everyone who made that experience possible, which includes the staff of the MIT Energy Initiative and the MIT-Portugal Program, and to those who made it unforgettable, in particular to my co-supervisor Professor Ignacio J. Pérez-Arriaga, my colleagues at Raja Systems and the Tata Center for Technology and Design.

It would be difficult to over-state how grateful I am for the opportunity that Ignacio and Carlos Batlle gave me to spend a year at IIT-Comillas in Spain. I was fortunate to work with a unique group with outstanding professional and personal attributes, with whom I hope to be able to keep collaborating for many years.

It would have not been possible to complete this work without support of my family in Chile and especially of my wife Lua. Together with our son Pascual, she has shared with me a period of uncertainty, excitement and constant change, postponing important things for her. I would also like to express my gratitude to my classmates and friends from FEUP, to the Lithium Innovation Center and Energy Center from Universidad de Chile, and to the Universal Access team from MIT-Comillas.

This work was supported by:

- MIT-Portugal FCT grant: SFRH/BD/51131/2010;
- Becas-Chile CONICYT grant;
- Instituto de Investigación Tecnológica, Universidad Pontificia Comillas, Madrid, Spain;
- Energy Initiative, Massachusetts Institute of Technology, Cambridge, Massachusetts;

This work was also made in the framework of the BEST CASE project (NORTE-07-0124-FEDER-000056) financed by the North Portugal Regional Operational Programme (ON.2 O Novo Norte), under the National Strategic Reference Framework (NSRF), through the European Regional Development Fund (ERDF), and by national funds, through the Foundation for Science and Technology (FCT).

Summary

Over the course of the last two centuries, energy systems have become one of the cornerstones of the complex mechanism that supports human activity. Along this path, a combination of pure science, abstract models and experimentation has provided a background of technical resources which have enabled these systems to achieve increasing levels of efficiency, effectiveness and resiliency.

During the last 30 years, the market pull for portable electronic devices encouraged major efforts to improve the technical performance and the economics of electrochemical storage devices. This, combined with an increase in the share of energy supplied by variable energy resources such as photovoltaic and wind generators, has propitiated application niches where battery energy storage systems (BESS) could create value streams which exceed their cost.

Reversible energy storage, in the form of hydroelectric pumping stations, has been part of the EPS mix for a long time and is relatively well understood in most timescales and feasible applications. However, the increasing protagonism of BESSs require additional modeling efforts for the following reasons: a) The energy conversion process is fundamentally different from pumped-hydro in several aspects which are relevant in most timescales and applications, b) The smaller size, modularity and operational flexibility of BESSs enables applications that previously did not exist.

Although the BESS technology is notably diverse, the survey of the currently dominant and most promising ones done in this research reveals that it can be understood in terms of components and mechanisms that apply to most of them. In summary, when two electron-conductive bodies (electrodes) are in simultaneous contact with an ion-conductive body (electrolyte), all of them with proper chemical compositions, a constant electric potential difference appears between the electrodes. This potential difference can be modulated by solid-state switches to create a voltage waveform (of one or more phases) closely sinusoidal and similar enough in magnitude and phase to the one in a connection point in an EPS, thus being able to operate in synchronism with it through a coupling inductor. By changing modulation parameters, active and reactive power can flow between the EPS and the electrochemical device. On the cell end, this is followed by a deviation from the equilibrium electric charge conditions, which causes the reactions

at the electrode/electrolyte interface (EEI) to occur faster and the potential difference between electrodes to drop if electrons leaves the negative terminal, or to increase if they leave the positive one. The increase in the reaction rate at the EEI decreases the ionic concentration there, which drives ionic diffusion mechanisms, and the imbalanced electric field contributes with a force in the same direction. The movement of ions because of these two gradients (electric potential and concentration) creates a ionic flow that balances the current through the external load (in this case, the inverter). As the ratio between reactants and products in the electrodes decreases (discharge), or increases (charge) the equilibrium voltage changes and the over-potentials associated with the reactions and ionic movements increase (with different sign for charge and discharge), which results in lower (charge) or higher (discharge) terminal voltage for the same current. At a certain point, the over-potentials are high enough to drive side-reactions which degrade the cell or even damage it, and the process needs to be slowed-down or stopped (end of charge or end of discharge). In fact, side-reactions and other aging mechanisms are present during normal operation for most chemical compositions, and they explain why a cell which is some years old does not behave in the same way as a new one. When the difference from the initial performance exceeds an arbitrary threshold, it is considered that the cell has reached its end of life.

Both short-term operational performance parameters (mainly energy losses and maximum power) and the variation of longer-term constructive characteristics (like available electrode reaction area, electrode resistance and EEI interface resistance) that condition them are related to the utilization profile of the cell, and both groups will impact the technical and economic performance of the BESS as a whole. The model developed in this Thesis allows the explicit formulation of the trade-offs between various long-term and short term revenue and cost drivers in different applications, and defines a parametric representation of a BESS which is adequate to solve these through optimization when the device is performing one or more functions simultaneously.

The complete analytical formulation presented can be coherently simplified and implemented in a variety of studies for electric power systems, and three application cases are developed in the Thesis. In the first one, the battery utilization profile is determine exogenously to reduce the impact of photovoltaic generation over a distribution network, and the BESS model is used to simulate the performance of the battery during its lifetime. The second application introduces the frequency regulation and state of charge

control features to obtain the simulated response of the BESS in response to a frequency measurement over a year of operation for different combinations of frequency response parameters which remain fixed during the analysis period. Finally, the BESS model is integrated into a day-ahead optimization model for a residential customer participating in energy and ancillary services markets.

It is found that the results from the application of the presented models and methodologies allow designers, operators and policymakers to improve their understanding of cost-value causal relationships of electrochemical storage technologies, and about how different technical and regulatory contexts influence them.

Resumo

Ao longo dos últimos dois séculos, os sistemas de energia tornaram-se um dos pilares do complexo mecanismo que suporta a atividade humana. Ao longo deste caminho, uma combinação de ciência pura, modelos abstratos e experimentação tem proporcionado um fundo de recursos técnicos que que têm permitido níveis crescentes de eficiência, eficácia e resiliência para estes sistemas.

Durante os últimos 30 anos, o mercado para dispositivos eletronicos portáteis incentivou esforços para melhorar o desempenho técnico e a economia dos dispositivos de armazenamento eletroquímicos. Esta evolução, combinada com um aumento da percentagem de eletricidade fornecida por fontes de energia variáveis, tais como geradores fotovoltaicos e geradores eólicos, propiciou nichos de aplicação onde os sistemas de armazenamento de energia da bateria (BESS) poderiam criar fluxos de valor maior do que o seu custo. O armazenamento de energia reversível, na forma de estações de bombeamento hidroelétricas, constitui já parte do mix de EPS e é relativamente bem entendido na maioria dos prazos e aplicações viáveis. No entanto, o crescente protagonismo dos BESS exigirá esforços adicionais de modelação, pelas seguintes razões: a) O processo de conversão de energia é fundamentalmente diferente do bombeamento hídrico em vários aspectos que são relevantes na maioria dos prazos e aplicações, b) O menor tamanho, modularidade e flexibilidade operacional dos BESS permite aplicações novas.

Embora a tecnologia dos BESS seja notavelmente diversificada, o levantamento das tecnologias atualmente dominantes e mais promissoras efectuado neste trabalho revela que estas podem ser entendidas em termos de um conjunto de componentes e mecanismos que se aplicam à maioria dos sistemas. Em resumo, quando dois corpos condutores de electrões(eléctrodos) estão em contacto simultâneo com um corpo condutor de iões (electrólito), com composições químicas adequadas, surge uma diferença de potencial eléctrico constante entre os eléctrodos. Esta diferença de potencial pode ser modulada por comutadores de estado sólido para criar uma onda de tensão (de uma ou mais fases) de forma aproximadamente sinusoidal e suficientemente semelhante em amplitude e fase às ondas de tensão num ponto de ligação num EPS, sendo portanto capaz de operar em sincronização com este através de um indutor de acoplamento. A mudança dos parâmetros de modulação permite o fluxo de potência ativa e reativa entre o EPS e o dispositivo eletroquímico. Do lado das células electroquímicas, este processo produz um

desvio em relação às condições de equilíbrio de carga eléctrica, resultando em reações mais rápidas na interface eléctrodo / electrólito (IEE) e numa diminuição da diferença de potencial entre os eléctrodos, caso os electrões migrem a partir do terminal negativo, ou aumento da diferença de potencial caso os mesmos migrem a partir do terminal positivo. O aumento na velocidade de reação na EEI diminui a concentração iónica na interface, acionando assim os mecanismos de difusão iónica, e o desequilíbrio no campo eléctrico contribui com uma força na mesma direção. O movimento de iões por causa destes dois gradientes (de concentração e potenciais eléctricos) cria um fluxo iónico que equilibra a corrente através da carga externa (neste caso, o inversor). Como a relação entre reagentes e produtos nos eletrodos diminui (descarga), ou aumenta (carga) as variações de tensão de equilíbrio e os potenciais associadas com as reações e os movimentos iônicos aumentam (com sinais opostos para carga e descarga), o que resulta em menor (descarga) ou superior (carga) tensão terminal para a mesma corrente. Quando os potenciais atingem um valor suficientemente elevado para produzir reações secundárias que degradam ou danificam as células, o processo deve ser retardado ou parado (final de carga ou no final de descarga). De facto, as reações secundárias e outros mecanismos de envelhecimento estão presentes durante a operação normal na maior parte das composições químicas, o que explica a diferença de comportamento entre células com alguns anos de utilização e células novas. Quando a diferença entre o desempenho inicial excede um limite arbitrário, considera-se que a célula atinge o fim de vida.

Tanto os parâmetros de desempenho operacional de curto prazo (principalmente perdas de energia e de potência máxima) como a variação de características construtivas de longo prazo que os condicionam (como área de reação eletrodo disponíveis, a resistência do eletrodo e da resistência de interface EEI) estão relacionados com o perfil de utilização da célula, e ambos terão impacto sobre o desempenho técnico e económico da BESS como um todo. O modelo desenvolvido nesta Tese permite formular explicitamente os trade-offs entre vários drivers de receitas e de custos de longo e curto prazo em diferentes aplicações, e definir uma representação paramétrica de uma BESS, adequada à resolução destes trade-offs, através da otimização da operação do dispositivo quando este realiza uma ou mais funções simultaneamente.

A formulação analítica apresentada pode ser coerentemente simplificada e implementada no seu conjunto numa variedade de estudos de sistemas de energia elétrica, sendo desenvolvidos três casos de aplicação nesta Tese. No primeiro, o perfil de utilização da bateria

é determinado exogenamente para reduzir o impacto da produção fotovoltaica através de uma rede de distribuição, em que o modelo BESS é usado para simular o desempenho da bateria durante o seu tempo de vida. A segunda aplicação apresenta os recursos de regulação de frequência e controlo do estado de carga para obter a resposta simulada do BESS resultante de uma medição de frequência ao longo de um ano de operação, para diferentes combinações de parâmetros de resposta de frequência, que permanecem fixos durante o período analisado. Finalmente, o modelo BESS é integrado num modelo de otimização de "day-ahead" para um cliente residencial que participa nos mercados de energia e de serviços auxiliares.

Verifica-se que os resultados da aplicação dos modelos e metodologias aqui apresentados permitem que designers e operadores de sistemas e decisores políticos melhorem a sua compreensão das relações causais de custo-beneficio inerentes à tecnologia, bem como o impacto do contexto técnico e regulatório sobre istas relações .

Contents

List of Figures

List of Tables

Abbreviations

AGC	**A**utomatic **G**eneration **C**ontrol.
AGM	**A**bsorbed **G**lass **M**att.
AVR	**A**utomatic **V**oltage **R**egulator.
BESS	**B**attery **E**nergy **S**torage **S**ystem
BMS	**B**attery **M**anagement **S**ystem
CAES	**C**ompressed **A**ir **E**nergy **S**torage.
CCGT	**C**ombined **C**ycle **G**as **T**urbine
CERTS	**C**onsortium for **E**lectric **R**eliability **T**echnology **S**olutions.
COP	**C**oefficient **O**f **P**erformance.
CSP	**C**oncentrated **S**olar **P**ower.
DB	**D**ead **B**and.
DN	**D**istribution **N**etwork.
DER	**D**istributed **E**nergy **R**esource.
DER-CAM	**D**istributed **E**nergy **R**esources **C**ustomer **A**doption **M**odel.
DES	**D**istributed **E**nergy **S**ystem.
DisCo	**Dis**stibution **Com**pany.
DFT	**D**ensity **F**unctionals **T**heory.
DMU	**D**ecision - **M**aking **U**nit.
DOD	**D**epth **O**f **D**ischarge.
DOE	**D**epartment **O**f **E**nergy, U.S.A.
DPR	**D**ynamic **P**ower **R**esource.
DSM	**D**emand - **S**ide **M**anagement.
ECM	**E**lectro - **C**hemical **M**odel.
EES	**E**lectrochemical **E**nergy **S**torage.

EMF	**E**lectro **M**otive **F**orce
EOL	**E**nd **O**f **L**ife.
EPSO	**E**volutionary **P**article **S**warm **O**ptimization.
ESS	**E**nergy **S**torage **S**ystem.
EV	**E**lectric **V**ehicle.
FACTS	**F**lexible **A**lternating **C**urrent **T**ransmission **S**ystem.
FERC	**F**ederal **E**nergy **R**egulatory **C**ommission, U.S.A.
FES	**F**lywheel **E**nergy **S**torage.
HVAC	**H**eating **V**entilation and **A**ir **C**onditioning
HOMER	**H**ybrid **O**ptimization **M**odel for **E**lectric **R**enewables.
ICT	**I**nformation and **C**ommunication **T**echnology.
IEA	**I**nternational **E**nergy **A**gency.
IGBT	**I**nsulated **G**ate **B**ipolar **T**ransistor.
IIT	**I**nstituto de **I**nvestigacion **T**ecnologica, Universidad Pontificia Comillas, Spain.
INESC-TEC	**I**nstituto de **E**letronica **E** **S**istemas de **C**omputadores -**T**ecnologia **E** **C**iencia, Portugal.
IOU	**I**nvestor - **O**wned **U**tility.
ISO	**I**ndependent **S**ystem **O**perator.
KiBaM	**Ki**netic **Ba**ttery **Mo**del.
LAB	**L**ead **A**cid **B**attery.
LIB	**L**ithium **I**on **B**attery.
LMB	**L**iquid **M**etal **B**attery.
LMP	**L**ocational **M**arginal **P**rice.
MCU	**M**easurement and **C**ontrol **U**nit.
MILP	**M**ixed - **I**nteger **L**inear **P**rogramming.
MOSFET	**M**etal - **O**xide **S**emiconductor **F**ield **E**ffect **T**ransistor.
MSE	**M**ean **S**quared **E**rror.
MIT	**M**assachusetts **I**nstitute of **T**echnology, U.S.A.
NPC	**N**et **P**resent **C**ost.
NREL	**N**ational **R**enewable **E**nergy **L**aboratory. U.S.A.
OCV	**O**pen **C**ircuit **V**oltage

OLTC	**O**n **L**oad **T**ap **Changer**.
PCC	**P**oint of **C**ommon **C**oupling.
PCS	**P**ower **C**onversion **S**ystem.
PSS	**P**ower **S**ystem **S**tabilizer.
PF	**P**ower **F**actor.
PV	**P**hoto **V**oltaic.
PWM	**P**ulse **W**idth **M**odulation.
RTO	**R**egional **T**ransmission **O**rganization.
RMS	**R**oot **M**ean **S**quare.
RNM	**R**eference **N**etwork **M**odel.
SEI	**S**olid **E**lectrolyte **I**nterface.
SMES	**S**uperconductive **M**agnetic **E**nergy **S**torage.
SOC	**S**tate **O**f **C**harge.
SOH	**S**tate **O**f **H**health.
SOP	**S**tate **O**f **P**ower.
SSC	**S**torage **S**ervice **C**ommitment.
STATCOM	**STA**tic synchronous **COM**pensator.
SVC	**S**tatic **V**Ar **C**ompensator.
TMY3	**T**ypical **M**etheorological **Y**ear **3**.
UC	**U**nit **C**ommitment.
UPFC	**U**nified **P**ower **F**low **C**ontroller.
VER	**V**ariable **E**nergy **R**esource.
VRLA	**V**alve - **R**egulated **L**ead **A**cid battery.

Physical Constants

Atmospheric pressure	P_a	$=$	$101,325$	Pa
Boltzmann constant	k	$\approx$	$1.3806503 \cdot 10^{-23}$	$\frac{m^2 \cdot kg}{s^2}$
Electric permittivity of vacuum	ε_0	$\approx$	$8.854187 \cdot 10^{-12}$	$\frac{m}{s}$
Electron charge	e	$\approx$	$1.60217646 \cdot 10^{-19}$	C
Faraday constant	F	$\approx$	$9.64853415 \cdot 10^{4}$	$\frac{C}{mol}$
Ideal gasses constant	R	$\approx$	8.3144621	$\frac{J}{mol \cdot K}$
Imaginary number	j	$=$	$\sqrt{-1}$	
Speed of light in vacuum	c	$=$	299,792,458	$\frac{m}{s}$

Symbols

A	Cross-sectional area of an electrochemical cell	m^2
a	Area	m^2
$\mathbf{B}$	Magnetic field	T
b	Binary variable	binary
C	Capacitance	F
C	Charge	$\mathrm{A} \cdot \mathrm{h}$
Cv	Specific heat at constant volume	$\frac{\mathrm{K}}{\mathrm{J}}$
$\mathrm{C}-\mathrm{rate}$	Current that depletes a cell of nominal charge capacity C in $\frac{1}{\mathrm{C-rate}}$ hours	A
D	Diffusion coefficient	m^2/s
$\mathbf{E}$	Electric field	$\frac{\mathrm{N}}{\mathrm{C}}$
e	Energy	J
$\mathbf{F}$	Force	N
f	Frequency	Hz
g^{Li}	Species generation or absorption rate	$\frac{\mathrm{mol}}{\mathrm{m}^3 \cdot \mathrm{s}}$
G	Gibbs' free energy	J
H	Enthalpy	J
H	Inertia constant	s
IG	Internal heat gains	W
i	Electric current	A
J	Moment of inertia	$\mathrm{kg} \cdot \mathrm{m}^2$
j	Electric current density	$\frac{\mathrm{A}}{\mathrm{m}^2}$
j^{Li}	Volumetric electric current generation or absorption rate	$\frac{\mathrm{A}}{\mathrm{m}^3}$
k	Fitting coefficients	
L	Inductance	H
m	Mass	kg

m	Modulation index	
n	Number of electrons transferred in a electrochemical reaction	
n	charge density per unit length	$\frac{\mathrm{C}}{\mathrm{m}}$
N	Number of turns in a coil of wire	
P	Pressure	Pa
p	Power	W
$\mathbf{p}$	Linear momentum	$\frac{\mathrm{kg \cdot m}}{\mathrm{s}}$
q	Electric charge	C
q	Reactive power	VAr
Q	Heat	J
R	Electric resistance	Ω
S	Entropy	$\frac{\mathrm{J}}{\mathrm{K}}$
S	Surface area	m
$\boldsymbol{S}$	Stoichiometric coefficient	
T	Temperature	K
t	Time	s
U	Internal energy	J
U	Open-circuit potential	V
S	Stoichiometric coefficient	
V	Volume	m^3
$\boldsymbol{v}$	Velocity	$\frac{\mathrm{m}}{\mathrm{s}}$
v	Electric potential difference	V
W	Work	J
X	Electric reactance	Ω
α	Apparent transfer coefficient	
δ	Phase angle	Rad
ε	Electromotive force	V
ζ	Species concentration	$\frac{\mathrm{mol}}{\mathrm{m}^3}$
ζ	Number of charge-discharge cycles	
Θ	Ratio of reactants to products in the context of an chemical reaction	
θ	Angle	Rad
ϑ	Amplitude of a charge-discharge cycle	p.u.
μ	Mobility of a chemical species	$\frac{\mathrm{m}^2}{\mathrm{V \cdot s}}$

ν	Overpotential associated to an electrochemical reaction	V
ν	Frequency of a particle	V
ρ	Amount of electric charge in a region	C
τ	Torque	$\mathrm{N} \cdot \mathrm{m}$
Υ	Species amount is a cell domain	mol
ϕ	Electric potential	V
ψ	Flux of a chemical species	$\frac{\mathrm{mol}}{\mathrm{m}^2}$
ω	Angular speed	$\frac{\mathrm{rad}}{\mathrm{s}}$

Chapter 1

Introduction

These are great days for engineers. Electric power systems (EPS), the machinery largely responsible for the unprecedented technological development during the 20^{th} century on one hand, and also an important contributor to the accelerated consumption of fossil fuels on the other, is undergoing deep changes. What previous generations of engineers succeeded to make powerful, ours will reshape into efficient, resilient, flexible and clean. A relevant part of this challenge deals both with the integration of clean variable energy resources (VER) such as wind and solar, and with the improvement of the operational regime of conventional power plants (powered by fossil fuels, hydro, nuclear) in the face of increasing variability. Indeed, the optimal operation of conventional units does not match typical load profiles, and this is exacerbated by the large amount of VERs, which are currently considered a key component of future low-emissions EPSs. Energy storage is one of the available options to improve the operation of the electric grid under this scenario.

This Thesis describes contributions to the analysis of some problems in the field of energy storage in electric power systems (EPS) developed in the context of the MIT-Portugal Doctoral Program on Sustainable Energy Systems at the Engineering Faculty of Porto University.

The central enquire is about whether battery energy storage systems (BESS) can play a relevant role in EPSs, and which factors influence the scope of this role. The relevance of

this rests primarily in an increased need for flexibility in electric power systems, driven by a higher penetration of variable energy resources (VER), and is further increased by the possibility that available BESS solutions in the market may be getting close to economic viability. More concisely, the aim is to develop models and methodologies to predict the effect of operation on the total value generated/capture during the lifetime of a BESS technology of a given size on a given place.

The research interest of the topic is related to two main knowledge gaps. First, it is currently not clear which revenue streams can be exploited by a BESS connected to an EPS. This is related to a lack of understanding of the value that they can provide, which in turn prevents the emergence of a regulatory framework that allows for that value to be either captured by the owner of the BESS or perceived as such by the society. Second, the utilization cost of a BESS is not sufficiently well understood to either obtain reasonable lifetime and performance estimates at the planning stage or to make the best decisions during its operation. This dissertation is an attempt to help overcome these difficulties for a selection of BESS technologies, functions and EPS structures.

1.1 Chapter overview

The purpose of this chapter is to give a brief description of the context of the Thesis and to establish the research boundaries within this context. Section 1.2 attempts to communicate the essence of the type of questions for which the models and methodologies described in the next chapters aims to be useful. Section 1.3 sets the limits and objectives of the work, and section1.4 describes the structure of the thesis and the content of each chapter.

1.2 Motivation

If electricity in a usable form was as abundant as salty water in the oceans, it is not unlikely that mankind could have achieved the present level of technological development several thousand years ago. The fact that it is not, and a significant amount of technology is involved in producing, converting and delivering it to the places where it serves its final purpose. At a high level, electricity is not too different from any other commodity:

It is very useful and the means to produce it are limited. However, its obtention requires primary energy forms (one cannot "mine" electricity) and so far it has been not practical to store it in significant quantities.

1.2.1 Why do we need institutions?

Agriculture emerged around 12,000 years ago as a technology that deeply disrupted the incumbent regime, dominated by hunter-gatherers. Early adopters quickly realized that growing plants and domesticating animals made it easier for them to remain well fed and simultaneously have more free time, which could be allotted to training, leisure, technology development, etc. Thus, these early adopters started dominating the landscape: Agriculture was clearly a superior strategy to hunting and collection for most cases. An interesting fact about agriculture is that it has significant economies of scale. However, to take advantage of that it is necessary to coordinate an increasingly large number of people, which led to the first social structures, to the specialization of labor and to public services like armies to protect the fields from other groups. The process is compatible with a selfish individual perspective: *if I work the fields and don't cause problems, I'll have food and safety.* Then, the same economies of scale and the access to slave labor encouraged leaders to invade other fields to increase their power. This led to a loss of welfare, since the battles involved burning fields and villages, killing workforce and destroying other infrastructure.

Feudal regimes prevailed until one of the groups was able to dominate over several other, and its leader became king. Of course, the new king wanted to maximize the tribute that defeated leaders can pay him, and having feudal lords fighting each other doesn't help: peace is imposed mainly from economic motivations in the form of a collection of institutions [27] [1] designed to keep the social-ecological system in the desired regime. In this way, properly defined institutions will cause that the welfare of a given agent decreases if it adopts strategies that tend to disturb the equilibrium, and that it will remain constant or increase if the strategies contribute to it. However, although one can identify an imperfect institutional arrangement when agents evolve stable strategies that go against this principle, it is not evident how one collection of institutions is better than another in the face of the regimes they propitiate.

[1] Examples of institutions in the present are laws, informal agreements, procedures, etc. Refer to [28] for a very good discussion of how institutions shape stable regimes.

In the next phase, this relatively protected environment enables peaceful commercial transactions between feuds and peace enforcement becomes less necessary within the kingdom. Local economic signals, perceived by the stakeholders, indicate that local trade is more beneficial than local war without the need of an active institution. What follows is a succession of rules being lifted, each of them unlocking opportunities to create value. But eventually this de-regulatory trend bounces back.

As a matter of fact, complete de-regulation has not been successful anywhere. In a few words, a system where economic signals alone are enough to achieve a stable regime with a set of characteristics consensually labeled as *desirable* seems to be beyond the grasp of present human capabilities, and hence formal institutions are required[2].

Successful institutions must be well grounded in the technical reality of their subject, and this is particulary evident in the case of electricity.

1.2.2 Power systems regulation in a nutshell

Electricity, an exemplary fruit of curiosity-driven research and inventiveness, is another example of a disruptive technology, probably the fourth in terms of impact after agriculture, writing and the steam engine. After an initial period dominated by lightly-regulated private companies, the possibility of increased welfare from access to this new energy vector and economies of scale required to come up with institutions that could steer companies in the direction of common good. Utilities were endowed with exclusivity benefits across all the layers of infrastructure that are necessary to bring electric power from primary energy sources to the points where it would be converted in valuable services like lighting, motive power, communication devices, etc. For around to a century, many economic signals hibernated, standards developed and this new actor in the global scene experienced an impressive growth, becoming familiar to many people.

The beginning of the decade of the 1980's saw the first pioneers who took seriously the possibility that it was possible to unlock efficiency sources by changing some rules. The basic idea is that in large power systems, it is possible to allow for competition in generation. It is surprising that this started in the small Chilean system, which at the time had just a few GW of installed capacity. In brief, the rationale behind this is that if

[2]Examples of this are the allocation of externalities related to big infrastructure projects and the perpetuation of large social gaps in most developing countries.

you remunerate electricity at the marginal cost, private investment in generation will be attracted and the load will be met at minimum cost. Most people call the global-level process that came afterwards de-regulation, which can be misleading since probably the number of rules has increased. Some of the key new rules needed were: vertical disintegration, open-access to transmission infrastructure and new market mechanisms. Although this regime-shift towards a more liberalized energy system has had different levels of success in different countries, most policy-makers agree in that it was a good idea.

More recently, advances in information processing and communications technologies (ICTs) are revealing opportunities to unlock efficient economic signals at different levels. For example, and in contrast with industrial consumers, residential consumers of electricity have been shielded from price fluctuations in the wholesale market through regulated tariffs. This made sense, since there were neither means to communicate the real price to the final consumer nor metering infrastructure capable of recording when energy was consumed. As these are becoming cheaper, it is possible that the economic gains from having price-responsive consumers could be larger than the cost to acquire and setup the new devices. The details about how this will exactly happen are not clear yet, although several countries have done pilot tests and advanced regulation, there's still significant disagreement about things like data visibility, meter ownership, enforcement of standards, among others.

The competitiveness of energy storage in general, and of batteries in particular, depends on a combination of technological and regulatory factors. However, a policy decision about encouraging market pull for batteries can be done on different grounds, such as to cost reductions through research or economies of scale. The models explained in this Thesis can be useful to evaluate competitiveness thresholds for battery technologies and also to identify key technical parameters to be improved.

1.2.3 Potential and realizable value of storage

An example[3] can serve to illustrate the relevance of models and regulation in technical decisions at the distribution level. Consider the feeder represented by the single-line diagram in figure 1.1, where two loads, both turned on at 3 AM and disconnected at 2

[3]Details about the simulation setup can be found in Appendix A

PM, were expected to be there before the feeder was built. With the voltage at the grid connection point considered fixed, the basic design of the feeder is trivial, resulting in the cheapest wires which are able to maintain the voltage at the end of the feeder above a minimum threshold when both loads are connected, and below a maximum value when both loads are disconnected.

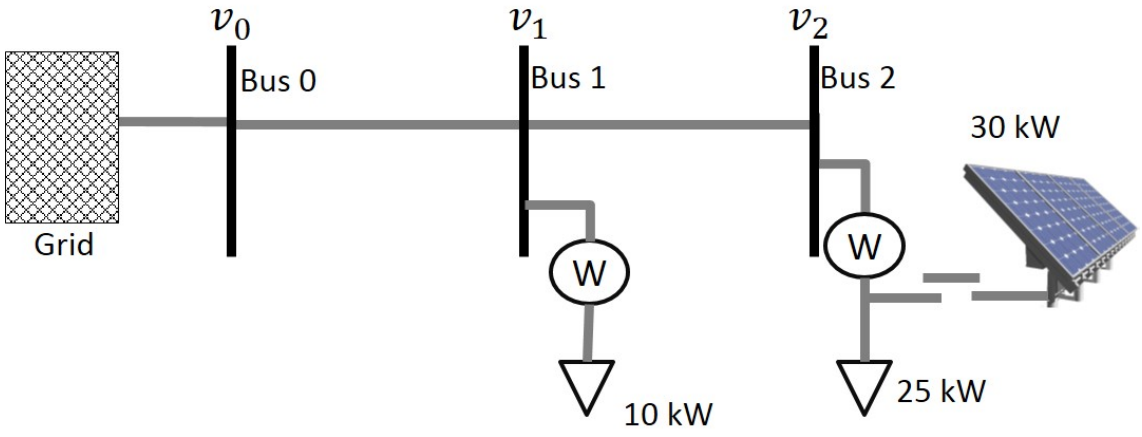

Figure 1.1: Single-line representation of the example case.

Suppose that now the owner of the load connected to the second busbar installs the photovoltaic panel shown in the figure, for which the expected generation profile on a clear summer day is the one shown in figure 1.2a. Evidently, when the loads disconnect at 2 pm, a power flow towards the grid comparable with the design capacity of the feeder will happen. Since the worst case scenario considered to size the wires was zero power, the negative power situation will likely cause the voltage to rise above the allowed value. One possibility to deal with this problem is to install a voltage regulator[4] in the second busbar. The operation of this device, as shown in figure 1.3a for a clear-sky day, is such that when the voltage exceeds a prescribed value, the transformation rate is decreased by discrete amounts, and the opposite happens for low-voltage condition. For the smooth PV generation curve this results in 7 operations of the tap changer per day. The number of operations is important because the remaining useful life of the device is roughly inversely-proportional to this number. The situation gets worse when intermittency is taken into account. The profile in Figure 1.2b corresponds to real PV production from a system in Madrid, Spain, for a day with intermittent clouds, and figure 1.3b shows the corresponding operation of the tap changer of the voltage

[4]For example, an autotransformer with 1:1 nominal conversion ratio and a number of taps in the secondary winding.

regulator, which increases from 7 to 14. Could it be argued that the long-term cost of voltage regulation for that feeder doubles because of intermittency? Maybe not, because there must be ways to repair a worn-out tap changer, but the important concept is that the impact of intermittency is likely to be noticeable, and incremental over the cost of smooth variability.

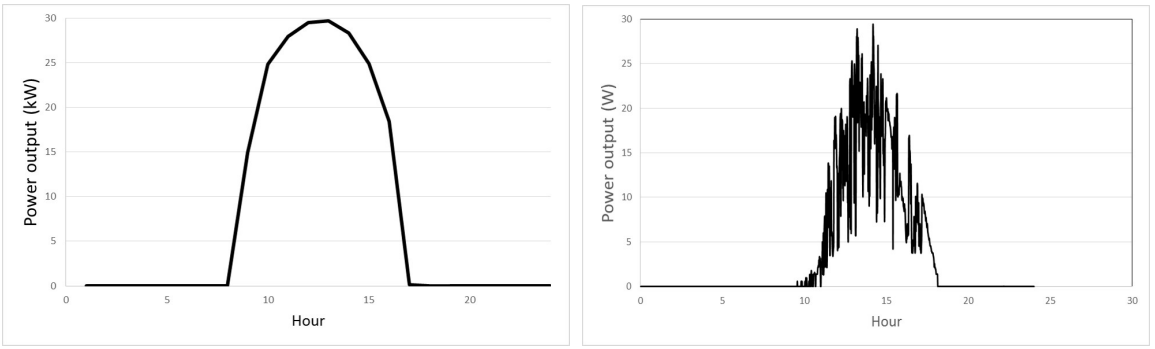

(a) Day with clear sky. **(b) Day with fast partial clouds.**

Figure 1.2: Examples of photovoltaic power output profiles.

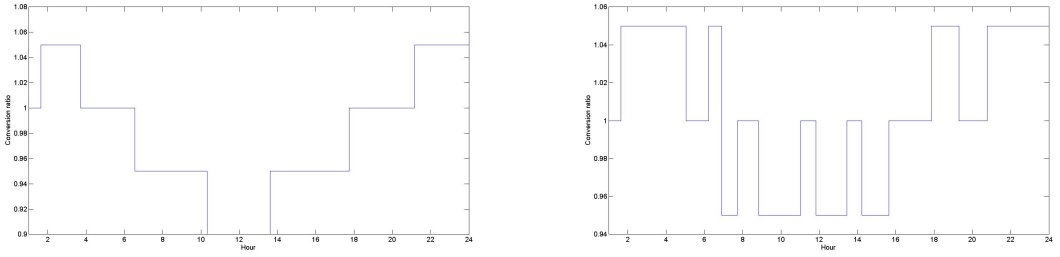

(a) Day with clear sky. **(b) Day with fast partial clouds.**

Figure 1.3: Daily operation of the voltage regulator connected to the second busbar.

The natural follow-up question to the discussion above is: who pays for the new network costs?. Although the answer differs from system to system and from time to time, often times the cost of network reinforcements to maintain the quality of service is socialized among all the users of the network; however, not everyone bears the same fraction of that cost. A popular method to allocate the network cost is in proportion to the net energy consumed over a pre-defined period of time. For the sake of the argument, let's assume that the capacity factor of the PV panel is 0.2, and that the meter is read once every year. Then, the yearly net energy balance before installing the panel is the power of the load times the number of hours it is connected each day, times the days in a year: $E_2 = 25 \cdot 11 \cdot 365 = 100,375$kWh. When the PV panel is connected, it will offset this value by $30 \cdot 0.2 \cdot 8760 = 52,560$, which is roughly half of the original value. In summary,

we have that an agent who makes a decision which produces an extra cost for the system is rewarded for it. In contrast, the other agents who don't install a PV panel will see their payments increase.

It is interesting to explore whether the extra cost could be avoided, or better allocated, if the right economic signals were in place. For example, it is likely that there will be some margin in the feeder to accommodate moderate reverse power flows without voltage problems, and also that the PV panel will not produce at full capacity every day. If the PV power production during no-load hours is limited to the amount that the feeder can tolerate, there will be a certain loss of revenue compared with an unrestricted scenario. One could argue that economic rationality dictates that if the annual loss of revenue is smaller than the annual cost of a voltage regulator[5], the device should not be installed and, in the absence of other options, the power of the PV generator should be curtailed. The fact that this doesn't happen in reality for scenarios like the one described here reveals imperfections in the way economic signals are generated and perceived. The owner of the PV panel has no incentive to curtail PV production or to buy a battery to move the energy produced during peak hours because, under the regulatory assumptions explained, if he did so his revenue would decrease and his costs would increase. In the same way, intermittency is nowhere to be found in the "objective function" of the private agent, although it is very clear how it impacts the cost to provide him electricity; and it could be that dealing with intermittency is cheaper for the owner of the panel than it is for the distribution company.

1.2.4 Unlocking economic efficiency

A fictitious regulatory scenario based on the situation described in the previous section can be used to explain how rules can unlock efficient economic signals. Suppose that the distribution company has found that the number of operations of the tap changer starts increasing when the average PV production ramp exceeds $6 \cdot 10^{-}4\frac{\text{p.u.}}{\text{s}}$ and that it increases linearly until $3 \cdot 10^{-}3\frac{\text{p.u.}}{\text{s}}$, where it is double of the number of operations due to the ideal solar radiation cycle.

A candidate economic signal could be embodied in the rule: *if the average ramp of the net output of a customer who owns a grid-connected PV panel exceeds a certain threshold*

[5]Corresponding to the annuity of the investment plus annual operation and maintenance costs.

(e.g., $6 \cdot 10^{-}4\frac{\text{p.u.}}{\text{s}}$*) an additional per-kW charge will be applied. This charge will be proportional to the difference between the measured average ramp and the threshold, up to a maximum value.* In simple words, the message is: if the ramps in your solar panel can be reduced, you could save money. Although in principle curtailment could also be used to reduce the ramps through restrictions on the power electronics[6], energy storage could be a better alternative. Figure 1.4 shows how the PV production profile can change when different amounts of energy storage are used to compensate intermittency, and figure 1.5 shows the effect that this has in the simulated voltage controller.

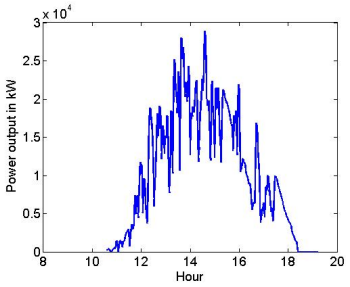

(a) 1.44 kWh.

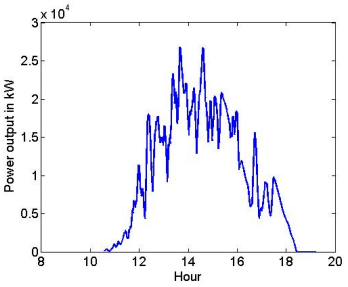

(b) 3.09 kWh.

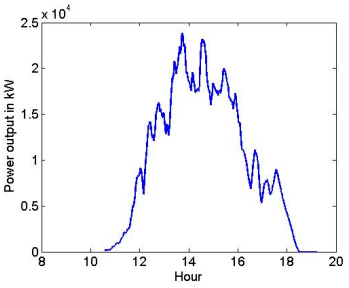

(c) 5.89 kWh .

Figure 1.4: Power output of the PV system for different values of storage.

[6]Positive PV power ramps are easy to control, whereas negative ones require that the panel operates permanently under its maximum power curve.

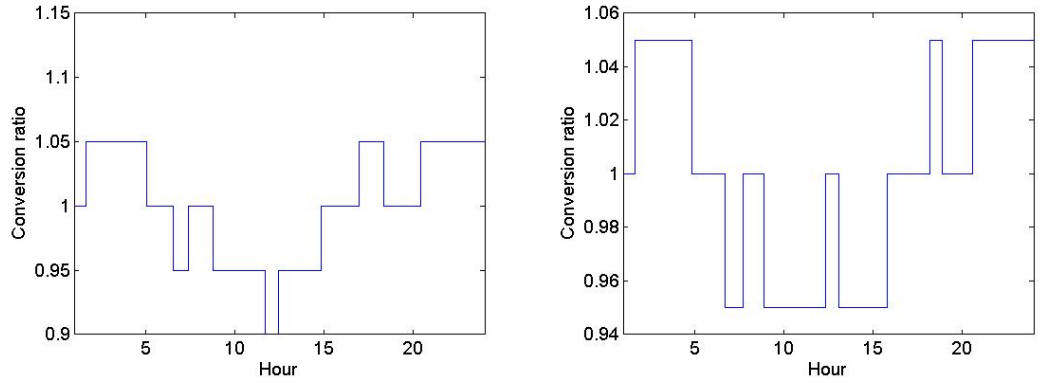

(a) 1.44 kWh.

(b) 3.09 kWh.

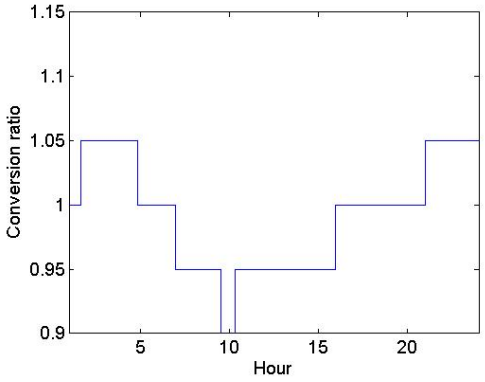

(c) 5.89 kWh.

Figure 1.5: Behavior of the voltage regulator for different values of smoothing storage.

Simulating for several battery sizes, we can obtain a curve that relates storage size with number of operations of the tap changer (figure 1.6). If the numbers are correctly calculated, the extra capacity charge should reflect, on average, the extra cost for the distribution company in terms of replacement or maintenance of voltage regulators. Then it is up to the private agent to decide about whether it prefers to pay this or reduce the power intermittency buying a battery (or doing something else), and there will likely be cases in which either makes economic sense.

Another interesting family of signals are those which require a coordinated action of several agents. For example, the owner of a PV panel could agree, in principle, to sell cheap electricity to a grain mill connected to the same busbar in times of high PV production. If the arrangement is done properly, there could be neither a need to install a voltage regulator nor to curtail generation. It seems convenient that those transactions occur in a local marketplace, leading to a new agent: the *aggregator*.

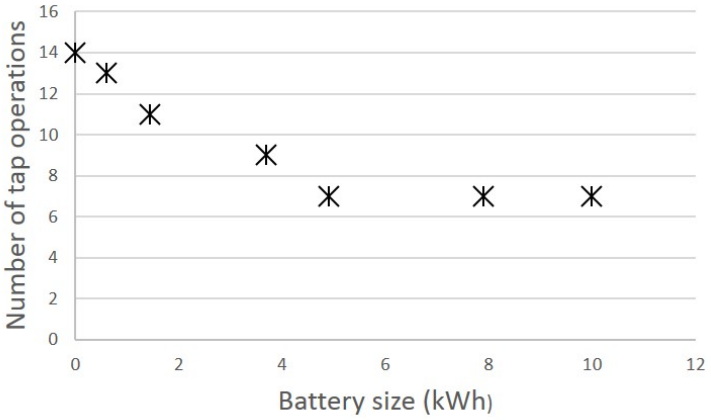

Figure 1.6: Number of tap changes as a function of the installed energy storage capacity.

The viability of either the individual or aggregated response to the economic signal related to intermittency will depend on the cost/performance relationship of available technologies. Both concepts, cost and performance, are not straightforward to defined. Cost can be disaggregated at least into investment, financial, operation and maintenance components, with the lifetime of the storage device being of foremost importance. Performance is also elusive to define, and in general it will be seen differently from the private and public perspective if rules are imperfect. There will also be a dependency between cost and performance. The intention of models and methodologies proposed in this Thesis is to help the study of these dependencies.

1.3 Scope and objectives

This research is motivated by the possibility of using electrochemical accumulators to improve the operation of current and future power systems, as expressed by the research question:

How Should Electrochemical Accumulators be Exploited to Support the Operation of Electric Power Systems?

It is important to note that this enquire, in particular the word *should*, can be approached at least from two perspectives corresponding to hypothetical agents:

1. Agent C is responsible for planning and operating a power system to support power flows between a set of generators and loads at minimum cost. The relevant question

for agent A is whether including BESSs in his catalog of equipment will lead to a lower total net present cost, assuming some evaluation period and including fixed and variable costs;

2. Agent P is deciding about buying a battery as an investment, and what he cares about is that the net present value of the investment at an attractive discount rate is positive using an evaluation period lower than the lifetime of the battery.

Each agent needs, in order to evaluate his/hers options, to consider a set of technologies and go through the process in figure 1.7. The three circles on the figure form an iterative process. To calculate the centralized (agent C) or private (agent P) economic value of a BESS technology in a power system, three basic decisions need to be made:

1. The electrical location of the BESS. The services that the asset is able to provide are sensitive to this; for example, a device connected to a transmission substation will be able to provide frequency regulation but not distribution voltage control;

2. The size of the BESS in terms of power and energy. Most applications will have associated an optimal size; for example, if the battery is going to be used to do energy arbitrage on a isolated microgrid based on photovoltaic generation, a too small battery will likely lead to energy spillage, while a too large one will be under-utilized;

3. The operational strategy of the BESS. Evidently, the generation of value for the power system is directly related to how the BESS is run, and hence agent C needs to make sure that the value calculation for given technology in a given place and of a given size is done under operational assumptions that are close to the optimal ones taking into account the system as a whole. Agent P also needs a reasonable assumption about the operation, but in his case the objective is to maximize the captured value, not the generated value. This is a fundamental difference between the two perspectives, since agent P has no incentive to operate the BESS taking into account value streams that cannot be captured, i.e., translated into revenue. However, if the correct economic signals are in place, both agents should arrive to the same decision.

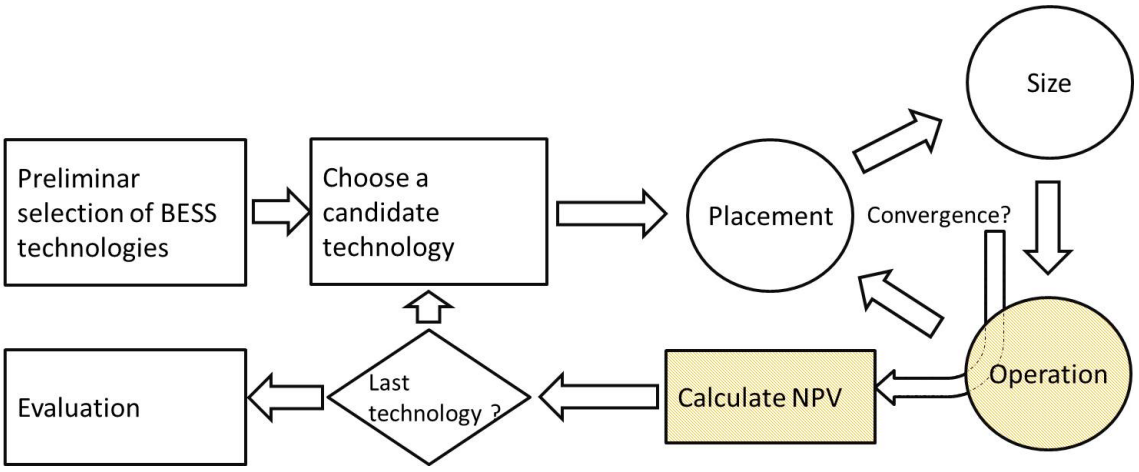

Figure 1.7: Evaluation process for storage technologies

The process in figure 1.7 defines the context where the techniques developed in this thesis are most relevant. However, the formulations have intentionally been developed with enough electrochemical consistency to also allow developers of electrochemical storage technologies to identify which are the most relevant parameters of these devices in order to generate value for power systems [7].

The scope of this dissertation is then broadly constrained to the development of analysis tools to support the execution of the highlighted blocks in figure 1.7. Although optimization techniques are needed for some intermediate steps and to formulate reasonable case studies, the focus of the work is on a convenient evaluation of their objective function rather than on the verification of optimality and/or the computational performance of the solution algorithms. In brief, one can state that:

The objective of the present research is to develop models and methodologies that can assess the technical and economical performance of electrochemical accumulators connected to electric power systems.

1.3.1 Specific objectives

Electrochemical cell models For secondary cells with static electrolyte, develop models that are capable to represent:

[7] For example, a developer of lead-acid battery could use this to do a sensitivity analysis on a single constructive parameter of his/hers cells, such as the concentration of the electrolyte, and the lifecycle economic performance on a specific power system for an specific set of services. This can make viable to include model-driven customization of electrochemical storage devices.

1. The variation of steady-state open-circuit voltage as a function of the state of charge and the temperature;
2. The efficiency as a function of the state of charge, temperature and current;
3. The cell terminal voltage for a given current in both steady-state and transient conditions;
4. The thermal behavior of one or more cells;
5. The evolution of the relations above over the lifetime of the cell for different utilization patterns.

Power conversion system (PCS) Taking into account a three-arms inverter bridge with sinusoidal pulse width modulation (PWM), develop models that are able to represent:

1. Voltage and frequency regulation functions for quasi-steady-state conditions;
2. Emulated inertia;
3. Non-ideal DC sources, in particular a simplified battery model;

Monitoring and control unit (MCU) Develop a model that is adequate to:

1. Constrain the operation of the PCS in order to keep the cells operating within their nominal range;
2. Control the thermal management system of the BESS;
3. Automatically adjust the behavior of the PCS to implement the following functionalities:
   (a) Frequency regulation;
   (b) Voltage control;
   (c) Energy arbitrage;
   (d) Peak shaving and valley-filling.

4. Adjust the participation of the BESS in the mentioned services over time in order to:

   (a) Maximize the total profit of the owner of the battery, taking into account a set of regulations and their associated economic signals;

   (b) Follow participation setpoints from the operator(s) of the EPS.

Distribution network expansion planning Develop a model that is able to predict the impact that a large number of batteries connected to the distribution network and operated following arbitrary rules would have over the necessary investments to cope with changes in the utilization of the network, in particular the increase in demand and the introduction of distributed generation.

Bulk energy arbitrage Develop a model that can represent the behavior of a BESS that is buying and selling energy from the grid.

Bulk frequency regulation Develop a model that can assess the performance of a large amount of BESS power capacity providing frequency regulation and inertial response. In particular, the model needs to take into account the ramping limitations related to the battery chemistry.

Microgrid design Develop a model that can aid the design process of grid-connected[8] and permanently islanded microgrids. In particular, the model should be able to represent the lifecycle economics of the battery including lifetime, losses and an evaluation of its participation in ancillary services.

Microgrid operation Develop a model that can conveniently represent a battery in day-ahead operation planning optimization algorithms. In particular, the model should be able to represent time-varying power limits, efficiency and utilization costs.

[8]This type of systems can temporarily disconnect from the larger EPS to which they are connected.

1.4 Organization of the thesis

The document is organized in 7 chapters, with chapters 2 to 6 corresponding to the development of the research question and chapter 7 concludes. Chapters 2 and 3 are used to place the research in a coherent context with respect to theory and the latest developments in the field, which are used as starting point in chapter 4 to formulate a coherent representation of battery energy storage in electric power systems studies. Chapter 5 explains how simplified versions of the representation can be incorporated into some selected models which are useful to answer questions related to EPSs, and chapter 6 uses these in application cases studied through simulations.

Chapter 2

The technology

Since the topic of this Thesis contains elements from the power systems and electrochemistry fields, this chapter aims to provide some minimum background for researchers and developers from both. Electric engineers will likely appreciate the synthetic introduction to the basic principles that govern electrochemical systems, as will electrochemists regarding the basic explanations of the constructive and operational principles of power systems. Moreover since, as far as the author is aware, the electrically-coupled dynamics of synchronous machines, heat engines and electrochemical accumulators is not commonly presented in a coupled way, the inclusion of their fundamental relations is considered relevant.

2.1 Chapter overview

This chapter gives some basic notions related to the relevant domains that will be treated in the rest of the chapters. Section 2.2 enunciates the foundations of the domain where the research is developed, section 2.3 broadly classifies energy systems and describes the most important processes that characterize them, section 2.4 goes through the structure and features of electric power systems and section 2.5 explains the principles that rule the behavior of electrochemical energy storage systems.

2.2 Basic principles

Although the step-by-step derivations are not included, the developments in this chapter can, in principle, be traced back to classical physics and thermodynamics. With the purpose to keep a coherent nomenclature throughout the document, this section presents the subset of relations that are relevant for the developments in later chapters. Unless otherwise noted, the base international system of units is used

Maxwell's equations They establish relationships for the electric field $\mathbf{E}$ in N/C, the magnetic field $\mathbf{B}$ in Tesla ($\mathrm{T} = (\mathrm{N} \cdot \mathrm{s})/(\mathrm{C} \cdot \mathrm{m})$) for an arbitrary distribution of electric charge.

1. The flux of $\mathbf{E}$ through a closed surface equals the charge inside divided by ε_0:

$$\nabla \cdot \boldsymbol{E} = \frac{\rho}{\varepsilon_0} \tag{2.1}$$

2. The rate of change of the flux of $\boldsymbol{B}$ through a loop is equal to the line integral of $\boldsymbol{E}$ in the loop:

$$\nabla \times \boldsymbol{E} = -\frac{\partial \boldsymbol{B}}{\partial t} \tag{2.2}$$

3. There are no magnetic monopoles!:

$$\nabla \cdot \boldsymbol{B} = 0 \tag{2.3}$$

4. The line integral of $\boldsymbol{B}$ around a loop is proportional to a linear combination of the current through the loop and the rate of change of the flux of $\boldsymbol{E}$ through the loop:

$$\mathrm{c}^2 \cdot \nabla \times \boldsymbol{B} = \frac{\boldsymbol{j}}{\varepsilon_0} + \frac{\partial \boldsymbol{E}}{\partial t} \tag{2.4}$$

Conservation of charge The net flux of current through a closed surface is equal to the rate of change of the charge inside it:

$$\nabla \cdot \boldsymbol{j} = -\frac{\partial \rho}{\partial t} \tag{2.5}$$

Lorentz force A charge at rest is affected by a force proportional to the local value of the electric field and in the same direction. A moving charge, in addition, is affected by a force proportional to its velocity and to the local magnetic field, with a direction perpendicular to both vectors:

$$\mathbf{F} = q \cdot (\boldsymbol{E} + \boldsymbol{v} \times \boldsymbol{B}) \tag{2.6}$$

Newton's equation of motion The rate of change in the momentum of an object is proportional to the total force applied:

$$\frac{d\boldsymbol{p}}{dt} = \boldsymbol{F} \tag{2.7}$$

Laws of thermodynamics

1. First law: Heat put into a system + Work done on a system = Increase in internal energy of the system:

$$dQ = dW + dU \tag{2.8}$$

2. Second law: A process whose *only* net result is to take heat from a reservoir and convert it to work is impossible. No heat engine taking heat Q_1 from a source at T_1 and delivering heat Q_2 to a source at temperature T_2 can do more work than a reversible engine, for which:

$$W = Q_1 - Q_2 = Q_1 \frac{T_1 - T_2}{T_1} \tag{2.9}$$

The *entropy* of a system is defined on this way:

- If heat ΔQ is added reversibly to a system at temperature T, the increase in entropy of the system is $\Delta S = \Delta Q/T$;
- At $T = 0$, $S = 0$ (third law).

In a *reversible change*, the total entropy of all parts of the system (including reservoirs) does not change.

In *irreversible change*, the total entropy of the system always increases.

It should also be possible to rework the explanations replacing thermodynamics by a combination of statistical and quantum physics. However, there are at least three important issues that make that approach inconvenient:

1. The analytical description of real materials is difficult, and many approximations are needed to produce workable formulas.

2. Even if the formulas can be worked out, there's no known analytical solution for many of them, and the time-step required to obtain a convergent numerical solution (usually nanoseconds) makes the simulation of their behavior incompatible with power systems simulations because of computational power constraints.

3. Although the insight gained from a deep theoretical understanding of the internal workings of electrochemical reactions is extremely valuable to develop new materials and devices, it does not shed significant light on the central topics of this dissertation.

The following sections explain the most relevant definitions and results that will be used to do a coupled study of electromechanical and electrochemical energy systems from a practical point of view. Readers familiar with both domains may prefer to skip to chapter 3.

2.3 Energy systems

A big number of feedback loops constitute our planetary life support system, and most of them involve relevant energy transfer and conversion processes. Since we will use the expressions *system* and *energy* in several ways, it is convenient to properly define them and summarize some of their relevant properties and applications.

Definition 2.1. *System*: a collection of physical entities that exist in a region of the space limited by a geometric boundary. The region outside the boundary is called the *environment*.

Here, systems will be understood from the point of view of thermodynamics. *"Initially, thermodynamics was the study of heat and its ability to generate motion; then it merged with the larger subject of energy and its interconversion from one form to another. With time, thermodynamics evolved into a theory that describes transformations of states of matter in general, motion generated by heat being a consequence of particular transformations"* [29]. The ideas used in thermodynamics are sufficiently well defined from an operational point of view to be used to unify the range of phenomena discussed in this document. In particular, we can classify systems as:

Definition 2.2. *Thermodynamic system types*[29]: Isolated systems do not exchange energy or matter with the environment; closed systems exchange only energy; open systems exchange energy and matter.

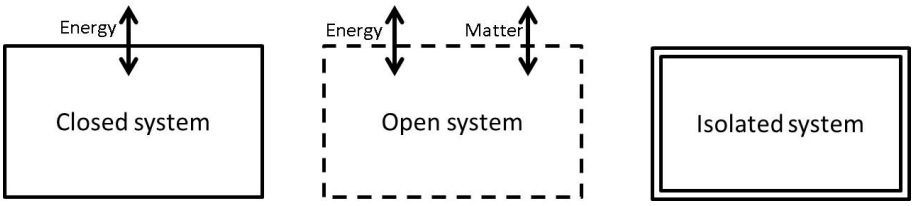

Figure 2.1: Classification of systems from a thermodynamic point of view

According to this, we can set the boundary of electric power systems in order for them to be considered closed. In concrete terms, we imagine that only generators, and not prime-movers, are inside the geometric boundary of the system.

2.3.1 Energy

Defining energy is not straightforward, and we can't avoid using the definition of isolated system, for which we used the energy concept on the first place. But this is more an ontological discrepancy than a practical one and we can use this quantity regardless of it. *"It is important to realize that in physics today, we have no knowledge of what energy is. We do not have a picture that energy comes in little blobs of a definite amount. It is not that way. However, there are formulas for calculating some numerical quantity, and when we add it all together it gives "28"always the same number. It is an abstract thing in that it does not tell us the mechanism or the reasons for the various formulas"* [30].

Definition 2.3. *Energy* is a numerical quantity that does not change over time in an isolated system, which can be related to the potential to perform mechanical work inside the system.

This definition includes both situations in which the potential comes from the existence of force fields acting over the components of the system and the possibility that moving parts of the system produce movement by interacting with other parts of it. It is not intended to mean *useful* or *macroscopic* work, which requires additional knowledge about the surroundings of the system and is related to the concept *exergy*.

There are many formulas to calculate the energy of a system on a given instant, and the reader is referred to [30] for an excellent description of them. There is a certain bias towards mechanical energy implicit in the way units are defined though. The International System (SI) unit for energy is the joule (J), which is defined through the relation $\mathrm{J} = \mathrm{N} \cdot \mathrm{m}$. In other words, to move an object 1 meter against a force of 1 newton we need 1 J of mechanical energy.

2.3.2 Primary energy forms

Primary energy refers to energy forms that have not gone through any artificial transformations [31]. When hydrocarbons are converted into thermal energy through combustion carbon dioxide can be released to the atmosphere and increase the ability of the atmosphere to retain low-wavelength electromagnetic radiation, which is known as $radiative forcing$ or *greenhouse effect*. There is clear evidence that this effect leads to an increase in the long term temperature of the atmosphere, which may jeopardize global life-support systems.CO_2 emissions are estimated to be responsible for over 70% of the increase in radiative forcing since the year 1750 [32], and the electric power sector accounts for over 40% of these emissions. Table 2.1 shows an estimation of the contribution of different primary energy sources to the satisfaction of energy demand published in 2013 by the International Energy Agency (IEA). The New Policies Scenario analyses the evolution of energy markets based on the continuation of existing policies and measures as well as cautious implementation of policies that have been announced by governments but are yet to be given effect. The Current Policies Scenario takes account only of policies already enacted as of mid-2013. The 450 Scenario shows what it takes

to set the energy system on track to have a 50% chance of keeping to 2 °C the long-term increase in average global temperature [23].

			New Policies Scenario		Current Policies Scenario		450 Scenario	
	2000	2011	2020	2035	2020	2035	2020	2035
Coal	2357	3773	4202	4428	4483	5435	3715	2533
Oil	3664	4108	4470	4661	4546	5094	4264	3577
Gas	2073	2787	3273	4119	3335	4369	3148	3357
Nuclear	676	674	886	1119	866	1020	924	1521
Hydro	225	300	392	501	379	471	401	550
Bioenergy*	1016	1300	1493	1847	1472	1729	1522	2205
Other renewables	60	127	309	711	278	528	342	1164
Clean sources	9.54%	8.42%	10.56%	13.41%	9.92%	10.83%	11.64%	21.70%
Renewable energy	13%	13%	15%	18%	14%	15%	16%	26%
Clean renewable energy	3%	3%	5%	7%	4%	5%	5%	11%
Total (Mtoe)	10071	13070	15025	17387	15359	18646	14316	14908
CO2 Emissions (Gt)	23.7	31.2	34.6	37.2	36.1	43.1	31.7	21.6

Table 2.1: Estimated and forecasted World primary energy demand and energy related emissions by scenario [23].

It is clear that the role of the energy sector in the moderation of global warming is paramount, especially if is possible to increase the share on non-polluting primary energy forms.

2.3.3 Energy services

With the exception of the chemical energy intake in the form of food[1], the relevance of energy rests in the provision of services that require it as an input. Most people in developed countries require a combination of energy forms to satisfy their needs. For example, households use energy for heating and cooling, transportation, lighting, cooking and for the operation of electronic devices. The final energy forms that can be used to provide these services include electricity, heat, and fuel. The concept of energy service is particularly relevant in contexts of poverty, since the basic needs of lighting, cooking and heating are essential to achieve an acceptable standard of living:

"Current energy systems are inadequate to meet the needs of the worlds poor and are jeopardizing the achievement of the Millennium Development Goals (MDGs). For instance, in the absence of reliable energy services, neither health clinics nor schools can function properly. Access to clean water and sanitation is constrained without effective

[1]This is a very interesting energy conversion process. Curious readers are encourage to read the book *Bicycle Science* by David Gordon Wilson

pumping capacity. Food security is adversely affected, often with devastating impact on vulnerable population." [33]

The utilization of primary energy resources to perform energy services requires a complex web of technical and financial coordinations, centered in energy conversion and transfer [2] processes.

2.3.4 Energy conversion

Suppose we have 1 kg of propane stored in a vessel at a pressure of 20 MPa and a temperature of 300 K. The vessel is in a room at atmospheric pressure ($\approx$ 100 kPa) and at 300 K. There are several ways in which we can extract energy from it, among them:

1. Let it expand inside a piston and move something. If done very slowly, the amount of work that is obtained is $W = N \cdot \mathrm{R} \cdot T \cdot ln\,(V_f/V_1)$, where V_f is the final volume, V_i is the initial volume, N is the number of moles, R is the universal ideal-gas constant and T is the absolute temperature [29];

2. Annihilate it entirely and convert the mass into energy. This energy is embodied in several particles, primarily photons, which can be absorbed by the medium and generate heat. The energy of each particle i is E_i=h $\cdot\, \nu_i$, where h is Planck's constant and ν is the frequency of the particle. We also get that $\sum_i E_i = m \cdot \mathrm{c}^2$ if all the mass m is annihilated [30];

3. Initiate a chemical reaction to turn propane into a different chemical species with lower energy. For example, this can be done through a combustion reaction with the following stoichiometric relation: $\mathrm{C_3H_8(g)} + 5\mathrm{O_2(g)} \rightarrow 3\mathrm{CO_2(g)} + 4\mathrm{H_2O(l)}$. To calculate the energy released through the reaction, we simply compare the standard formation enthalpy of the reactants and the products, weighed by their stoichiometric coefficients: $\mathrm{E} = (3\Delta\mathrm{H_f^0[CO_2]} + 4\Delta\mathrm{H_f^0[H_2O]}) - (\Delta\mathrm{H_f^0[C_3H_8]} + \Delta\mathrm{H_f^0[O_2]})$ [29].

4. Use a reformer to convert the propane into syngas, use the syngas to obtain electricity from a fuel cell and, finally, power an electromagnet with the electricity to move something. The syngas can obtained either by steam reforming

[2] Energy *transfer* is the term used in thermodynamics to describe the exchange of energy between systems or parts of a system. In electricity, it is more common to use *energy transmission* to refer to the case when wires mediate the transfer process. Finally, to refer to the movement of embodied energy, e.g., hydrocarbons on a ship, we use the term *energy transport*.

($C_3H_8 + 3H_2O \rightarrow 3CO + 7H_2$) or dry reforming ($C_3H_8 + 3CO_2 \rightarrow 6CO + 4H_2$), both processes requiring some energy input [34]. Then the hydrogen can be used as input to a fuel cell, where the reaction $2H_2 + O_2 \rightarrow 2H_2O$ yields 2 electrons at about 0.7 V. The electric current produced by the reaction can be used to move an electromagnet.

Note options 2 and 4 don't produce work directly, but just increase the heat content of the medium where the reaction occurs. To turn that heat into mechanical work, we need a *heat engine*.

Two energy conversion processes of particular relevance to electric power systems are from thermal to mechanical and from mechanical to electrical. Since one of the purposes of this Thesis is to develop a dynamic model that couples their dynamics with those of electrochemical accumulators, a brief description of both follows.

Thermo-mechanical energy conversion *"Everyone knows that heat can produce motion. That it possesses vast motive-power no one can doubt, in these days when the steam-engine is everywhere so well known. To heat also are due the vast movements which take place on the earth. It causes the agitations of the atmosphere, the ascension of clouds, the fall of rain and of meteors, the currents of water which channel the surface of the globe, and of which man has thus far employed but a small portion. Even earthquakes and volcanic eruptions are the result of heat. From this immense reservoir we may draw the moving force necessary for our purposes. Nature, in providing us with combustibles on all sides, has given us the power to produce, at all times and in all places, heat and the impelling power which is the result of it. To develop this power, to appropriate it to our uses, is the object of heat engines."*[35].

The most simple version of a heat engine is the piston shown in figure 2.2. The left side of the figure corresponds to t_0, when a propane burner is turned on to heat up an adiabatic container with N moles of air. In $t_1 = t_0 + \Delta t$, the burner is turned off. The first part of the cycle involves expansion of the working fluid by contact with a surface of higher temperature (the flame). The second part of the cycle corresponds to condensation by contact with a cold source (e.g., the air). Only using logical deductions, and before the energy conservation law was stated, Saidi Carnot proposed that when a quantity of heat Q_1 is extracted in this way from a body at constant temperature T_H,

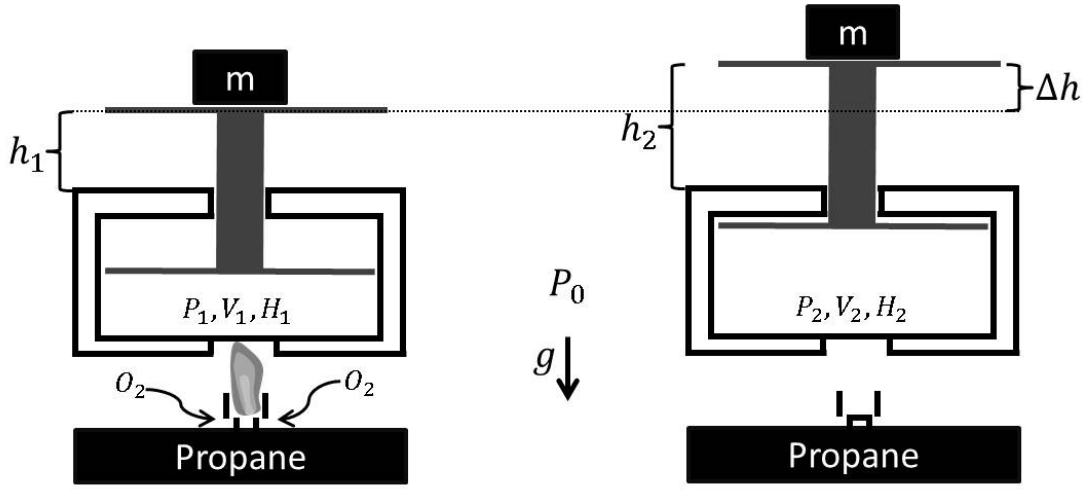

Figure 2.2: A piston can be used to convert heat into work

and a quantity of heat Q_2 is delivered to another body at constant temperature T_L, where $T_H \geq T_L$, the mechanical power W extracted from the system is constrained by equation (2.9), when the temperature is expressed in K. The surprising fact that even though Carnot wrongly assumed that $Q_1 = Q_2$ this expression works, supports the idea that wrong assumptions can lead to correct conclusions. Now we know, applying the first law of thermodynamics, that $Q_2 = Q_1 - W$. Equation (2.9) applies both to reciprocating (pistons) and continuous (turbines) single-cycle heat engines. In real applications, Q_2 is hot enough to drive a second thermodynamic cycle, and the overall conversion efficiency can be higher than equation (2.9). This arrangement is exploited in combined cycle gas turbines (CCGT).

Electromechanical energy conversion Consider the experimental arrangement in figure 2.3, which represents two identical ideal coils and an ideal resistor. The coils are immersed in uniform magnetic fields and free to rotate abut their axes.

Let θ be the angle between the plane of a coil and the magnetic field, S the internal surface of the coils and N their number of turns. Using the integral form of equation (2.2), we obtain that if coil number one on rotates with angular speed $\omega_1 = \mathrm{d}\theta_1/\mathrm{d}t$ an electromotive force ε_1 is induced:

$$\varepsilon_1 = \mathrm{N} \cdot |\boldsymbol{B}| \cdot S \cdot \omega_1 \cdot \sin(\omega_1 \cdot t)\,. \tag{2.10}$$

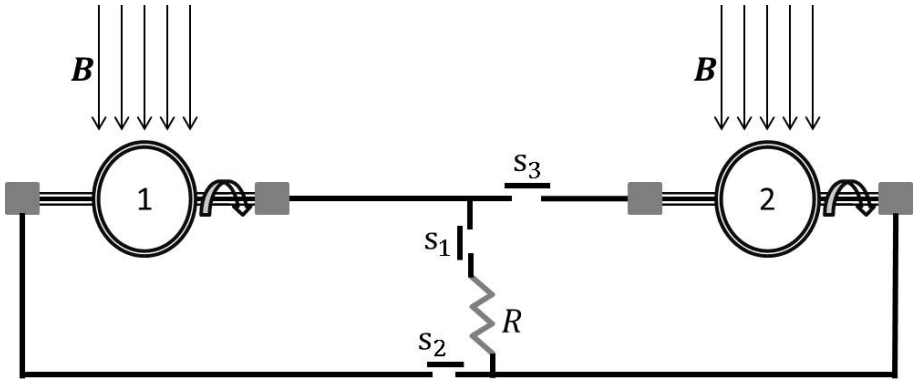

Figure 2.3: Electromechanical energy conversion with a rotating generator.

One can arbitrarily set the phase of this coil to zero. Making $E_1 = \mathrm{N} \cdot |\boldsymbol{B}| \cdot S \cdot \omega_1$ the phasor expression for the EMF, in Volts, is:

$$\varepsilon_1 = E_1 \cdot e^{\mathrm{j}0} = E_1 \angle 0. \tag{2.11}$$

By closing the switches S_1 and S_3 a current will flow through the left coil. If the inductance of the coil is constant of value L_1,

$$I_1 = \frac{E_1}{\mathrm{R} + \mathrm{j} \cdot w_1 \cdot \mathrm{L}_1} = \frac{|E_1|}{\sqrt{\mathrm{R}^2 + (w_1 \cdot \mathrm{L}_1)^2} e^{j \tan^{-1}\left(\frac{w_1 \cdot \mathrm{L}_1}{\mathrm{R}}\right)}} \tag{2.12}$$

If n is the charge density per unit length in the wire and $\mathbf{v}$ is the velocity of the charges, the force law in equation (2.6) implies that the power that is delivered to the loop is $P = \oint n \cdot \mathbf{v} \cdot F \cdot ds$. Since $\varepsilon = \oint E \cdot ds$ and $E = F/\mathrm{q}$, it results that the electric power delivered by the generator is:

$$P_1 = I_1 \cdot \mathrm{N} \cdot |\boldsymbol{B}| \cdot \boldsymbol{S_1} \cdot \omega_1 \cdot \sin(\omega_1 \cdot t) \tag{2.13}$$

On the other hand, the torque $\boldsymbol{\tau_1}$ in $\mathrm{N} \cdot \mathrm{m}$ about the coil's axis is proportional to the magnetic moment $M_1 = S \cdot I_1$ and to the projection of the magnetic field over the plane of the coil. Since the mechanical power $P_{mec} = \tau\omega$, we obtain equation (2.13). This implies that ideal electromechanical energy conversion processes are conservative. Note that when $\mathrm{R} = 0$, $\boldsymbol{I_1}$ is always perpendicular to the vector normal to $\boldsymbol{S_1}$, and

hence $\boldsymbol{\tau_1} = 0$. In general, if $\delta_1 = \tan^{-1}\left(\frac{w_1 L_1}{\mathrm{R}}\right) + \frac{\pi}{2}$ is the angle between S_1 and I_1 and $X_1 = w_1 \cdot L_1$, then:

$$P_1 = \frac{|E_1|\,|V_1| \sin\delta}{X_1}, \tag{2.14}$$

where V_1 is the terminal voltage of coil 1. Deriving equation (2.14) with respect to R and equating to zero yield that $R_{pmax} = |X_1|$, which is known as the *Maximum Power Transfer Theorem.* Now, if one opens switch S_3 and closes switch S_2, the current through coil 2 will induce a torque. If the mass and friction of coil 2 are small enough, by virtue of equation (2.14) a stable operation point will be reached in which $w_1 = w_2$. If we try to externally break coil 2, δ_2 increases in the precise amount to compensate the breaking power. For this reason, this type of machines remain in synchronism. Note however, that for $\delta > \pi/2$ the power delivered will start decreasing, and the system loses synchronism. Actual synchronous machines are much more complex to model, but follow the same principle. With some modifications, the same idea of shifted magnetic fields explains the operation of the induction machine, the other major electromechanical conversion device.

2.3.5 Energy storage

The value that can be realized from the provision of most energy services exhibits a strong temporal and spatial dependency. An example where this relationship is weaker, and that will serve to illustrate the relevance of the subject, is a farm with a grain grinder connected to a wind propeller. If the grinder is used to provide flour for the farm, in principle one does not care about when the grain is ground, as long as a certain amount is produced over a certain time, say one hundred kilograms each week. Hence, the perceived usefulness of this simple energy system is independent from when the wind blows. On the other hand, it is straightforward that the higher the fluctuations in wind speed the more the propeller and grinder need to be oversized in terms of instantaneous processing power. This additional investment increases the cost of providing the energy service, as illustrated in figures 2.4a and 2.4b: the fluctuations in the energy supply are mismatched with the ideal utilization patter of the equipment that provides the energy service.

Energy storage technologies can help to improve the performance of energy systems that exhibit temporal mismatches. In the case of the grinding process, there's nothing we can do to store wind, since it is a variable energy resource which we can either use or let it go. The mechanical output of the wind propeller is easier to handle, and it could for instance be used to operate a mechanical pump to compress air. A pneumatic motor could then be used to convert the potential mechanical energy in the compressed air into work in the shaft of the grinder. As depicted in figure 2.4c, the addition of this mechanical storage device would allows us to continuously operate a smaller grinder and keep the weekly flour output constant.

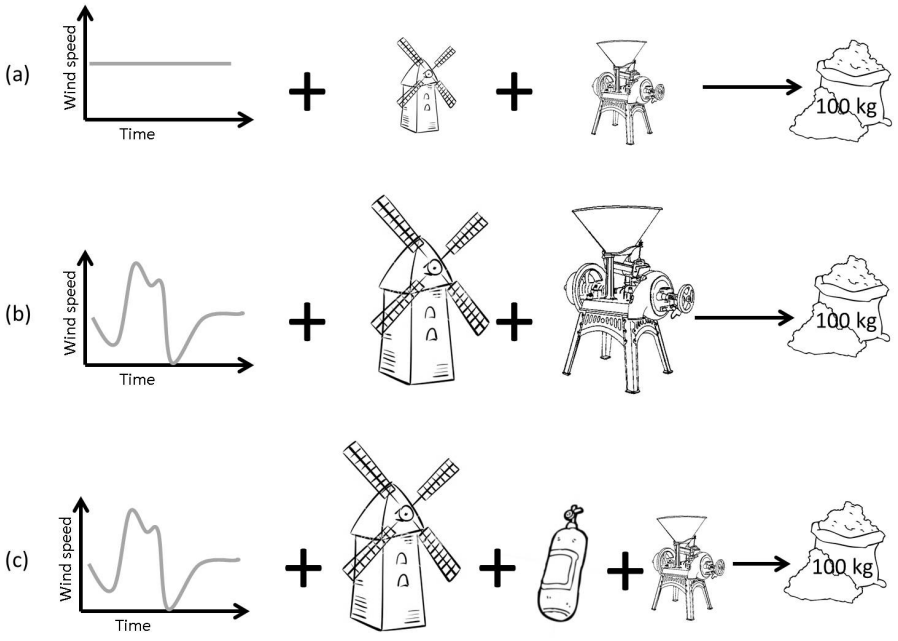

Figure 2.4: Grain grinding energy service example.

It is obvious that the inclusion of the energy storage device in the example will only be justified if it makes economic sense. In other words, the money saved because one doesn't have to buy a big grinder must be more than what needs to be paid for the pump, the air tank, the pneumatic motor and the conversion losses. Using this idea one can define the economic value of an energy storage asset in general:

Definition 2.4. *Economic value of an energy storage asset*: For an existing system or for one under design, the total net present savings obtained from the introduction and of the asset.

This definition contains a couple of degrees of freedom. There can be more than one way of introducing the asset in the energy system and also several ways in which it can be operated. The analysis of these aspects is one of the central motivation of this dissertation.

2.3.6 Energy transfers

In addition to temporal mismatches, the best places to execute an energy service (e.g., cooling for a hospital) usually don't coincide with where the primary energy resource is available (e.g., an oil rig in the ocean). Also, the energy conversion steps that need to be taken to convert the primary energy resource into a form that can be used to provide the service are often not compatible with the activities (refining, combustion, etc.). Hence, the energy needs a means of being transported from sources to sinks. When the distances involved are of more than some tens of meters, only some energy forms are transportable in practice:

1. Electric energy: electric transmission and distribution lines and cables;
2. Chemical: gas pipes, liquified gas cylinders, oil, electrochemical storage devices, hydrogen, etc;
3. Hydraulic: pressurized ducts, canals;
4. Mechanical potential: Pressurized air, springs (e.g., in clocks).

Of these, hydrocarbons and electricity are the most used for long distances and high volumes. Recently, electrochemical storage devices, in particular the lithium-ion type, have experienced a significant development related to mobile applications, a sector that is currently highly dependent on hydrocarbons. Since the location of the centers of consumption and bulk energy conversion/exploitation changes slowly, it has been convenient to build permanent infrastructures to support energy transport and distribution. This is an obvious fact for electric energy, since current needs wires to exist. In the case of hydrocarbons, pipelines span over thousands of kilometers. These two energy transfer systems interact heavily because a big share of prime movers connected to electricity generators use hydrocarbons to generate mechanical power.

2.4 Electric power systems

When Faraday first made public, in 1821, his remarkable discovery that a changing magnetic flux produces an EMF, he was asked (as anyone is asked when he discovers a new fact of nature), What is the use of it?" All he had found was the oddity that a tiny current was produced when he moved a wire near a magnet. Of what possible use could that be? His answer was: What is the use of a newborn baby?" [36]. This discovery started a technological revolution probably with an impact, in the last millennium, second only to the heat engine.

2.4.1 History

Fifty years later, the commercial exploitation of electricity began, when arc lamps were used for lighthouse illumination and street lighting [37]. After a brief period dominated by the direct current (DC) system, by the turn of the century the simplicity and flexibility of alternating current (AC) became evident. Alternating current generators remain in synchronism because of the self-regulating properties of their interconnection. If one machine deviates from its synchronous speed, power is transferred from the other generators in the system in such a way as to reduce the speed deviation [38]. One constraint derived from this principle is that all the machines in an AC power system have to generate electricity at the same frequency. In 1891, Westinghouse engineers in Pittsburgh selected 60 Hz as their new power frequency. That same year, AEG engineers in Berlin selected 50 Hz as their new power frequency. Although much has happened since 1891, these two frequencies remain the principal power frequencies in use worldwide [39].

The increasing need for transmitting larger amounts of power over longer distances created an incentive to use progressively higher voltage levels. The early power systems used 12, 44 and 60 kV. This rose to 165 kV in 1922, 220 kV in 1923, 287 kV in 1935, 330 kV, 500 kV in 1965, and a 765 kV line was introduced in the United States in 1969. After the 1950's high-voltage direct current transmission has become economical in special situations [37] and is becoming increasingly common as EPSs span across countries and the volumes of energy transported grow.

Currently, more than 2/3 of the world's population significantly relies on power systems to maintain their way of life. The barriers to achieving an acceptable quality of life that face the remainder should be a high priority for international agencies, governments and all institutions that try to eliminate poverty.

2.4.2 Structure and components

Electric power systems are basically a gigantic electric energy transfer infrastructure between generators and loads. The power magnitude and the distance involved in the transfers condition the selection of different voltage levels. This is conveniently understood as the hierarchical network structure shown in figure 2.5.

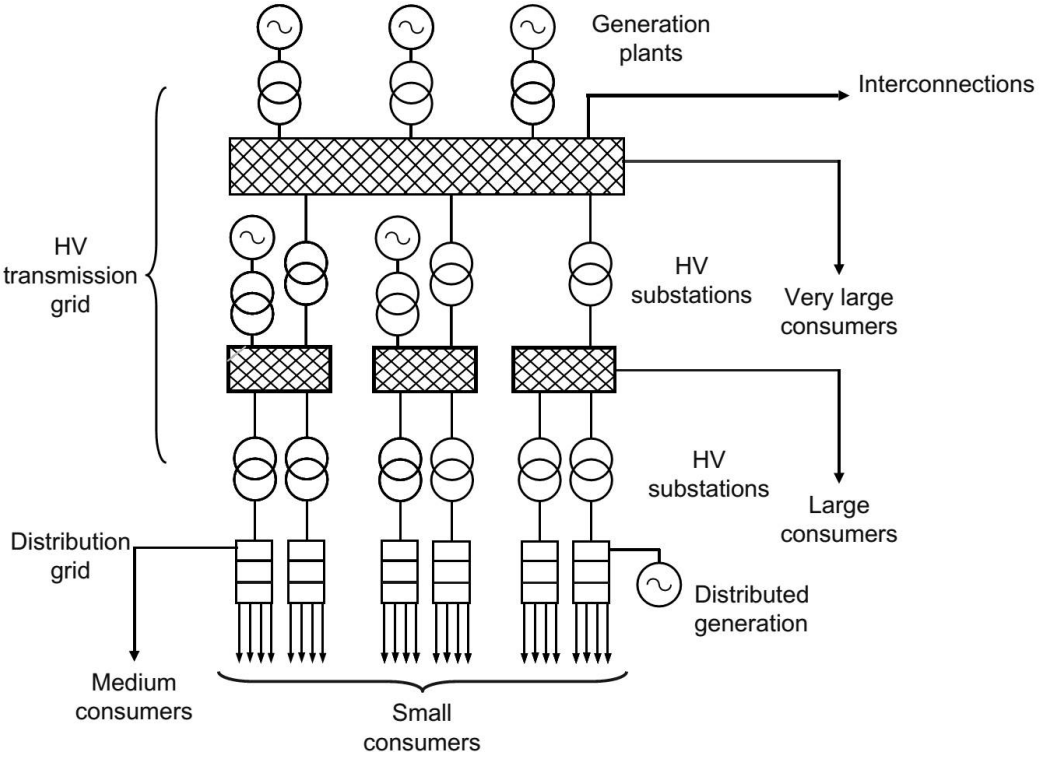

Figure 2.5: Typical structure of large electric power systems [1]

Generators Include all devices that inject energy into the system, in AC networks by producing an EMF with a phase angle that leads the one in their coupling point to the system, in DC networks by imposing a voltage higher that the open-circuit one. For the purpose of this dissertation, we're interested in three types:

1. Synchronous generators that are the backbone of large power systems, they are characterized by a proportional relationship between the mechanical rotation speed of the rotor and the frequency of the EMF;

2. Induction generators that are most frequently used in wind turbines and small hydro power plants. They are characterized by a nonlinear deviation from a proportional relationship between the mechanical rotation speed of the rotor and the frequency of the EMF. A relevant sub-type of these machines are doubly-fed induction machines, in which rotor currents are electronically controlled [37];

3. Electronic converters that use semiconducting devices like IGBTs and MOSFETs together with capacitors and inductors to approximate a sinusoidal EMF from either a DC (inverters)or AC (cycloconverter) electric power supply. They are used to connect PV panels, batteries, wind generators and high-speed rotating machines like microturbines.

Load Devices used to convert electric energy into services exhibit two types of fluctuations. The first one is in most cases very difficult to model and is associated to the behavior of the users of these services. Nevertheless, statistical data at the substation level allows for temporal patterns to be inferred for typical days. These estimations are more accurate the more customers exist in the area being analyzed, since averaging effects compensate for diversity in behavior and uncertainty. The second one corresponds to the reaction of the physical devices to changes in the characteristics of the supply. For example, a resistive load (e.g., an incandescent light bulb) will consume active power in proportion to the square of its supply voltage. These loads belong to the class named *constant impedance loads.* In contrast, devices connected through regulated power supplies are able to maintain the consumption constant for reasonable variations in the voltage, which is why they are called *constant power loads.* The last family of loads commonly used in steady-state models is the constant-current load, which draws a current from the system under all voltage conditions, hence the active and reactive power are proportional to the voltage. This type of load is representative of many systems and is sometimes used in the absence of better data [40]. These three load types can be combined in a polynomial expression commonly referred to as the *ZIP* model [37]:

$$
\begin{aligned}
p &= p_0 \left[p_1 \cdot \bar{V}^2 + p_2 \cdot \bar{V} + p_3 \cdot \right] \\
q &= q_0 \left[q_1 \cdot \bar{V}^2 + q_2 \cdot \bar{V} + q_3 \cdot \right],
\end{aligned}
\tag{2.15}
$$

where the voltages are expressed relative to the nominal value as $\bar{V} = V/V_0$. In dynamic studies, it is necessary to use more detailed model to represent the response of devices like induction machines to fast frequency and voltage changes.

Lines include both overhead conductors and cables. Their function is to allow the flow of electric current. A transmission line is characterized by the series resistance R due to conductor resistivity, shunt conductance G due to leakage currents between the phases and ground, series inductance L due to the magnetic field surrounding the conductors, and shunt capacitance C due to the electric field between the conductors and the ground plane [37]. Although these 4 are due to characteristics that occur continuously in space, models that represent them as equivalent circuits with lumped components like the one shown in figure 2.6 where $Z = R + \mathrm{j}\omega L$ and $Y_1 = Y_2 = (G + \mathrm{j}\omega C)/2$.

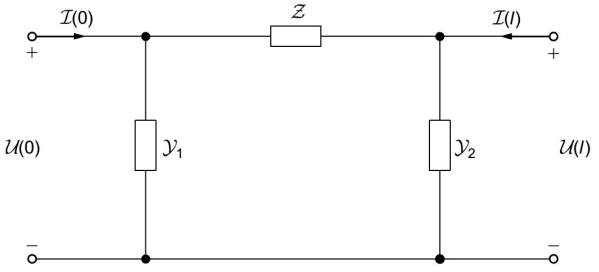

Figure 2.6: Equivalent π lumped parameters model for a transmission line [1]

Transformers Their primary function is to allow power flows between lines at different voltage levels. They can also be used to correct angle issues (phase-shifting transformers) and to regulate the voltage magnitude on a feeder. Their operation is based on two or more magnetically-coupled coils wound around a ferromagnetic core. For coils that link the same magnetic flux, the ratio between terminal voltages is approximately proportional to the ratio in the number of turns. The non-ideality of the core as a magnetic conductor induces several non-linearities and losses that are difficult to model. Figure 2.7 shows a "reasonable" representation of a transformer in terms of electric components.

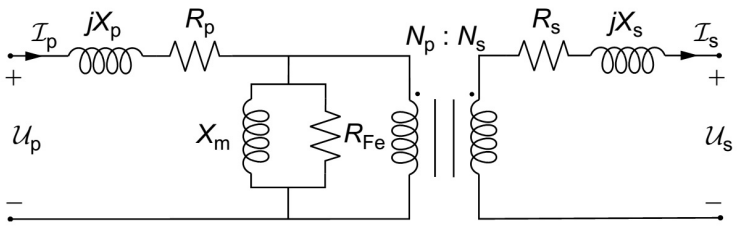

Figure 2.7: Equivalent circuit for a single-pase two winding transformer [1]

Switches, breakers and protections Changes in the operational regime and faults often times require to modify the topology of the network. Breakers are able to interrupt a current within a certain range, and switches are devices usually operated under supervision and on a circuit where a breaker has previously stopped the current. In the event of a fault, the section of the network with problems is isolated by the automatic action of breakers commanded by protection relays. The protection relay contains an electronic implementation of a reaction logic that sets off a trip signal when a combination of conditions are present. Common logics are the overcurrent, differential, frequency and distance protections [1].

Voltage regulation equipment The devices used for this purpose may be classified as: a) sources or sinks of reactive power; b) line reactance compensators, such as series capacitors; c)regulating transformers [37]. Since voltage problems are not usually permanent, these devices need to be able to automatically change their parameters. For example, regulating transformers achieve different conversion ratios by "tapping" on a different number of coil turns. Doing this under load supposes the presence of adequate switching equipment whose lifetime will be related to the number of operations. The operational schedule of a tap-changer can be defined a-priory based on knowledge about the power flow regimes in the line, or in response to a local, remote or virtual measurement (estimating the value of a remote node from a model and local measurements).

Filters The saturation of ferromagnetic cores and the existence of non-linear devices in the network causes a distortion in the voltage waveform. This is inconvenient, since many devices cannot operate properly with a distorted waveform, and the abnormal frequency components can excite resonances in the network leading to voltage and current spikes that can make protections trip. To alleviate these issues, passive and active

filters are used. They vary widely in complexity, from simple L-C circuits to complex arrangements of passive elements and power electronics [41].

Flexible AC transmission systems (FACTS) Using power electronics it is possible to modify the electric characteristics of transmission lines in a controlled way or to strategically inject or consume reactive power to do voltage control. For example, the left-side arrangement in figure 2.8, known as thyristor-controlled series capacitor, allows to control the series line impedance with the firing angle of the thyristors. The device on the right-side of 2.8, known as the static VAr compensator (SVC), can control the shunt impedance. Other examples of FACTS devices are the unified power flow controller (UPFC) and the static synchronous compensator (STATCOM) [2]. This last is basically a three-phase inverter used to provide reactive power support, an hence it doesn't require an active power supply on the DC link. When the capacitor in the DC link is replaced with a battery, the STATCOM can be used to also inject active power, a feature that can be useful to control fast voltage variations in distribution networks [42]. Also, the increase in distributed photovoltaic and wind generation has driven a larger number of inverters connected to the grid, opening the possibility of using the excess power capacity of these devices as STATCOMs [43].

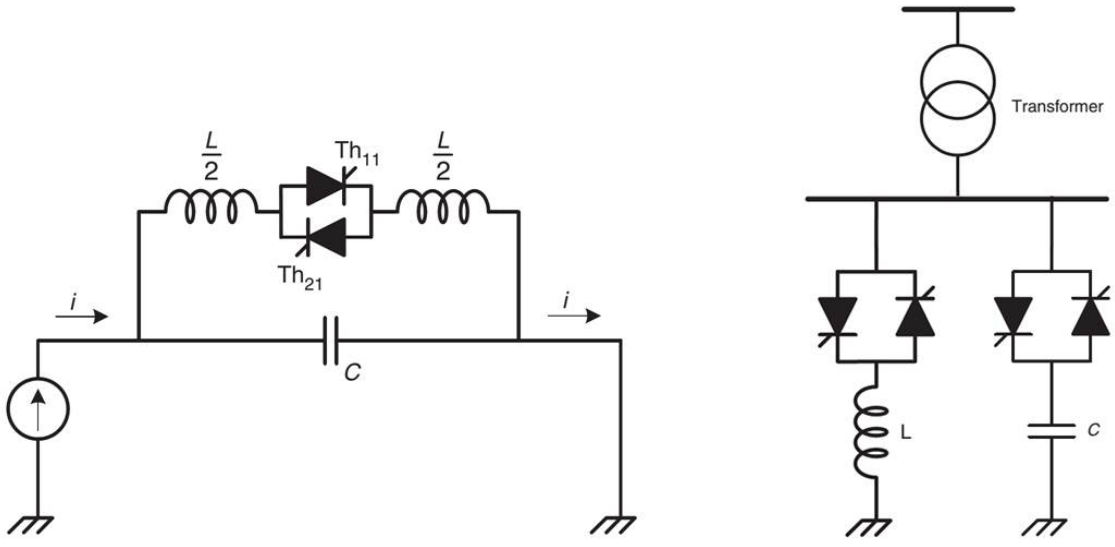

Figure 2.8: SVC and TCSC [2]

2.4.3 Stability considerations

Power systems are rarely found in equilibrium, but instead operate in continuous change. Historically, most of the variability in power flows has been explained by fluctuations on the load. More recently, a higher share of variable energy resources (VERs) have increased significantly the contribution of power sources. Thanks to a combination of the physics of synchronous machines, their inertia, and several levels of control, large networks can be kept in secure operation for decades. Two basic state variables need to be kept within a narrow interval, the frequency and the voltage. The former is considered a single variable for a synchronous area[3], while the latter can be likened to a scalar field in the network space. Due to this difference, the methods involved in the control of both are very different, although interdependent (reactions to correct frequency issues can cause voltage issues and vice-versa).

The swing equation The dynamics of the frequency is mainly related to the physics of synchronous machines and, on a lesser degree, to the physics of loads. In the test system of section 2.3.4, we assumed an ideal coil rotating at constant speed regardless of the power output. The underlying assumption was that the mechanism providing a mechanical power P_m could instantaneously adjust its output to match the electric power delivered to the load P_e and therefore the torque angle changes in steps. In real generators there are no prime movers that can react instantaneously, which causes power imbalances to occur. In turn, these power imbalances cause an accelerating power $P_a = P_m - P_e$. For a mechanical rotation speed $\omega_{\mathbf{m}}$, a mechanical torque $\tau_{\mathbf{m}}$ and using that $P = \tau \cdot \omega$, we get the equation of motion of the machine:

$$\mathrm{J}\frac{d\omega_{\mathrm{m}}}{dt} = \tau_{\mathrm{a}} = \tau_{\mathrm{m}} - \tau_{\mathrm{e}}, \tag{2.16}$$

where J in $\mathrm{kg} \cdot \mathrm{m}^2$ is the combined moment of inertia of the rotor of the synchronous machine and the rotating part of the prime mover, τ_a is known as the accelerating torque and τ_e is the electromagnetic torque [37]. If the inertia constant H, in s, is defined as:

[3]Nevertheless, for systems spanning several hundreds of km, a frequency perturbation can take some seconds to propagate.

$$\mathrm{H} = \frac{1}{2}\frac{\mathrm{J}\cdot\omega_{0m}^2}{\mathrm{VA}_{base}}, \tag{2.17}$$

where VA_{base} is the rated complex power of the generator in VA and if we also consider a damping term $\mathrm{K_D}$ proportional to the frequency deviation, equation (2.18) can be written as:

$$\frac{2\mathrm{H}}{\omega_0}\frac{d\omega}{dt} = \bar{\boldsymbol{\tau}}_{\boldsymbol{m}} - \bar{\boldsymbol{\tau}}_{\boldsymbol{e}} - \mathrm{K_D}\Delta\bar{\boldsymbol{\omega}}_{\boldsymbol{m}}, \tag{2.18}$$

Where the bars denote per-unit values with $\omega_{base} = |\boldsymbol{\omega_0}|$ and $\tau_{base} = \mathrm{VA}_{base}/\,|\boldsymbol{\omega_{base}}|$.

Power transfer limits in transmission lines There are four limiting factors:

1. Maximum voltage between conductors, conditioned by the quality of insulation, geometrical arrangement and atmospheric conditions;

2. Maximum operational temperature of the conductor, related to the thermal tolerance of the insulation in cables and to the minimum distance to the ground in overhead lines;

3. Voltage stability limit. The relationship between the power transferred and the voltage drop in a line is non-linear and increases abruptly after a certain threshold. Operating a line close to this limit supposes a risk, since sudden changes in the load on the receiving end (frequently related to starting induction motors) can lead to voltage collapse [37];

4. Angular stability limit. This can be understood from equation (2.14) considering that the sending and receiving ends are equivalent synchronous machines and the load angle δ being the measure of the relative positions of their rotors. Beyond the point of maximum power, an increase in the torque of the sending end machine results in an increase of δ, but the transmitted power decreases. This causes the sending end machine to accelerate and the receiving end machine to decelerate, resulting in a further increase of δ. This is a runaway situation, and the two machines (or the systems they represent) lose synchronism [37].

2.4.4 Operation principles

The existence of power generation and transfer limits in the devices that compose EPSs, together with the existence of unstable frequency and voltage characteristics makes the existence of feedback control loops indispensable for their stable operation. Also, since the load changes in time and the generation units are heterogeneous, a procedure to decide which units should be contributing on every instant to meet the load is needed. Finally, the composition of the demand will not remain fixed over periods of time of several years, and other procedures are needed to plan adaptations accordingly. The difference in time scales between these procedures is, as figure 2.9 shows, overwhelming.

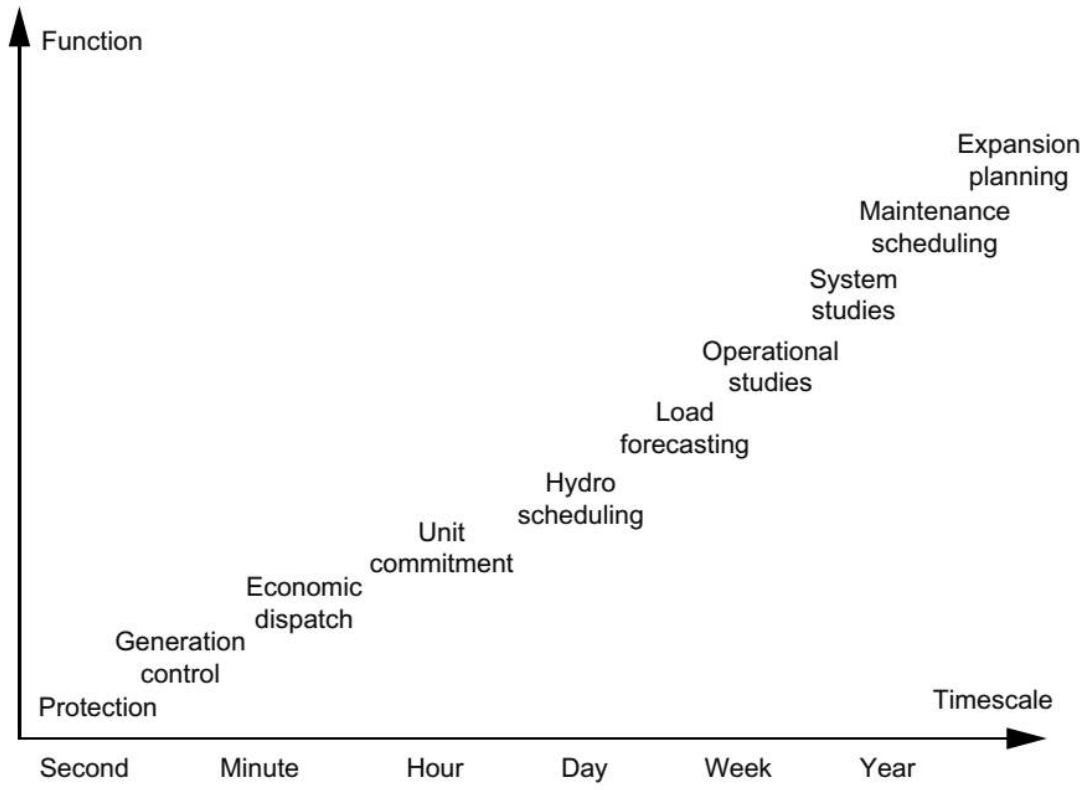

Figure 2.9: Representative time scale for different correction loops designed to ensure the long-term reliable operation of electric power systems [1].

Load balancing and frequency control By virtue of equations (2.18) and 2.14, when an imbalance between the power output of all the prime-movers in the system and the load occurs, it causes an instantaneous change in the kinetic energy of the rotors. The amount that each generator contributes is initially only a function of its electrical

location with respect to the origin of the variation, and subsequently proportional to the machine's inertia. If the power output of the prime-movers is not adjusted promptly in the opposite direction of the disturbance, the frequency of the entire system will go out of the safe operation range, triggering frequency-sensitive protections. In order to prevent this situation, the whole or part of the hierarchy of control loops shown in figure 2.10 is implemented.

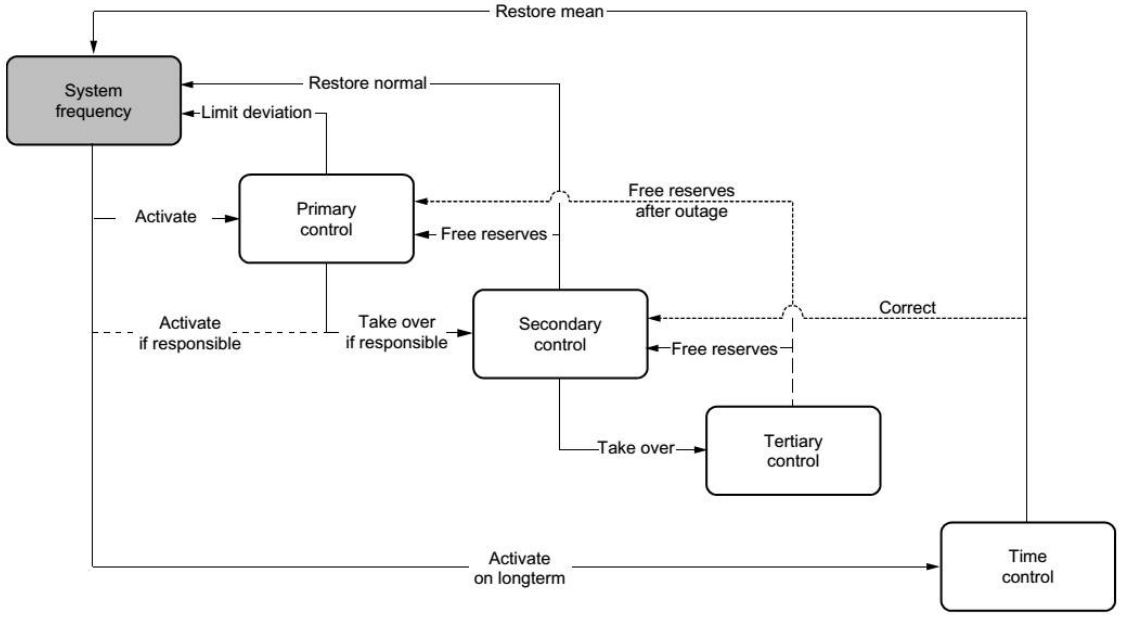

Figure 2.10: Functional definition of balancing services [3].

Primary frequency control can be implemented either exclusively through speed regulators or *governors* in the generators themselves, or also using in addition a frequency control signal from the system operator. For this first control loop to work, there needs to be enough operational margin in the machines present at the time of the imbalance and they need to be able to react fast enough so that the frequency doesn't drop out of the safety margins. It is the role of secondary reserve to bring frequency back to the nominal value and to correct the flows between control areas. In very large power system, this function is performed by the automatic generation control (AGC) routine. Tertiary control uses reserves that need to be activated manually in case of observed or expected sustained activation of secondary control to reestablish the secondary reserve levels [3] .

Voltage control In contrast to frequency, voltage control is a strongly local problem. At medium and high voltage, voltage deviations are mostly related to reactive power

imbalances and synchronous machines are the primary means to correct them. This function is done by the automatic voltage regulator (AVR), which acts over the excitation current that originates the permanent magnetic field, usually in the rotor. In lower voltage ($\tilde{0}.4$ kV) the high resistivity of the lines prevents reactive power control from being as effective as in higher voltage levels, being active power control or transformers with on-load tap changers (OLTCs) often more effective.

Economic operation The economic dispatch (ED) problem consists in allocating the total demand among generating units so that the production cost is minimized. Generating units have different production costs depending on the prime energy source used to produce electricity (mainly coal, oil, natural gas, uranium, and water stored in reservoirs). And these costs vary significantly [1]. The freedom to solve this, in principle simple, optimization problem, is restricted by several constraints. Evidently, the operation limits of the machines, their current state and their reaction speeds need to be taken into account, but also the capacity of the transmission lines that will make possible to deliver that power to the load. The dispatch is most strongly conditioned by the availability of units. For example, if the problem being solved is to be implemented in the next hour, all the machines that take more than one hour to start cannot be included. This conditioning comes from a previous analysis known as unit-commitment (UC), which calculates approximate setpoints for a period between one or two days and allows companies to plan starts and stops accordingly. The UC is also very relevant in systems that even without significant time constants in the generation units need to make time-coupled decisions about the utilization of limited storage resources like a BESS or a small water reservoir.

2.5 Electrochemical energy storage

As described in the previous sections, a characteristic of EPSs is the existence of spatial and temporal mismatches. One of the possibilities to deal with these is through the use of the storage devices commonly known as batteries, probably because of the French term *batterie d'accumulateurs*, which refers to a stack of devices capable of accumulating energy in chemical form. Although *Electrochemical Energy Accumulator* is probably the correct term to use from a formal point of view, in practical applications in power

systems the term "Battery Energy Storage Systems" or BESS is used to refer to a device comprising a stack of electrochemical accumulators plus a number of external components that allow the accumulator to be conveniently connected to an EPS and controlled. A BESS connected to an AC EPS includes at least the components shown in figure 2.11).

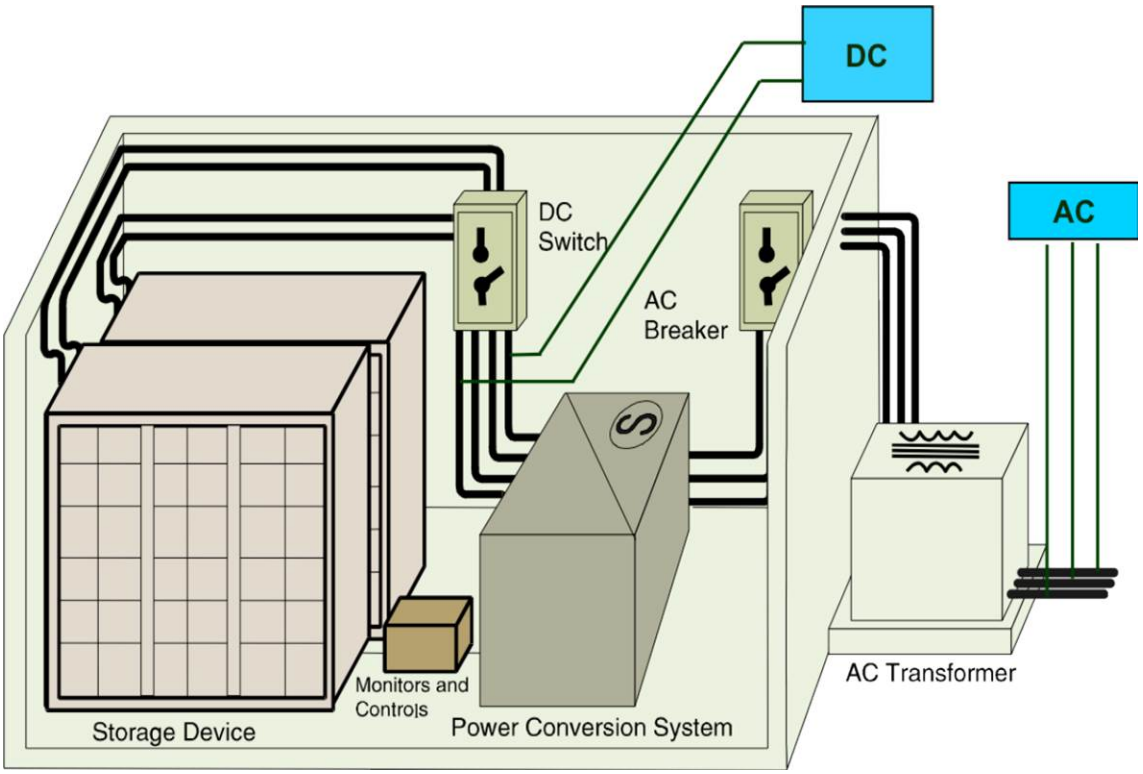

Figure 2.11: Referential configuration of a battery energy storage system [4]

Storage Devices correspond to individual electrochemical systems where the conversion between electrical and chemical energy occurs. They can be either open or closed thermodynamical systems.

Protections Most electrochemical storage devices are capable of high short-circuit current and can be permanently damaged or even explode or catch fire when operated outside of their safe range. To isolate the battery from the EPS, in the event of a fault outside the BESS, or from the PCS in the case of an internal fault, fast-acting breakers need to be installed. These are usually divided into *hard* and *soft* breakers. The first category involves a physical interruption of the circuit, while the second acts by changing the conductive properties of a semi-conductor.

Power conversion system (PCS) The reactions in electrochemical accumulators are vary sensitive to variations in the voltage of their terminals, and a direct connection to an AC power system would almost instantaneously set off the protections. To be able to control the flow of energy between the EPS and the accumulators, a power conditioning stage is needed. While a circuit that allows the charge of a cell from an AC power system can be built using passive components (diodes, capacitors and resistors), bi-directional flow necessarily requires the use of power electronics. An extensive description of this stage is given in Chapter 3.

Monitoring and control unit (MCU) Although the electrochemical cell is governed by electrochemical equations, a modern BESS is a digitally controlled device. The MCU takes care of responding to external functional requests and/or implementing pre-programmed behavior, while at the same time keeping the battery operation in the safe range. In Chapter 3 the MCU is described as a hierarchical control system that enables the BESS to interact with the EPS at a physical and financial level.

AC transformer and filters Depending on the difference between the nominal voltage of the battery stack and the EPS-side of the point of common coupling (PCC), and also on the nature of the PCS, a transformer is necessary to adapt the output voltage of the PCS. The transformer itself and additional passive components also contribute to reduce the harmonic content of the current and voltage waveforms originated at the PCS, which contain distortions from a pure sinusoid of different magnitude depending on the modulation technique and electronic topology used.

2.5.1 Electrochemical systems fundamentals

The first practical electrochemical system was the Volta pile, invented by Alexander Volta in 1800 [44]. It consisted on zinc (Zn) and silver (Ag) plates separated by paper soaked in salt water H_2O. When he connected both plates with a wire, electric current flowed through it. Electrochemical systems are characterized by the existence of chemical reactions that can be controlled through electrical variables, in particular the electric potential or voltage. The experimental setup illustrated in Figure 2.12 is used

to explain the phenomena of interest. The dominant discharge reactions in the positive and negative electrodes are shown in equations (2.19) and (2.20) respectively.

$$Ag_2O + H_2O + 2e^- \rightarrow 2Ag + 2OH^- \tag{2.19}$$

$$Zn + 2OH^- \rightarrow ZnO + H2O + 2e^- \tag{2.20}$$

Reaction (2.19), two electrons are absorbed from the external circuit to reduce a silver oxide molecule (Ag_2O) to silver ions. Conversely, reaction (2.20) involves the oxidation of zinc into zinc oxide, which releases two electrons to the external circuit.

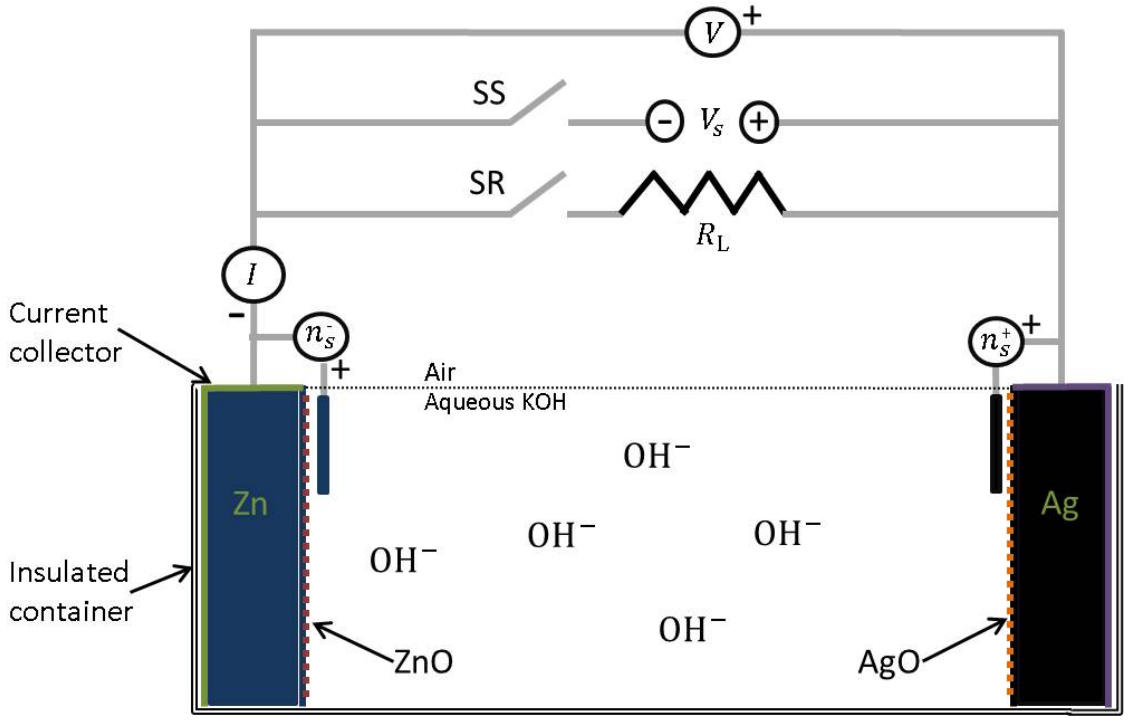

Figure 2.12: Experimental setup for the Silver - Zinc electrochemical reactor

Thermodynamics and potential Driving forces for reaction are determined by the thermodynamic properties of the electrodes and electrolyte. The open-circuit steady-state potential U, in Volts, can be calculated from the difference in the Gibbs free energy G of the two electrodes as:

$$U = \frac{\mathrm{F}}{\mathrm{n} \cdot \Delta G} \tag{2.21}$$

Where n is the number of electrons transferred per reaction and F is Faraday's constant. In general, ΔG is a function of the electrochemical potential of all the species participating in reactions on each electrode:

$$\Delta G = \left(\sum_i S_i \cdot \xi_i \right)_{positive} - \left(\sum_i S_i \cdot \xi_i \right)_{negative} \tag{2.22}$$

Where S_i is the stoichiometric coefficient of species i in the reaction. The sign of this coefficient is determined by the direction of the reaction in which electrons are released. For example, in the positive (Silver) electrode of the Silver-Zinc cell of figure $S_{Ag_2O} = -1$, $S_{H_2O} = -1$, $S_{Ag} = 2$ and $S_{OH^-} = 2$. The formal definition of ξ_i is related to the molality m_i and activity γ_i of the species as:

$$\xi_i = \xi_i^0 + \mathrm{R}T \ln (m_i \gamma_i) \tag{2.23}$$

The parameter γ_i is difficult to determine in practice, which is why the calculation of the open-circuit potential makes use of standard potential tables for different half-cell reactions through the Nernst equation.

$$U = \mathrm{U}_0 - \mathrm{R}T \ln (\Theta) \tag{2.24}$$

Where U_0 is the open-circuit steady-state potential when the concentration of reactants and products is 1M, the temperature is 298K, the pressure is 1atm, and Θ is the ratio of the current concentrations of reactants to products.

Electrode kinetics By closing SR, the electrons in the negative electrode are allowed to flow through the circuit towards the positive electrode. This will cause the appearance of surface overpotentials in both electrodes in accordance to the Butler-Volmer equation:

$$j = j_0 \left[\exp\left(\frac{\alpha_\mathrm{a} \mathrm{F}}{\mathrm{RT}} \nu_s \right) - \exp\left(-\frac{\alpha_\mathrm{c} \mathrm{F}}{\mathrm{RT}} \nu_s \right) \right] \tag{2.25}$$

Surface overpotentials can be experimentally estimated using high-impedance voltmeters connected to reference electrodes places very close to the active electrodes as shown in figure 2.12. The sign of the current will determine the direction of reactions 2.19 and 2.20. Note that for significant overpotentials, one of the exponential terms in 4.16 will dominate strongly. The term j_0 is called *exchange current density*, which depends on the concentration of reactants and products, temperature and the nature of the electrode-electrolyte interface. j_0 can take values from over 1mA/cm^2 down to less than 10^{-7}mA/cm^2. The parameters α_a and α_c, called *apparent transfer coefficients* are additional kinetic parameters that relate how an applied potential favors one direction of reaction over the other, usually taking values between 0.2 and 2.

Ionic transport In order for reactions to be sustained, species [4] need to be transported to the electrodes at a sufficiently high rate to replenish electrons, in other words, the flow of change in the electrolyte needs to match the output current in the steady-state. The total current density in the electrolyte is related to the flux of the different relevant species $\boldsymbol{\psi_i}$ and to the number of electrons transferred n_i by each species as:

$$i = \sum_i \text{n}_\text{i}\text{F}\boldsymbol{\psi_i}, \tag{2.26}$$

where $\boldsymbol{\psi_i}$ is the flux of species i in $mol/(cm^2 s)$. There are three mechanisms that drive these flows: 1) convection and stirring, 2) electrically-driven migration and 3) diffusion.

$$\boldsymbol{\psi_{i,mig}} = -n_i \cdot \mu_i \cdot \zeta_i \cdot \Delta\phi, \tag{2.27}$$

where, for each species, μ is the mobility, ϕ is the electric potential in the solution and ζ is the concentration.

Another driver of ionic motion is diffusion, a process that occurs in response to concentration gradients:

$$\boldsymbol{\psi_{i,diff}} = -\text{D}_\text{i} \cdot \Delta\zeta_i, \tag{2.28}$$

[4] In electrochemistry, species are chemical compounds that do not dissociate in the electrolyte. The main species of interest here are the ions that migrate through the electrolyte to transport electric charge.

Where D_i is the diffusion coefficient of species i. Similarly, for convection:

$$\boldsymbol{\psi_{i,conv}} = \zeta_i \cdot \boldsymbol{v}, \tag{2.29}$$

where $\boldsymbol{v}$ is the velocity of the bulk fluid.

Degradation Batteries are a perishable product and deteriorate as a result of the chemical action that proceeds during storage. The design, electrochemical system, temperature, and length of storage period are factors which affect the shelf life or charge retention of the battery. The type of discharge following the storage period will also influence the shelf life of the battery. Usually the percentage charge retention following storage (comparing performance after and before storage) will be lower the more stringent the discharge condition [45].

Manufacturers give users tables that relate the decrease of battery capacity versus the number of charge-discharge cycles for different depths of discharge (DOD) cycles, and sometimes also for different rates. In this way, battery cycle life is defined as the number of complete chargedischarge cycles a battery can perform before its nominal capacity falls below 80% of its initial rated capacity. Another fact is that batteries degrade even if they are not cycled, this is known as "ageing"; also, ambient temperature and vibrations are relevant. The problem with the way this information is presented is that it doesn't link to the underlaying degradation processes and it prevents researchers to infer how the battery will degrade under different operating conditions than the ones specified in the battery datasheet.

The concept of state of health (SOH) is a more comprehensive terminology used in recent literature to refer to a set of parameters that allow to define a distance to the end of life (EOL) of the device in a particular application. Besides the capacity at a given C rate, the SOH can be defined taking into account aspects like the failure probability or the cycle efficiency.

2.5.2 Types and characteristic equations

To give an idea of the diversity of electrochemical systems, the following list briefly describes a set of promising mature and emerging electrochemical storage technologies

and their characteristic reactions [4]:

Sodium (Na)/Sulfur(S) Sodium-sulfur (NaS) batteries are a commercial energy storage technology finding applications in electric utility distribution grid support, wind power integration, and high-value grid services. NaS battery technology holds potential for use in grid services because of its long discharge period (6h approx). It is also capable of prompt, precise response to such grid needs as mitigation of power quality events and response to AGC signals for area regulation. The main reactions that describe this battery are [45]:

Negative electrode	$2Na \leftrightharpoons 2Na^{+} + 2e^{-}$
Positive electrode	$xS + 2e^{-} \leftrightharpoons S_x^{-2}$
Overall reaction	$2Na + xS \leftrightharpoons Na_2S_x$

Sodium (Na)/Nickel-Chloride (NiCl) Sodium-nickel-chloride batteries are high-temperature battery devices like NaS, with the particularity that it uses a solid Beta-Alumina electrolyte and two liquid electrodes. Another relevant characteristic of this battery is that there are no side-reactions. The reactions that describe this battery chemistry are given in [46] and are described by:

Negative electrode	$NiCl_2 + 2Na^{+} + 2e^{-} \leftrightharpoons Ni + 2NaCl$
Positive electrode	$2Na \leftrightharpoons 2Na^{+} + 2e^{-}$
Overall reaction	$NiCl_2 + 2Na \leftrightharpoons Ni + NaCl$

Lead (Pb)-acid (H_2SO_4) battery In the category of medium to large sized batteries, this is the most commonly manufactured rechargeable battery. The negative electrode for this battery is a lead paste covered grid, and the positive electrode is the plate or grid which has lead dioxide [46]. The main reactions that describe this battery chemistry are given in [45] and described by:

Negative electrode	$Pb + HSO_4^{-} \leftrightharpoons PbSO_4 + H^{+} + 2e^{-}$
Positive electrode	$PbO_2 + 3H^{+}HSO_4^{-} + 2e^{-} \leftrightharpoons 2H_2O + PbSO_4$
Overall reaction	$PbO_2 + Pb + 2H_2SO_4 \leftrightharpoons 2PbSO_4 + 2H_2O$

Lithium-ion battery The electrochemistry for the LIB is not substantially different from other batteries. Graphite is the active material in the negative terminal

and the positive terminal is made of lithium metal oxide compounds, such as $LiCoO_2$ and $LiNiO_2$. The element lithium is highly reactive and can catch fire, or even explode, when it comes in contact with water. So, the electrolyte used in the LIB is a nonaqueous solution, such as a combination of lithium salt ($LiPF_6$) with organic solvents, namely ethylene carbonate-dimethyl carbonate (EC-DMC) [46]. The reactions that describe this battery chemistry are described in [45] and given by:

Negative electrode	$\mathrm{C + xLi^+ + xe^- \leftrightharpoons Li_xC}$
Positive electrode	$\mathrm{LiMO_2 \leftrightharpoons Li_{1-x}MO_2 + xLi^+ + xe^-}$
Overall reaction	$\mathrm{LiMO_2 + C \leftrightharpoons Li_xC + Li_{1-x}MO_2}$

Zinc-Air battery The electrochemical coupling of a reactive anode to an air electrode provides a battery with an inexhaustible cathode reactant and, in some cases, very high specific energy and energy density. The capacity limit of such systems is determined by the Ampere-hour capacity of the anode and the technique for handling and storage of the reaction product. As a result of this performance potential, a significant effort has gone into metal/air battery development. Zinc is attractive for electrically rechargeable metal/air systems because of its relative stability in alkaline electrolytes and also because it is the most active metal that can be electrodeposited from an aqueous electrolyte. The development of a practical rechargeable zinc/air battery with an extended cycle life would provide a promising high-capacity power source for many portable applications (computers, communications equipment) as well as, in larger sizes, for electric vehicles. Problems of dendrite formation, nonuniform zinc dissolution and deposition, limited solubility of the reaction product, and unsatisfactory air electrode performance have slowed progress toward the development of a commercial rechargeable battery. However, there is a continued search for a practical system because of the potential of the zinc/air battery. The main reactions that describe this battery chemistry are given in [45] and described by:

Negative electrode	$\mathrm{H2O + O_2 + 2e^- \leftrightharpoons 2OH^- + O}$
Positive electrode	$\mathrm{2OH^- + Zn^+ \leftrightharpoons Zn(OH)_2 + 2e^-}$
Overall reaction	$\mathrm{Zn + \frac{1}{2}O_2 \leftrightharpoons ZnO}$

Vanadium (V) redox flow battery This is another example of a battery that uses liquid electrodes and a solid electrolyte. The novelty is that in contrast with the

Sodium/Nickel-Chloride cell, the electrodes of the Vanadium redox battery are circulated through storage tanks outside the cell. The reactions that describe this battery chemistry

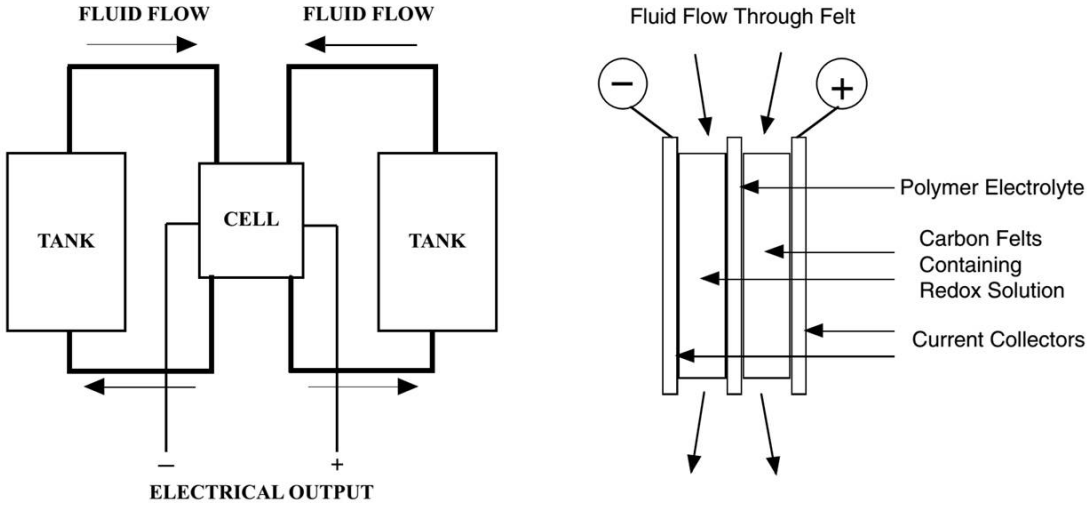

Figure 2.13: Arrangement of the elements of a flow battery (left) and the structure of the electrochemical energy conversion cell (right) [5].

are described in [47] and given by:

Negative electrode $\quad V^{2+} \leftrightharpoons V^{3+} + e^-$

Positive electrode $\quad VO_2^+ + 2H^+ + e^- \leftrightharpoons VO^{+2} + H_2O$

Magnesium(Mg)-Antimony(Sb) liquid metal battery (LMB) The particularity of this battery is that both electrodes and the electrolyte are liquid during the operation, which takes place at 700 ∘C. As shown in figure 2.14, During charging, the battery consumes energy to electrochemically extract Mg from the MgSb alloy electrode and deposited as liquid Mg on the top (negative) electrode. During discharging, the Mg electrode is consumed, and Mg is deposited into the MgSb liquid bottom (positive) electrode, supplying energy to the external circuit.

Negative electrode $\quad Mg \leftrightharpoons Mg^{2+} + 2e,$

Positive electrode $\quad Mg^{2+} + 2e \leftrightharpoons Mg_{Sb}$

2.6 Summary

This chapter has described the physical principles behind the structure and operation of the two energy systems that are the focus of this dissertation. On the one hand, electric power systems are a thermodynamically closed electromechanical system made mainly

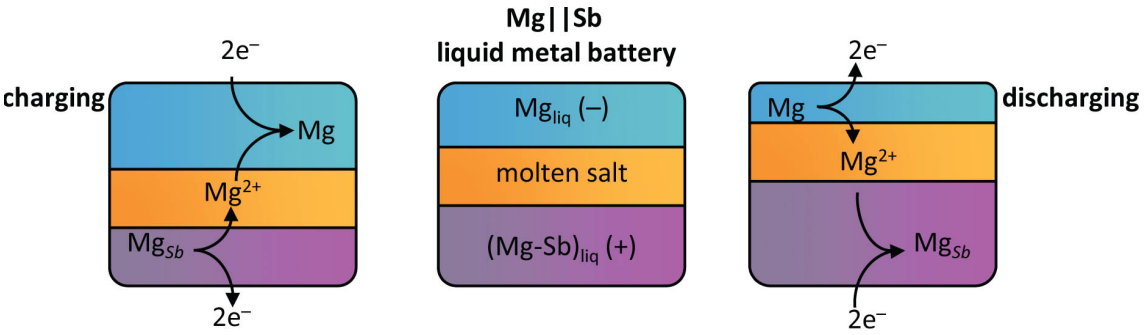

Figure 2.14: Schematic representation of the liquid metal battery [6].

of synchronous machines, lines, transformers and protections, which serve as a platform to transfer energy between devices that convert various primary energy resources into electric current and other devices that provide final energy services. On the other hand, electrochemical storage systems are thermodynamically open electrochemical systems that can convert between electric and chemical energy. With the aid of a proper electronic interface and control scheme, the resulting battery energy storage system can support the operation of electric power system in several ways. The basic equations presented in this section for electrochemical and electromechanical systems will serve as reference to build more complex models, often requiring justifiable simplifications.

Chapter 3

The state of the art

In one way or another, the ability to defer the use of energy has always been present in most energy systems. Firewood stocks, hot water bags and water towers are some timeless evidence of this fact. In electric power systems, until the mid-1980's energy storage was used to time-shift from coal off-peak to replace natural gas on-peak so that the coal units remained at their optimal output as system load varied, as well as to prevent the use of peaking units with high variable cost. These large pumped-hydro energy storage facilities stored excess electricity production during periods of low energy demand and price and discharged it during peak load times. This practice not only allowed the time-shifting of energy but also reduced the need for peaking capacity that would otherwise be provided by combustion turbines. Unfortunately, pumped-hydro units can only be installed in places with adequate geography, which are nowadays very scarce. By the mid-1980s, the push was stronger to develop battery and other storage technologies to provide services to the electric grid [4]. Although these technologies could not match the ability of pumped hydro to provide large storage capacities, there are several applications for which they are better suited, especially related to location-specific issues or to fast reaction times. In addition, the market pull for effective storage solutions for portable electronics since the turn of the century, and incipiently viable electric vehicles has propelled a variety of research and development (R&D) efforts worldwide to improve the performance and decrease the cost of devices capable of reversibly converting electric energy into other forms.

The complementary need to the situation described above is to develop analysis methods that can guide, in the direction of maximizing value creation:

1. The utilization of existing technologies;
2. The development of new technologies.

In order to prevent very time and money consuming trial and error processes, both aspects can greatly benefit from models that can reliably represent storage devices in simulation studies.

A variety of approaches are currently used to inform decisions related to planning and operation of EPSs. These are particularly complex for large systems, given the diversity and complexity of the technologies present, the number of actors and the big potential to realize saving. Since electrochemical storage is not a major contributor to the storage capacity of large EPSs, their representation in system-level models is coarse. However, the current prospect of a nested and distributed decision-making structure in EPSs has brought attention to the development of tools with reduced scope (targeted to an analysis subset of the larger EPS) which could benefit from a more accurate representation of individual components inside distributed energy systems (DES)[1].

Another case where a realistic representation of BESSs can be critical is in autonomous or semi-autonomous EPSs, also known as microgrids (μG). The former are being currently tested to provide high quality of service to remote locations, and often rely on a BESS as the solely responsible for load balancing and load-shifting. The latter coexist with large EPSs, to which they are connected through a single breaker known as point of common coupling (PCC). These grid-connected (μGs) can both increase the quality of supply behind the PCC and provide services to improve the operation of the larger EPS.

3.1 Overview

This chapter is mainly about existing models and approaches to represent mature electrochemical storage technologies in studies related to EPSs. The purpose of section

[1] A distributed energy system (DES) is an aggregation of distributed energy resources (DER). DERs include loads, generation, storage devices and aggregations of them.

3.2 shows the current state of deployment of energy storage in general and of electrochemical devices in particular, giving a more detailed description of the current state of development of Lithium-ion and Lead-acid batteries. Section 3.3 begins by defining the expected characteristics of models to represent electrochemical energy storage en EPS studies and reviews the most relevant proposals found in the literature. Finally, section 3.5 goes through the current practical and regulatory challenges relevant for the widespread utilization of energy storage in general.

3.2 Energy storage technologies

The number of energy forms that can be bi-directionally transformed in electricity is limited, and references [4, 48] do a very good job describing them in detail. The following table lists the storage media currently available for this purpose:

Principle	Embodiment
Electric field	Capacitors, super-capacitors, electric double-layer in batteries
Magnetic field	Inductors, super-conducting inductors
Mechanical - kinetic	Flywheels, generator rotors
Mechanical - potential	Pumped-hydro, compressed air
Thermal	Bi-directional heat pump
Chemical	Batteries and fuel-cells

3.2.1 Energy storage principles in power systems

Considering that the boundary that defines an EPS is located at the interface between prime-movers and generators, the only energy storage forms within them are electric fields, magnetic fields and the rotational kinetic mechanical energy in the rotors of generators and motors. Besides actual inductors and capacitors, the electric field is also present among conductors, and between them and the ground. Magnetic field exists around conductors and in the magnetic nuclei of transformers, generators and motors. Although the existence of this storage capacity explains the presence of reactive power and inrush currents during the energization of transformers and transmission lines, the volume of energy that can be stored in both fields is very small. Without the inertia of rotational machines (or other devices that emulate their behavior, as will be

explained in Chapter 4), the frequency of the system would change very fast under small perturbations, making it very difficult for speed regulators to react. Hence, the most relevant role of energy storage in power systems is to make the system stable. As it will be described below, in many cases it is necessary or convenient to complement the natural energy storage capacity of EPSs with devices whose main function is to absorb and release electric power in a controlled fashion, either to increase their stability or to improve their economic or environmental performance.

3.2.2 Technological landscape

Energy storage systems can be designed with a broad portfolio of technologies such as pumped hydro, compressed air energy storage (CAES), a large family of batteries, flywheels, capacitors and superconductive magnetic energy storage (SMES). Each technology has its own performance characteristics that makes it optimally suitable for certain grid services and less so for other grid applications. This ability of a storage system to match performance to different grid requirements also allows the same storage system to provide multiple services [24]. Table 3.1 is a qualitative visualization of the goodness of the match between seven currently deployed storage technologies and twelve services.

The U.S. Department of Energy (US-DOE) maintains an updated database of worldwide grid-connected storage sites [2]. The following discussion and figures are based on the analysis of that database, accessed in May 2014. As shown in Figure 3.1 pumped-hydro storage completely dominates the landscape, with 97.76% of the power and 96.28% of the energy of all currently operational sites, and therefore it is convenient to separate it from the other technologies in the analysis.

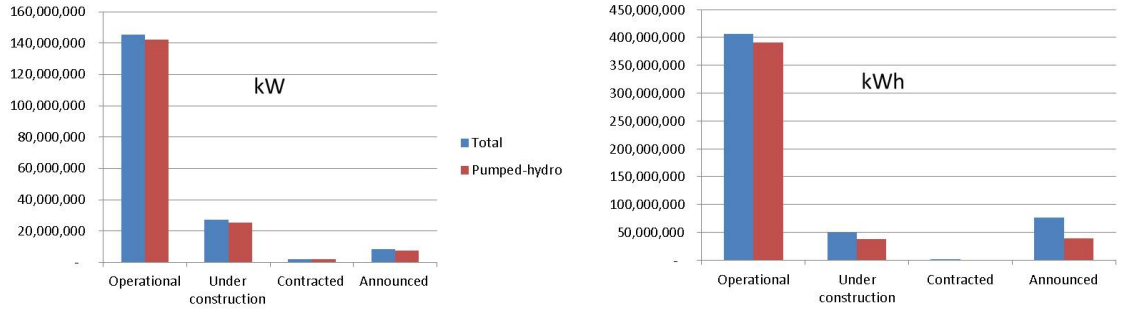

Figure 3.1: Worldwide energy storage power and energy

[2] http://www.energystorageexchange.org

Application	Description	CAES	Pumped Hydro	Flywheels	Lead-Acid	NaS	Li-ion	Flow Batteries
Off-to-on peak intermittent shifting and firming	Charge at the site of off peak renewable and/ or intermittent energy sources; discharge energy into the grid during on peak periods	◑	◑	○	●	●	●	●
On-peak intermittent energy smoothing and shaping	Charge/discharge seconds to minutes to smooth intermittent generation and/or charge/discharge minutes to hours to shape energy profile	○	◑	◑	●	●	●	●
Ancillary service provision	Provide ancillary service capacity in day ahead markets and respond to ISO signaling in real time	◑	◑	◑	◑	◑	◑	◑
Black start provision	Unit sits fully charged, discharging when black start capability is required	◑	◑	○	●	●	●	●
Transmission infrastructure	Use an energy storage device to defer upgrades in transmission	○	○	○	●	●	●	●
Distribution infrastructure	Use an energy storage device to defer upgrades in distribution	○	○	○	●	●	●	●
Transportable distribution-level outage mitigation	Use a transportable storage unit to provide supplemental power to end users during outages due to short term distribution overload situations	○	○	○	◑	●	●	●
Peak load shifting downstream of distribution system	Charge device during off peak downstream of the distribution system (below secondary transformer); discharge during 2-4 hour daily peek	○	○	○	●	●	●	●
Intermittent distributed generation integration	Charge/Discharge device to balance local energy use with generation. Sited between the distributed and generation and distribution grid to defer otherwise necessary distribution infrastructure upgrades	○	○	○	●	◑	◑	◑
End-user time-of-use rate optimization	Charge device when retail TOU prices are low and discharge when prices are high	◑	◑	○	◑	◑	◑	◑
Uninterruptible power supply	End user deploys energy storage to improve power quality and /or provide back up power during outages	○	○	◑	●	●	●	●
Micro grid formation	Energy storage is deployed in conjunction with local generation to separate from the grid, creating an islanded micro-grid	○	○	○	●	●	●	●

Definite suitability for application ● ; Possible use for application ◑ ; Unsuitable for application ○

Table 3.1: Suitability matrix for selected grid services and storage technologies extracted from the SANDIA-DOE report on energy storage [24]

By inspection of figures 3.2, 3.3 and 3.4, it is clear that although electrochemical storage is significantly larger in terms of number of projects for all time-frames, thermal storage and compressed air currently provide most of the bulk of non pumped-hydro storage

and will probably continue doing so. Note the very important contribution of flywheels to power and their negligible contribution to energy due to their low energy storage volume.

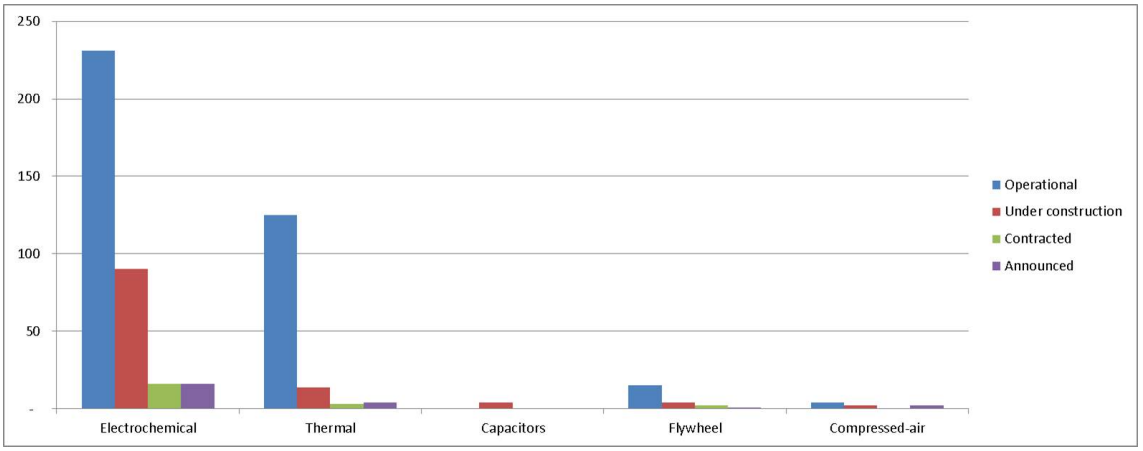

Figure 3.2: Worldwide energy storage sites excluding pumped-hydro

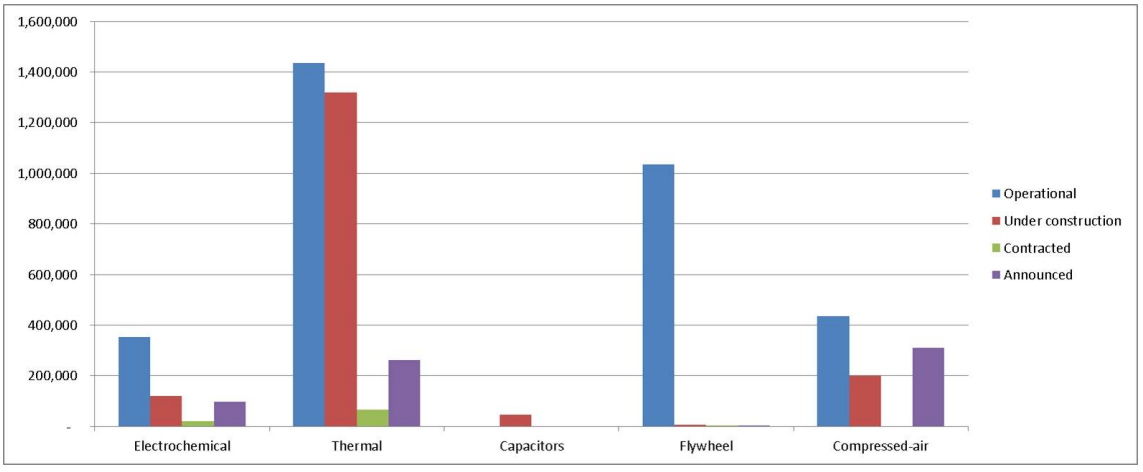

Figure 3.3: Worldwide storage capacity excluding pumped-hydro in kW

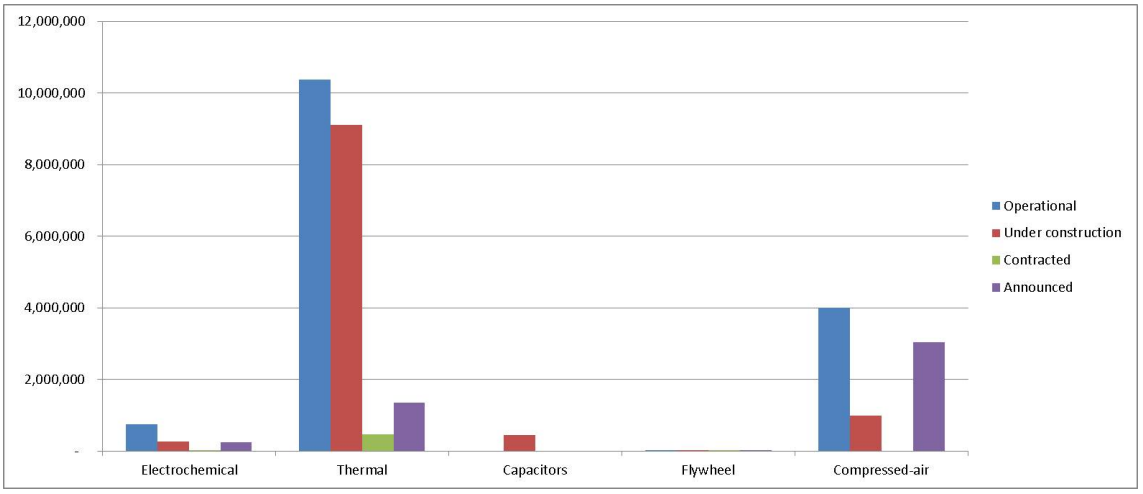

Figure 3.4: Worldwide energy storage energy excluding pumped-hydro in kWh

Figures 3.5, 3.6 and 3.7 decompose electrochemical storage into particular technologies, with Lithium-based, Lead-based and Sodium-Sulfur technologies as the clear forerunners. Interestingly, Lithium batteries take, by far, the largest share in terms of power, as does Sodium-Sulfur in terms of energy. Regardless of this last fact, the absence of projected Sodium-Sulfur sites is remarkable. It is reasonable to speculate an important contribution of a few -though very visible- safety failures of this technology a few years ago [3]. In contrast, Sodium-Nickel Chloride and both Zinc-based and Vanadium-based flow batteries are expected to increase their market share.

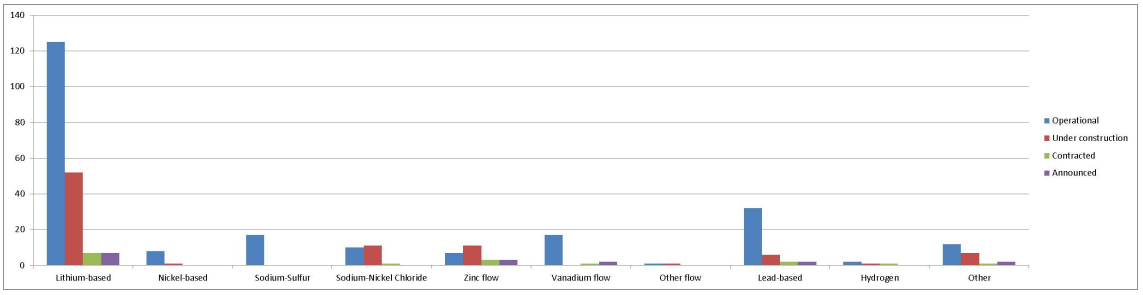

Figure 3.5: Worldwide installed electrochemical storage sites

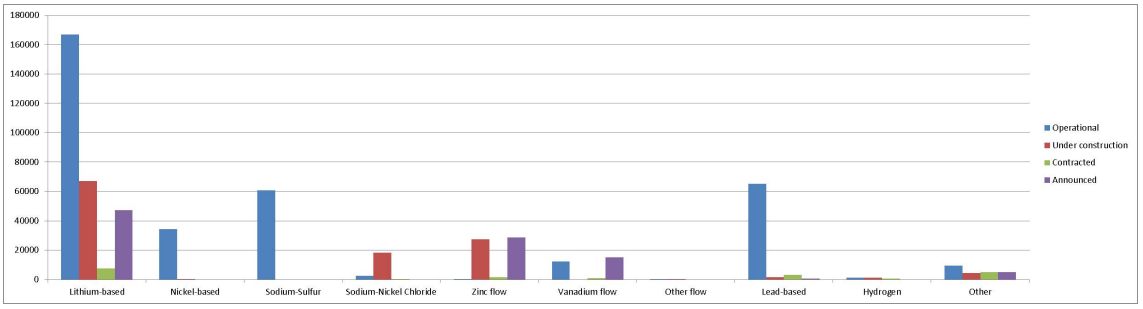

Figure 3.6: Worldwide electrochemical storage capacity in kW

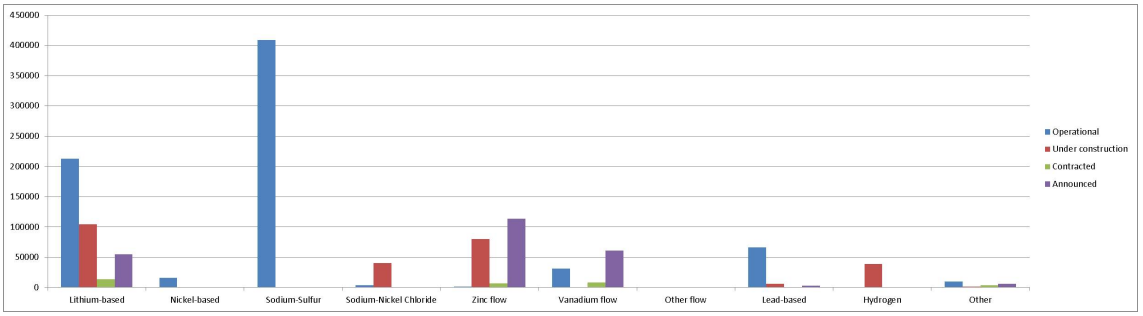

Figure 3.7: Worldwide electrochemical storage energy in kWh

Although most of the formulations developed in this document can be modified to represent most electrochemical storage technologies, the models will focus on the two most

[3] See for instance http://www.greentechmedia.com/articles/read/Exploding-Sodium-Sulfur-Batteries-From-NGK-Energy-Storage

mature and validated technologies available: Lithium-based and Lead-based. Although Lead-based batteries are expected to loose market share in grid-connected applications, their role in off-grid systems (rural electrification) and in single-home systems is very relevant, often being the only technology available. Each of these battery technologies can be further decomposed into a number of major chemical compositions.

3.2.2.1 Lithium-based batteries

Lithium-ion batteries (LIB) are comprised of cells that employ lithium intercalation compounds as the positive and negative materials. As a battery is cycled, lithium ions (Li^+) exchange between the positive and negative electrodes. They are also referred to as rocking-chair batteries as the lithium ions "rock" back and forth between the positive and negative electrodes as the cell is charged and discharged [45]. Graphite is the material of choice for the negative electrode in most present commercial lithium ion batteries, with the exception of the Lithium-Titanate cells. The positive electrode material can be either a metal oxide with a layered structure, such as lithium cobalt oxide ($LiCoO_2$), a material with a spinel structure, such as lithium manganese oxide ($LiMn_2O_4$) or with an olivine structure ($LiFePO_4$) [7] on a current collector of aluminum foil (see figure 3.8[4]). On top of these low-level structures, some manufacturers use proprietary nanotechnology and dopants to improve intercalation area, stability and kinetics [50]. In the charge/discharge process, Lithium ions are intercalated or extracted from interstitial space between atomic layers within the active materials. The term intercalation refers to a process whereby a guest molecule or ion is inserted into a host lattice. The structure of the guest host or intercalation compound is only slightly perturbed from the host structure and the reaction used to form the compound is either chemically or thermally reversible. Other terms such as insertion, inclusion, and topotactic reaction are also often used but fall under this general definition. Reactions involve adsorption of guest species on host crystals, exchange or insertion at the host surface, the formation of intermediate stages in layered compounds, and transport within the host lattice. Macroscopic effects such as variations in crystal size, dislocations, stacking faults, and pore mouth blockage can strongly influence the kinetics of intercalation [51].

[4]Where 3a, 3b and 8a follow Wyckoff's notation for positions in crystal latices [49]

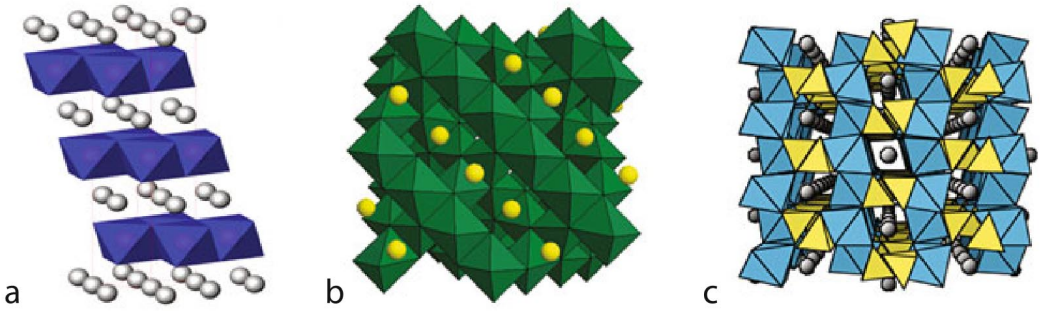

Figure 3.8: Structures of common cathode materials: (a) The layered structure of $LiCoO_2$ with c-axis oriented vertically. The octahedrally coordinated Li ions in 3a sites are represented as spheres and CoO_6 (Co in 3b sites) as octahedra; (b) the cubic structure of $LiMn_2O_4$ spinel, with tetrahedrally coordinated Li ions (in 8a sites) represented as spheres, and MnO_6(Mn in 16d sites) as octahedra; and (c) the olivine structure of $LiFePO_4$, looking down the b-axis. Octahedrally coordinated Li ions are represented as spheres, and FeO_6 and PO_4 as octahedra and tetrahedra, respectively [7]

The electrolyte for LIBs is a mixture of organic solvents and an electrolyte salt compound. The common solvents are a mixture of cyclic carbonate esters, such as ethylene carbonate and propylene carbonate, and linear carbonate esters, such as dimethyl carbonate and diethyl carbonate. The solution is completed with the addition of a salt compound such as $LiPF_6$ $LiBF_4$. Electrolyte solutions must enable the Li ions to transport freely, which requires both high dielectric constant and low viscosity. Cyclic carbonate esters have a high dielectric constant but high viscosity, while linear carbonate esters have low viscosity but low dielectric constant. Suitable electrolyte solutions are therefore obtained by mixing the two. Research on the electrolyte solution is generally focused on one of three areas: functional electrolyte additives, flame-resistant or nonflammable electrolyte solutions, and new electrolyte salts [52].

3.2.2.2 Lead-based batteries

The Lead-acid battery (LAB) is the most commonly manufactured rechargeable battery. The negative electrode for this battery is a lead paste covered grid, and the positive electrode is the plate or grid which has lead dioxide [46]. Typically, a charged positive electrode contains both $\alpha - PbO_2$ (orthorhombic) and $\alpha - PbO_2$(tetragonal). The α form has a larger, more compact crystal morphology which is less active electrochemically and slightly lower in capacity per unit weight; it does, however, promote longer cycle life. The electrolyte is a sulfuric acid solution, typically about 1.28 specific gravity or

37% acid by weight in a fully charged condition [45]. A recurrent issue with LABs is the evolution of hydrogen and oxygen through electrolysis. In vented cells, periodic water additions are necessary to maintain life. Lead alloys containing calcium were introduced to reduce water loss and ventilation requirements. Valve-regulated Lead-acid (VRLA) batteries have a one-way pressure relief valve that opens when the internal battery pressure increases to a specified valve design level between 1 and 30 psi. The valve closes when the internal battery pressure decreases. Some VRLA batteries have grids made of pure lead or pure lead with a little tin added. The design intent is to facilitate the recombination of the oxygen and hydrogen within the cell by re-forming the water during charge [7].

Two types of electrolyte systems are used to immobilize the liquid battery acid. The first design, which was developed in Germany, is called a "gel" battery because finely divided silica is added to "gel" or thicken the electrolyte. Gelling prevents the aqueous sulfuric acid from leaking or spilling if the battery is tipped. The other method, developed in the USA in about 1970, is absorbing a more highly concentrated acid in a porous glass mat (AGM). This reduces the water volume in each cell and makes the battery more sensitive to dry-out in hot environments. However, the AGM design has the advantage of higher discharge power compared to a gel battery design.

3.3 Electrochemical storage models

Battery modelling is a challenging field that has been receiving a great amount of interest recently due to two main commercial drives: the desire for longer-lasting portable electronic devices, and the great push for hybrid and battery electric vehicles by the automotive industry [53]. This section reviews different approaches to represent intercalation batteries in studies related to electric power systems (EPSs). As starting point, the following list of desirable properties of these representations is proposed:

3.3.1 Functional aspects

1. **Energy balance.** This is the minimum explanatory level for any model that represents a battery. If $e(t_1)$ and $e(t_2)$ are the energy content of the battery in two instants, and $p(t)$ is the power leaving the battery, then:

$$e(t_2) = e(t_1) - \int_{t_1}^{t_2} p(t)dt. \tag{3.1}$$

This equation alone is useful when the size of the battery is defined a-posteriori as:

$$max(e) - min(e) = e_{max}, \tag{3.2}$$

where the initial condition is arbitrary and the domain of the maximum and minimum functions is the total simulation time. In the alternative case, with a given e_{max}, equation (3.2) becomes

$$max(e) - min(e) \leq e_{max}. \tag{3.3}$$

2. **Charge and discharge power limits.** In a similar way, the rated power of the battery can be defined trivially a-posteriori as $p_{max} = max(p)$ and $p_{min} = min(p)$, where $p < 0$ indicates charging. For a given real battery, though, the power transfer limits change in time with respect to several state variables, notably:

   (a) State of charge (SOC): A value between 0 and 1 corresponding to an estimation of the amount of charge in a cell as a fraction of its rated ampere-hour capacity;

   (b) State of health (SOH); A value between 0 and 1 corresponding to the ampere-hour capacity of a cell as a fraction of its rated ampere-hour capacity;

   (c) Temperature;

   (d) Spatial ionic concentration distribution in the electrolyte.

   Power limits can be viewed in two ways. The first one is related to the actual physical limits of the battery to transfer charge in a sustained way and is mostly linked to the appearance of overpotentials that decrease the terminal voltage as the current increases. The second corresponds to the battery management system (BMS) perspective, which is in charge of assuring a safe operation (e.g., prevent premature failures, overheating or other dangerous situations), promoting a reasonable useful life and performance. These last two considerations are the most

important when defining either fixed or time varying power limits, and BMS developers are usually required to follow the recommendations of the manufacturer of the cells as part of their warranty requirements.

3. **Efficiency.** Each overpotential happening inside the cell which is linked to charge transfer is a cause of losses in the form of heat. All the factors that impact power limits also impact the magnitude of the overpotentials. For example, the charging efficiency of a cell is going to be smaller when it is close to full charge compared with a lower state of charge, and the opposite will happen with the discharge efficiency. Another energy loss mechanism are Faradic losses, which correspond to electrons participating in side reactions leading to the formation of compounds and to the generation of heat (e.g., Joule losses due to electronic conductivity in the electrolyte). Another factor that influences the amount of energy that can be retrieved from a charged battery is changes on its temperature. In practice, high-level systems designers are concerned with the average round trip efficiency for a given application, defined as

$$\bar{\eta} = \frac{\int_0^{\mathrm{T}} p_{out}(t)dt}{\int_0^{\mathrm{T}} p_{in}(t)dt} \tag{3.4}$$

where T is the assessment period and P_{out} , P_{in} are the power leaving and entering the battery, respectively;

4. **Current-Voltage relationship.** From the electrochemical point of view, electric power and energy are abstractions with no direct correlate in the internal state of the cell, which is defined in terms of concentrations, potentials and charges. These properties give rise and govern the relationship between the instantaneous measurable quantities voltage and current. This relationship changes over time and with respect to the utilization profile, and it is very relevant when designing components that will be connected to the battery. For example, the terminal voltage of a LIB can easily fluctuate between 2V and 4V, which means doubling the current for a fixed power. Since power electronics and protections are mainly current-limited, wider fluctuations in terminal voltage increase their cost;

5. **Rate of change limits** Transport phenomena in the electrolyte limit the speed at which the cell can react to a change in the load. This is seen as a voltage dip

after a current step. Although in most energy-related applications this limit is never reached, it is not the case for inertial response and power quality services.

6. **Temperature.** There's a two-way interaction between the chemistry and the thermal behavior of electrochemical cells. On one hand, all the reactions and properties of the battery show some degree of temperature dependency. On the other hand, temperature is affected by both the environment and by the heat produced by the reactions inside the cell. LIBs are particularly prone to the phenomenon known as *thermal runaway*, which refers to a process which is accelerated by increased temperature, in turn releasing energy that further increases temperature. This is for example the case of internal short-circuits [52];

7. **Degradation.** Applications concerned with the long-term behavior and economics of batteries require some means to represent the fact that in most chemistries the parameters of the cell will change over time due to the existence of secondary chemical reactions. One part of this, called "ageing", is usually related to changes not related to the operation of the battery, while the rest of degradation mechanisms are strongly influenced by it.

3.3.2 Non-functional aspects

In addition to their explanatory power, when comparing between models to represent cells in a given application it is also important to take into consideration the following:

1. **Computational burden** This is particularly relevant in models to support the operation of BESSs, and makes impractical approaches that rely on a very granular physical representation of the battery. For example, the method of finite elements, commonly used to simulate the temperature and potential distribution in structures, relies on a discrete solution of the laws of physics for a large number of physical domains. Even for design purposes, the solution involving time-domain models that include fast chemical dynamics, represented through non-linear partial differential equations, requires computationally-intensive numerical methods.

2. **Parameters estimation** The complex structure of real cells, added to the existence of proprietary information about them, prevents a theoretical calculation of the parameters of the model. Hence, the availability of procedures to extract

these from measurements is paramount. Jointly, the model's structure and the parameters estimation technique can be evaluated in terms of two related aspects: a) experimental requirements and b) extrapolative performance. It is commonly found that the more parameters a model contains, the more experimental requirements for a target ability to extrapolate behavior. Two extreme cases are ab-initio and black-box models. In the first one, there are no parameters to fit and the behavior of the cell can be predicted theoretically without error under the assumption of perfectly known boundary conditions. In the second type, both the structure of the model and its parameters are derived from experimental tests, the extrapolation capacity of the model is in general uncertain, and therefore extensive tests are required in order to be able to predict behavior by interpolation of results. A larger number of parameters also makes more difficult to keep track of their slow changes during the lifetime of the cell[5]. Accurate estimation of the battery electrical parameters allows testing battery cells with different real mission profiles by simulation. Consequently, the experimental efforts are diminished, which leads to reduced costs and testing time [54];

3. **State estimation** Operational decisions can benefit from non-measurable information about the internal state of the battery. The most relevant of these is the SOC because of its usefulness when predicting the runtime of the battery. Also important for this is to know the current value of variables that explain the internal losses. Obviously, the initial requirement for this is that the model individualizes those variables. The long-term operational performance can also benefit from models that can estimate the value of variables linked to side-reactions related to ageing[6].

3.3.3 Review of existing modelling approaches

It is important to stress, in accordance with sections 3.3.1 and 3.3.2, that accuracy is not the most important characteristic of a model to represent an electrochemical cell in a given application. Indeed, while supporting the development of better batteries can

[5]For example, if the determination of the SOH requires one day of testing, it would be impractical to do the procedure more than a few times a year.

[6]Take for example the case of a model which could predict the overpotential of an electrolysis reaction in Lead-acid cells. A battery management system with access to this information would then be able to constrain the operation of the BESS to avoid excessive water loss in order to decrease maintenance requirements and the probability of a failure.

greatly benefit from the representation of local phenomena such as the ionic current or temperature spatial distributions, these would make little sense in a study aimed at determining the optimal storage size on a microgrid. A survey of the literature revealed three groups of models, which will be described in this section: electrochemical, analytical and equivalent circuits. Circuits and electrochemical modelling are the most frequent choice for automotive applications [53] since they enable accurate predictions of the dynamic response of the cell and the estimation of non-measurable state variables such as the SOC and the SOH. Mathematical models, mostly too abstract to embody any practical meaning but still useful to system designers, adopt empirical equations or mathematical methods [15].

The following discussion starts with the most exact models electrochemical models that are still computationally tractable in some power systems studies, followed by a discussion of analytical models that express important emergent properties of the former in a simplified mathematical form. Finally, some examples of equivalent circuits are given and explained, when possible, in relation to the electrochemical models.

3.3.3.1 Electrochemical Models

Electrochemical models (ECM) are mainly used to optimize battery cell design and to identify processes that limit battery cell performance, being able to describe the mass, energy, and momentum transport of each species for each phase and component of the cell. The advantage of electrochemical models is their ability to predict, with high accuracy, both macroscopic quantities (e.g., cell voltage and current) and microscopic quantities (e.g., local distribution of concentration, potential, current, and temperature inside the cell)[54]. Since ECMs inherently capture the relationships between measurable quantities and the internal state of the battery [55],they provide a sharp understanding of the specific physical and chemical phenomena occurring during battery utilizations [56].

Typically, an electrochemical model ends up as a system of coupled partial differential equations that has to be solved in time for all the spatial dimensions that are needed. Consequently, since many parameters have to be determined. The solution of these systems requires complicated numerical algorithms, and battery specific information that are difficult to obtain [54]. In this section, the focus will be to review approaches

aimed mainly at Lithium-ion batteries. However, most of the formulations also apply to the Lead-acid battery.

The mathematical 1-D model of the lithium-ion battery was introduced by Doyle et al. [57, 58], and it was recently improved by Smith and Wang by experimental validation [59], and by thermal modeling in [20]. Figure 3.9 shows the referential 1-D physical representation of the cell [8], which comprises three domains, corresponding to the two electrodes and the separator, and two substrates, namely the electrolyte (liquid) and the electrodes (solid). The electrodes are represented by connected arrangements of spherical particles of radius R_s made of the active material (e.g., Lithium carbonate for the negative electrode and Lithium-metal oxide for the positive electrode).

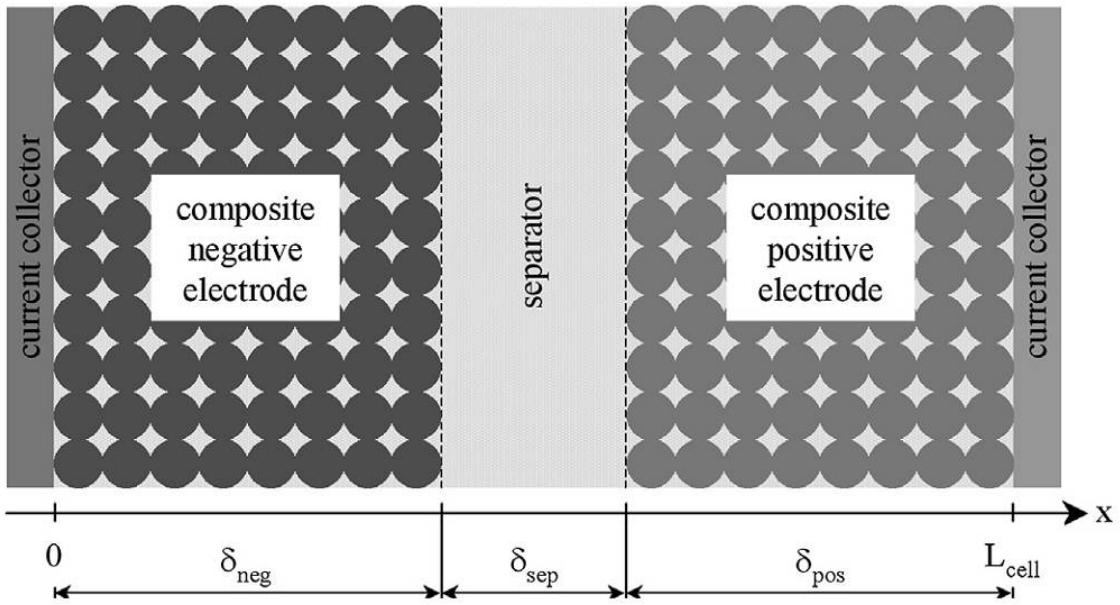

Figure 3.9: Physical representation of a electrochemical cell used for the electrochemical model in [8].

Table 3.2 shows the main equations for the four unknowns: The ionic concentration $\zeta_e(x,t)$ of Lithium ions in the electrolyte, the Lithium concentration in the spherical particles $\zeta_s(r,t)$, the electric potential in the electrolyte $\phi_e(x,t)$ and in the solid particles $\phi_s(r,t)$. These relationships are explained in more detail in section 4.3.3.

Recently, Legrand et. al. [9] showed that the previously described model leads to a physical error when the double layer capacitance is included that, under certain conditions, could translate (they studied the effect through simulations) in several tens of mV in the predicted cell voltage. It is argued that describing electric double-layer phenomenon is necessary for system applications, for which short-time effects are essential.

Unknown	Partial differential equations	Boundary conditions
c_s	$\begin{cases} \varphi_s(r) = -D_s \cdot \frac{\partial c_s(r)}{\partial r} \\ \frac{\partial c_s(r)}{\partial t} = \frac{1}{r^2} \cdot \frac{\partial}{\partial r}\left(D_s \cdot r^2 \cdot \frac{\partial c_s(r)}{\partial r}\right) \end{cases}$	$\begin{cases} \varphi_s(0) = 0 \\ \varphi_s(R_s) = \frac{j^{Li}(x)}{a_s \cdot F} \end{cases}$
ϕ_s	$\begin{cases} J_s(x) = -\sigma_{s,eff} \cdot \frac{\partial \phi_s(x)}{\partial x} \\ \frac{\partial J_s(x)}{\partial x} = -j^{Li}(x) \end{cases}$	$\begin{cases} J_s(0) = I_{cell}/A_{cell} \\ J_s(\delta_{neg}) = 0 \\ J_s(L_{cell} - \delta_{pos}) = 0 \\ J_s(L_{cell}) = I_{cell}/A_{cell} \end{cases}$
c_e	$\varepsilon_e \cdot \frac{\partial c_e(x)}{\partial t} = \frac{\partial}{\partial x}\left(D_{e,eff} \cdot \frac{\partial c_e(x)}{\partial x}\right) + (1 - t_p) \cdot \frac{j^{Li}(x)}{F}$	$\begin{cases} \frac{\partial c_e}{\partial x}(0) = 0 \\ \frac{\partial c_e}{\partial x}(L_{cell}) = 0 \end{cases}$
ϕ_e	$\begin{cases} J_e(x) = -\sigma_{e,eff}(x) \cdot \frac{\partial \phi_e(x)}{\partial x} - \sigma_{De,eff}(x) \cdot \frac{\partial \ln(c_e(x))}{\partial x} \\ \frac{\partial J_e(x)}{\partial x} = j^{Li}(x) \end{cases}$	$\begin{cases} \frac{\partial \phi_e}{\partial x}(0) = 0 \\ \frac{\partial \phi_e}{\partial x}(L_{cell}) = 0 \end{cases}$

Table 3.2: Electrochemical equations of the Lithium-ion cell [9].

As a matter of fact, in many applications e.g., uninterruptible power supplies, or board networks in transportation, batteries are often connected to power electronic converters as a link or energy buffer to other sources e.g., industrial grid, fuel cells, photovoltaic generators, wind turbines, or to variable loads e.g., electrical motors. For safety reasons, these converters usually include very fast current controllers, with a response time constant to a step perturbation lower than 10 ms. Therefore, accurate knowledge of the battery resistive and capacitive behavior at high frequency i.e., above a few hundred Hz is required to calculate with accuracy regulator parameters and stability margins of the system. Moreover, power electronic converters generate battery current ripples at switching frequency, so that RMS and mean currents may significantly differ from each other, especially at low mean current level [9].

The mathematical model for the electric double layer is formulated in [60], considering that in a rigorous manner, the current density j_s at the electrolyte/solid active material interface has faradaic j^{Li} and non-faradaic j^{DL} current contributions. The second one is related to the transient change in charge state of the double layer capacitance, and is expressed in $\mathrm{A} \cdot \mathrm{m}^{-3}$ as:

$$j^{DL}(x) = \mathrm{a_s} \cdot \mathrm{C_{DL}} \cdot \frac{\partial(\phi_s(x) - \phi_e(x))}{\partial t}, \tag{3.5}$$

where C_{DL} is the surface double layer capacitance ($F \cdot m^{-2}$) exhibited at the electrolyte/-solid active material interface and a_s is the specific area by volume in $\frac{m^2}{m^3}$. In the positive and negative electrodes, charge conservation equations including the double layer contribution can be established, as shown schematically in figure 3.10.

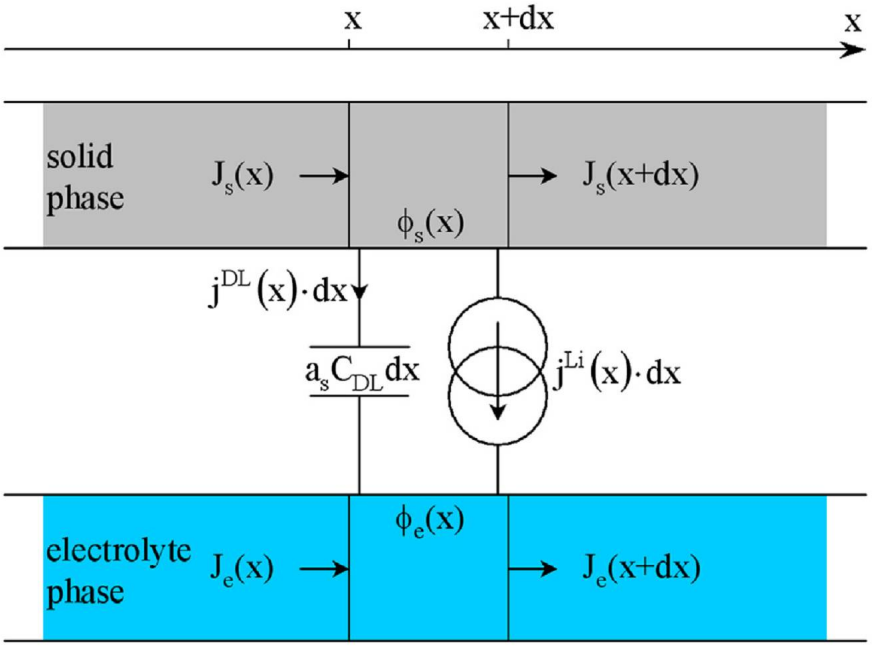

Figure 3.10: Schematic representation of local charge conservation in both electrodes, including the double layer current contribution [9].

This leads to:

$$\begin{aligned} j_s(x) &= j(s)(x + \mathrm{d}x) + j^{Li}(x) \cdot \mathrm{d}x + j^{DL}(x) \cdot \mathrm{d}x \\ j(s)(x + \mathrm{d}x) &= j_e(x) + j^{Li}(x) \cdot \mathrm{d}x + j^{DL}(x) \cdot \mathrm{d}x. \end{aligned} \tag{3.6}$$

The model described above (including the addition of the double-layer capacitance) constitutes the state of the art in terms of a tractable electrochemical formulation to describe short-term charge-discharge dynamics [7] Long-term effects are more complex to model, in part because of the lack of consensus about their underlying mechanisms. Numerous capacity fading mechanisms of lithium ion battery have been proposed, including electrolyte decomposition, active material degradation, surface film formation,

[7] In the model described in chapters 4 and 5 we have neglected this effect since the application examples did not require a very detailed representation of transient battery behavior

overcharging, self-discharging, and phase change. It is believed that the irreversible capacity loss during the first few charge-discharge cycles is primarily due to the formation of a passivating film on the negative electrode surface. This so-called solid electrolyte interphase layer (SEI) is formed at the first time when the electrode enters in contact with the solvent. It can isolate the negative electrode from the electrolyte solvent and minimize further reduction reactions of electrolyte components, through which the lithium ions are transported by vacancies and interstitials to reach the active electrode. Typically, the SEI consists of two distinct layers: an inorganic layer and an organic layer. The inorganic layer is a compact layer. It is close to the electrode and is several nanometers thick. The organic layer is a porous layer and on the electrolyte side, which is usually on the order of hundred nanometers thick. The SEI formation can act as a barrier to prevent the electrolyte solvent co-intercalation, but the excessive SEI formation may lead to undesirable lithium ions consumption and active electrode area reduction, which finally causes irreversible capacity fading [61]. Reference [61] proposes a detailed multiphysics model through which the relationship between SEI growth and charging/discharging rate, operation temperature and electrolyte salt concentration were studied. Alternative formulations can be found in references [62–64].

3.3.3.2 Mathematical Models

Mathematical models are developed based on empirical equations or stochastic approaches and are able to predict the battery capacity, efficiency, and runtime. However, usually these models are too abstract to comprehend any practical meaning and provide less-accurate results [54] than ECMs or equivalent circuits. The most basic mathematical model is the energy accumulator. If $e(t_1)$ and $e(t_2)$ are the energy contents of the battery in two instants, and $p(t)$ is the power leaving the battery, then:

$$e(t_2) = e(t_1) - \int_{t_1}^{t_2} e(t)dt. \tag{3.7}$$

Considering the formulations presented in section 3.3.3.1, the energy accumulator neglects the energy losses because of overpotentials, transport dynamics and electrode kinetics. This representation is useful for back of the envelope calculations like prefeasibility or market studies [65], producing an optimistic estimate of the performance of the device. The most commonly found formulation adds constant efficiency, energy

and power limits. In discrete form:

$$e(t_2) = \begin{cases} e(t_1) - \frac{p(t_1)}{\eta}, & \text{if } p(t-1) \geq 0 \\ e(t_1) - \eta p(t_1), & \text{if } p(t-1) < 0 \end{cases}, \tag{3.8}$$

with the constraints:

$$\begin{aligned} e_{min} \leq e(t) \leq e_{max} \\ p_{min} \leq p(t) \leq p_{max} \end{aligned} \tag{3.9}$$

This formulation is widely used in studies with a relatively large time step (several minutes to a few hours) to do battery sizing or scheduling [66, 67], including the distributed energy resources customer adoption model (DER-CAM) [68]. It is possible to enhance the capabilities of this formulation considering the power limits [69] and the efficiency [70] as variables that depend on the stored energy as a functions of $e(t)$, which approximates the dependency of overpotentials and kinetics with the concentration of species as expressed by the Nernst and Butler-Volmer equations.

Analytical approaches to battery life have also been proposed. The Miner's Rule method of evaluating battery aging was first introduced by Facinelli in 1983, who observed that cycling damage to a battery is primarily a function of the depth of discharge (and corresponding recharge) to which the battery is subjected. The magnitude of the cycle was found to be more important than the average depth of discharge during the cycle. Thus the effect, for example, of going from 10% to 30% discharge and back was seen to be approximately the same as from going from 50%to 70% and back. Facinelli's Miner's Rule method was originally developed for discrete, non-overlapping cycles, that might typically be found in photovoltaic based battery charging systems. These would be subject to approximately one cycle per day. When batteries are subjected to more irregular cycling, Facinelli's Miner's Rule approach cannot be applied directly. Such irregular cycling has been found to occur in modeling of wind/diesel systems. For example, a relatively long, deep cycle might be interrupted by shorter, shallower cycles. To deal with such irregular, overlapping cycles a cycle counting method was developed in [71]. The cycle counting method used is known as "rainflow" counting. It is typically

used in metal fatigue estimates. The damage to batteries due to cycling is modeled primarily as a function of depth of charge/discharge cycles. Battery lifetime prediction is then based on empirical curves that relate number of cycles to battery failure as a function of the magnitude of the cycles. This relationship is approximated with a double exponential curve fit:

$$\eth_f = \mathrm{k}_1 + \mathrm{k}_2 \exp(\mathrm{k}_3 \cdot \vartheta)\mathrm{k}_4 \cdot \exp(\mathrm{k}_5 \cdot \vartheta), \tag{3.10}$$

where $\eth_f$ is the number of cycles to failure the cycles to failure, $\mathrm{k_i}$ are fitting constants and ϑ is the range of the cycle (fractional depth of discharge). An alternative analytical model to represent the evolution of the state of health is proposed in [72]:

$$\begin{aligned} SOH(t = -\infty) &= 1 \\ SOH(t) &= \int_{-\infty}^{t} \mathrm{k_T} + \mathrm{k_{wz}} \mathrm{d}t \\ \eta_T &= \alpha_\mathrm{T} \left| T - \mathrm{T_{ref}} \right| + \beta_\mathrm{T} \end{aligned} \tag{3.11}$$

where α_T and β_T are temperature fitting factors and k_{wz} is a working-zone factor, taken from tables of experimental results, that changes its value with respect to the temperature and the SOC. The advantage of this model over (3.10) is that it doesn't require the concept of cycle.

Another important improvement to analytic models was the incorporation of a representation of the battery kinetics with the discrete KiBaM model proposed by Manwell and McGowan, which is used in the popular software HOMER [11], which is actually a first-order approximation [10] of the later simplified diffusion model proposed by Rakhmatov and Vrudhula [73]. As explained in section 2.5.1, the relationship between the terminal voltage drop and the current is related to the presence of overpotentials. In particular, the electrode surface overpotential is related to the concentration of species through the parameter i_0 in the Butler-Volmer equation (4.16). The reaction in the electrode reduces

the concentration, giving rise to the restoration mechanisms described in the same section. The aim of both models is to represent the fact that, because of the limited rate of ionic transport processes, not all the charge in the battery is available at a given time.

The Rakhmatov-Vrudhula (RV) model represents all the ionic transport mechanisms through a one-dimensional diffusion model for symmetrical electrodes. The evolution of the concentration C in time and space is described by Fick's laws:

$$\begin{aligned} -j(x,t) &= \mathrm{D}\frac{\partial \psi(x,t)}{\partial x} \\ \frac{\partial \psi(x,t)}{\partial t} &= \mathrm{D}\frac{\partial^2 \psi(x,t)}{\partial x^2}, \end{aligned} \tag{3.12}$$

where ψ is the molar flow in the x direction in $\frac{\mathrm{mol}}{\mathrm{m^2 s}}$ and D is a diffusion coefficient. The assumption of symmetric electrodes allows to model only one of them, with the flux at the electrode surface being proportional to the current and the flow in the other extreme of the diffusion region of width w equal to zero; formally:

$$\begin{aligned} D\frac{\partial \psi(x,t)}{\partial x}|_{x=0} &= \frac{i(t)}{v\mathrm{F}\cdot \mathrm{a}} \\ D\frac{\partial \psi(x,t)}{\partial x}|_{x=w} &= \frac{i(t)}{v\mathrm{F}\cdot \mathrm{a}} \end{aligned} \tag{3.13}$$

Solving using Laplace transforms yields an expression for the apparent charge lost $\varrho(t)$

$$\varrho(t) = \int_0^t i(\tau)d\tau + \int_0^t i(\tau)\left(2\sum_{m=1}^{\infty} e^{-\beta^2 m^2 (t-\tau)}\right)d\tau, \tag{3.14}$$

where $\beta = \pi\sqrt{D}/w$. The battery is completely discharged when the apparent charge lost is equal to the battery capacity. Note that the term $(t-\tau)$ in the negative exponential of equation (3.14) has the effect of discounting past values of the current. Hence, the second term on the right-hand side of the equation vanishes when the current stops for a long time. The advantages of this model are that it can represent well the available charge of batteries, and that it links them to actual physical parameters of the cell. The

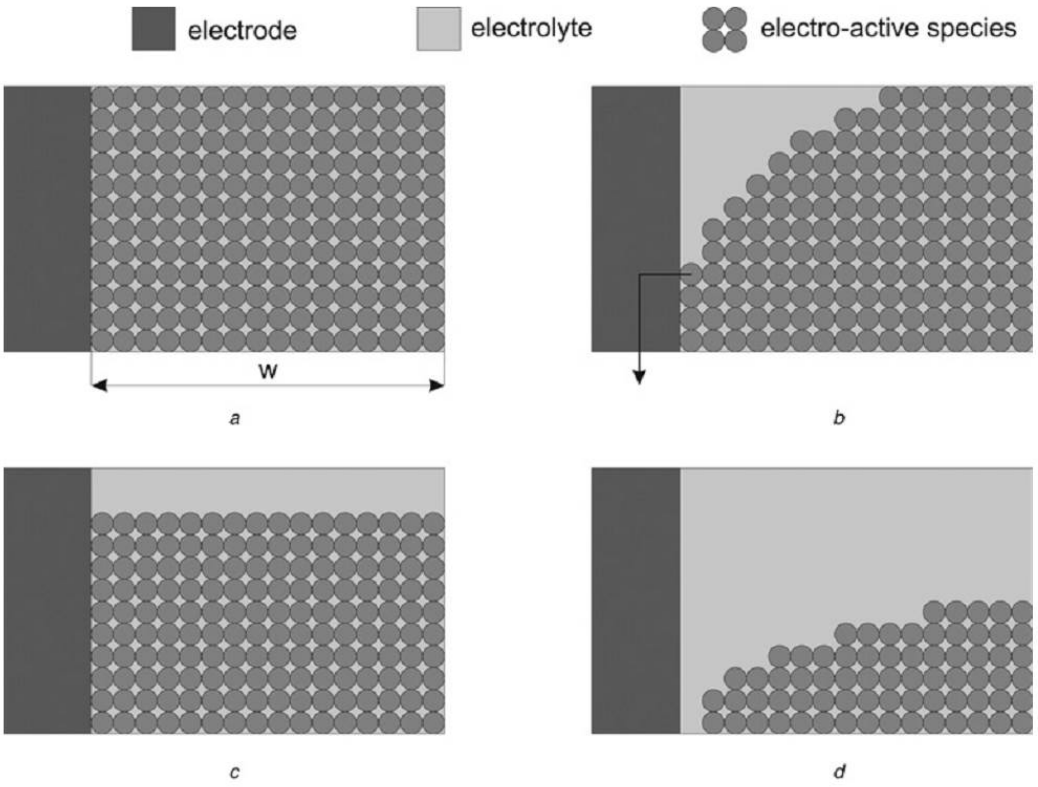

Figure 3.11: Physical picture of the model by Rakhmatov and Vrudhula [10]

main disadvantage is that equation (3.14) doesn't lend itself to be solved analytically for an arbitrary current profile.

The KiBaM model is grounded on the same principles but uses a very simplified representation of the underlying physics. Nevertheless, the results obtained are very close to the RV model when predicting the runtime of batteries. Instead of using a continuous diffusion model, the KiBaM model abstracts the concepts of available and total charge through the equivalent two-well model of figure 3.12.

Let C be the total battery capacity in Wh and y_1, y_2 the amount of energy on each well and consider a linear valve between the wells that lets charge flow in proportion to the height difference as shown in figure 3.12, then:

$$\begin{aligned} \frac{\mathrm{d}y_1}{\mathrm{d}t} &= -i(t) + k(h_2 - h_1) \\ \frac{\mathrm{d}y_2}{\mathrm{d}t} &= -k(h_2 - h_1) \end{aligned} \tag{3.15}$$

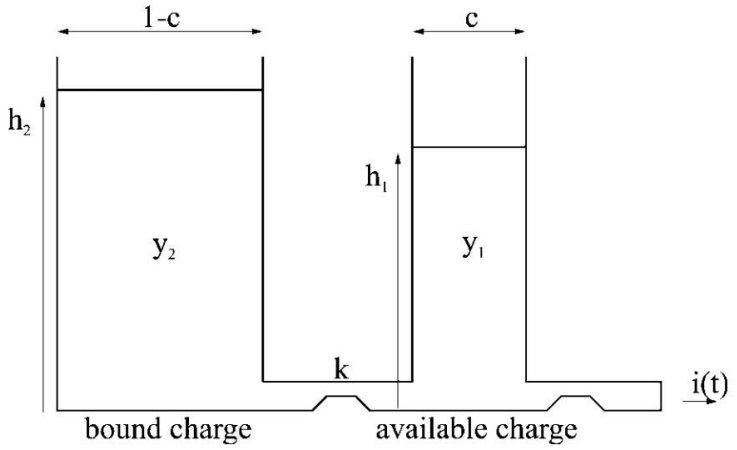

Figure 3.12: Two-well model of the KiBaM [11]

The initial conditions are $y_1(0) = c \cdot C$ and $y_2(0) = (1-c) \cdot C$. Making $\delta = h_2 - h_1$, $\gamma = y_1 + y_2$ and $k' = k/(c(1-c)$, the equations (3.12) are decoupled and the solution for constant discharge current is given by [10]:

$$\begin{aligned} \gamma(t) &= C - I \cdot t \\ \delta(t) &= \frac{I}{c}\frac{1 - e^{-k't}}{k'} \end{aligned} \tag{3.16}$$

which shows similar properties as equation (3.14). Finally, a Laplace-domain representation of the power response of a BESS under droop control for small signal stability studies is used in [74] using a first order lag:

$$\frac{\Delta P_{BESS}}{\Delta f} = \frac{k_{BESS}}{1 + sT_{BESS}}, \tag{3.17}$$

where k_{BESS} is the droop gain and T_{BESS} is the reaction time constant of the BESS.

3.3.3.3 Electrical Models

Electrical models are electrical equivalent circuits that use combinations of voltage sources, capacitors, and resistors and can offer good information about the performance of batteries. The I-V relationships that these provide are a fundamental requirement for

models that include the electrical representation of external components with a relative high accuracy (1% to 5% error [15]) in I-V relationships, while having a relative low modeling complexity. Although some of these models intend to map their parameters into electrochemical phenomena, they are usually estimated through curve-fitting without taking the reactions explicitly into account, why they have very limited extrapolation capacity to other material combinations or cell designs.

Although in some recent studies the battery is still represented by a constant-voltage source [75, 76], the simplest circuit model with a variable I-V relationship computes the terminal voltage using a fixed internal resistance R and a fixed internal potential U, and is given by:

$$V(t) = \mathrm{U} - \mathrm{R} \cdot I(t), \tag{3.18}$$

which is equivalent to neglecting the charge-voltage relationship given by the Nernst equation and the non-linear transport and reaction overpotentials that cause the terminal voltage drops. The formulation keeps track of the SOC with respect to a nominal capacity $\mathrm{C_n}$ through Coulomb-counting, which consists in integrating the current I that enters the positive terminal of the battery:

$$SOC(t) = SOC(t_0) + \frac{1}{\mathrm{C_n}} \int_{t_0}^{t} \cdot I(\tau)(d)\tau, \tag{3.19}$$

which neglects faradic losses and hence suffers from drift in practical applications, being accurate only for short durations, or when the battery is frequently recharged to a known SOC [53]. However, for systems simulations Coulomb-counting is acceptable. Another limitation of this model is that it doesn't capture the dynamic response of the battery, which is limited by transport and kinetics. The Thévenin representation in figure 3.13 was introduced in early representations of BESSs for dynamic studies [12], and is still widely used to study stability [77–79]. The parameters ($\mathrm{R_1}, \mathrm{C_1}$ and ($\mathrm{R_2}, \mathrm{C_2}$ can be assimilated to the diffusion in the electrolyte and solid phases, $\mathrm{L_T}$ to the mass movement in the electrolyte and $\mathrm{R_T}$ to the resistance of the electrodes.

Several modifications to the Thévenin equivalent circuit have been proposed which introduce more reactive components, time-varying (typically as a function of the SOC),

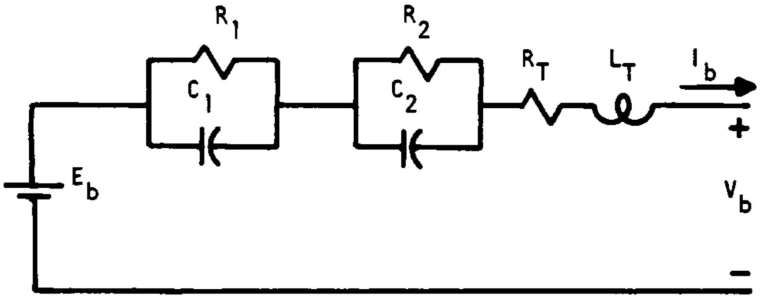

Figure 3.13: Thévenin equivalent circuit with two R-C networks [12].

mode-dependent (charge or discharge) parameters and/or shunt branches to account for parasitic losses [13, 14, 80, 81]. For example, $R_{dis}(SOC)$ and $R_{ch}(SOC)$ in figure 3.14a account for the direction-dependent relationship between the terminal voltage and the current implicit in the Butler-Volmer equation with regards to the concentration of species in the electrodes, and in figure 3.14b a shunt branch is added to account for faradic losses.

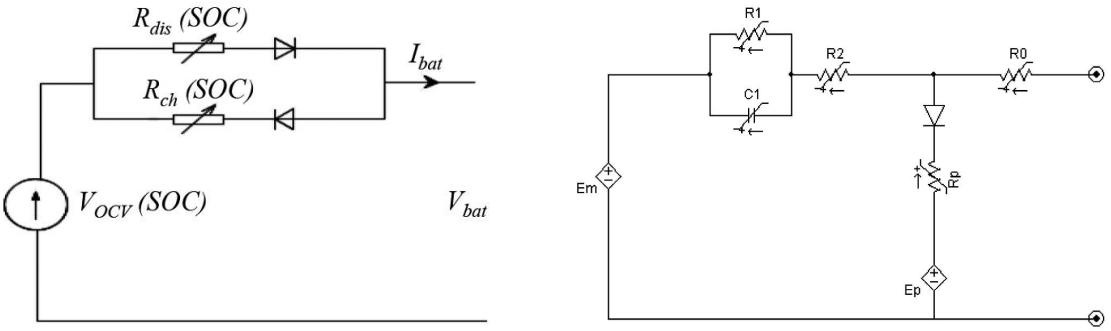

(a) **(b)**

Figure 3.14: Variations of the Thévenin equivalent circuit: a) direction-sensitive parameters [13]; b) time-varying parameters and shunt branch [14].

More recently, the model in figure 3.15 has been intensively[8]used for discharge modeling. The circuit decouples the short-term dynamics of the current-voltage parameters, represented by the R-C network on the right-hand side of figure 3.15, from the slower evolution of the state of charge, represented as the charge in $C_{capacity}$ in the left-hand side of the same figure. Longer terms effects are represented by an analytical relationship for the value of the charge storage capacity of the charge-storing capacitor in Coulombs as [15]:

[8]According to http://scholar.google.com the article had 625 citations by May 2014.

$$C_{capacity} = 3600 \cdot \text{capacity} \cdot \text{f}_1(cycles) \cdot \text{f}_2(temperature), \tag{3.20}$$

where capacity is the nominal Ah rating of the cell and f_1, f_2 are functions that can be obtained from experimental data through curve-fitting

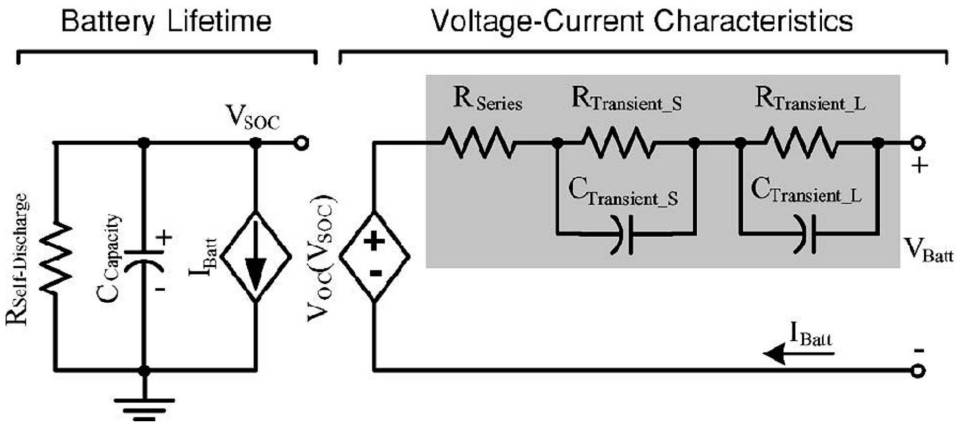

Figure 3.15: Equivalent-circuit model proposed in [15].

One of the main drawbacks of equivalent circuit models is their inability to model correctly the open-circuit voltage. A simplified version of Nernst's equation is proposed in [82]:

$$V_{oc} = \text{V}_{\text{nom}} + \text{k} \cdot \frac{\text{R}}{\text{F}} \cdot T \cdot \ln\left(\frac{SOC}{\text{C}_{\text{nom}} - SOC}\right), \tag{3.21}$$

where the SOC is expressed in Ah, V_{nom} is the nominal voltage, k a sensitivity parameter of V_{oc} to the SOC, R is the gas constant, F is the Faraday constant, T is the battery temperature and C_{nom} is the nominal battery Coulomb capacity in Ah. However, this model is unable to capture the nonlinear capacity behaviors, such as the rate capacity effect and recovery effect, of the battery due to the use of a constant capacitance to represent the remaining usable capacity of the battery. This reduces the model accuracy when predicting the battery performance at various load current conditions [16]. To overcome this, [16] proposed an hybridization with the KiBaM model, which is described in figure 3.16.

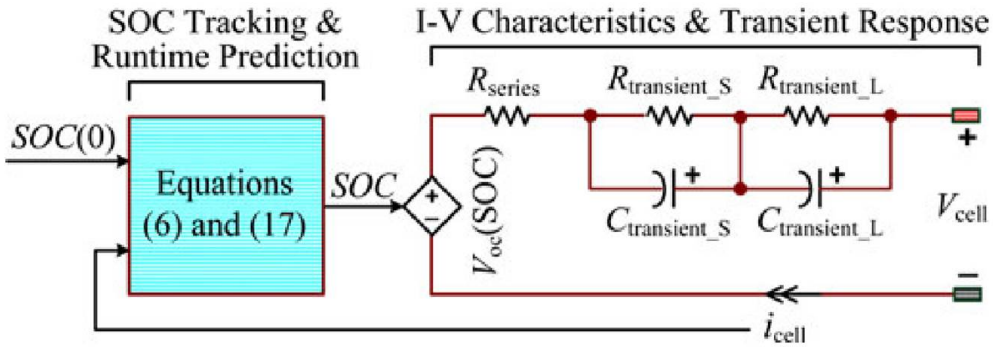

$$\mathrm{SOC}(t) = \mathrm{SOC}_{\mathrm{initial}} - \frac{1}{C_{\max}}\left[\int i_{\mathrm{cell}}(t)dt + C_{\mathrm{unavaiable}}(t)\right] \quad (6)$$

$$C_{\mathrm{unavailable}}(t) = \begin{cases} C_{\mathrm{unavailable}}(t_0)e^{-k'\cdot(t-t_0)} + (1-c)\dfrac{I}{c}\cdot\dfrac{1-e^{-k'\cdot(t-t_0)}}{k'}, & t_0 < t < t_d \\ C_{\mathrm{unavailable}}(t_d)e^{-k'\cdot(t-t_d)}, & t_d < t < t_r \end{cases} \quad (17)$$

Figure 3.16: Hybrid model proposed in [16].

3.4 Applications

This section describes examples of real applications an of proposals found in the literature.

3.4.1 Existing applications

The database of worldwide energy storage applications maintained by the United State's Department of Energy[9] was used, which includes information about the functions in which each site is participating as summarized in figure 3.17. A brief description of an example of each application is given below.

Transmission congestion relief: Orkney storage park The project aims at demonstrating power supply stabilization in the region by introducing a container-housed large capacity energy storage system using lithium-ion rechargeable batteries, with a power output/input capability of 2MW. The energy storage system will be installed at SHEPD's Kirkwall Power Station. In the cases of power shortage or power surplus on the Orkney Islands, power is transmitted from/to the mainland through two 33kV

[9] http://www.energystorageexchange.org

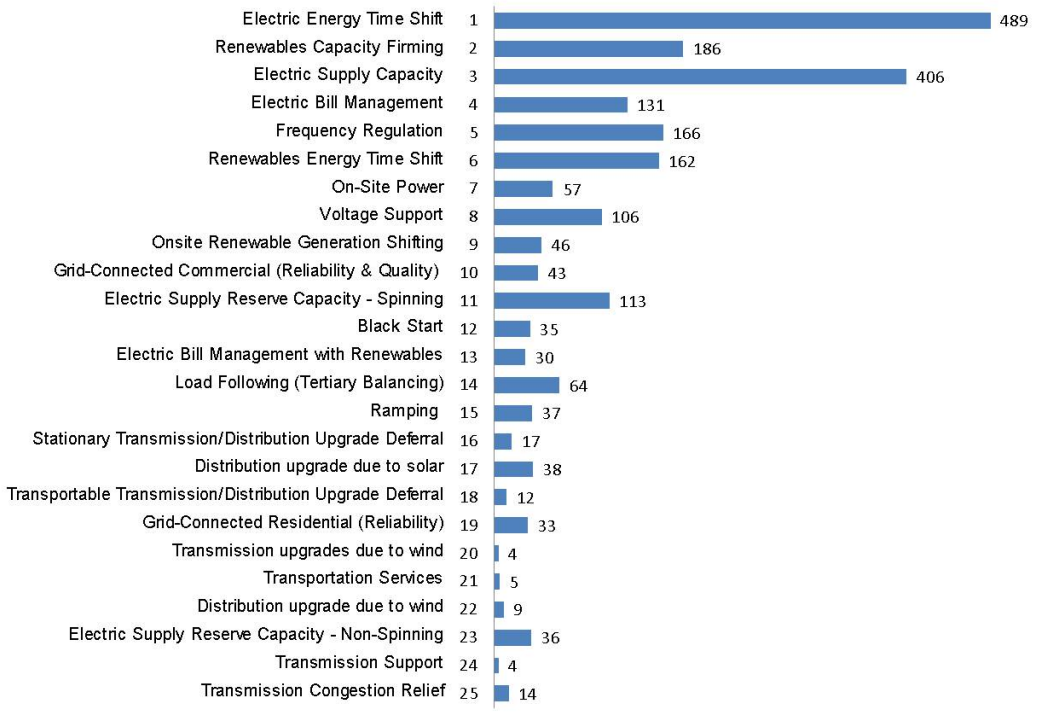

Figure 3.17: Count of battery applications for the 890 energy storage systems in the DOE database. One ESS can participate in more than one application simultaneously.

submarine cables. When there is too much renewable energy, exceeding the export capacity of the cable to the mainland, the energy storage system will import part of the excess energy, reducing the need to constrain renewable generation on the islands.

Transmission support: Smart city Malaga There is a block of power storage modules connected in MV to the network as backup. This project aims to prove the benefits of power storage in the daily performance of the network[10].

Electric supply reserve capacity- Non-spinning: Kaua'i Island Utility Cooperative The KIUC dynamic power resource (DPR) is designed to mitigate the variability of a 3 MW solar PV project for the Kauai Island Utility Cooperative, as well as provide critical grid support services for the island grid. The DPR will provide responsive reserves to the island utility and correct any frequency and voltage deviations.

[10]See http://www.endesa.com/es/conoceendesa/lineasnegocio/principalesproyectos/Malaga_SmartCity.

Distribution upgrade due to wind: Clear Creek Flywheel Wind Farm Project Temporal Powers flywheel energy storage (FES) technology is currently being deployed by Hydro One Networks Inc. to provide renewable energy integration support in Ontario, Canada. This 10-flywheel 5MW installation will provide local power quality support, by balancing real and reactive power flows from a 20MW wind farm [11].

Transportation services: INGRID Hydrogen Demonstration Project The project aims to balance the power grid by making it possible to store surplus electricity and use it to provide additional energy as required, to supply the hydrogen market by delivering green solid hydrogen storage to customers, and to test mobility by providing the electricity generated from hydrogen to the electric vehicle charging station [12].

Transmission upgrades due to wind: MAREX The flexible diversion of wind power into storage ensures maximum utility for the wind farms and permits over 2000 MW of wind to be connected to market using only 1500 MW of transmission cable [13].

Grid-Connected Residential (Reliability): Detroit Edison community energy storage (CES) The CES is designed to improve electricity service to customers whose circuits are often heavily loaded and would benefit from the power conditioning advantages provided from a CES [14].

Transportable Transmission/Distribution Upgrade Deferral: Churubusco NaS Battery Energy Storage System The units buy the utility time to decide whether to redesign a substation, build generation, or keep the storage units in place permanently. (All of the NaS systems are capable of being relocated for an estimated $85,000 to $115,000 if and when the companys needs for storage change)[15].

[11] See http://temporalpower.com/what-we-do/applications/grid-balancing/.
[12] See http://www.ingridproject.eu/.
[13] See http://www.organicpower.ie/pdf/glinsk/OP_Brochure_Marex.pdf.
[14] See http://energy.gov/sites/prod/files/DTE.pdf.
[15] See https://www.aepohio.com/save/efforts/SuperBatteries.aspx.

Distribution upgrade due to solar: Sacramento Municipal Utility District In this project there are 2 Cabinets of Sodium-Nickel Chloride batteries (620V 23,5kWh), which enable EV charging, PV smoothing, and load shifting [16].

Stationary Transmission/Distribution Upgrade Deferral: Ausgrid RedFlow has supplied 40 energy storage systems for the SGSC Project, that have been grid-feeding since early 2012. Each system contains a RedFlow 5kW/10kWh zinc-bromide battery, resulting in a total 200kW and 400kWh of storage. The demonstration project gathers information about the benefits and costs of different smart grid technologies in an Australian setting [17].

Ramping: Auwahi Wind Farm This 11MW, 4.4MWh lithium ion battery system was provided by A123 Systems and performs wind ramp management for a 21MW wind farm located on the island of Maui [18].

Load Following (Tertiary Balancing): Catalina Island Energy Storage The island has daily load variations from approximately 2 MW in the very early morning to approximately 5 MW in the late afternoon.In response to diesel engine emission reviews, the utility installed a 1 MW battery system to help stabilize the generation fluctuations.

Electric Bill Management with Renewables: Santa Rita Jail 2MW / 12 MWh Lithium Iron Phosphate Battery for the reduction of peak power and integration of renewables in the largest CERTS-based microgrid in the United States [19].

Black Start: Kraftwerk Huntorf 1st commercial CAES plant, operational since 1978. The 321-MW plant utilizes nuclear-sourced night-time power for compression and produces peak power during the day via a natural gas turbine. One cavern is cycled on a diurnal basis. The second cavern serves as a black start asset if the nearby nuclear power plant unexpectedly goes down.

[16] See https://www.smud.org/en/index.htm
[17] See http://www.smartgridsmartcity.com.au/.
[18] See http://www.neces.com/smart-grid-storage.htm?mform=redirect.
[19] See http://www.acgov.org/government/news/smartgrid.htm.

Electric Supply Reserve Capacity - Spinning: Metlakatla BESS Metlakatla Power and Light (MP&L)installation consisting of VRLA cells, providing rapid spinning reserve, frequency control, and better power quality. Beginning operation in 1997, the BESS has a 1 MW peak power output, and 1.4 MWh energy capacity. Nearly 5 MW of hydroelectric generation capacity provides almost all of MP&Ls power, with a 3.3 MW diesel generation system relegated to reserve duty. MP&Ls two hydroelectric plants, Purple Lake and Chester Lake, have reservoir storage capacity, though the hydro generators were too slow to respond to sudden load fluctuations. At the time of the BESSs initial operations, the MP&L peak load was approximately 4 MW. A lumber mill in Metlakatla (since closed down) caused large, sudden power spikes on the communitys islanded power system, and the BESS was installed to provide fast response for the mills rapid load changes [20].

Grid-Connected Commercial (Reliability & Quality): Gills Onion's Prudent Energy's Vanadium-redox flow batter provides peak-shaving and demand charge avoidance services to reduce Gills Onions' monthly electric utility bill[21].

On-site Renewable Generation Shifting:OptiGrid Burlington This OptiGrid system is a 1 MW installation which is used by an industrial manufacturer to offset curtailment from the local utility[22].

Voltage Support: Marble Bar Power Store Flywheel Project PowerStore acts like a STATCOM, and in addition is capable of rapidly absorbing or injecting real power within an isolated power network. It can stabilize both voltage and frequency, hold 18 MWs (megawatt seconds) of energy and shift from full absorption to full injection in 1 millisecond to stabilize the grid [23].

On-Site Power: SkyGrid Energy Off-grid 100kW wind powered commercial scale water pumping system utilizing a grid forming 100kW 4-quadrant 3-phase inverter,

[20] See http://www.irena.org/documentdownloads/events/VanuatuJuly2012/7_Srinivas_Bharadwaj.pdf.
[21] See http://www.pdenergy.com/pdfs/GillsOnions-PrudentEnergy-WhitePaper-July2012.pdf
[22] See http://www.energystorageexchange.org/projects/174
[23] See http://www.horizonpower.com.au/marble_bar_nullagine_power_stations.html

100kW lithium titanate battery bank, variable frequency drive and PCL based supervisory controls to operate a 50hp submersible pump. This completely off-grid system is capable of producing over 30 million gallons of water per year. Can also utilize solar as a source of renewable energy [24].

Renewables Energy Time Shift: Minera El Tesoro CSP Plant The 10.5 MW_{th} concentrated solar power plant in the Atacama Desert incorporates thermal energy storage that allows the delivery of thermal energy for up to 6.5 hours at rated power after the sun goes down[25].

Frequency Regulation: Angamos The 20 MW lithium-ion energy storage installation provides critical contingency services to maintain the stability of the electric grid in Northern Chile, an important mining area. It is designed to operate for 15 minutes at full power, allowing the system operator to resolve the event or bring other standby units online [26].

Electric Bill Management: Southern California Edison - HVAC Optimization Program with energy storage The Ice Bears[27] from Ice Energy redistribute thermal energy use to off-peak hours when rates are much lower, thereby increasing efficiency and reducing costs. Customers include a chain of diners (24 kW), a high-tech manufacturing plant (30 kW), two wineries (127 kW) and a Southern California Public Power Authority (SCPPA) project (38 kW).

Electric Supply Capacity: BC Hydro Energy Storage 1MW NAS battery installed 50km along 25kV feeder from Golden, BC substation close to Field, BC. Battery system is able to operate islanded from the grid in order to provide back-up power to Field in the event of a feeder outage and is also set up to discharge over the peak hours from 4pm to 8pm every day and recharge over night[28].

[24] See http://skygridenergy.com

[25] See http://www.abengoasolar.com/web/en/nuestras_plantas/plantas_para_terceros/chile/index.html

[26] See http://energystorage.org/energy-storage/case-studies/bringing-stability-grid-aes-energy-storage-

[27] See http://www.ice-energy.com/technology/

[28] https://www.bchydro.com/energy-in-bc/projects/field-battery.html.

Renewables Capacity Firming: Kaheawa Wind Power Park On the island of Maui, a 10-MW/45 minute Xtreme Power advanced lead-acid system is being integrated with the 21-MW Kaheawa Wind Power II project, built by First Wind, to provide utility-scale power storage and management [29].

Electric Energy Time Shift: Bath County Pumped Storage Station This project consists of a 3GW Pumped Hydro storage plant in Virginia that pumps water to an elevated reservoir at night and lets it run back down to generate electricity during the day[30].

3.4.2 Empirical affinity of application stacking

As shown in figure 3.18, it is most common that these applications do not occur in isolation, because some functions do not prevent the execution of others from a technical point of view, and the participation in many can give access to additional revenue streams with the proper market rules. Figure 3.19 lists pair-wise information about simultaneity in terms of occurrences and figure 3.19 does it in terms of a relative frequency $f_{i,j}$, which is calculated as:

$$f_{i,j} = \frac{n_{i,j}}{n_i + n_j}, \tag{3.22}$$

where n_i , n_j are the number of sites in the database that provide service i and service j respectively, and $n_{i,j}$ is the number of those that simultaneously provide services i and j.

One could speculate that the numbers in figure 3.20 relate to the probability of finding a given pair of applications simultaneously, and that the quantity $d_{i,j} = 1 - f_{i,j}$ reveals a metric on a hypothetical "application space". This metric can be used to identify groups of "compatible" services with the aid of graph visualization algorithms like the Kamada-Kawai force-directed one [83], which is used here used to produce figure 3.21.

Although this is by no means a rigourous map, insightful affinity relationships between applications can be inferred. For example, the most distant applications in the map are

[29] http://www.xtremepower.com.
[30] https://www.dom.com/about/stations/hydro/bath-county-pumped-storage-station.jsp

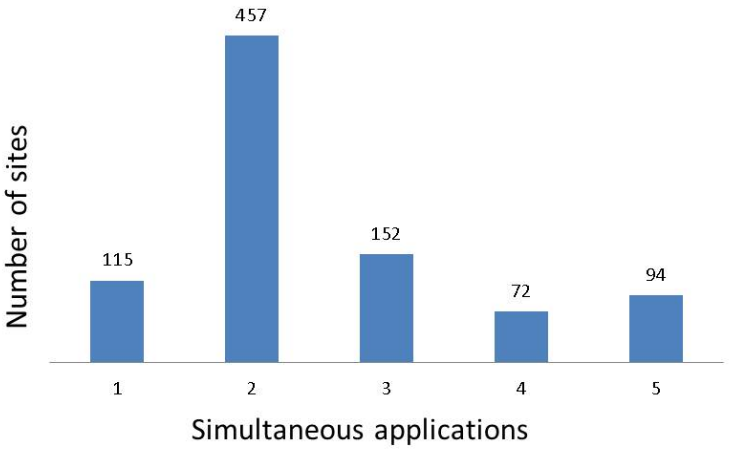

Figure 3.18: Number of simultaneous occurrences for pairs of services, numbered according to figure 3.17

	1																								
1	489	2																							
2	31	186	3																						
3	325	10	406	4																					
4	54	4	49	131	5																				
5	81	32	52	5	166	6																			
6	34	114	14	6	28	162	7																		
7	7	13	17	6	3	7	57	8																	
8	46	32	29	2	64	17	2	106	9																
9	6	21	6	4	3	13	3	6	46	10															
10	11	7	6	10	10	6	4	8	3	43	11														
11	89	11	56	4	57	11	0	31	3	2	113	12													
12	17	5	9	2	12	6	3	9	3	1	11	35	13												
13	7	12	6	5	2	3	2	4	15	7	1	1	30	14											
14	41	12	22	0	20	17	1	14	7	5	24	4	0	64	15										
15	9	18	5	0	18	10	1	11	2	1	5	3	1	3	37	16									
16	7	2	1	0	3	7	0	5	0	6	1	0	0	2	0	17	17								
17	9	6	21	2	0	12	16	0	4	2	0	1	3	7	2	3	38	18							
18	9	4	3	2	0	3	0	1	1	0	4	0	2	2	1	0	0	12	19						
19	14	11	3	3	4	11	1	5	6	5	3	0	7	1	0	4	0	1	33	20					
20	0	1	0	0	0	2	0	0	1	0	0	0	0	0	0	0	0	1	0	4	21				
21	0	3	0	0	1	2	2	0	0	0	1	0	0	0	1	0	0	0	1	0	5	22			
22	1	1	2	0	0	4	1	2	2	1	1	1	2	0	2	0	4	0	0	0	0	9	23		
23	24	4	8	18	6	5	1	5	2	6	5	2	2	3	1	2	0	0	0	0	0	0	36	24	
24	1	2	0	0	0	0	1	2	0	0	1	0	0	0	1	0	0	0	0	0	0	0	0	4	25
25	8	4	3	1	0	3	0	2	0	1	3	1	1	2	1	2	0	2	0	1	0	0	2	0	14

Figure 3.19: Number of simultaneous occurrences for pairs of services, numbered according to figure 3.17

number 20, corresponding to transmission upgrades due to wind, and 22, corresponding to distribution upgrades due to wind, which is a reasonable conclusion since a device connected to the transmission system cannot offer services at the distribution level, and devices connected to the distribution system will often be of a too small size to provide meaningful transmission support. On the other hand, services 11 (spinning reserve), 15(ramping), 1(energy time shift), 2(renewables capacity firming) and 6(renewable energy time shift) are close by and, as will be shown in chapters 5 and 7 indeed can be provided by a single storage asset. Finally, it is important to emphasize that the map in figure 3.21 comes from data of real projects and provides a relevant data point to

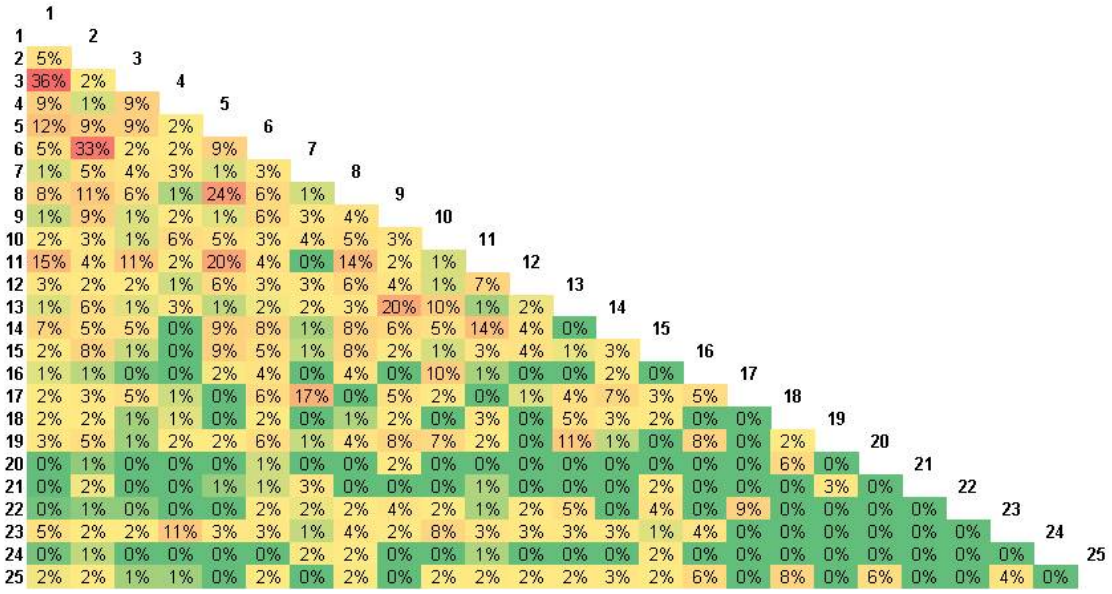

Figure 3.20: Relative fraction of simultaneous services, numbered according to figure 3.17

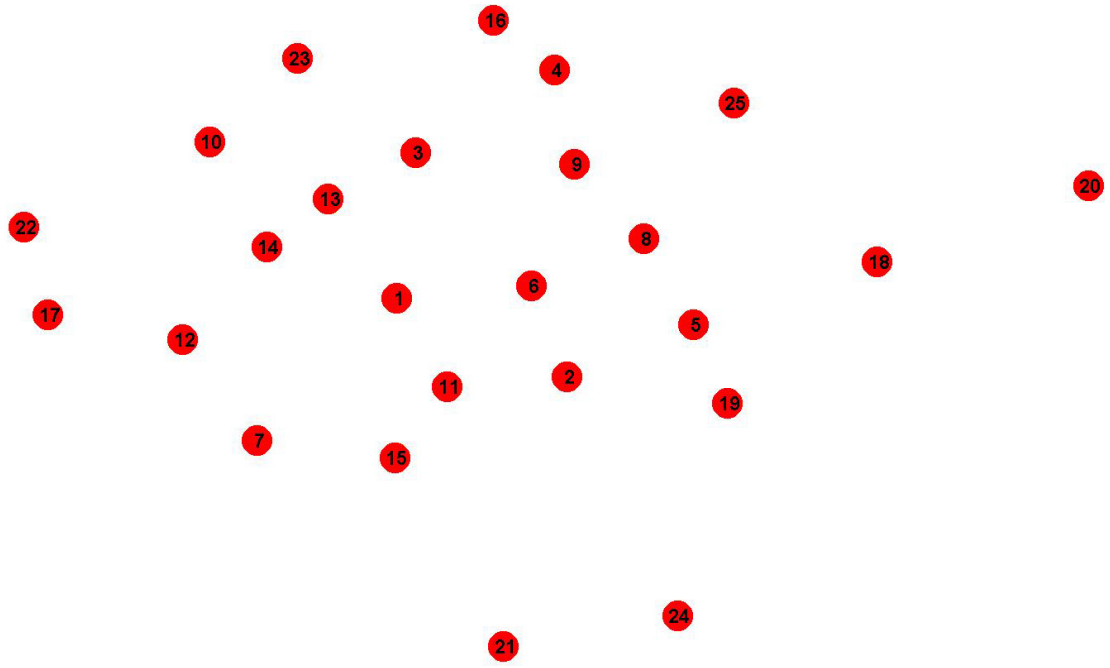

Figure 3.21: Relative position of storage applications in a two-dimensional space induced by $d_{i,j}$ and the Kamada-Kawai graph visualization algorithm, the numbering is according to figure 3.17.

compare with results obtained through models.

3.4.3 Academic perspective

In academic research, applications of energy storage, and of other types of flexible devices, to electric power systems is a fertile and active field. The expected growth in the number of flexible devices in the next decade has been regarded as an excellent opportunity to integrate them as part of a demand side management approach to network operation [84, 85], specially when power fluctuations are expected as result of an increasing penetration of renewable energy sources with stochastic nature such as wind and solar [86]. When a suitable control scheme is available, the elements can be converted into grid supporting devices and provide frequency and voltage support [87], enabling them to provide ancillary services.

There's apparently a widespread misunderstanding or over-valuation of electric energy storage in the literature, because it is too often referred to as unavoidable in a context of a big share of variable energy resources [88–90], which is plainly wrong. In contrast to other applications like portable electronics (without lithium-ion batteries, the decade of the laptops, tablets and smart phones, would not have progressed like it did [91]), EPSs count with several means to compensate fluctuations and temporal mismatches. As discussed in section 2.3.5, the value of energy storage in different applications should be understood, according to definition 2.4, through a careful calculation of the economic advantages that the introduction of a given means has for the power system as a whole, which in turn requires that one first understands the electric grid [92] in order to understand how existing functions could be substituted or new ones emerge that improve current quality standards. However, this alone does not imply that a private storage project is economically viable, since market imperfections prevent agents to capture all the value that their assets could provide, hence leading to a potential sub-utilization of them.

Regarding the quantification of value, one possibility is to estimate the cost savings from the hypothetical alleviation of a relevant problem. For example, the yearly economic losses in the United States explained by short-duration electricity service interruptions has been calculated in eighty thousand million dollars [93], which can be understood as a potential revenue cap for a commercial segment of providers of reliability through storage devices. A rigourous methodology to quantify the value of storage for specific services is given in [25], from which table 3.3 is copied literarily:

		Functional Use	Value Metric	Analysis Methods
Bulk Energy	1	Electric Energy Time-Shift	The price differential between energy price during charge and discharge. This includes: • arbitrage • renewable energy firming and integration • electric supply capacity: The avoided cost of new generation capacity (procurement or build capital cost) to meet requirements.	Production cost modeling; optimization using historical and projected data; use specific valuation tools; long term planning models.
T&D Services	2	Transmission Upgrade Deferral	The avoided cost of deferred infrastructure to address the issue.	Long term planning models.
	3	Distribution Upgrade Deferral	The avoided cost of deferred infrastructure to address the issue.	Long term planning models.
	4	Transmission Voltage Support	The avoided cost of procuring voltage support services through other means.	Power flow modeling
	5	Distribution Voltage Support	The avoided cost of procuring voltage support services through other means.	Power flow modeling
Reserve Services	6	Synchronous Reserve	*Regulated environment*: the avoided cost of procuring reserve service through other means. *Market environment*: the market price for synchronous reserve.	Production cost modeling; optimization using historical and projected data; use specific valuation tools.
	7	Non-Synchronous Reserve	*Regulated environment*: the avoided cost of procuring reserve service through other means. *Market environment*: the market price for non-synchronous reserve.	Production cost modeling; optimization using historical and projected data; use specific valuation tools
	8	Frequency Regulation	*Regulated environment*: the avoided cost of procuring service through other means. *Market environment*: the market price for frequency regulation service.	High resolution production cost modeling; optimization using historical and projected data; use specific valuation tools.
Customer	9	Power Reliability	The avoided cost of new resources to meet reliability requirements.	Distribution modeling: power flow; use specific valuation tools; simple internal modeling.
	10	Power Quality	The avoided cost of new resources to meet power quality requirements, or avoided penalties if requirements not being met.	Distribution modeling: power flow; use specific valuation tools; simple internal modeling.

Table 3.3: Functional uses for EES systems and their associated value metrics, from [25].

In terms of practical replacement feasibility, they could substitute the frequency regulation requirement to wind parks, which in order to provide the service need to operated below the maximum power point extraction curve [94]. Also, in the special case of isolated systems, which can be either remote hybrid systems or a part of a larger power system that disconnected during a contingency, the behavior of storage-capable, curtailable units and loads is particularly critical given the inherent weakness of the network

[95]. Other approaches to this are found in [96], for the case of electric vehicles with droop response to voltage and frequency deviations, in [97] for on-off control of appliances in response to frequency thresholds and in [98] for the optimization of a combined system with pumped-hydro and wind generators.

3.5 Policy considerations

Before claiming categorically that more storage should be introduced, it is important to have a comprehensive understanding of the eventual functions that electricity storage has to fulfill, together with other grid, generation, and demand side assets of the power system [17]. Hence, the utilization of eligible storage devices for the provision of the ancillary and system services in table 3.1 is contingent to the possibility to capture enough revenue to justify the investment. In addition to the specific characteristics of the technology, two contextual aspects significantly influence this: 1) the electrical location of the device, depicted in figure 3.22 and 2) the relevant regulatory environment. The first aspect reveals itself as a technical imperative. For example, congestion management, voltage regulation and distribution peak-shaving cannot be provided from devices connected in any location, which is not the case for frequency regulation; energy arbitrage will also be limited by the capacity of the electric network to which the device is connected, and compensation of fast renewable energy fluctuations will be more effective if the target generator is close by.

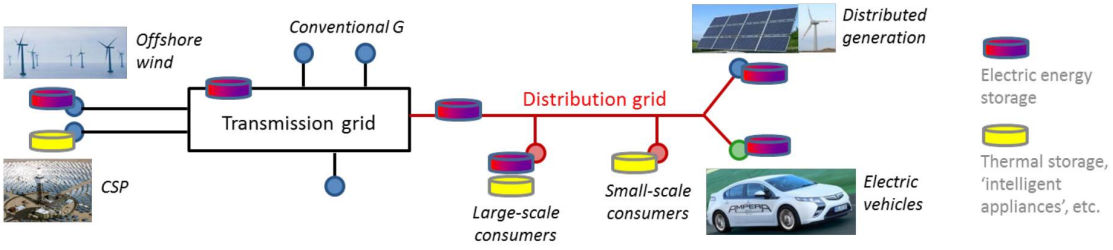

Figure 3.22: Possible locations of application in the future power system [17].

Numerous studies have been undertaken to assess the value of specific uses of storage. Some focus on the arbitrage value of electricity storage in the electricity spot market, others on the estimation of the value of electricity storage when providing primary regulation services, in their use to optimize the generation portfolio, or into the use at transmission or distribution level. End-user applications are typically studied in the

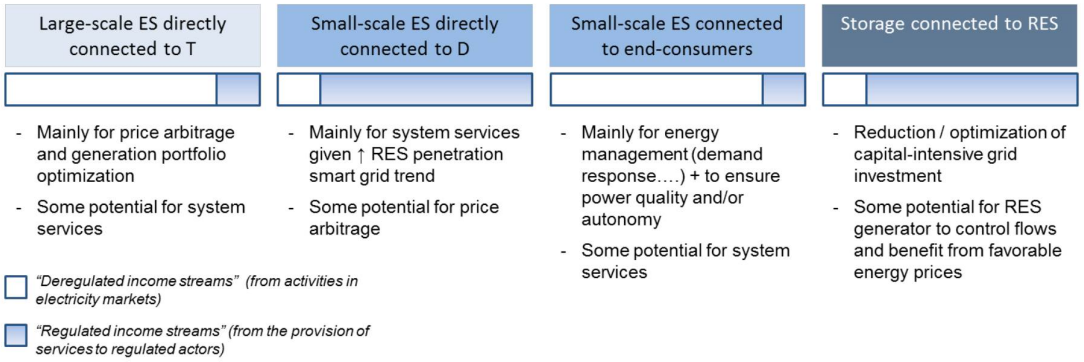

Figure 3.23: Location of storage against the most plausible type of business model today [17].

scope of distributed energy storage systems. Most of the analyses mentioned above cannot show profitability of storage by providing only one specific service in the current market context. But this does not necessarily imply that electricity storage is not an economic business or valuable solution for the power system. To reveal the overall value of storage for the whole system, it is necessary to investigate the way to aggregate the benefits of storage for different services or even different actors that encompass both regulated and competitive activities [17]. Additionally, there is a concurrent need to quantify the value of storage in the various services it may provide to the grid, individually and in multiple or "stacked" services, where a single storage system has the potential to capture several revenue streams to achieve economic viability [24].

3.5.1 Enables for a widespread use of energy storage

Considering that policy should facilitate the creation of value, where there is room for it. A summary of the enablers for a widespread development of storage applications is given in [24] and is described next:

Cost competitive energy storage systems The total cost of storage systems, including all the subsystem components, installation, and integration costs need to be cost competitive with other non-storage options available to electric utilities. While there is a strong focus on reducing the cost of the "storage" components, such as batteries or the flywheel, the storage component still constitute only 30% to 40% of the total system cost, thus the focus needs to be on the entire system.

Validated performance and safety The process for evaluating and reporting the performance of existing storage systems on a unified basis needs to be created. This combined with industry accepted codes and standards to specify desired performance parameters for each storage service, will lead to a wider acceptance of energy storage systems. For example, there is significant uncertainty over the usable life of batteries [31]and the length of time that a storage installation can generate revenue; both of these issues directly impact investment calculations.

Equitable Regulatory Environment Currently, a consistent pricing or market plan for providing grid storage does not exist and the uncertainty surrounding use-case economics inhibits investment. Without an established revenue generation model for storage operators, the case for investment will remain muted. While there have been demonstrations in areas such as frequency regulation, there are still enough revenue uncertainties in other applications to dissuade investment. Also, the viability of a certain business models is directly related to the value of market prices. The availability of market prices is a precondition to conceive relevant business models, and the credibility of market prices affects the credibility of the result of the business model [17].

Note that it is unlikely that but a few regulators will be able to foresee the relevance of business models which could unlock opportunities to increase the economical and technical efficiency of power systems under new scenarios. An example of this is the recent increment in the penetration of variable energy resources, which is occurring fast and the rules are being adapted in the face of undeniable evidence of their inadequacy. Simulation models have a relevant role to play in the elaboration of roadmaps and projections to enable a timely discussion of eventual regulatory changes.

Industry Acceptance Currently, system operators have limited experience using deployed storage resources; stakeholder input suggests that development of algorithms to employ storage technology effectively and profitably could encourage investments. Similarly, today's utility planning, transmission and distribution design tools do not have the capability to analyze energy storage as an option on a consistent basis.

[31]For example, at a recent roundtable with several key stakeholders from utilities and energy companies, there was particular skepticism over claims of 20-years of high-efficiency charging/discharging that some battery manufacturers make [24].

3.5.2 Examples

The growing awareness of about the potential of energy storage is being evidenced by the emergence of schemes to encourage their introduction in different countries, mainly in Europe and the United States. As means of example, the cases of California, Germany, and the latest orders from the Federal Energy Regulatory Commission (FERC, U.S.A.) are summarized in this section.

3.5.2.1 German residential energy storage support program

This program is available for systems installed after January 2013 and with an installed PV capacity up to 30 kW. It distinguishes between new PV systems, where a BESS is part of the project, and existing ones, where the battery is considered an upgrade:

$$S = \begin{cases} \min\left(0.3 \cdot C_s, 660 \cdot P_{PV}\right) & \text{for new systems} \\ \min\left(0.3 \cdot C_s, 600 \cdot P_{PV}\right) & \text{for upgrades,} \end{cases} \tag{3.23}$$

where P_{PV} is the nominal AC capacity of the photovoltaic system and C_s is the cost of the storage device. To be eligible for the support, the operator of the PV-storage system must agree to operate the battery in such a way that it keeps the net feed-in capacity to 60% of the capacity of the system. For example, for a system connected to the grid through a 10 kW inverter, the maximum power injection would be 6 kW. Also, only battery systems under a minimum 7-year manufacturer's guarantee can be included [99].

3.5.2.2 California energy storage procurement framework and design program

In the face of increasing penetration of photovoltaic generation to meet an ambitious goal of 33% of generation from renewable resources by year 2020, the government of the state of California established in 2013 a target of 1 325 MW of energy storage to be procured by the same year, and installed no later than 2024. The procurement process is biennial and started on March 2014, with specific targets for the three investor-owned utilities (IOUs) operating in the state as shown in table 3.4:

Storage Grid Domain (Point of Interconnection)	2014	2016	2018	2020	Total
Southern California Edison					
Transmission	50	65	85	110	310
Distribution	30	40	50	65	185
Customer	10	15	25	35	85
Subtotal SCE	**90**	**120**	**160**	**210**	**580**
Pacific Gas and Electric					
Transmission	50	65	85	110	310
Distribution	30	40	50	65	185
Customer	10	15	25	35	85
Subtotal PG&E	**90**	**120**	**160**	**210**	**580**
San Diego Gas & Electric					
Transmission	10	15	22	33	80
Distribution	7	10	15	23	55
Customer	3	5	8	14	30
Subtotal SDG&E	**20**	**30**	**45**	**70**	**165**
Total - all 3 utilities	**200**	**270**	**365**	**490**	**1,325**

Table 3.4: Energy storage procurement targets in MW [26].

The process to procure energy storage consists in competitive solicitations for third party-owned or aggregated resources, which can include any technology (including non-stationary such as electric vehicles), except for pumped-hydro resources over 50 MW. Existing energy storage projects can be discounted from the IOU's target if they were installed after January 1, 2010 [26].

3.5.2.3 FERC orders 745, 755 and 784

In 2011, FERC issued order 745 to allow that *"when a demand response resource participating in an organized wholesale energy market administered by a Regional Transmission Organization (RTO) or Independent System Operator (ISO) has the capability to balance supply and demand as an alternative to a generation resource and when dispatch of that demand response resource is cost-effective as determined by the net benefits test described in this rule, that demand response resource must be compensated for the service it provides to the energy market at the market price for energy, referred to as the locational*

marginal price (LMP)". This order enabled the consideration of load reductions at the same level of generation, a concept sometimes referred to as *negaWatts*.

Order 745 was followed in the same year by order 755, which intends to *"remedy undue discrimination in the procurement of frequency regulation in the organized wholesale electric markets and ensure that providers of frequency regulation receive just and reasonable and not unduly discriminatory or preferential rates."* by the requiring the introduction of the *pay for performance* concept, based on how closely the device follows AGC signals.

Despite orders 745 and 755, third-party ancillary services providers were restricted to provide them under the Avista order, according to which the users of the transmission system had two alternatives to procure their share of ancillary services: from the local utility or using their own resources, as long as these were deemed comparable with the ones used by public utilities. Hence, if the customer had access to fast acting batteries to provide its frequency regulation needs, this was not recognized if the utility didn't did something similar. Order 784, by enforcing a comparison on a performance basis, allows customers cater to their needs by buying faster or more accurate frequency regulation means. The order also includes directives related to how utilities should account for the use of storage devices.

3.6 Remarks

This chapter has shown that several models have been proposed to represent batteries in particular applications. Analytical models are the most frequent choice for energy-related services with slow dynamics, equivalent circuits are preferred for the design of devices and to simulate the performance of BESSs in dynamic response, and electrochemical models offer advantages when the underlying physics need to be accurately represented in order to predict the effect that variables such as discharge rate, temperature and secondary reactions have in both the short-term performance of the cell and in slower parameter changes related to ageing.

Also, evidence has been provided to support that counting with a coherent formulation can simultaneously: a) estimate the value of an energy storage asset participating in several services, and b) represent the performance of the device in terms of the quality of the service provided and the associated cost (in electrochemical devices, mainly due to

lifetime and efficiency considerations). The development of such a formulation is what motivates the present dissertation.

Chapter 4

Models for battery energy storage systems

When an engineer wants to model a system that includes a combined cycle gas turbine, there is a reasonable consensus in the literature about acceptable ways to model its performance in different contexts. For example, for dynamic studies both the synchronous machine and the gas turbine have been studied in detail and depending of the relevant analysis time frame there are a known number of modeling simplifications that lead to results which closely approximate data from real operation.

However, when it comes to represent electrochemical storage devices the path is not clear for a number of reasons:

1. The constructive characteristics of the devices are not always known because: a) the manufacturing process is not completely controllable or observable, b) the parameters change over time, c) manufacturers don't disclose proprietary information;
2. The technology is changing fast;
3. As opposed to, for example, synchronous machines, the response of a BESS cannot be defined purely in terms of physics, but a substantial part is related to different levels of control;

4. Frequently only a part of the reactions are known. For example, degradation mechanisms are still being studied at an experimental level for many technologies.

This chapter proposes a comprehensive model to represent battery energy storage systems in several types of studies. The formulation, developed starting from recent proposals for the different parts of the BESS, is intended to be sufficient, although not always necessary, to produce useful performance predictions when the correct parameters for the electrochemical device of interest are used. The next chapter discusses how for different power systems problems the proposed model can be simplified.

4.1 Model architecture

Figure 4.1, taken from a commercial brochure, displays the arrangement of components of a BESS in an actual system in production. The purpose of this section is to describe all the energy and information flows between the model blocks that represent such a system in the proposed formulation.

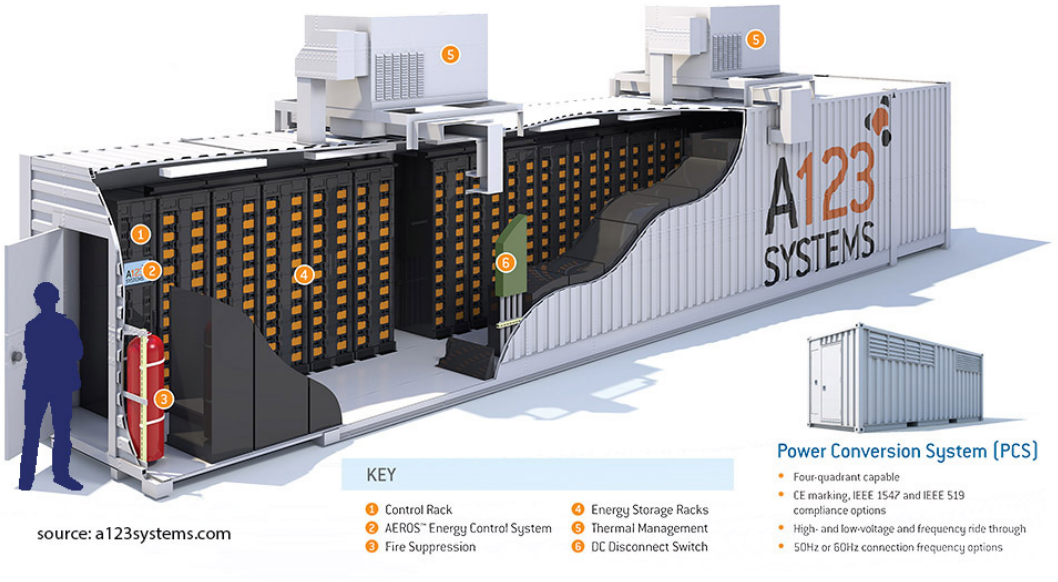

Figure 4.1: Commercial BESS assembled by A123 Systems [18].

Figure 4.2 corresponds to the general schematic representation of the entities considered and the interactions between them. The blocks bounded by solid lines are part of the BESS model, and those with dashed lines are external to it.

The interactions between the BESS and the external entities are as follows:

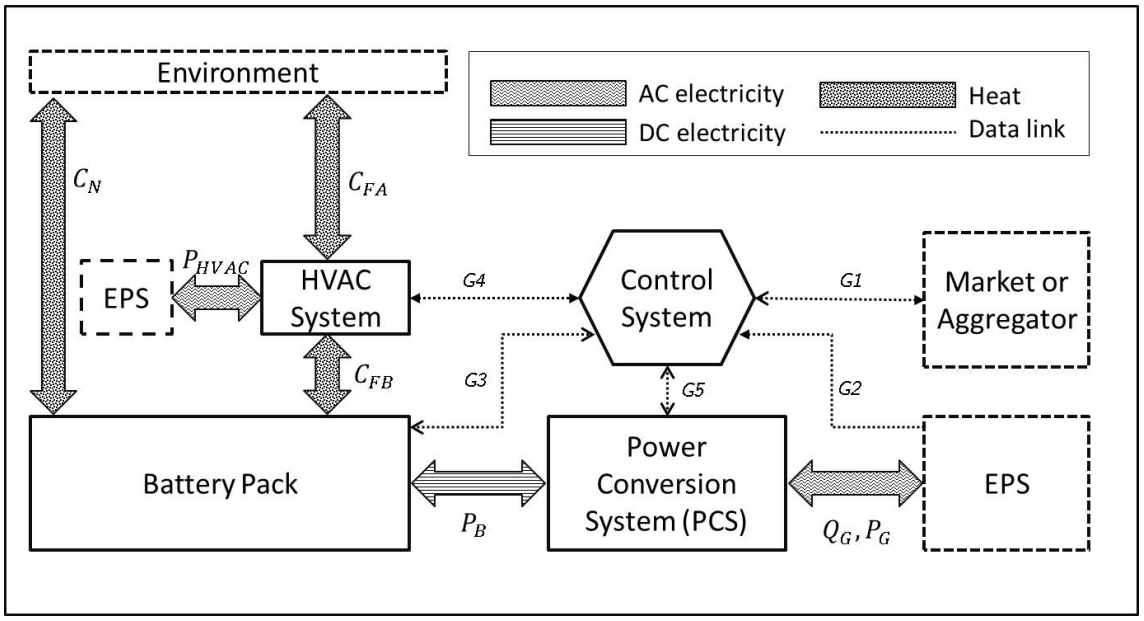

Figure 4.2: General block diagram.

Environment This corresponds to the physical envelop where the BESS is placed. In the model it is considered that the ambient is an ideal heat source at a temperature that changes in time according to a known profile which is independent of the power exchanged with the BESS. The sign and magnitude of the natural heat exchange Q_N is calculated using a factor h_{th} such that:

$$Q_N = h_{th} \cdot (T_a - T_p)\,, \tag{4.1}$$

where T_a is the ambient temperature and T_p is the temperature of the battery pack, which is considered to be uniform. Regarding the forced heat exchange Q_F, it is determined by the operation of the HVAC system and will be explained later.

EPS The main interaction between the BESS and the EPS is the exchange of active and reactive power p and q. In addition to this, the temperature control system (HVAC, for Heating, Ventilation and Air Conditioning) uses electricity to operate a heat pump. The provision of a given service may also require access to remote measurements, represented by the signal $G2$

Market or aggregator The behavior of the BESS is decided against a business model. The signal $G1$ represents a codification of the rules that describe how payments

for energy and ancillary services are calculated, including performance requirements, and the response of the BESS controller to calls for services.

4.2 Power Conversion System (PCS)

The PCS is modeled through an ideal single-level three-phase inverter bridge operated as a voltage-source inverter (VSI) with sinusoidal pulse width modulation (SPWM) [19]. Figure 4.3 shows the arrangements of power electronic components in the device, for example insulated gate bipolar transistors (IGBTs).

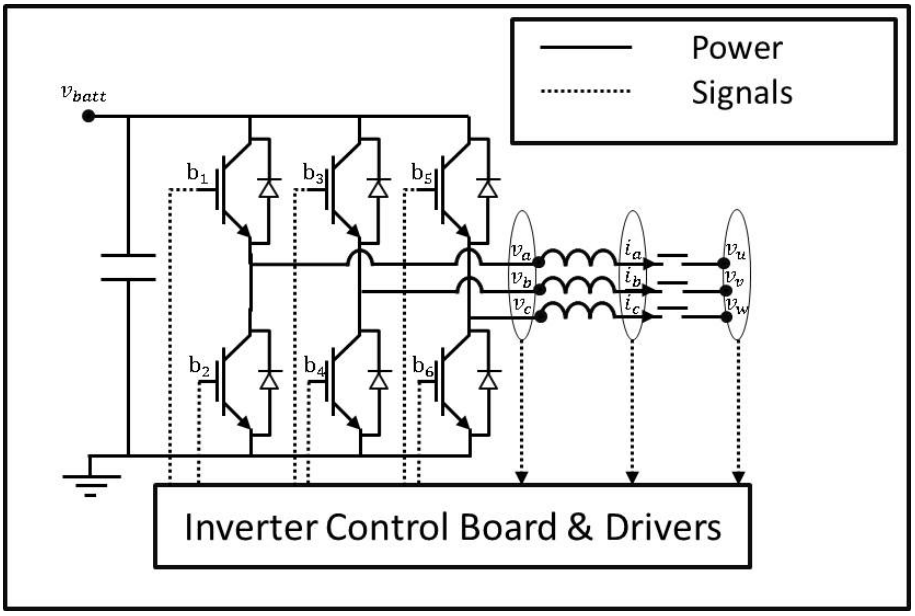

Figure 4.3: Inverter schematic.

4.2.1 Modulation

The SPWM technique calculates the state of the switches b_i by comparing three reference sinusoidal waveforms, shifted in 120 degrees, (modulating signals) with a triangular waveform (carrier signal). As shown in figure 4.4, the result of this are three variable-width pulse-trains which are usually filtered to reduce the contribution with voltage harmonics to the network. For steady-state and stability simulations, a fundamental-frequency model can be used where the ideal, loss-less converter can be modelled by a DC-voltage controlled AC-voltage source conserving active power between AC and DC sides as explained in [100].

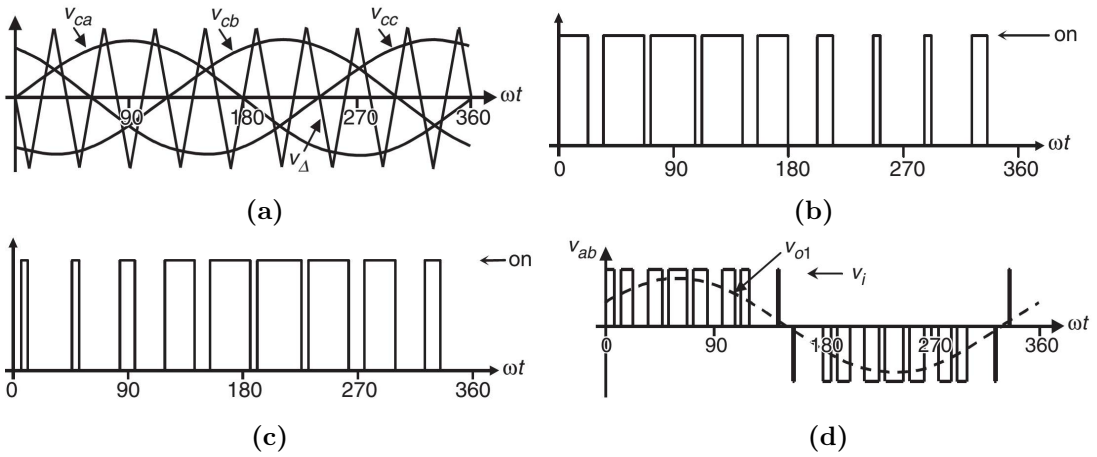

Figure 4.4: Characteristic waveforms of the SPWM modulation: a)carrier and modulating signals; b) b_1 state; c) b_3 state; d) raw and filtered output waveform for $u_{ab} = u_a - u_b$ [19].

For a sinusoidal modulating signal Pm of frequency f_m and amplitude a_m; and a triangular carrier Pc of frequency f_c and amplitude a_c, the modulation index m_a is defined as:

$$m_a = \frac{a_m}{a_c} \tag{4.2}$$

For values of $m_a < 1$, the real and imaginary parts of the fundamental frequency component of the output voltage are:

$$\begin{aligned} U_{ab_r} &= \mathrm{K0} \cdot Pm_r \cdot v_{in} \\ U_{ab_i} &= \mathrm{K0} \cdot Pm_i \cdot v_{in} \end{aligned} \tag{4.3}$$

The fundamental frequency equations are completed by the active-power conservation between AC and DC sides:

$$P_{AC} = Re\left(U_{ab} \cdot I_a^*\right) = v_{in} \cdot i_{in} = P_{DC} \tag{4.4}$$

The variables in equations (4.3) and (4.4) are defined as follows:

- U_{ab}: voltage phasor between phases a and b (RMS value);

- I_a: current phasor of phase a;
- v_{in}: DC voltage in the battery terminals;
- i_{in}: DC current entering the positive inverter terminal;
- P_{DC}: Power entering the inverter;
- P_{AC}: Active power leaving the inverter towards the grid;
- U_{ab_r}: Real part of the phasor U_{ab};
- U_{ab_i}: Imaginary part of the phasor U_{ab};
- $K0$: Constant depending on the modulation method. For SPWM, $K0 = \frac{\sqrt{3}}{2\sqrt{2}}$;
- Pm_r: Real part of the modulation phasor;
- Pm_i: Imaginary part of the modulation phasor.

The reference frame of the modulation signal can be obtained in two ways. The simplest option, appropriate for isolated applications where the inverter behaves as a grid-forming unit, is to define an internal reference signal with arbitrary phase, frequency and amplitude ($|Pm|$). Alternatively, the reference frame can be obtained from the grid-side voltage measurements v_u, v_v and v_w through a phase-locked loop (PLL)[100]. The latter scheme is shown in figure 4.5 for a balanced three-phase system[1], where v_r and v_i be the positive-sequence voltage real and imaginary components in p.u. respectively.

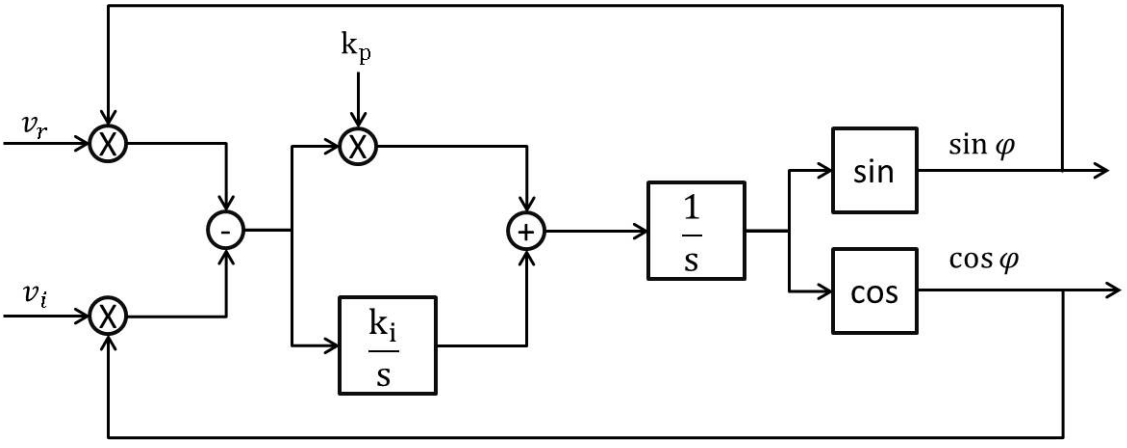

Figure 4.5: Block diagram for the proportional-integral (PI) phase-locked loop (PLL) in the Laplace domain

[1] extensions for unbalanced systems are beyond the scope of this thesis.

4.2.2 Power transfer

Let δ_u and δ_v be the angle of the phasors u and v with respect to an arbitrary global reference frame, then, the power across the coupling (purely inductive) reactance $\mathrm{X_s}$ is equivalent to a cylindric rotor synchronous machine:

$$\begin{aligned} p &= \frac{U \cdot V \cdot \sin(\delta_u - \delta_v)}{\mathrm{X_s}} \\ q &= \frac{V\left(U\cos(\delta_u - \delta_v) - V\right)}{\mathrm{X_s}} \end{aligned} \tag{4.5}$$

Note that, by virtue of equations (4.3) and (4.5), the active and reactive power output of the inverter is completely controllable through the modulation signal. When such a signal is referred to the reference frame coming from a measurement at the grid connection point processed by an ideal PLL, a fixed-phase modulation signal guarantees constant power. However, real PLLs cannot follow the reference signal instantaneously and therefore fast variations in δ_v will be followed by non-controllable changes in the power output of the inverter. The direction of this change, from equation (4.5) will be such that when δ_v gets closer to δ_{u_0}, the power output of the inverter will decrease since the phase of the modulation signal will remain in the same δ_u because of the phase estimation lag. As the PLL converges to the new value of δ_u, the power will be reestablished to the original value. Consider the particular case shown in figure 4.6, where the synchronous machine is assumed to have enough inertia to keep the frequency constant during the analysis interval after the load L2 is connected in $\mathrm{t_0}$. With a fast PLL, since δ_2 comes from a modulation signal referred to δ_0, the angle across X_2 remains constant. If the voltage magnitudes don't change appreciably, this means that the power from the inverter does not change. In contrast, δ_1 does not come from a modulation signal referred to δ_0, but instead from the internal voltage of a synchronous machine with considerable inertia. Hence, it cannot change abruptly after the connection of L2 and the synchronous machine absorbs all the imbalance, a behavior known as *inertial response*.

When a slow PLL is used in the inverter, the reference frame for the modulation signal lingers in the old phase value for δ_0 and progressively gets closer to it. This causes the inverter to provide an open-loop inertial response that closely resembles the reaction of

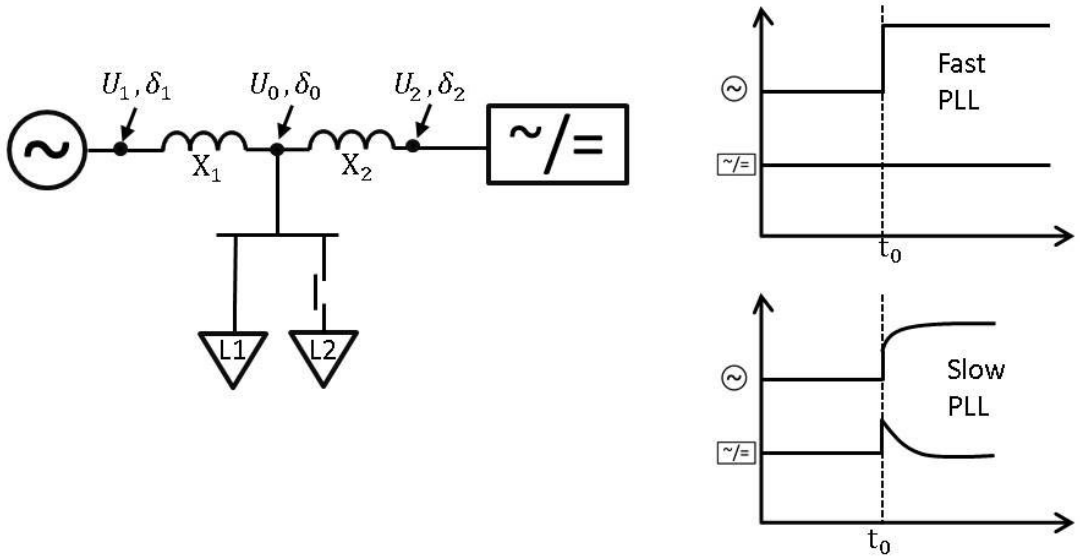

Figure 4.6: Effect of the PLL speed in the transient power share between an inverter and a synchronous machine.

a synchronous machine. This is fundamentally different from approaches that rely on a measurement of the frequency and provide a reaction proportional to its derivative. True inertial response can also be implemented in inverters without the need of a PLL using the following relationship:

$$f_m = f_0 - \frac{p - p_{set}}{2\mathrm{H}}, \tag{4.6}$$

where p_{set} is the quasi-steady-state power setpoint of the inverter.

4.3 Battery pack

Presently available storage units are much more than a collection of electrochemical cell in series-parallel arrangements. Especially for chemistries which are sensitive to being operated out of their nominal range, sophisticated electronics for monitoring, protection and "housekeeping" operations are included by default and tampering with them always voids the warranty of the unit.

4.3.1 Structure

The components of the battery pack considered in this model are shown in figure 4.7. Although the HVAC system is not part of the pack according to figure 4.2, since its function has indirect relation with it has been included in the scheme for clarity. All the boundaries defined by dashed lines are open, and the ones with solid lines are closed in the sense of figure 2.1.

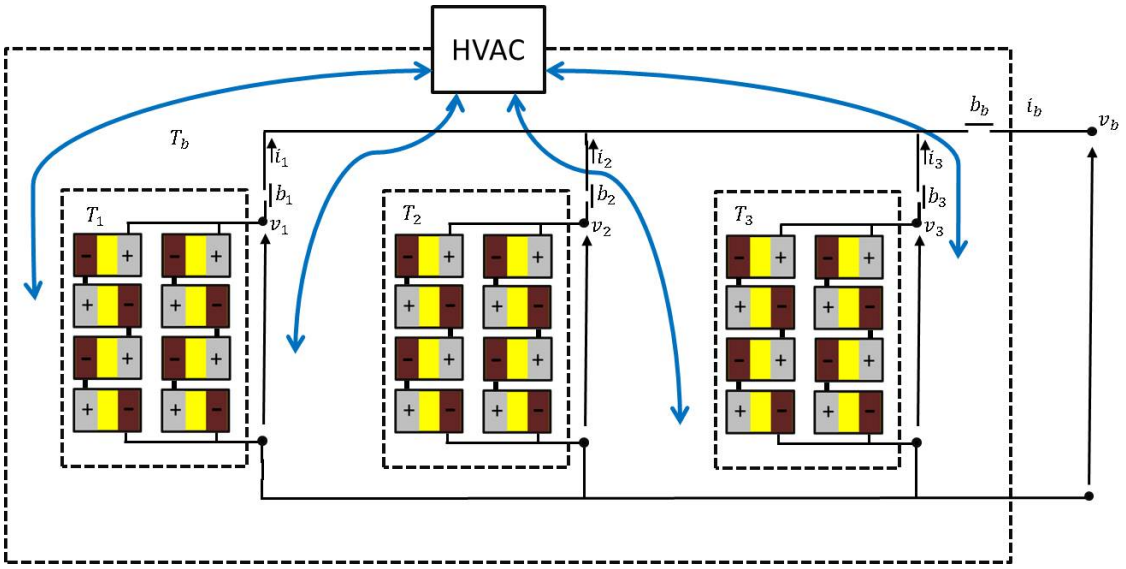

Figure 4.7: Battery pack structure considered in the model.

An arbitrary number of modules, in this case three for illustration, are placed inside a container that protects them from the environment. Each module consists in an arbitrary arrangement of electrochemical cells with a combination of series-parallel connection such that the total cell voltage is v_i and the current is i_i. All cells in a module are of the same technology and parameters at any point of their lifetime. Hence, for a given module power pm_i, the power output of each of its n_i cells, $pc_{j,i}$, is the same and independent of the internal connections of the pack:

$$pc_{i,j} = \frac{pm_i}{n_i}, \forall j \in (1, 2, ..., n_i) \tag{4.7}$$

The distinction between individual modules and not between individual cells is done because the module is commonly the minimum unit of failure/replacement, which is why it is likely that modules with different parameters could coexist in the same battery pack.

The binary variables b_i, define the status of the breakers of each module and of the complete pack. The BMS controls those switches to isolate faults and perform thermal equalization.

4.3.2 Thermal model and climatization

The behavior of electrochemical cells is sensitive to the temperature at which the reactions and the movement of ions take place. Since the evolution of this state variable is conditioned by the space surrounding the cell and by the cell's internal losses, it is convenient to represent this dynamic through a simplified thermal model with lumped parameters. For this purpose, the following thermal domains are considered: a) each cell module; b) the part of the pack external to the modules; and c) the environment external to the pack. The air inside the container is considered to be perfectly mixed and at uniform temperature T_b and constant atmospheric pressure. In the same way, the temperature T_i inside each module is considered uniform. The evolution of temperatures is given by the net caloric energy balance:

$$\begin{aligned} \frac{\mathrm{d}T_i}{\mathrm{d}t} &= \frac{\mathrm{IG}_i + h_{i,b}\,(T_b - T_i)}{\mathrm{Cv_i}} \\ \frac{\mathrm{d}T_b}{\mathrm{d}t} &= \frac{h_{a,b}\cdot(T_a - T_b) + h_{i,b}\cdot(T_i - T_b) + HVAC_{th}}{\mathrm{Cv_b}} \end{aligned} \tag{4.8}$$

where $\mathrm{Cv_i}$ is the specific heat for each module, which includes the thermal inertia of the cells and the air inside the module; $\mathrm{Cv_b}$ is the specific heat of the battery pack excluding the modules (air, other equipment, wires, container, etc.); $HVAC_{th}$ is the heat entering the pack through the climatization system; and IG_i are the internal gains of each module, equal to the thermal losses of their constituent cells.

The climatization system is modeled as a reversible heat pump[2] moved by an electric motor. A temperature setpoint T_{set} and a temperature dead-band T_{db} are received from the central controller and the electric motor is turned on and off according to figure 4.8.

There will be a trade-off between the cost of the energy to run the climatization system and the benefits derived from it, such as lower losses and longer battery life. From the

[2] A heat pump is the name given to a thermal engine (2.2) operated in reverse

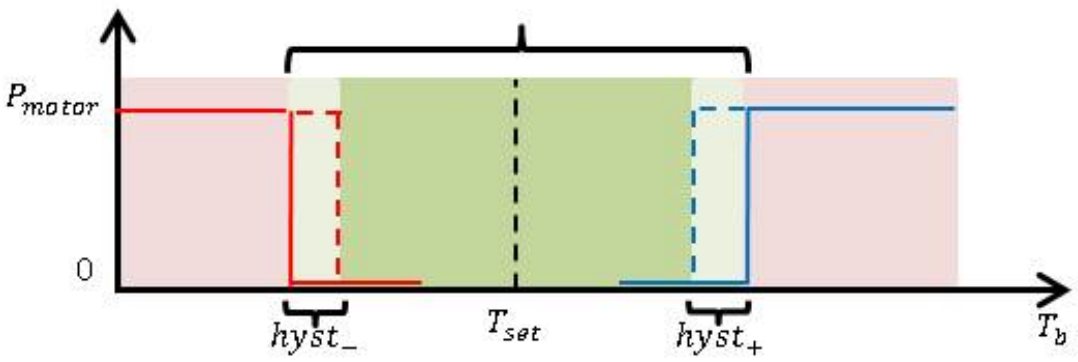

Figure 4.8: Reaction curve of the electric motor as a function of the temperature with two hysteresis loops. The solid lines apply when the motor is off and the dashed lines when it is on. Blue lines correspond to cooling mode and red lines to heating mode.

point of view of the thermal system, the variables that can be manipulated in order to control the temperature are $HVAC_{th}$ and IG_i. The latter is related to the operation of the cells, and will only be used to control the temperature in extreme cases, for example through the breaker control variables b_i. The former, however, is not really a manipulated variable but a consequence of the action of the motor. Let $HVAC_{el}$ be the electric power consumed by the heat pump, and let η_{m} be the constant electromechanical efficiency of the motor. The relationship between the $HVAC_{th}$ and $HVAC_{el}$ is given by the coefficient of performance (COP) of the heat pump:

$$COP = \frac{|HVAC_{th}|}{\eta_{\mathrm{m}} \cdot HVAC_{el}} \tag{4.9}$$

The COP is a function of the temperature difference between the heat sink and source. When the heat flows against the temperature gradient, i.e., from a cold source at temperature $\mathrm{T_{cold}}$ to a hot source at temperature $\mathrm{T_{hot}}$, the theoretical COP limit is given by:

$$COP \leq \begin{cases} \frac{T_{hot}}{T_{hot}-T_{cold}} & \text{Cooling mode} \\ \frac{T_{cold}}{T_{hot}-T_{cold}} & \text{Heating mode} \end{cases} \tag{4.10}$$

In practice, the COP for the expected operation conditions can be interpolated from the manufacturer's data sheet.

4.3.3 Electrochemical cell

A discrete state-space formulation for the electrochemical cell based on the model proposed in [8] and improved in [9] is explained in this section. Following the 1-D representation of the cell in figure 4.9, and as described in chapter 3, the state variables considered by the model are:

- $\zeta_s(r,t)$: Lithium concentration in the spherical particles in $\frac{\text{mol}}{\text{m}^3}$;
- $\phi_s(x,t)$: Electrical potential in the solid phase in V;
- $\zeta_e(x,t)$: Concentration of lithium ions in the electrolyte in $\frac{\text{mol}}{\text{m}^3}$; and
- $\phi_e(x,t)$: Electric potential in the electrolyte in V.

Assumptions:

1. The temperature is homogeneous throughout the cell;
2. In the electrolyte phase, mass and charge transports are one-dimensional, along the $\hat{\mathbf{x}}$ direction in figure 4.9. They are both due to diffusion (Ficks diffusion law) and advection driven by the electric field (Ohms law). Convection of the electrolyte substrate where the ions are suspended is neglected;
3. The spherical active material particles, in or out which lithium diffuses along the $\hat{\mathbf{r}}$ dimension, are supposed to be purely diffusive. Particle radius is considered small enough compared with electrode thicknesses, so that lithium concentration at solid/electrolyte interface is computed as a continuous function of the space variable x;
4. Electron transport through migration is one-dimensional, along the direction $\hat{\mathbf{x}}$.

The referential parameters in 4.1 are used when needed to generate numerical results.

Let Υ be the amount of lithium in an electrode in moles. Then, according to the data in table 4.1the lithium storage capacity of each one of them is:

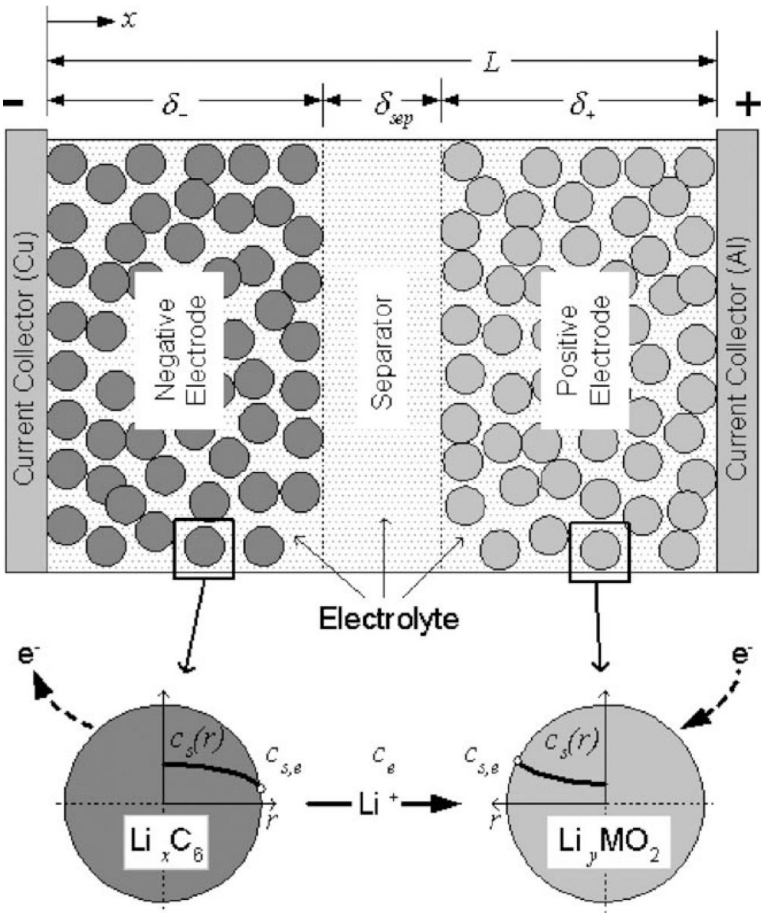

Figure 4.9: Physical representation of a electrochemical cell used for the electrochemical model in [20].

Parameter	Unit	Negative elect.	Separator	Positive elec.
Thickness	m	$\delta^- = 50 \cdot 10^-6$	$\delta^{\mathrm{s}} = 25.4 \cdot 10^-6$	$\delta^+ = 36.4 \cdot 10^-6$
Active material volume fraction		$\varepsilon_{\mathrm{s}}^- = 0.58$		$\varepsilon_{\mathrm{s}}^+ = 0.5$
Planar area	m^2	$\mathrm{A}^- = 1.0452$	$\mathrm{A}^{\mathrm{s}} = 1.0452$	$\mathrm{A}^+ = 1.0452$
Maximum lithium concentration	$\frac{mol}{m^3}$	$\zeta_{\max}^- = 16.1 \cdot 10^3$		$\zeta_{\max}^+ = 23.9 \cdot 10^3$
Initial lithium charge	mol	$\zeta_0^- = 0.244$		$\zeta_0^+ = 0.227$

Table 4.1: Parameter of a referential Li-Metal oxide cell from [20].

$$\begin{aligned} \Upsilon_{\max}^- &= \varepsilon_{\mathrm{s}}^- \cdot \delta^- \cdot \mathrm{A}^- \cdot \zeta_{\max}^- = 0.488\,\mathrm{mol} \\ \Upsilon_{\max}^+ &= \varepsilon_{\mathrm{s}}^+ \cdot \delta^+ \cdot \mathrm{A}^+ \cdot \zeta_{\max}^+ = 0.454\,\mathrm{mol}. \end{aligned} \tag{4.11}$$

Taking into account that $1\,\mathrm{mol} = 6.02 \cdot 10^{23}\mathrm{e}^-$, the positive electrode therefore limits the charge capacity to $2.733 \cdot 10^{23}$ electrons, $0.438 \cdot 10^5$ C or 12.1 Ah.

4.3.3.1 Equilibrium and non-equilibrium potential

At any given point in time, the thermodynamical potentials of each electrode U^- and U^+ are given by equation 2.24, where Θ is the ratio between the present concentration and the maximum concentration. The magnitude $U^{cell} = U^+ - U^-$ corresponds to what one would measure after the cell has been at rest for a long enough time so that all concentration gradients have disappeared.

$$U^{cell} = \left[\mathrm{U}_0^+ - \frac{\mathrm{R}}{\mathrm{F}} \cdot T \cdot \ln\left(\frac{\Upsilon^+_{\max}}{\Upsilon^+}\right)\right] - \left[\mathrm{U}_0^- - \frac{\mathrm{R}}{\mathrm{F}} \cdot T \cdot \ln\left(\frac{\Upsilon^-_{\max}}{\Upsilon^-}\right)\right]. \tag{4.12}$$

In equation 4.12, Θ has been replaced by the ratio between the maximum concentration $\Upsilon_{\max}$ and the concentration Υ for both electrodes. Defining $\mathrm{U}_0^{\mathrm{cell}} = \mathrm{U}_0^+ - \mathrm{U}_0^-$, $SOC^+ = \frac{\Upsilon^+}{\Upsilon^+_{\max}}$ and $SOC^- = \frac{S^-}{\Upsilon^-_{\max}}$, equation 4.12 can be written as:

$$U^{cell} = \mathrm{U}_0^{\mathrm{cell}} - \frac{\mathrm{R}}{\mathrm{F}} \cdot T \cdot \ln\left(\frac{SOC^+}{SOC^-}\right). \tag{4.13}$$

Note that for the initial lithium charge in table 4.1 $SOC^+ = SOC^-$, and therefore $U^{cell} = \mathrm{U}_0^{\mathrm{cell}}$. If the ionic concentration in the electrolyte is constant, U^{cell} can be calculated as a function of the charge leaving the cell Δq in Ah as:

$$U^{cell} = \mathrm{U}_0^{\mathrm{cell}} - \frac{\mathrm{R}}{\mathrm{F}} \cdot T \cdot \ln\left(\frac{0.5 + \frac{\Delta q}{\Upsilon^+_{max} \cdot 26.8}}{0.5 - \frac{\Delta q}{\Upsilon^-_{max} \cdot 26.8}}\right). \tag{4.14}$$

Figure 4.10 illustrates the dependency of the open-circuit voltage with the charge processed for a constant temperature of 25 °C. It is important to have in mind that because diffusion-derived over-potentials, the OCV is only measurable after several hours of inactivity.

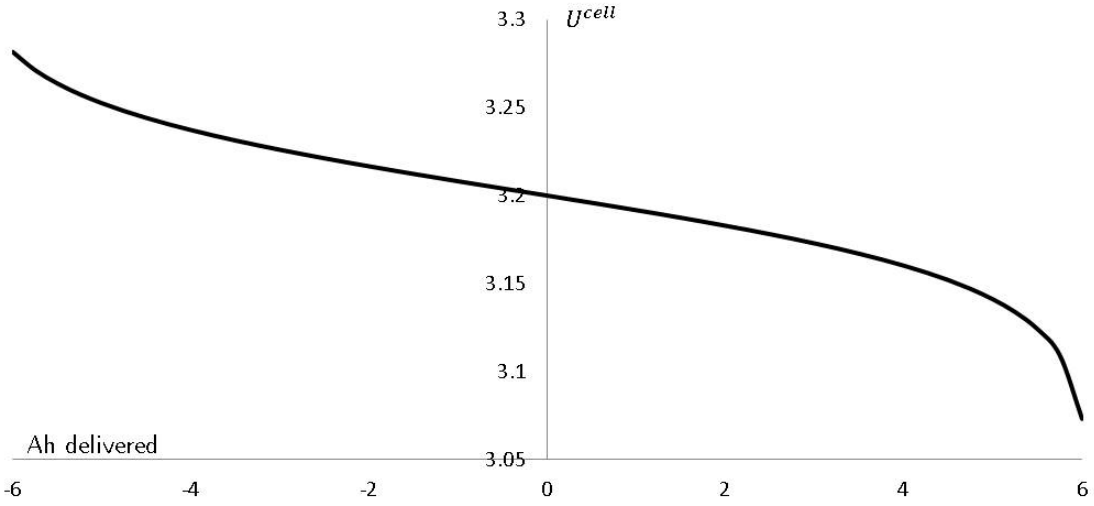

Figure 4.10: Open-circuit voltage as a function of the charge delivered. Negative numbers indicate charging.

The terminal voltage of the cell, v, depends, in addition to the VOC, on the present discharge rate and the cell's recent operation through the relation:

$$v(t) = \phi_s(L,t) - \phi_s(0,t) - \mathrm{R_c(t)} \cdot i(t), \tag{4.15}$$

where $\mathrm{R_c}$ is the sum of the contact resistance of both electrodes. The two first terms of equation 4.15 deviate from equilibrium as a consequence of the processes in the cell, which can be divided in two groups: transport and reaction. Transport overpotentials are due to the movement of charge in the solid and liquid phases. The reaction overpotential is normally the deviation from equilibrium that is required to drive the intercalation and release of lithium from the electrodes, although it can include terms related to side-reactions. The following sections describe the models for these phenomena.

4.3.3.2 Electrochemical reaction rate

The insertion-release process of lithium ions in the structure of both electrodes occurs quasi-continuously along the horizontal direction. We can therefore talk about a volumetric rate $g^{Li}(x)$ in $\frac{\mathrm{mole}}{\mathrm{m^3 \cdot s}}$ that refers to the release or insertion of lithium ions at the solid/electrolyte interface. The counterpart of this rate is the volumetric current generation $j^{Li}(x)$ in $\frac{\mathrm{A}}{\mathrm{m^3}}$. The process is driven by a local deviation from the electrode's equilibrium potential through the Butler-Volmer equation:

$$g^{Li}(x) = \frac{j^{Li}(x)}{\mathrm{F}} = \frac{a_s}{\mathrm{F}} \cdot j_0 \cdot \left[\exp\left(\alpha_{\mathrm{o}} \frac{\nu(x)}{v_T}\right) - \exp\left(-\alpha_{\mathrm{r}} \frac{\nu(x)}{v_T}\right) \right], \tag{4.16}$$

where:

- j_0: Exchange current density in $\frac{\mathrm{A}}{\mathrm{m}^3}$. It exhibits a modest dependency on electrolyte and solid surface ionic concentrations, ζ_e and $\zeta_{s,e}$ respectively, according to $i_0 = (\zeta_e)^{\alpha_o} \cdot (\zeta_{\mathrm{s,max}} - \zeta_{s,e})^{\alpha_o} \cdot (\zeta_{s,e})^{\alpha_r}$ [59];
- a_s: Electrode active area per unit volume in $\frac{\mathrm{m}^2}{\mathrm{m}^3}$;
- $\nu(x)$: Deviation from the equilibrium interface potential, or surface overpotential, in V;
- α_o, α_r: Oxidation and reduction transfer coefficients;
- $v_T = \frac{\mathrm{R}}{\mathrm{F}} \cdot T$: Thermal voltage.

4.3.3.3 Lithium transport in the active material

The active material is represented by spherical particles of radius $\mathrm{R_s}$, each with a crystalline structure like the ones shown in figure 3.8. Here the transport of ions inside each particle is considered to be purely diffusive, and figure 4.11 illustrates this concept for the reduction reaction.

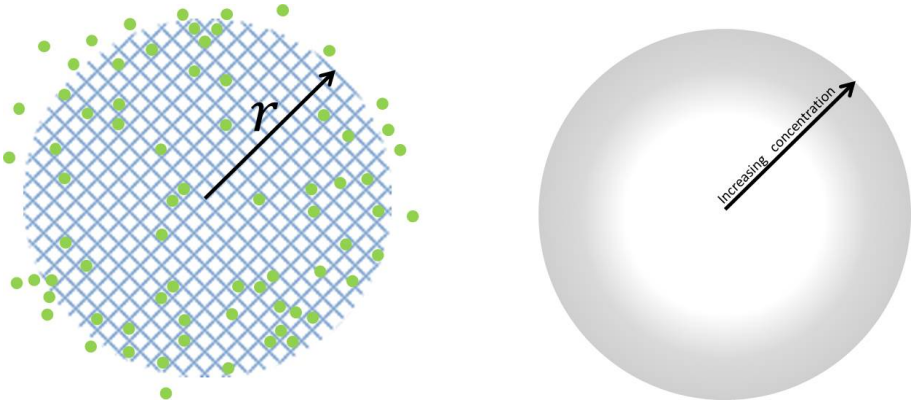

Figure 4.11: Left: schematic 2-D representation of the diffusion of lithium in a spherical particle. Right: assuming radial symmetry allows for a 1-D treatment along the r direction.

The outer layer of the particle is in contact with the electrolyte, which is where the Li ions are. The Li ions are driven towards the particles following concentration gradients

(diffusion) and the electric field (mobility). Once in the particle they become neutral by gaining an electron and are no longer affected by electric fields. However, the Li concentration gradient in the particle promotes particle displacement. In a 1-D approximation of the particle along the radial direction:

$$\varphi_s(r) = -\mathrm{D_s} \cdot \frac{\partial \zeta_s(r)}{\partial r} \tag{4.17}$$

The conservation of mass imposes equal ionic flows through spheres of different radii. Combining this with the diffusion equation yields:

$$\frac{\partial \zeta_s(r)}{\partial t} = \frac{1}{r^2} \cdot \frac{\partial}{\partial r} \left(\mathrm{D_s} \cdot r^2 \cdot \frac{\partial \zeta_s(r)}{\partial r} \right), \tag{4.18}$$

with the boundary conditions:

$$\begin{aligned} \varphi_s(0) &= 0 \\ \varphi_s(R_s) &= \frac{g^{Li}(x)}{a_s} \end{aligned} \tag{4.19}$$

4.3.3.4 Electronic transport in the active material

The electrons coming in and out of the lithium atoms find their way to the current collectors following the electric field according to Ohms law:

$$j_s(x) = -\sigma_s \cdot \frac{\partial \phi_s(x)}{\partial x}, \tag{4.20}$$

where:

- $j_s(x)$: Electronic current density in the solid phase in the direction perpendicular to the electrode plane, in $\frac{\mathrm{A}}{\mathrm{m}^2}$;
- σ_s: Electronic conductivity of the solid phase in $\frac{1}{\mathrm{ohm}}$.

And charge conservation implies:

$$\frac{\partial j_s(x)}{\partial x} = -j^{Li}(x) \tag{4.21}$$

Assuming that the separator is an electronic insulator and that the current density in the current collectors of area $\mathrm{A_{cell}}$ is constant, we have the boundary conditions:

$$\begin{aligned} j_s(\delta_{neg}) &= 0 \\ j_s(\delta_{neg} + \delta_{sep}) &= 0 \\ j_s(0) &= \frac{i}{A_{cell}} \\ j_s(\mathrm{L_{cell}}) &= \frac{i}{\mathrm{A_{cell}}} \end{aligned} \tag{4.22}$$

4.3.3.5 Charge transport in the electrolyte

The formulation for the electrolyte phase, introduced in [9], is described hereafter. The total ion current density $j_e(x)$ associated with ion transport in the electrolyte phase is the sum of two conduction components for potential gradient-induced migration of anion and cation and two diffusion terms for anion and cation transport:

$$\begin{aligned} j_e(x) &= j_n(x) + j_p(x) \\ j_n(x) &= -\sigma_{\mathrm{n}} \cdot \frac{\partial \phi_e}{\partial x} + \sigma_{\mathrm{n}} \cdot \upsilon_T \cdot \frac{\partial \left(\ln\left(\zeta_e\right)\right)}{\partial x} \\ j_p(x) &= -\sigma_{\mathrm{p}} \cdot \frac{\partial \phi_e}{\partial x} - \sigma_{\mathrm{p}} \cdot \upsilon_T \cdot \frac{\partial \left(\ln\left(\zeta_e\right)\right)}{\partial x} \end{aligned} \tag{4.23}$$

where j_n and j_p are the anion and cation current densities, and $\mathrm{sigma_n}$ and σ_{p} are the anion and cation conductivities of the electrolyte, respectively. Combining the equations yields:

$$J_e = -\sigma_{\mathrm{e}} \cdot \frac{\partial \phi_e}{\partial x} + (\sigma_{\mathrm{n}} - \sigma_{\mathrm{p}}) \cdot v_T \cdot \frac{\partial \left(\ln\left(\zeta_e\right)\right)}{\partial x}, \tag{4.24}$$

where σ_e is the ionic conductivity of the electrolyte, which can be related to ζ_e through the following empirical relation in ref [20]:

$$\sigma_e(x) = 0.00158 \cdot \zeta_e(x) \cdot \exp\left(-5.363 \cdot 10^{-5} \cdot \zeta_e^{1.4}(x)\right) \tag{4.25}$$

4.3.3.6 Cell degradation

The capacity loss is modeled as a decrease in the electrode useful area due to 4 combined causes: natural ageing, temperature, state of charge (SOC) and reaction rate (($I_{ion}(t)$). In [101] is proposed that this phenomenon is similar to the evolution of cracks in solids. Therefore, the rate of electrode loss would follow the Zhurkov equation:

$$\frac{\delta S_a(t)}{\delta t} = exp\left(\frac{g \cdot S(t) - \beta_1}{k \cdot T(t)}\right) \tag{4.26}$$

The factor S is the stress level, which is calculated in [101] for every cycle as a combined effect between the average SOC during the cycle and the cycle's amplitude. The disadvantage of this approach in this case is that is that a cell participating in frequency regulation will experience a variety of SOC fluctuations that do not match the concept of cycle. To overcome this, an expression that makes use of instantaneous current, temperature and SOC values is proposed (equation (4.27)). Note that the dependency with the state of charge is related to the direction of the current, which is coherent with the damage from over-charge and over-discharge observed in Lithium-ion cells.

$$S(t) = \begin{cases} \beta_2 \cdot i(t) \cdot (1 - \Theta(t)) & \text{if } i(t) > 0 \\ \beta_3 \cdot i(t) \cdot \Theta(t) & \text{if } i(t) <= 0. \end{cases} \tag{4.27}$$

During a period of time Δt, the area loss is given by:

$$\Delta S_a(\Delta t) = exp\left(\frac{S(t) - \beta_1}{k \cdot \frac{T(t)}{T_0}}\right) \cdot \Delta t \tag{4.28}$$

4.3.4 Battery Management System (BMS)

Battery management systems (BMS) have been designed to provide monitoring, diagnosis, and control functions to enhance the operations of battery. In this model, the BMS is responsible for the estimation of the following indicators:

State of charge (SOC) Theoretically, the SOC is related to the concentration of species in the electrodes. For example, if the positive electrode of a LIB has n lattice sites that can host lithium ions, and currently only m of them are occupied, then $SOC = m/\mathrm{n}$. More commonly, the SOC is expressed in terms of volumetric concentration:

$$SOC = \frac{Current\ concentration\ of\ ionic\ species}{\text{Maximum concentration of ionic species}} \tag{4.29}$$

Practical applications use the SOC to predict the moment when the battery would be depleted for a hypothetical operation, and it can only be estimated (not measured) during the operation of the cell, for which filter algorithms are presently a better solution compared to coulomb-counting or impedance spectroscopy since they can effectively avoid the problems from noise, inaccurate current sensor, accumulated round off error and so on [102].

State of power (SOP) The energy discharge rate that can be safely obtained from a cell is constrained by its voltage drop due to overpotentials and temperature. As discussed before, overpotentials behave as if a non-linear internal resistor was between the internal voltage and the battery terminals, which will limit the power transfer. Also, temperature increments from sustained operation at high currents or extreme environments can prevent the realization of this maximum power. In terms of SOP estimation, some methods have been presented to guarantee safe, efficient, and durable operations of the traction batteries under demanding driving conditions, which have been reviewed in ref [103].

State of health (SOH) This is a generic figure of merit for the current conditions of the battery compared to the reference conditions. The proposed model distinguishes between three sub-categories of SOH, all of them expressed in per-unit relative to the

ideal conditions: a) SOH_c is the charge storage capacity, related to the number of lattice intercalation sites; b) SOH_p is the power rating of the battery for representative SOC and temperature conditions; and c) SOH_η is the average efficiency of the cell.

The BMS can also take protective control actions through the binary variables b_b and b_i in case the battery operating conditions (in particular voltage, current or temperature), leave the interval considered safe.

4.4 Control system

This section describes the model of the BESS as an agent that participates in several functions that give access to various revenue streams. Since a BESS is a limited resource with a reduced number of degrees of freedom, an abstraction is presented through parametric behavioral rules. In other words, a set of decision variables are proposed which are sufficient to calculate the power exchanged between the BESS and the power system at any given time.

For each parameter, an analysis interval of duration Λ is divided into segments of length δ_{x}, where the subscript x indicates that the value of δ is in principle different for each parameter. For simulation purposes, one needs to make sure that $\forall x, \delta_{\mathrm{x}}$ is an integer divider of Λ.

4.4.1 Regulatory and market assumptions

Characterizing the revenue derived from behavioral rules running the BESS requires a clear definition of the conventions used to calculate it, which are part of the regulatory environment associated to the electric power system to which the BESS is connected. While there's currently no widely accepted set for these, they should in principle be technology-neutral and reflect the value that any responsive device can provide to the EPS and to other agents. Another aspect that needs to be considered is the interaction between agents. For example, if the price of frequency response comes from a daily auction, a greater number of agents that can provide that service will be translated into a lower price. In the context of this dissertation, the following assumptions and simplifications are made:

1. The formulae to calculate the payments to an agent for its participation in ancillary services are defined in a centralized way and are invariant in relation to the behavior of the agents;

2. The calculation parameters of the aforementioned formulae are calculated in accordance to the marginal benefit that the EPS obtains from the provision of the service;

3. All agents have access to all the available price signals, independently of their size.

4.4.2 Arbitrage

A BESS can access a revenue stream derived from the changes in energy price. In this formulation we assume that the price π_k is accessible in real time and that is the same for buying and selling energy. This situation can be encountered in existing power systems when the device is connected at wholesale level, or when the distribution network charges are independent from the direction of the flow.

The service is characterized by the following decision variables, which are constant during each period k of uniform duration δ_a:

- The steady-state power exchange setpoint in kW: for each period k, p_k^{set} is calculated in advance in order to maximize the net revenue.
- The price-elasticity of power setpoint in $\frac{\text{p.u.kW}}{\text{p.u.\$}}$: for each period, k_p corresponds to the real-time correction of p_k^{set} in order to correct for errors in the price forecasts.

Note that these decision variables imply that after they have been set the BESS is no longer under the control of the optimization engine, which may either be located at some aggregating entity or be too slow to re-optimize the setpoints. In contrast, the price signal is broadcasted to many units, making efficient use of communication networks.

The net revenue due to energy arbitrage over N periods can be expressed as:

$$R_a = \sum_{k=1}^{\mathrm{N}} p_k \cdot \pi_k \cdot \delta_{\mathrm{k}} \tag{4.30}$$

The battery power P_k is assumed constant during the period and is calculated as:

$$p_k = \begin{cases} max(p_k^{set} - k_p \cdot (\pi_k^e - \hat{\pi}_k^e), p_k^{min}) \text{ if } p_k^{set} \leq 0 \\ min(p_k^{set} - k_p \cdot (\pi_k^e - \hat{\pi}_k^e), p_k^{max}) \text{ if } p_k^{set} > 0 \end{cases} \tag{4.31}$$

The variable π_k corresponds to the real price of period k, while $\hat{\pi_k}$ corresponds to the estimation of π_k that was used to determine p_k^{set}. p_k^{min} and p_k^{max} are the power limits of the BESS imposed by the BMS.

4.4.3 Frequency regulation and voltage control

Short-term imbalances between generation and load are reflected in frequency fluctuations which can be measured by storage devices. Two representations of the frequency regulation service are proposed:

The purpose of this stage is to adapt active power set points to frequency and voltage changes. Reactive power is not considered and it is assumed that the unit keeps a unity power factor. The extension to a controller with droop reactive power behavior is explained in [95]. p_{set} is calculated based in p_{ref}, the device limits and the measured system frequency and voltage at the connection point. For normal operation, $p_{set} = p_{ref}$. Otherwise, it is obtained through the droop curves shown in Figures 4.12 and 4.13. There, the deviation from p_{ref} is plotted against the voltage and the frequency around nominal values. Three reaction zones are identified in both curves: first, for deviations less than a defined dead band, there is no reaction; then, for deviations between defined critical values, there is a reaction with moderate slope; finally, when the excursions surpass the critical values, the slope is increased to provide emergency reaction. Obviously, the complete curves only apply to units with bidirectional power flow capability. For pure loads or pure generators only the corresponding quadrant is considered. The frequency and voltage responses are combined in the following way:

1. If both magnitudes are within the critical values, voltage and frequency reactions are added;

2. If one of the magnitudes exceeds a critical value, the other is added only if the direction of both reactions match;

3. If both magnitudes exceed a critical value and the reaction directions do not match, the voltage reaction is not added. Otherwise, voltage and frequency reactions are added.

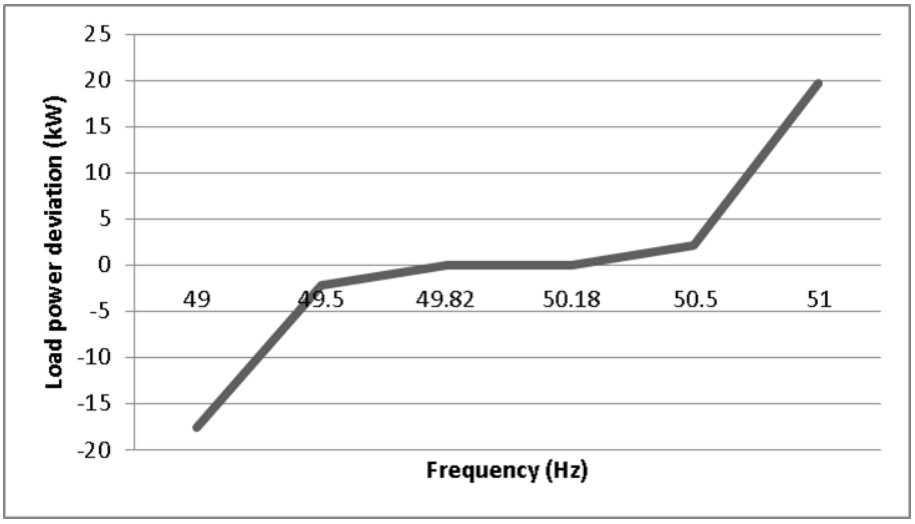

Figure 4.12: Control rule for the power response to frequency deviations.

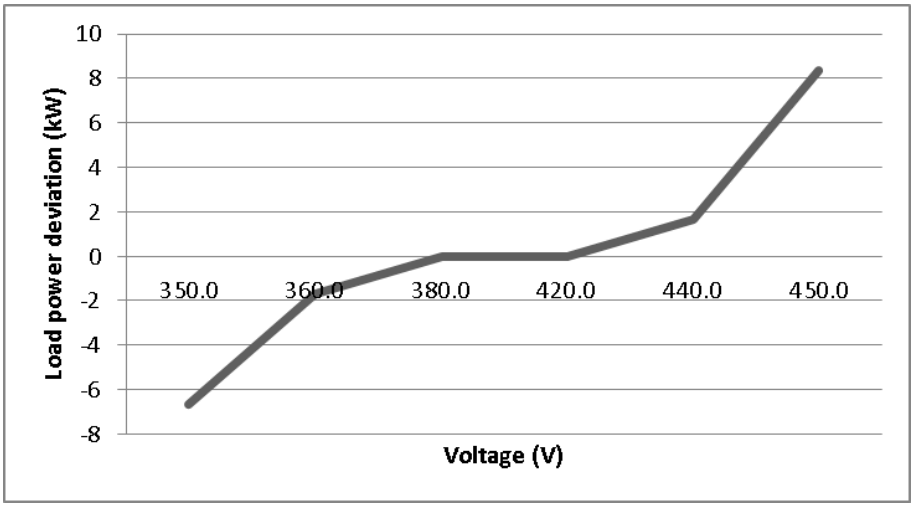

Figure 4.13: Control rule for the power response to voltage deviations.

The simultaneous action of frequency and voltage corrections allows that areas with voltage problems naturally provide less frequency regulation, which helps avoiding undesirable local voltage problems. The critical override condition is justified by the possibility that, as mentioned above, in some cases voltage problems require a response that demands a power deviation with a direction that is opposite to the one needed to react to a concurrent frequency event.

This two-segment reaction curve naturally defines two types of primary frequency regulation: the first one resembles conventional droop response of synchronous machines, while the second is similar (but in a continuous version) to the operation of load or generation shedding relays. If the penetration of flexible devices reaches important levels, the use of this controller results in the existence of two values for the network stiffness: the quasi-steady-state stiffness and the transient, or emergency, stiffness. This second is particulary relevant in the case of isolated systems or areas within large power systems that disconnect during and emergency (Microgrids [104]). For a high penetration scenario is important to mention that [105] finds potential stability problems for widespread implementation of frequency responsive devices because of the non-instantaneous propagation of frequency waves due to the existence of reactive components in the network. This means that when a power imbalance close to a power plant causes it to slow down, the frequency measured in a node several hundreds of kilometers from it will take an interval in the order of seconds to reflect it. This calls for a stability analysis and possibly to the need of including a power system stabilizer (PSS) in the responsive controllers.

It is proposed that the payments to storage devices for the provision of the mentioned services are computed in $\frac{\$}{\text{kWh}}$ for the available power and for the execution energy. For the power component, the following performance characteristics are taken into account differentiating between upwards and downwards adjustments:

1. **Hold time** Minimum guaranteed time that the regulation power offered can be sustained,

2. **Slew rate** Maximum rate of change of the power output of the storage device, differentiating upwards and downwards adjustments.

The price paid for the provision of frequency regulation could therefore be non-homogeneous across devices, being the highest for fast devices with long guaranteed hold times. However, it would be better if the operator of the power system can run separate auctions for different characteristics.

4.4.3.1 Peak-shaving

This service is offered in reference to an existing facility or group of facilities, and it consists in capping their net power to a pre-defined value as shown in figure 4.14 The revenue stream derived from this service is a potential reduction in the contracted capacity of the facility.

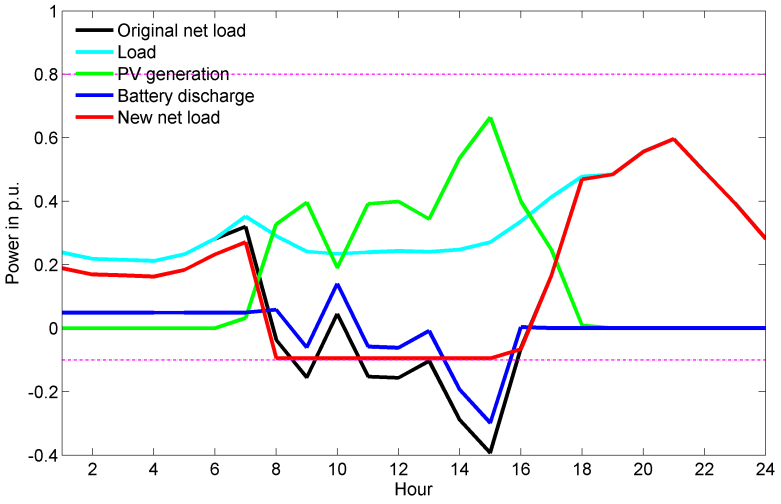

Figure 4.14

4.4.4 Decision making unit and service bundling considerations

Each one of the described services gives the BESS access to a revenue stream while at the same time it constrains the possibilities of the rest. For example, we have seen that the degradation processes have dual dependency from current intensity and state of charge. This means that when the state of charge is low, providing upwards frequency regulation is more costly than doing it at medium state of charge.

Another example is the participation in energy arbitrage and peak shaving. Suppose that the peak shaving service is being offered by a BESS connected to the LV network to a distribution company with the purpose of deferring the upgrade of a LV/MV transformer due to power flowing towards the LV network. If the transformer's peak consistently coincides with low energy marginal costs, the behavior that maximizes the energy arbitrage benefit will be at odds with the peak shaving service.

The role of the decision making unit (DMU) is dual:

1. To decide in advance about the allocation of the limited capabilities of the BESS to different services, which will henceforth be called storage service commitment or SSC. This process can happen at several moments before real time, and will depend on the required characteristics of the services. For example, a frequency response service may be contracted one day ahead, while a peak shaving one may require several months of compliance.

2. To correct in real time the planned operation in order to correct imperfect forecasts and simulations. When because of unforeseen reasons it is not possible to provide the ancillary services in the planned way, a procedure needs to be established to decide which one of them is going to be restricted. While the decision here could be contingent on the penalties for failing to deliver, it is proposed to establish a hierarchy where commitments with third-parties take precedence. A possible order of priorities is

   (a) Peak shaving

   (b) Frequency response

   (c) Primary frequency regulation

   (d) Voltage control

   (e) Secondary frequency regulation

   (f) Energy arbitrage

4.5 Remarks

This chapter has presented the formulations to represent, theoretically, battery energy storage systems in simulations at different time scales. The models described here are used as the foundation to include BESSs in the different methodologies described in the next chapter. Regarding the decision-making unit, an autonomous operation is assumed as opposed to a remotely-controlled one. In that case, the decisions can be either made the system operator or by an entity that aggregates several assets to provide system services, frequently termed *aggregator*.

Chapter 5

Integration with models for electric power systems

Our expectations over simulation and decision-support tools drive the selection of the models deemed adequate to represent physical components and control algorithms inside them. However, this selection is not obvious. Although it seems reasonable to impose that the complexity of the models should not exceed our understanding of the physical reality (software and hardware) of the system, the viewpoint that adding complexity can reveal emergent properties which can expand that understanding is also compelling. For instance, electrode kinetics and the growth of the solid-electrolyte interface layer could be represented, among others, through:

1. An empirical exponential relationship, which involves relatively small complexity and no understanding of the subjacent phenomena;
2. The Butler-Volmer equation, which is more complex and contains electrochemical understanding; or
3. Density functional theory (DFT), which is rather complex and implies an understanding of the materials in terms of quantum electrodynamics (with no electrochemical explanation whatsoever).

If the modeler is evaluating a particular technology and enough experimental data is available, the first approach in the list may be adequate to characterize lifecycle economics and to compare between control approaches, as done in [106]. The main drawbacks of this approach are that: a) it is not possible to map the parameters of the model to constructive parameters of the cell, and therefore to infer the characteristics that should be changed in order to improve the performance; and b) it is not possible to apply the results to evaluate other cells, even when the constructive parameters are similar.

The second approach requires a model of surface kinetics, whose parameters can be obtained through significantly less demanding experiments than the polynomial case. Since the parameters map directly to physical characteristics of the cell, it is possible to evaluate the benefits obtained from variations of them. For example, the surface area per unit volume a_s described in section 4.3.3.2 has a major influence in the appearance of a surface overpotential. This means that when simulations show that a given application is being constrained by this voltage drop component, a system designer can consider looking for a similar technology with a higher a_s value, or a cell researchers can choose a promising research direction to enhance the performance for the target application. An example of this was the development of electronically conductive phospho-olivines as lithium storage electrodes [107], which later became the commercial material Nanophosphate®described in [50]:

"Typical lithium-ion batteries store energy via a reaction between lithium ions and the cathode and anode material. The lithium ions are inserted or removed in active materials through a process called *intercalation*. However, these chemical reactions are generally slow, limiting the rate capability, or power output, of the battery. Thus, traditional lithium-ion batteries have high energy, but low power. Conversely, the chemical reactions created in the Nanophosphate®technology increase the cathode surface area with the electrolyte, which allows for faster lithium insertion and thus more power. At the same time, however, all of the bulk volume is still used to store energy, like other battery materials."

A123, the manufacturer of Nanophosphate®, found an initial commercial niche in battery powered tools, and later moved to electric vehicles and grid storage.

A deeper understanding of the physical processes in the electrodes allows for a computational approach to materials design. Diffusion, voltage and stability depend significantly on crystal structure. DFT has been successful in predicting the structure of materials and their stability, recently being used to computationally predict stable new electrode materials [108].

This chapter shows how the detailed model presented in the previous chapter can be used in two applications: a) the day-ahead use allocation of a BESS and b) the utilization of distributed storage to defer upgrades in distribution networks.

5.1 Formulation for day-ahead optimization

The operation of modern electric power systems benefits from preliminary decisions taken in advance. For example, if an offline generation unit takes 3 hours to be ready to inject power, the operator of the system has to know at least that time in advance that the unit will be needed. The decision-support tool used to plan in advance the dispatch is known as unit commitment or pre-dispatch. In the case of a BESS, although the start time is negligible, its ability to store energy and release it later makes it convenient to consider several time periods instead of just the present one when deciding about the operation of the BESS. The number of degrees of freedom of these devices and the variety of applications they can participate in makes them challenging from the pre-dispatch point of view ant it is reasonable to expect a variety of ways to formulate the decision-making problem, from expert rules to mathematical optimization. The latter approach is advantageous because:

- Expert rules are both difficult to obtain, and their performance mainly depends on the inventiveness of the rules-developer;
- Expert rules have an inherently constrained validity range. For example, if the BESS technology or the regulatory conditions change, a new rule may be needed, and there's no systematic procedure to do this;
- Optimization assures that the maximum possible value from the BESS is obtained.

However, optimization also has a number of drawbacks:

- It requires a forecast of the stochastic variables for the optimization interval;
- It requires more computational power;
- It requires more sophisticated algorithms.

For a particular system there will be a trade-off between both approaches, and this section presents a formulation appropriate for optimization. The reason for this is that the BESS model related expert rules can be understood to be embedded in the expert knowledge of the rule designer and hence implicit in the rule itself, however not directly recognizable[1].

5.1.1 Problem definition

It is evident that the formulation does not only depend on the representation of the BESS, but also significantly on the point of view of the optimization and on the characteristics of the system to which the battery is connected. In general, one is concerned with the maximization of the net value obtained, calculated as the difference between benefits and costs. Considering that the benefits are mostly context-dependent, the formulation presented in this section will focus on the representation of the BESS-related costs and the specification of the decision variables.

Consider an optimization window W to be a collection of n uniform periods p of duration d seconds each. For each period, the decision variables are represented by a vector $\boldsymbol{X_p}$ of real numbers:

$$\begin{aligned}\boldsymbol{X_p} = \{&Pref_p, H_p, DB_p^{UF}, DB_p^{OV}, kD1_p^{UF}, DB_p^{OV}, kD1_p^{UF}, kD1_p^{OF},\\ &kD2_p^{UV}, kD2_p^{OV}, Rmax_p^U, Rmax_p^D, PC_p^L, PC_p^G\},\end{aligned} \tag{5.1}$$

where:

[1] For example, a rule for a BESS in an isolated system may contain the statement: *when PV generation is less than the load, discharge the battery to meet the load. However, if the state of charge of the BESS is less than 0.2, restrict the discharge power to 50% of the nominal power.* The designer may have chosen this formulation to protect the battery from over-discharge damage, to minimize losses, to keep a reserve margin, etc., all of which are not explicit in the rule itself.

- $Pref$: Steady-state reference to for the power controller of the BESS. Note that it is not possible to pre-dispatch the actual power of the battery, which will be the results of control and physical variables that may not be directly controllable. This also applies to most of the decision variables described in the following paragraphs;
- H: Emulated inertia constant, corresponding to the rate of change of the angular speed of the fundamental frequency component of the voltage waveform for fast deviations between the expected power of the BESS and its real power. Physical parameters will mediate the actual inertial response of the device;
- DB^{UF} and DB^{OF} : No-reaction interval of the frequency controller in Hz for under-frequency and over-frequency;
- DB^{UV} and DB^{OV} : No-reaction interval of the voltage controller in V for under-voltage and over-voltage;
- $kD1^{UF}$ and $kD1^{OF}$: Droop constants for the low-risk frequency interval in p.u. Watt per p.u. Hertz;
- $kD2^{UF}$ and $kD2^{OF}$: Droop constants for the high-risk frequency interval in p.u. Watt per p.u. Hertz;
- $kD1^{UV}$ and $kD1^{OV}$: Droop constants for the low-risk voltage interval in p.u. Watt per p.u. Volt;
- $kD2^{UV}$ and $kD2^{OV}$: Droop constants for the high-risk voltage interval in p.u. Watt per p.u. Volt;
- $Rmax^{U}$ and $Rmax^{D}$: Constraint for the upwards and downwards power rate of change in p.u. Watt per p.u. seconds;
- PC^{L} and PC^{G} : Load and generation power caps, considering that the battery is controlling the net power flow from either a load, generator or prosumer.

5.1.2 Objective function

If it is possible to calculate the costs and benefits from the operation of the battery on each period independently, one would like to maximize the total benefits minus the costs for all the periods. Although this is not true in general since non-continuous coupling

between periods can occur[2]. Considering that those can be represented as a function F that operates over the results vectors, the general objective function has the form:

$$\text{OF} = F(\boldsymbol{S}, \boldsymbol{U}) + \sum_{p=1}^{n} \text{Benefits}(\boldsymbol{X_p}, \boldsymbol{S_p}, \boldsymbol{U_p}) - \text{Costs}(\boldsymbol{X_p}, \boldsymbol{S_p}, \boldsymbol{U_p}), \tag{5.2}$$

The functions that compute the costs and benefits on a per-period basis have as arguments: a) the decision vector $\boldsymbol{X_p}$, b) the state vector $\boldsymbol{S_p}$, and c) the context/input vector $\boldsymbol{U_p}$, which are structured as described in the following sections.

5.1.2.1 Context/input vector

Includes variables that are not influenced by the BESS and that influence the value of the objective function either directly (e.g., energy price) or indirectly (Like the temperature, through battery degradation or energy expenditure related to temperature control).

$$\boldsymbol{U_p} = \{Ta_p, f_p, v_p, \pi_p^{sell}, \pi_p^{buy}, \ldots\}, \tag{5.3}$$

where:

1. T_a : Ambient temperature in K;
2. f : Frequency of the fundamental voltage waveform in the connection point of the BESS in Hz;
3. π^{sell} : Remuneration for the energy injected by the BESS into it's connection point in $\frac{\$}{\text{kWh}}$;
4. π^{buy} : Expenditure for the energy withdrawn by the BESS from it's connection point;

[2]Examples of this are when the battery reaches the end of life within the optimization window, when a service constraint becomes active (e.g., the maximum number of times that the battery can fail to respond to a frequency regulation request) or when the result of the optimization is not physically implementable. The latter is less likely to happen when less approximations are used.

5.1.2.2 State vector

This set of variables describe the state of the battery and serve to couple different periods.

$$\boldsymbol{S_p} = \{Tb_p, \zeta s_{r,p}, \zeta e_{x,p}, \phi e_{x,p}, \phi s_{x,p}\}, \tag{5.4}$$

where:

1. Tb : Average temperature of the battery pack;
2. ζs : Concentration of the charge-transport species in the solid particles in the electrodes, assumed uniform for all the particles;
3. ζe : Concentration of charge-transport species in the electrolyte;
4. ϕe : Electric potential in the electrolyte;
5. ϕs : Electric potential in the solid phase;

It is also convenient to consider some calculation variables which, although can be calculated from the state, help express the state evolution in a more condensed way:

1. js : Electronic current density in the solid phase in the $\hat{\text{x}}$ direction;
2. je : Ionic current density in the electrolyte phase;
3. φ_s : Molar flow of species in the particles of the solid phase in the $\hat{\text{x}}$ direction.

5.1.3 State evolution

In numeric simulations, the evolution of the state can be calculated from the 1-D model presented in chapter 4 through a uniform discrete representation of space and time in steps of δx and δr meters and δt seconds. This section describes how to compute the state in period $p+1$ from the state in period p and the input vector in period p.

Step 1: Calculation of the open-circuit potential Let $\zeta_{\mathrm{Rs}}^{\max}$ be the maximum surface concentration of species in the spherical particles of radii Rs. Then, the open-circuit potential is obtained from the Nernst equation (4.12) as:

$$U_p^{cell} = \mathrm{U}_0^{\mathrm{cell}} - \frac{\mathrm{R}}{\mathrm{F}} \cdot T \cdot \ln\left(\frac{\zeta s_{Rs,p}}{\zeta \mathrm{s}_{\mathrm{Rs}}^{\max}}\right). \tag{5.5}$$

Step 2: Calculation of mass and charge flows

$$\begin{aligned} js_{x,p} &= -\sigma_s \cdot \frac{\phi s_{p,(x+\delta x)} - \phi s_{p,(x-\delta x)}}{2 \cdot \delta x} \\ je_{x,p} &= -\sigma_e \cdot \frac{\phi e_{p,(x+\delta x)} - \phi e_{p,(x-\delta x)}}{2 \cdot \delta x} \\ \varphi_{r,p} &= -D_s \cdot \frac{\zeta s_{p,(r+\delta r)} - \zeta s_{p,(r-\delta r)}}{2 \cdot \delta r} \end{aligned} \tag{5.6}$$

Step 3: Calculation of the reaction overpotential Applying logarithm to both sides of the Butler-Volmer equation (4.16) and considering the dominant reaction only yields:

$$\ln(i) = \ln\left(\mathrm{a_s} \cdot j_0 \cdot \mathrm{V_e}\right) + \frac{\alpha \cdot \nu_r}{v_T} \tag{5.7}$$

Where $\mathrm{V_e}$ is the total volume of the electrode. Solving for the reaction overpotential ν_r yields:

$$\nu_r = \frac{v_T}{\alpha} \cdot \ln\left(\frac{i}{\mathrm{j_0} \cdot \mathrm{a_s} \cdot \mathrm{V_e}}\right) \tag{5.8}$$

Step 3: Update concentration

$$\begin{aligned} \zeta s_{r,p+1} &= \zeta s_{r,p} + (\varphi_{r+\delta_r,p} - \varphi_{r-\delta_r,p}) \cdot \delta_{\mathrm{t}} \\ \zeta e_{x,p+1} &= \zeta e_{x,p} + (je_{x+\delta_x,p} - je_{x-\delta_x,p}) \cdot \delta_{\mathrm{t}} \end{aligned} \tag{5.9}$$

Step 4: Calculation of the potential in the solid and electrolyte phases

$$\begin{aligned} \phi s_{p,(x+\delta \mathrm{x})} &= \phi s_{p,(x-\delta \mathrm{x})} - \frac{j s_{x,p}}{\sigma_s} \cdot \delta \mathrm{x} \\ \phi e_{p,(x+\delta \mathrm{x})} &= \phi e_{p,(x-\delta \mathrm{x})} - \frac{j e_{x,p}}{\sigma_e} \cdot \delta \mathrm{x} \end{aligned} \tag{5.10}$$

Calculation of the terminal voltage and losses

$$v_p = \phi s_{p,x_{max}} - \phi s_{p,0} \tag{5.11}$$

$$L_p = (v_p - U_p^{cell}) \cdot i_p \tag{5.12}$$

Heat exchanged with the environment

$$Q_p = (\mathrm{Ta}_p - T_p) \cdot h0 \tag{5.13}$$

Temperature update

$$T_{p+1} = T_p + \frac{L_p + Q_p}{\mathrm{cp}} \tag{5.14}$$

Stress parameter

$$S_p = \begin{cases} \beta_2 \cdot I_p \cdot \left(1 - \frac{Cs_{Rs,p}}{\mathrm{Cs}_{\mathrm{Rs}}^{\max}}\right) & \text{if } I_p > 0 \\ \beta_3 \cdot I_{ion}(t) \cdot \frac{Cs_{Rs,p}}{\mathrm{Cs}_{\mathrm{Rs}}^{\max}} & \text{if } I_p <= 0 \end{cases} \tag{5.15}$$

Electrode degradation

$$\mathrm{Sa}_p = \mathrm{Sa}_{p-1} - exp\left(\frac{\mathrm{Sa}_{p-1} - \beta_1}{k \cdot \frac{T_p}{T_0}}\right) \cdot \delta \mathrm{t} \tag{5.16}$$

5.1.3.1 Solution methods

These expressions are used to compute the evolution of the state of the battery, which on each particular study is used to compute costs and benefits. Because the formulation

contains discontinuities and non-linearities, the optimization problem cannot be solved directly and the optimality conditions for the solution cannot be verified. In practice, one approach that strikes a reasonable trade-off between computing time and the quality of the solution is the use of meta-heuristics such as the evolutionary particle swarm optimization (EPSO) algorithm, as described in section 6.4.

In some applications, the day-ahead utilization problem is used as a sub-routine in planning algorithms. For example, if the problem involves determining simultaneously the sizes of the battery, diesel generator and photovoltaic panels for an isolated system, the cost results from the optimal operation, for a relevant sample of intervals, of a given combination of component sizes become part of the objective function of the planning stage. Typically, solving the planning problem involves a large number of objective function evaluations and therefore the execution time of each of them becomes relevant. The experiments carried out throughout this thesis revealed that although meta-heuristics can solve the problem fast enough to calculate day-ahead setpoints more than once a day, the execution time is excessive to be a viable alternative in planning applications. However, if the sample of intervals is small and the planning problem is found to be well behaved (i.e., unlikely to have discontinuities or local minima) local methods that look at the steepest-descent direction can be used in combination with meta-heuristic operational optimization. During the course of this research, meta-heuristics at both the planning and operation level were also used, with partial success. This approach may be adequate when the planning problem is not well-behaved.

The following section explains how the battery can be simplified to represent it in operational optimization problems to be solved through mixed integer linear programming (MILP) methods.

5.1.4 Formulation for the resolution through mixed-integer linear programming (MILP) methods

Since pumped-hydro energy storage dominates large electric power systems, the representation of electrochemical storage devices in pre-dispatch algorithms used therein has not been given much attention. In contrast, in distributed energy systems (DES) the battery is often times the only means to store electricity. Given the large number of decision variables in the optimization problem and the non-continuous nature of

decisions such as the availability of thermal power plants, makes inviable to solve the problem using an exact representation of the components. Techniques grouped under the term *mixed integer linear programming* allow for an efficient search of the feasible space to obtain a solution which is within a known maximum distance from the true optimal solution. Although the explanation of these techniques is beyond the scope of this Thesis, and approximate formulation to represent electrochemical accumulators in them is presented in this section.

5.1.4.1 Energy balance

The non-linear voltage-current relationship is not compatible with MILP, and therefore the state of charge needs to be expressed in kWh instead of Ah.

Let's begin by defining E_{max} to be the maximum storage capacity of a battery in kWh, E_p as the energy stored at the beginning of period p, PC_b and PC_p as the average power leaving the battery during period p in kW, and P_l as the average power of the losses during period p. Then, for an analysis interval of duration δt small compared to the lifetime of the battery:

$$E_{p+1} = E_p - (P_b + P_l) \cdot \delta t. \tag{5.17}$$

$$SOC_p = \frac{E_p}{Emax} \tag{5.18}$$

5.1.4.2 Power limits

There are two reasons to limit the charge or discharge rate of a battery in a simulation model:

1. The device has physical limitations such as the fact that when ionic density in the SEI is low, the over-potential related to electrode kinetics causes the terminal voltage to collapse. This implies that regardless of the power setpoint at the level of power electronics, the cell will limit the power that can be injected or extracted.

2. Battery life. As explained in chapter 2, side-reactions are present in most battery technologies, and their speed is controlled mainly by the temperature and by deviations from an equilibrium potential.

In a MILP formulation, the voltage of the battery is not an accessible quantity, and therefore cannot be used to represent the first consideration. Regarding degradation, the underlying mechanisms are also non-linear function in terms of internal variables not present in this simplified model. One possibility to overcome these difficulties is to represent both of them through linear approximations taken from the exact model.

Physical power limits are mainly a function of the state of charge and recent history. The mathematical form of the part corresponding to the state of charge is, following the Butler-Volmer equation, exponential as in figure 5.1.

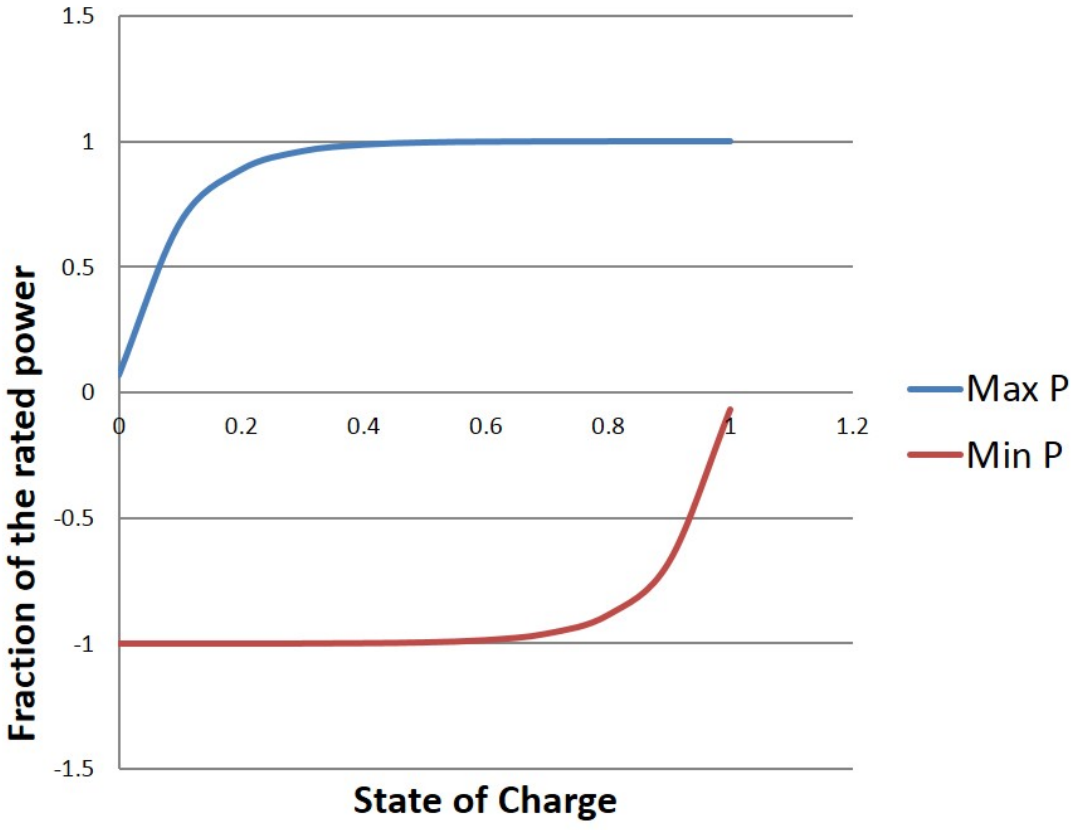

Figure 5.1: Representation of the physical power limit of the battery.

According to the KiBaM model, the relevant state of charge has to be calculated taking into account the diffusion processes inside the battery. Following this, let's define the auxiliary variables $E1$ and $E2$, which are calculated through the following equations:

$$\begin{aligned} E1_p + E2_p &= E_p \\ E1_{p+1} = E1_p - Pb_p - Pl_p + \frac{E2_p - E1_p}{k_e} \\ E2_{p+1} = E2_p - \frac{E2_p - E1_p}{k_e}, \end{aligned} \tag{5.19}$$

where k_e is a dimensionless diffusion coefficient. Curves similar to the one shown in figure 5.1 can also be used to approximate the degradation equation 4.28 and the losses, with the added complexity that the quantities not only vary with the state of charge, but also with the current and temperature. In all cases, the curves need to be decomposed into linear sections, and auxiliary or binary variables are necessary to select the adequate section. The next section illustrates how to proceed for the case of discharge losses. The other cases can be formulated using the same procedure.

5.1.4.3 Energy losses

A reasonable approximation to energy losses is to consider a polynomial dependency with respect to the discharge power and an exponential one with the state of charge. This can be summarized in the set of curves shown in figure 5.2. Each curve on the figure represents the polynomial relationship for a given state of charge. Under the assumption that during one period the state of charge does not change significantly, only one of the curves is relevant for each period. The following equations intend to be generic for other variables (power limits, degradation, etc.), and hence the variable x is used instead of output power, and the variable y instead of the state of charge.

Let x be a continuous variable defined over the interval $[\underline{\mathrm{x}}, \overline{\mathrm{x}}]$ and let's define a partition.

$$\text{Part} : \{\mathrm{x}_0 = \underline{\mathrm{x}} < \mathrm{x}_1 < \cdots < \mathrm{x}_\mathrm{i} < \cdots < \overline{\mathrm{x}} = \mathrm{x}_\mathrm{n}\}. \tag{5.20}$$

Also, consider the activation function $u = \{u_j,\ j = 1 \cdots \mathrm{n}\}$, where n is the number of curves.

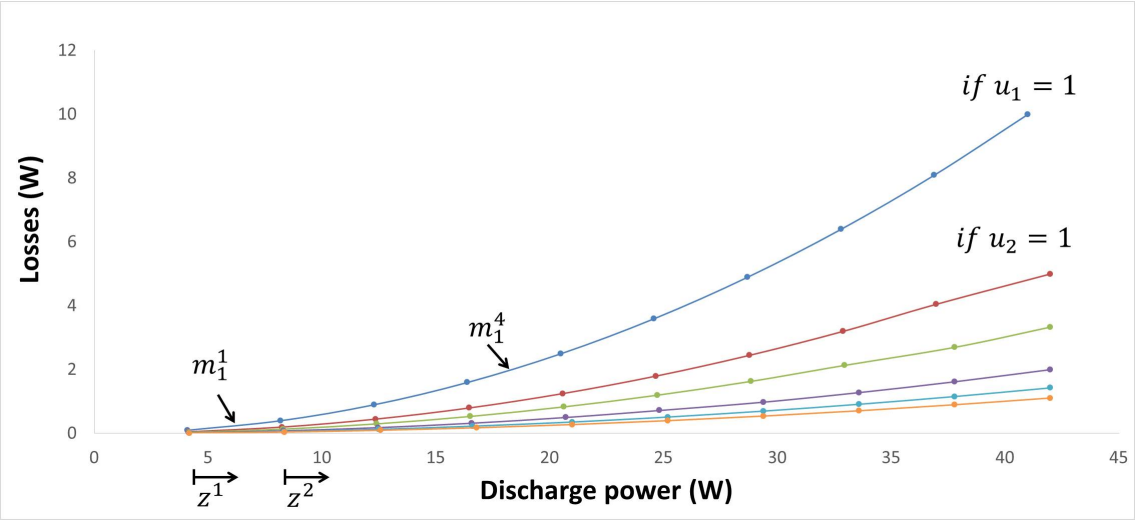

Figure 5.2: Representation of the losses of the battery.

$$u_i = \begin{cases} 1 \Leftrightarrow x \in [x_{i-1}, x_i[\\ 0 \Leftrightarrow x \notin [x_{i-1}, x_i[\end{cases} \tag{5.21}$$

For the case of the losses, the variable x corresponds to the state of charge. The binary variables respect the following constraints:

$$\begin{gathered} \sum_{i=1}^{n} u_i = 1 \\ x \leq \sum_{i=1}^{n} x_i \cdot u_i \\ x \geq \sum_{i=1}^{n} x_{i-1} \cdot u_i \end{gathered} \tag{5.22}$$

To calculate the losses, auxiliary variables z are used to represent the output power in m intervals:

$$
\begin{aligned}
P_{loss} &\leq \sum_{i=1}^{n} z_i \cdot m_i^1 + K_{loss} \cdot (1 - u_1) \\
P_{loss} &\geq \sum_{i=1}^{n} z_i \cdot m_i^1 - K_{loss} \cdot (1 - u_1) \\
P_{loss} &\leq \sum_{i=1}^{n} z_i \cdot m_i^2 + K_{loss} \cdot (1 - u_2) \\
P_{loss} &\geq \sum_{i=1}^{n} z_i \cdot m_i^2 - K_{loss} \cdot (1 - u_2) \\
&\vdots \\
P_{loss} &\leq \sum_{i=1}^{n} z_i \cdot m_i^n + K_{loss} \cdot (1 - u_n) \\
P_{loss} &\geq \sum_{i=1}^{n} z_i \cdot m_i^n - K_{loss} \cdot (1 - u_n) \\
P_d &= \sum_{i=1}^{n} z_i
\end{aligned}
\tag{5.23}
$$

This formulation was used to incorporate a battery in the microgrid energy management system described in a master thesis supervised by the author [109].

5.2 Formulation for distribution grid expansion and impact studies

Historically, the most extended practice is to design passive distribution networks prepared to cope with a certain worst-case scenario, mainly in terms of voltage drops under maximum load. When an unexpected situation happens, like a high penetration of PV generators on a feeder, network reinforcements, voltage regulation equipment or operational constraints are applied. More recently, active network management has emerged as an attractive solution, including on-line feeder reconfiguration, dynamic protection

settings and coordinated Volt/VAR control [110]. At the same time, demand-side management (DSM) has re-emerged as a tool able to improve the optimal functioning of power systems and simultaneously contributing to the integration of renewables [111–114].

In a smart grid context, another option to integrate VERs is the use of storage systems [115–117], and in particular battery energy storage systems (BESS). Recently, the value of these devices in distribution networks has been widely discussed, in part because of the prospect of a large number of electric vehicles in the future [87]. Also, having a substantial amount of energy storage connected to the grid can have other benefits, for example by decreasing both the ramping requirements and number of starts for thermal units participating in frequency control, which would also represent additional revenue streams for the owner of the storage asset. Regarding stationary BESS, several techniques have been proposed to determine their optimal operation [118–121] optimal placement [122] and value [110, 123, 124]. While these studies provide very useful insights and tools to support the design and evaluation of storage solutions for distribution networks, we identify two shortcomings that impede a cost/beneffit analysis for their large scale introduction:

The results are specific to the case studied. Distribution networks are diverse in terms of, for example, topology, load magnitude, dispersion and load profiles. Therefore, a judgement about the convenience of energy storage over other solutions for renewable energy integration that can guide policy requires an statistical approach with sensitivity analysis. A second driver of diversity is the amount of distributed generation as a proportion of the load.

The battery models used cannot explain the effect of operation over useful life. This limitation prevents the determination of a realistic cost of ownership or annuity of the storage solution since the battery replacement frequency is unknown.

5.2.1 Battery sizing and control

To estimate the benefits and costs derived from the introduction of energy storage, we need to define: 1) the characteristics of every storage asset in the system; and 2) the

way each storage asset is operated. This section explains the calculation process for both using Figure 4.14. We begin defining some parameters that are common for all the assets. The basis for all the parameters in p.u. is the annual maximum load of each customer.

- Upper net-load power limit, P_{ub} in p.u. ;
- Lower net-load power limit, P_{lb} in p.u. ;
- Charging efficiency of the storage asset, Eff_{in} ;
- Discharging efficiency of the storage asset, Eff_{out} ;
- Usable fraction of the storage asset, E_{usable}.

Using these parameters and the yearly net hourly load profile for a given customer, we need to define:

- Hourly storage power profile, $P_{storage}$;
- Nominal storage energy storage capacity, E_{nom} ;
- Nominal storage power, P_{nom}.

Imposing that every day the state of charge in hour 1 has to be the same as in hour 24, the problem is divided into 365 sub-problems[3]. Each of these is solved by minimizing the required storage energy subject to power limit constraints. Let P_{net} and $P_{storage}$ be 24-hour power profiles for the net load and the storage utilization, then we solve:

[3]This constraint is most-likely sub-optimal, but is good enough to produce reasonable results as will be shown in the case study described in section 6.2. Alternatively, one could impose that the final state of charge is a function of the expected conditions of the next day.

$$\underset{P_{storage}}{\text{minimize:}}$$

$$f(P_{storage}) = \frac{SOC_{max}(P_{storage}) - SOC_{min}(P_{storage})}{E_{usable}}$$

subject to:

$$max(P_{net} - P_{storage}) \leq P_{ub};$$

$$min(P_{net} - P_{storage}) \geq P_{lb};$$

$$averageP_{storage} = 0;$$

$$SOC(1) = SOC(24).$$

The result from the optimization corresponds to the power setpoints of the battery. Note that the restriction over the average storage power implies an initial assumption of unitary storage efficiency, done to simplify the optimization problem. To correct for this we add a constant charging power to the optimal profile. The necessary energy storage capacity of the battery for each day is obtained directly from the value of the objective function, and the necessary power is obtained from the profile:

$$E_{nom} = max_{year}\left(\frac{SOC_{max}(P_{storage}) - SOC_{min}(P_{storage})}{E_{usable}}\right) \tag{5.24}$$

In other words, the necessary storage capacity to be installed will be the minimum value that meets the daily energy requirement for all the days in the year. In a similar fashion, the rated power of the device has to be able to meet the maximum instantaneous value for all the year:

$$P_{nom} = max_{year}\left(|P_{storage}|\right) \tag{5.25}$$

As will be shown in the case study of section 6.2, imposing perfect compliance for year one does not imply that this will be the case later in the life of the battery, because of capacity-fade. The optimal size of the battery will therefore related to acceptable quality of the service provided. Although the determination of this value is out of the scope of this dissertation, the proposed model can be used to evaluate different sizing criteria.

5.2.2 Performance simulation

The simple model and optimization procedure presented in the previous section is necessary since the application of storage to distribution networks usually involves several hundred devices. To verify that the expected performance is technically feasible, the operation needs to be verified using the full model. When the results of both models differ more than an allowable threshold, some strategic parameters can be adjusted:

- Increase the number of segments in the piece-wise representation of nonlinear functions, or change the limits of the segments (non-uniform sampling);
- Decrease the simulation and/or optimization time steps;
- Establish hard constraints to prevent problematic operation zones. An example of this is to change the minimum discharge level in the optimization step.

5.3 Remarks

This chapter has shown how features of the battery model described in chapter 4 can be integrated into models to answer questions related to the operation and planning of electric power systems at three levels: a) a non-linear models for simulation and heuristic optimization, b)a linear model for optimization, c) a methodology to assess the utilization of distributed battery energy storage. The application cases in chapter 6 illustrate how different studies can benefit from the incorporation of greater physical detail in the BESS model, revealing advantages compared to more simplified approaches.

Although the non-linear models explained in this chapter already are a simplified version of those explained in chapter 4, their level of detail is still greater that what is needed in the applications of chapter 6, where the relevant simplifications are explained. The linear model described this chapter was not used on any of the case studied, partial results were reported in [109].

Chapter 6

Application cases

6.1 Overview

Modelers, including the author, can easily spend a significant amount of time accounting for the endless details in the objects and situations being studied, but that doesn't necessarily means that they neither will get much practical benefit from that effort, nor that it will be useful to run simulations more effectively. The practical benefit aspect is related to the ability to make decisions, since there will likely be a point after which, although modeling improvements may change the results obtained, they will not impact decisions at any level or provide any additional insight. The usefulness objection can be sustained on computational grounds (more accuracy in general requires smaller time steps, more mathematical operations and more memory) and, perhaps more importantly, on input data intensity since the extraction of model parameters for a given real component requires extensive testing and computation.

This chapter presents some applications to show that the level of detail in the proposed models actually leads to changes in decisions and to insights which can be useful when designing systems that include battery energy storage. The next three sections go through selected case studies to show how the models and methodologies developed throughout the Thesis can help study applications of battery energy storage in electric power systems.

The first case study is about the use of batteries to support the integration of photovoltaic generation in distribution networks. The analysis is separated in three parts:

First, a methodology to quantify the impact of PV generation over distribution networks is explained and used to establish a baseline. Then, the model and methodology presented in section 5.2 is used to determine the size and daily operation of several BESSs to provide peak-shaving and valley-filling, obtaining preliminary yearly battery utilization profiles. Finally, the lumped-parameters version of the model proposed in section 4[1], is used to verify the operation of the battery until its end of life.

The second case study adds the frequency regulation module described in section 4.4.3 to study the dependency between reaction parameters and the cost of use of the battery for a BESS. The power system to which the BESS is connected is represented by an historical frequency signal. In contrast with the previous case, here the service simulation and the cost of use is calculated simultaneously.

The third case study combines the lumped-parameters nonlinear model with the EPSO meta-heuristic to study the optimal combined operation of a residential BESS an electric vehicle and a set of domestic appliances under different tariff schemes.

With the exception of the RNM, all the simulations were implemented in Matlab version 2013.

6.2 Case 1: Distribution network planning under high penetration of variable energy resources

Most distribution networks are designed to maintain the quality of supply to final customers considering that the load on each be anywhere between zero and a positive number. Distributed generation, in particular non-controllable one like photovoltaic, affects these expected power flow patterns, causing various well-documented problems that drive relevant upgrades and modifications to maintain an acceptable service and also have an influence in the magnitude of the energy losses. Using the methodology explained in section 5.2, this section investigates how energy storage can reduce these impacts.

[1] see Appendix B.

6.2.1 Case description

The number of grid-connected photovoltaic (PV) systems has exploded in the last decade [125, 126], imposing new operational regimes on networks which were designed to passively allow for the flow of electric power from large generation facilities towards consumers. Of the nearly 70 GW of nameplate PV capacity in Europe, it is estimated that 96% is connected to the distribution network in either medium voltage (MV) or low voltage (LV), and the size of each system ranges from a few kilowatt peak (kW_p) in LV up to 5 MW_p in MV [126]. In the residential sector the share of electricity produced based on renewables has been increasing, mainly due to the economic incentives and the availability of new technologies [127]. This concentration of PV generation in the lower voltage levels is the motivation for studying its economic impact on distribution systems and the feasibility of reducing the overall integration cost through energy storage devices.

There are several studies [128–132], facts and forecasts [133] that confirm the cost drivers associated with distributed PV for many particular cases. Also, the need for new analysis tools has been recognized [134–136], for a revision of the methods used to calculate the allowed remuneration of distribution companies, as well as for new methods to calculate the network chargers to the users of the infrastructure [137–139]. The published studies have analyzed the problem either looking at a few characteristic feeders or through stakeholder surveys. Quantifications like the maximum theoretical hosting capacity of a feeder and information about actual costs incurred by utilities provide valuable data points to guide policy decisions.

In most systems, the users of the electric network pay a network tariff that is calculated taking into account not only the cost of the particular feeder where they are connected but also a wider collection of infrastructure in the surrounding area. This implies that the cost-tariff relationship is diffuse, since the causal loop is closed under aggregation, hence making it difficult to allocate payments based strictly in cost-causality. Another factor that adds to this indetermination is the lumped nature of network investments. For example, consider a 50 kW distribution transformer serving 40 loads which reaches full capacity at some periods. If one of the loads increases its rated power (e.g., a bakery buys a second oven), the distribution company may have to replace the transformer for another with higher capacity. Since transformers only are manufactured in so many

sizes, and sice the replacement process involves fixed costs which are independent from the rating such as installation and testing, the DisCo will probably opt for a 75 kW transformer that will be enough to accommodate load increases for another 10 years. Although one could argue that customer 41 is driving this investment, allocating the cost to him will usually be perceived as unfair.

6.2.2 Methodology

In order to estimate the value of energy storage as a component of distribution network, it is first necessary to compute a baseline scenario where storage is not present, and then calculate the savings derived from its introduction.

A model-based approach is used to explore and illustrate the link between the future introduction of PV generation in distribution networks and all the costs related to the power distribution function from an aggregate point of view. Subsequently, the value of distributed energy storage as an integration strategy is calculated using the methodology in section 5.2 to size and operate the devices, and a simplified version of the model described in chapter 4 is used to assess their lifetime performance. The argument has eight parts:

1. *Definition of the Consumer Space*: Select a set of parameters that conveniently represent the diversity of clusters of consumers regarding their location and load profiles (See figure 6.1). Subsequently, assign values to the selected parameters in order to obtain a representative sample of the space;

2. *Design of host networks*: Determination of the topology and equipment that would realistically be used to provide a pre-defined quality of service to the customers in the network space sample and its costs;

3. *Formulation of PV integration scenarios*: Formulate assumptions about the introduction of PV generators in the future scenario in terms of capacity and location. This involves also the determination of the typical PV power production profiles (See figure 6.1);

4. *Calculation of baseline new distribution and losses costs*: Determine the network reinforcements that would be required to maintain the quality of service for each integration scenario and its costs, assuming that storage is not used;

5. *Storage allocation and control*: Define a number of storage introduction scenarios and the storage operation rule;

6. *Calculation of distribution and losses cost for different storage scenarios*: Re-calculate the network reinforcements required to maintain the quality of service, for each storage introduction scenario, and their cost;

7. *Calculation of storage utilization profiles*: For each storage scenario, calculate the yearly utilization profile;

8. *Calculation of storage lifetime*: Assuming that a particular Lithium-ion battery type is used as storage media, estimate the capacity loss as a function of time and calculate the expected time to the end of life;

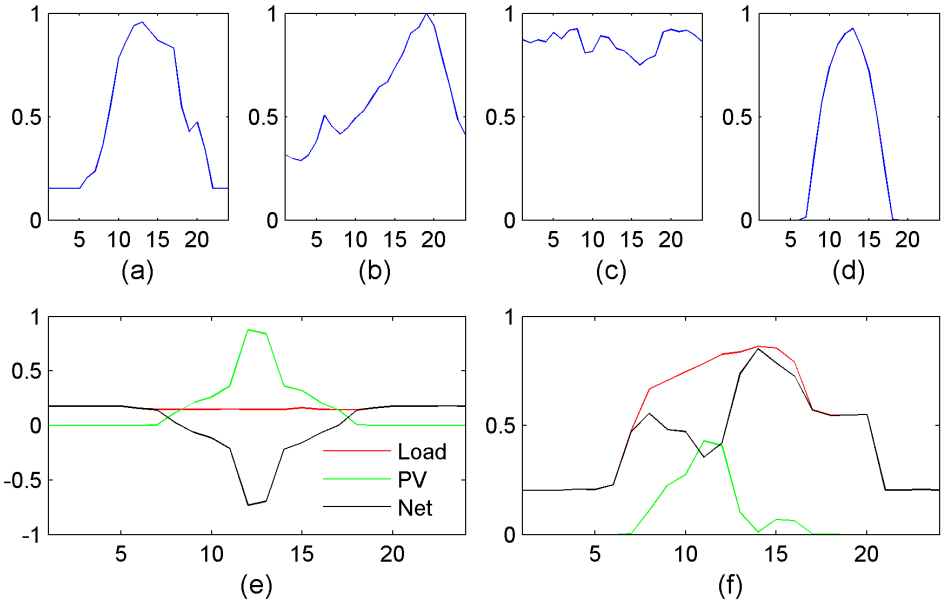

Figure 6.1: Example for typical hourly power profiles for PV generation (d) and different types of loads: commercial (a), residential (b) and industrial (c). Specially in the case of PV, the profile can change significantly between days. For example, (e) shows, for a particular customer, a day where the net injection is maximum, and (f) shows the one of maximum net load.

Distribution networks are at least as diverse as the places they serve, and different companies have come to their own engineering and design practices through studies and trial-and-error processes, conditioned by the local availability of products and services.

Therefore, establishing a relationship between a change in the characteristics of the users of the network, like the introduction of PV systems on rooftops, and its impact on distribution costs and losses is complex if general results are sought. For this reason we chose not to study a few existing systems, but instead to build, via simulation, several prototype networks with different characteristics, designed to cover a wide range of network types. In general, the configuration of a particular network will be conditioned by the users therein. The following section explains how populations of customers are created.

6.2.2.1 Consumer space

Two characteristics that vary across locations are considered: 1) the electricity consumption characteristic; 2) the relative geographical location of consumers. To represent the variability in both, the following procedure is followed[2]:

1. The 6 locations in the United States shown in Figure 6.2 are chosen. The sampling criterion is to be representative in terms of insolation and latitude;
2. For each location, two areas with different population densities are selected (Table 6.1;
3. Values for the parameters in Table 6.2 are determined from demographic information and used to create a population of consumers;
4. The created consumption points are given relative geographic locations. This is done using the street map of the chosen cities as scaffold.

State	Low density	High density
Connecticut	Torrington	Hartford
Texas	San Marcos	Austin
California	Lancaster	Los Angeles
Washington	Covington	Seattle
Colorado	Eaton	Boulder
Iowa	Altoona	Des Moines

Table 6.1: Reference locations for the synthetic networks

[2]For details about the base networks used for the study, see Appendix C.

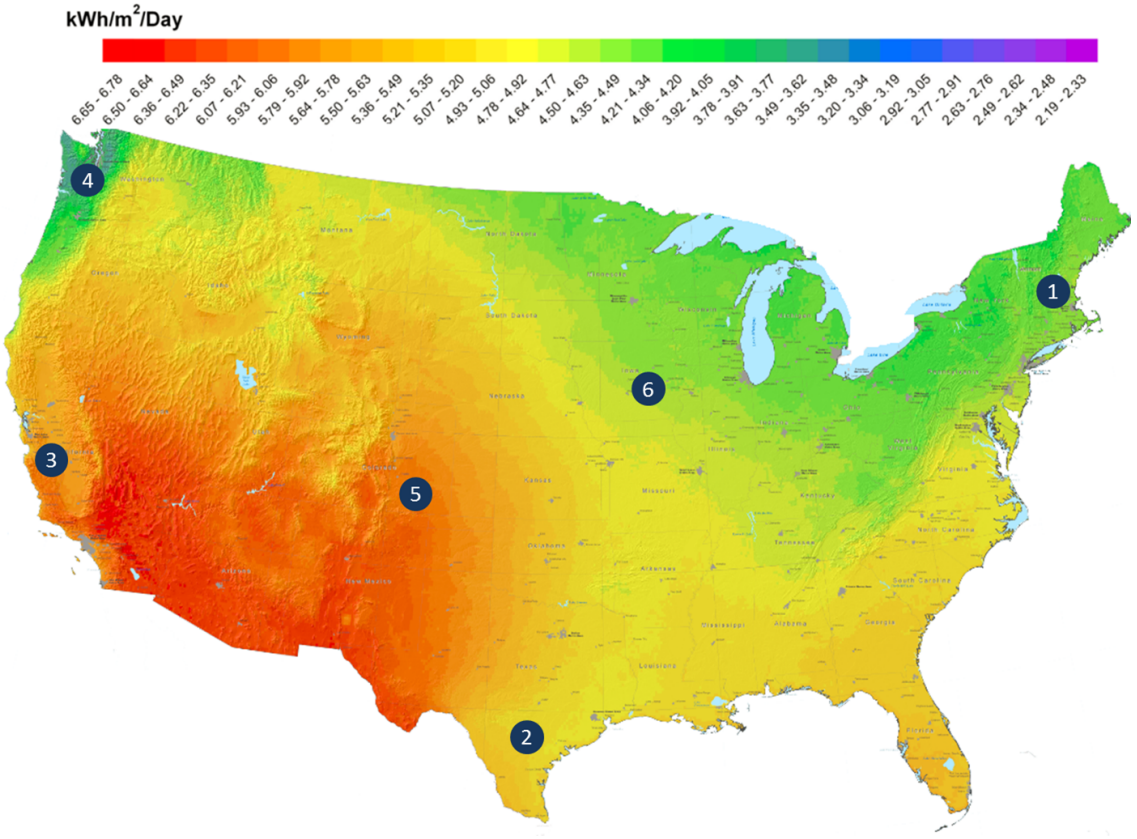

Figure 6.2: Irradiation map of the United States and the selected locations for the study (NREL, data from 2006 to 2009)

Nomenclature	Description	Unit
Dl_j	Load power density	$\frac{kW}{km^2}$
$\overline{PL_j}$	Load average peak power	kW
$\overline{PFL_j}$	Load average PF	p.u.
σPL_j	Load StDev power	p.u.
σPFL_j	Load StDev PF	p.u.
Ind_j	Industrial profile share	p.u.
Com_j	Commercial profile share	p.u.
Res_j	Residential profile share	p.u.

Table 6.2: Example for a set of parameters that define the load space, the index j refers to the voltage level: 1=LV; 2=MV; 3=HV.

6.2.2.2 Generation of load sets

The translation of the values in Table 6.2 into individual loads deserves further explanation. Each load is defined by its 1) maximum power; 2) average power factor; 3) typical daily active and reactive power profiles. For each location l The number of customers connected to each voltage level is calculated as:

$$nLoads_{j,l} = \frac{A_l \cdot Dl_{l,j}}{\overline{PL_{j,l}}} \tag{6.1}$$

The maximum power, power factor and annual energy consumed are:

$$P_{i,j,l} \sim N\left(\mu P_{j,l}, \sigma P_{j,l}\right) \tag{6.2}$$

$$PF_{i,j,l} \sim N\left(\mu PF_{j,l}, \sigma PF_{j,l}\right) \tag{6.3}$$

Next, the daily profile of electricity consumption is defined considering three basic load types: residential, commercial and industrial. Residential and commercial load profiles are obtained from the simulation of a set of standard building types [140] using the simulation software Energy Plus [141] using TMY3 [142] weather data for the 6 selected locations. Simulations results for all TMY3 locations are publicly available [143]. Since industrial profiles are very dependent of the particular process they supply, we assumed a nearly-constant consumption with 10% hourly variability. Figures 6.5(a), 6.5(b) and 6.5(c) show example profiles for the three load types.

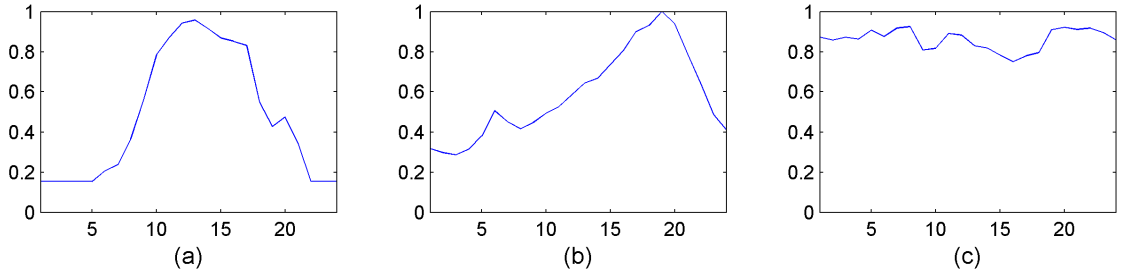

Figure 6.3: Example residential(a), commercial(b) and industrial(c) load profiles.

Load placement Street maps of each location are used as scaffold to assign relative geographic locations to the loads. For example, Figure 6.4b shows the resulting viable connection points after processing a street map of the area around Torrington. constraining the existence of connection points only along the streets with equal probability per unit of street length.

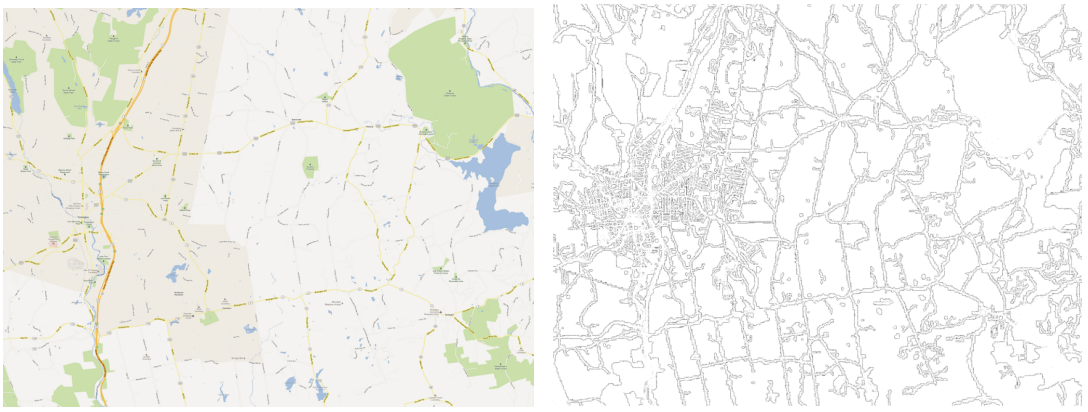

(a) **(b)**

Figure 6.4: Viable load and generation connection points (b) obtained from a street map (a).

Each viable point from the image has associated an index from 1 to N. To associate indexes with customers, a sequential uniform integer random sampling without replacement is used

$$I_i = U(\{1...N\} - \{I_1...I_{i-1}\}) \tag{6.4}$$

The design of the network is using a Reference Network Model (RNM), which was developed by IIT researchers, and later adopted by the Spanish regulator, with the approval of the Spanish distribution companies. A detailed explanation of how the model works can be found in [144]. This model emulates the engineering design process of a DisCo, and it specifies all the components between the transmission substation and the final customers that compose the minimum cost network which respects power quality constraints. The RNM is able to do *greenfield* and *brownfield* network planning. In the former, the maximum power on each connection point is used in conjunction with simultaneity factors to create the base network. The latter is used to determine the required modifications to maintain the quality of service in the face of changes in the load/generation characteristics of the users of the network and the appearance of new ones. The base networks are created using the information about the location and electric characteristics of the load together with a standard file that contains technical and cost information about the equipment and other strategic parameters. Similar studies to the one described here, wi for PV penetration have been done by researchers at IIT and MIT, although without distributed storage.

6.2.3 Study of energy share scenarios

Taking the 12 load-only networks as the reference case, the consequences of supplying a portion of the load with distributed PV generation are evaluated. The energy share is chosen instead of the penetration (maximum fraction of the power that is supplied by PV) as independent variable because it is directly related to the value that the system gets from the existence of the devices. Eight values of energy share are simulated for each one of the baseline networks. The dependent variable will be the sum of the additional network costs required to maintain the quality of service and the cost of the additional losses caused by the presence of PV generation.

6.2.3.1 Formulation

It is considered that PV generators can be connected either to LV, MV, or HV. A single study case involves an assumption about the amount of PV that is going to be connected and its distribution among voltage levels. For LV and MV, it is assumed that the generators are going to be associated to existing customers, and the rule used to match customers with generators was to minimize the net power at the time of maximum PV generation. For the ones connected to HV, their location was constrained to a number of pre-defined places in the map. The size of all the generators was obtained randomly from a gaussian distribution with different mean and standard deviation for each voltage level. The parameters used to define one energy share scenario are listed in Table 6.3. The determination of the total installed capacity to be shared among the generators is a function of the desired energy share and the capacity factor of the location:

$$P_{total} = \frac{Load_{year} \cdot eShare}{CFG} \tag{6.5}$$

Starting with the information from the scenarios, the existing connection points are modified and new ones are created. Since the PV generation is expected to occur in some (non-specified) future, a 2 % increase in the load is assumed. Other values of demand growth between 0% and 30% were tested, and it was determined that this assumption doesn't affect qualitatively the results.

Nomenclature	Name	Unit
$\overline{PG_j}$	PV average power	kW
$\overline{CFG_j}$	PV average capacity factor	p.u.
$\overline{PFG_j}$	PV average PF	p.u.
σPG_j	PV StDev power	p.u.
σCFG_j	PV StDev capacity factor	p.u.
σPFG_j	PV StDev PF	p.u.

Table 6.3: Set of parameters that define a penetration study case, the index j refers to the voltage level: 1=LV; 2=MV; 3=HV.

6.2.3.2 Determination of the new costs

The determination of the new costs is done using the RNM in brownfield mode. Since the electrical impact of PV generators is related to their power profile, location in the network and the profiles of other customers, the determination of the profiles that will be used by the RNM has to be representative of the interaction between load and generation. For example, a generator placed on a building with much more load than generation at 1 pm will drive much less network modifications that another in a residential suburb with many PV panels on rooftops which will be injecting power at a time when most of the dwellers are downtown at work. Since PV is not a dispatchable resource, the extreme scenarios need to be considered to design the network. These correspond to the days when the peak load and peak generation are reached.

Net profiles calculation To find out the critical days, we combine the yearly load profiles of the customers with simulated PV generation profiles obtained using the PVWatts online calculator [145], which is based on the same TMY3 weather database that was used to create the load profiles. In this way, correlations between weather-driven loads and PV generation are correctly captured.

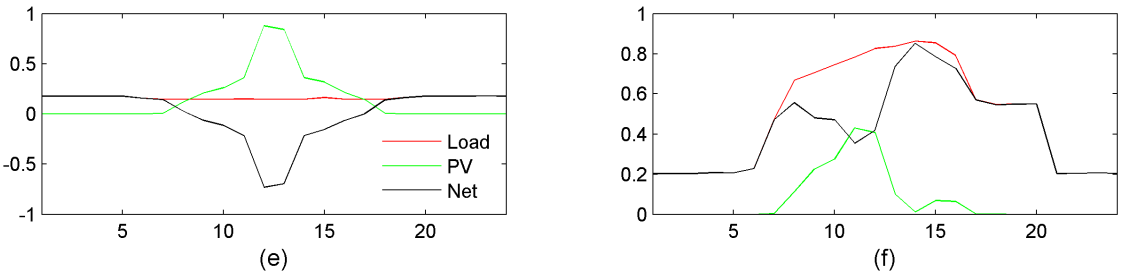

Figure 6.5: Extreme net load and generation days for a commercial customer in Lancaster, CA.

6.2.3.3 PV generation impact results

The results for the no-storage scenarios shown in Figure 6.6, reveal that a significant penetration of PV generation is a relevant cost driver in distribution networks, assuming that our sample represents well the diversity of networks that can be found in the power industry. The main sources for the new costs are related to conductor reinforcements and voltage regulators to correct over-voltage problems. Note that the X axis in most of the figures corresponds to the ratio of annual PV energy production to the total annual load, and that a color scale has been used to identify the capacity factor of the location considered on each particular simulation.

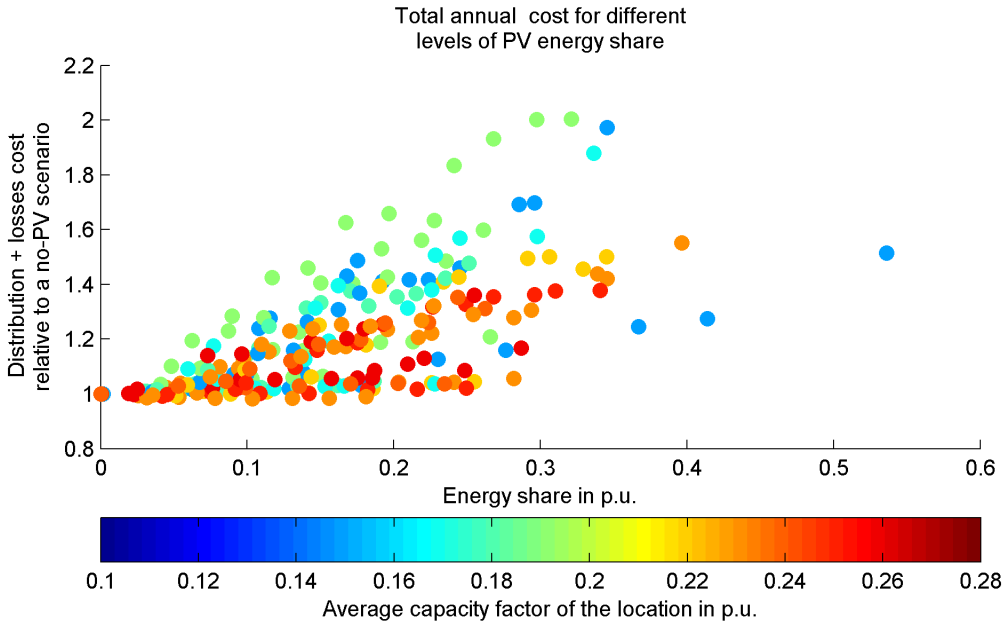

(a)

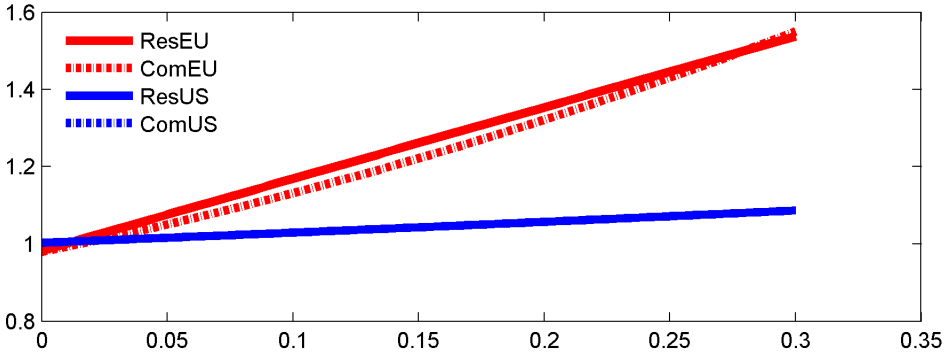

(b)

Figure 6.6: Total network cost after the introduction of PV generators, for all study cases using equipment representing engineering practices in Europe, relative to the cost of the respective base networks. Each dot represents one case study (energy share and relative cost). The colors of markers correspond to the average capacity factor of the generators in that location.

The logic that underlies these results is simple. As will be further explained in the following sections, a distribution network without a high penetration of non-controllable generation needs to be prepared only for the maximum load scenario. As the penetration increases, more neighborhoods become net generators at certain hours, and a second design restriction appears: the feeders now need to be ready to cope with the power flows in the maximum generation scenario as well. There are also other costs related to the connection of distributed generation.

Impact on energy losses As depicted in Figure 6.7, the cost of network losses has a general tendency to decrease as the share of PV energy in that distribution network increases. There are two drivers that, combined, explain this:

1. Part of the original load has been offset by local generation. As long as the net power is, in magnitude, less than the original load, the losses are going to be smaller.

2. In the places where the net generation is significant, over-voltage issues in specific hours demand wire reinforcements that will contribute to decrease losses in all hours. These voltage problems are partly due to the fact that peak PV production does not usually coincide with the peak load, which means that reverse flows will occur, giving rise to voltage issues, which are especially significant in low voltage networks because of the large resistance to reactance ratio of the conductors.

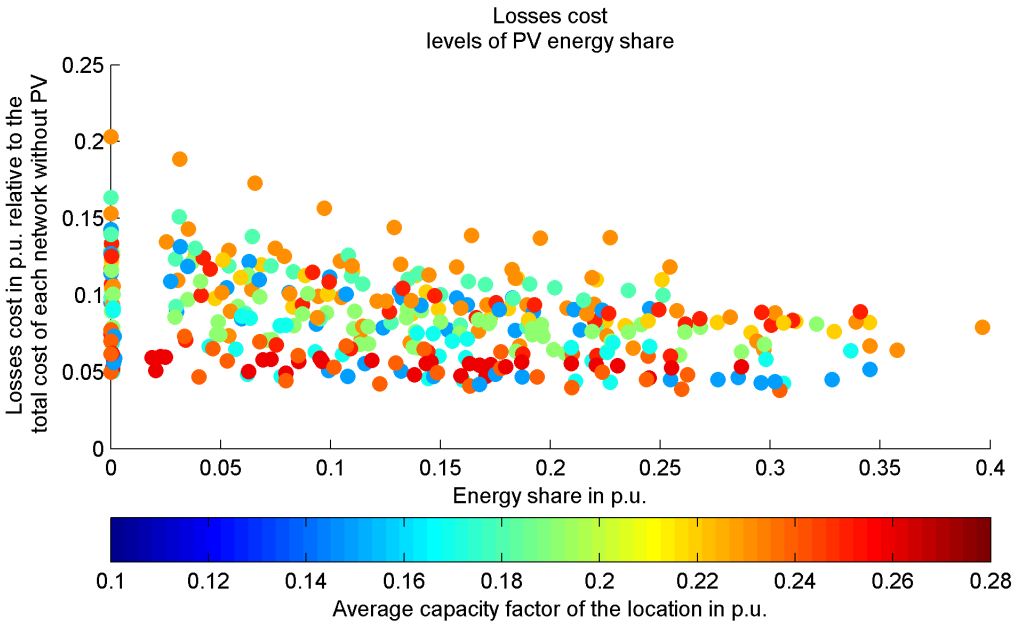

(a)

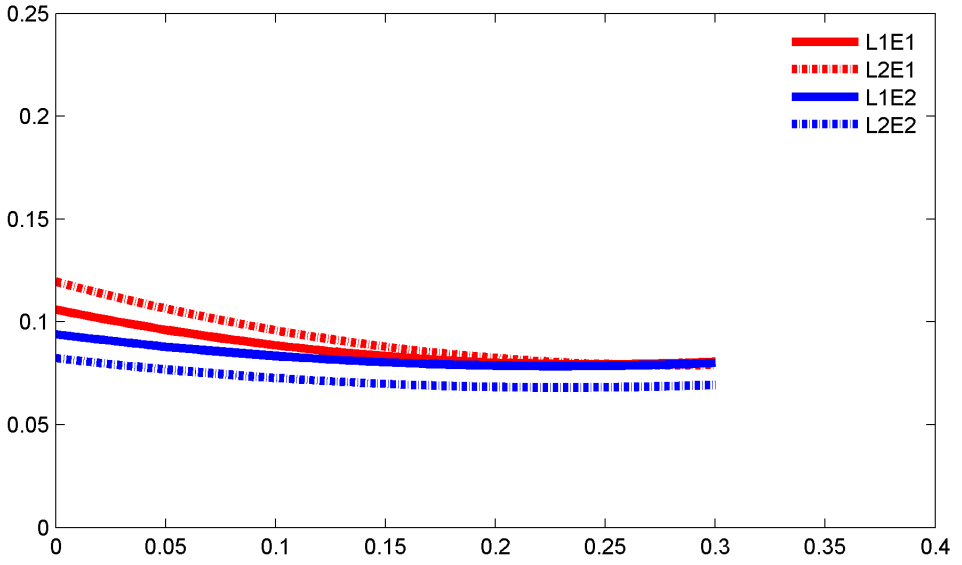

(b)

Figure 6.7: Annual cost of network losses after the introduction of PV generators, relative to the total cost (including losses) of the respective base networks. Each dot represents one case study (energy share and relative cost). The colors of markers correspond to the average capacity factor of the generators in that location.

A closer look at what happens in the left side of Figures 6.6a reveals that total costs remain basically flat for low shares of PV energy. This happens in part because for small PV penetration levels at most a very small number of power flows have changed direction (most generation goes to offset local load) compared to the flows in the reference case

with no PV, and also because the decrease in losses is enough to offset the additional costs derived from them.

Cost drivers A more detailed inspection of the results reveals some additional facts that help to understand the impact of PV generation in the distribution network:

1. The extra network cost as a function of PV energy share is going to be lower in places with higher capacity factor. This is because the network has to be able to cope with the maximum generation profile (e.g. clear sky day in summer) when the PV output is going to reach capacity, and since a place with lower insolation will require a higher installed PV capacity to achieve the same energy output, the stress over the network at times of peak radiation is going to be larger.

2. The gradual impact of PV penetration in the first interval of Figure 6.6 can be understood in terms of two drivers. First, small penetrations imply that almost no sector of the network will be a generator in net terms in any hour of the day, in particular for the hour of maximum PV generation, which is no longer true for a significant penetration. Distribution network problems are strongly local, mainly related to voltage issues, which implies that many of the sectors would violate power quality constrains should no upgrades be applied.

Another interesting indicator results from dividing the total incremental net present cost (NPC) by the total installed PV capacity in every scenario. The results in Figure 6.8 show that 1 kW_p of PV can, in some cases, explain some tens of dollars of annual network cost increase.

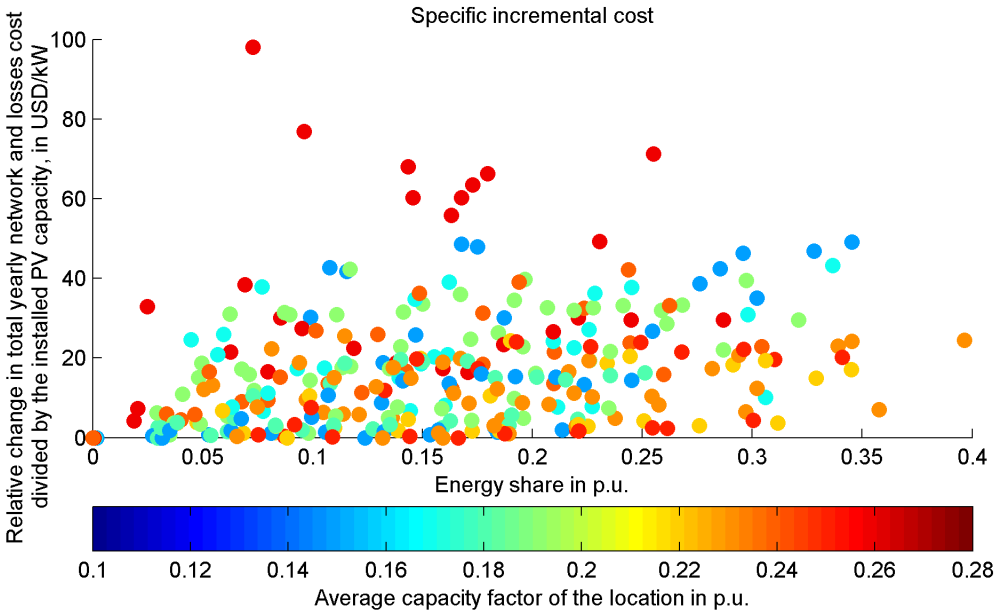

(a)

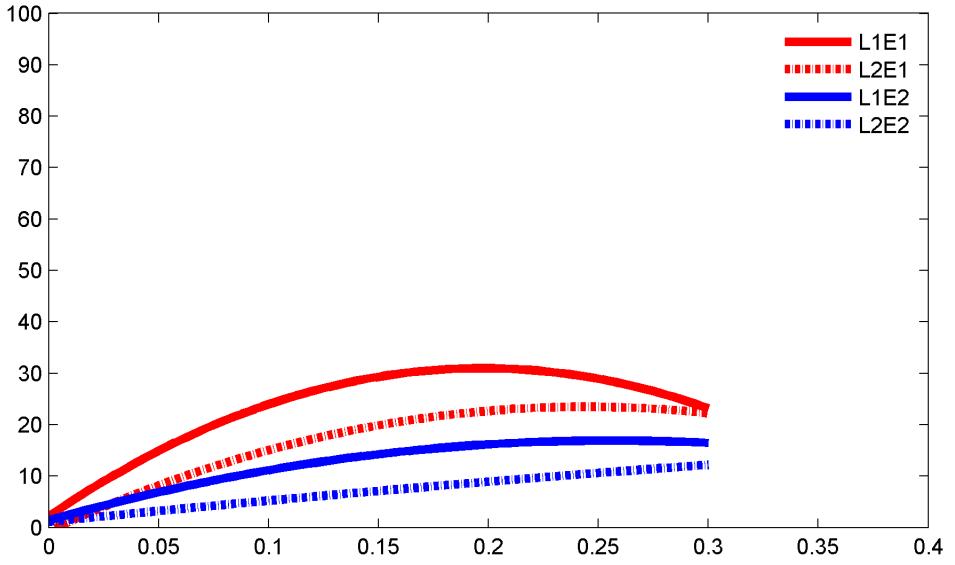

(b)

Figure 6.8: Total incremental annual costs divided by the installed PV capacity.

6.2.4 Value of energy storage

The need for network upgrades is mainly driven by the installed PV capacity, which may create significant reverse power flows at certain hours. Since "smoothing" the flow profile would alleviate the problem derived from this and therefore prevent or reduce

additional investments, energy storage can be seen as an alternative solution to conventional network equipment in high penetration scenarios.

The results shown in figure 6.9 compare the previously calculated additional network cost (red dots) with the new ones in which storage devices are coupled to LV and MV PV systems. The size of the storage devices in both power and energy is calculated to be enough to eliminate power injections to the network at the times of maximum PV generation.

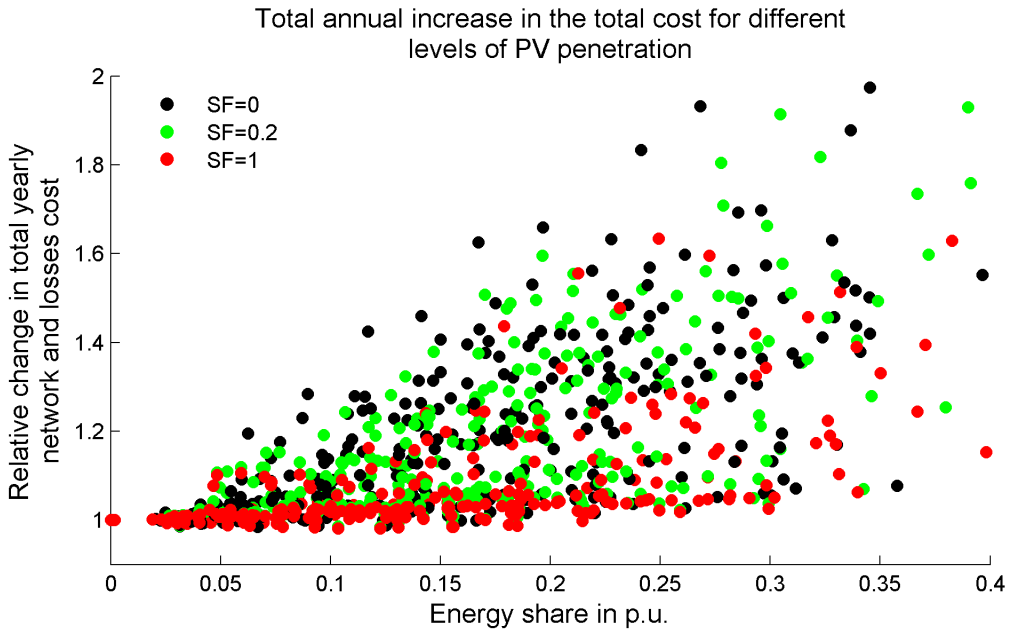

(a)

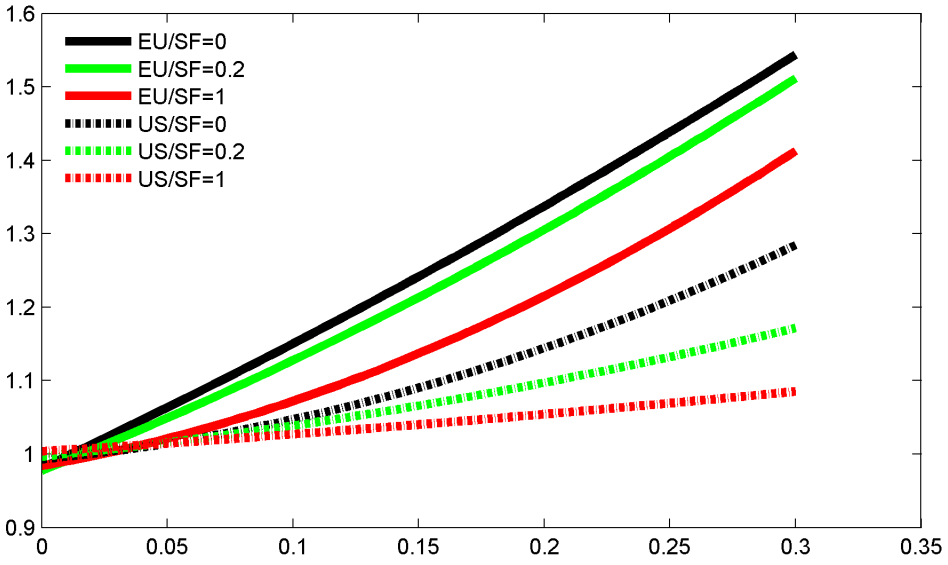

(b)

Figure 6.9: Contribution of energy storage to the integration of distributed PV generation. The representative cost-trajectories on the right were generated from the results using second-order polynomial interpolation and averaging.

When for each base network and penetration level we subtract the cost results of both runs and divide those savings by the total amount of storage installed, the result is an indication of the annual value of distributed energy storage. For the cases studied here, we obtain the values shown in Figure 6.10.

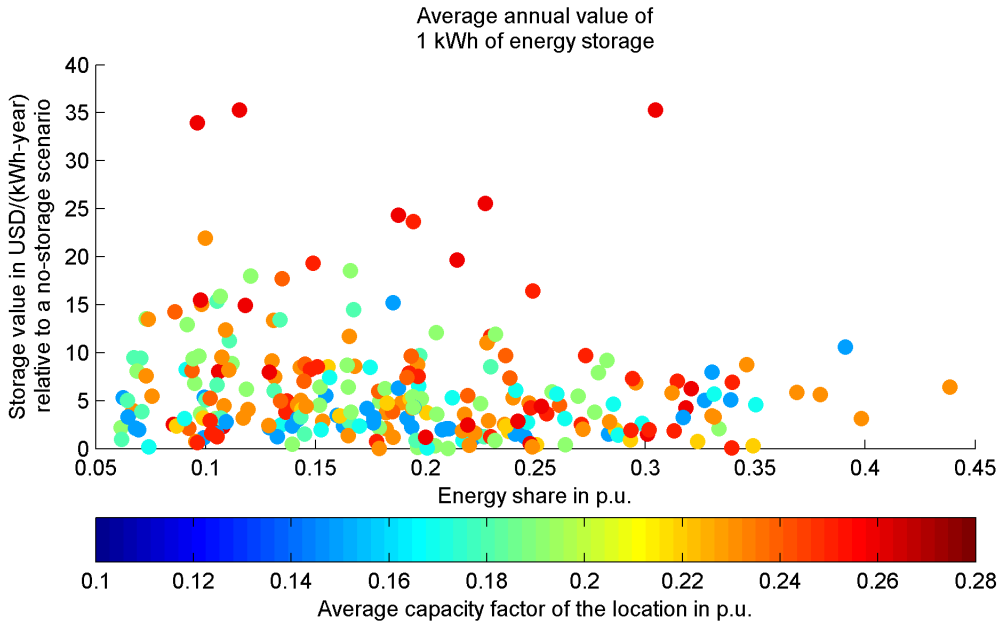

Figure 6.10: Value of energy storage in different cases

6.2.5 BESS lifetime and performance calculation

In order to get a notion of the viability of using existing energy storage technologies to support the operation of distribution systems, we combine the storage utilization profiles generated using the methodology explained in chapter 5 with a-posteriori simulations based on the BESS model described in chapter 4, fitted to the ANR26650 cell from A123 Systems, to estimate the useful life of the assets. The BESS considered includes the following components:

- ANR 26650 Electrochemical cells;
- A container with a known thermal insulation from the environment;
- An active temperature control system;
- A battery management system to ensure safe operation;
- A DC/AC bi-directional electronic power control interface.

6.2.5.1 Description of the battery utilization simulation

For the generation of battery utilization profiles, we consider a set of residential consumers on each one of the six locations. The simulations are setup considering that:

1. Each system has the same PV installed capacity as the peak load;
2. The batteries are sized and operated in order to respect a band of power between -0.1 and 0.8 p.u during one typical year;
3. The TMY3 database is used to determine yearly profiles for load, PV generation and ambient temperature;
4. When the heat pump is used, the power of the motor is sufficient to react according to figure 4.8.

As explained in chapter 5, the primary objective of the BESS is to keep the net power injection to the grid between prescribed limits, and the size of the battery the minimum that would comply with this for all days in a yearly simulation. Figure 6.11 shows an example of one day of battery planned operation according to the very simplified model in section 5.2. However, since that model does not take into account neither the electrical characteristics of the battery nor the effect of degradation, it is necessary to perform a lifecycle performance assessment including these aspects. In order to do this, a multi-year simulation is carried out. Since the load and PV production profiles are assumed to be constant from one year to the next, the only difference between consecutive years is the state of health of the battery. The simulation is stopped when the battery reaches 70% of the original capacity.

6.2.5.2 Lifecycle performance assessment

The power profile in figure 6.11 is used as the BESS power setpoint of the simulation. Instead of minimizing costs, hard voltage and state of charge limits are programmed into the BMS subroutine. Therefore, the power profile setpoint is only going to be achieved if, according to the BESS model, it is physically feasible at the time.

The simulation described in the previous section is used to analyze how the battery would behave during its lifetime. Figure 6.12 can be used to understand the utilization of the battery capacity in order to respect the power limits. It is clear that in the first years the available capacity is under-utilized in most days, while later in life the reduction of capacity requires a much more intensive use.

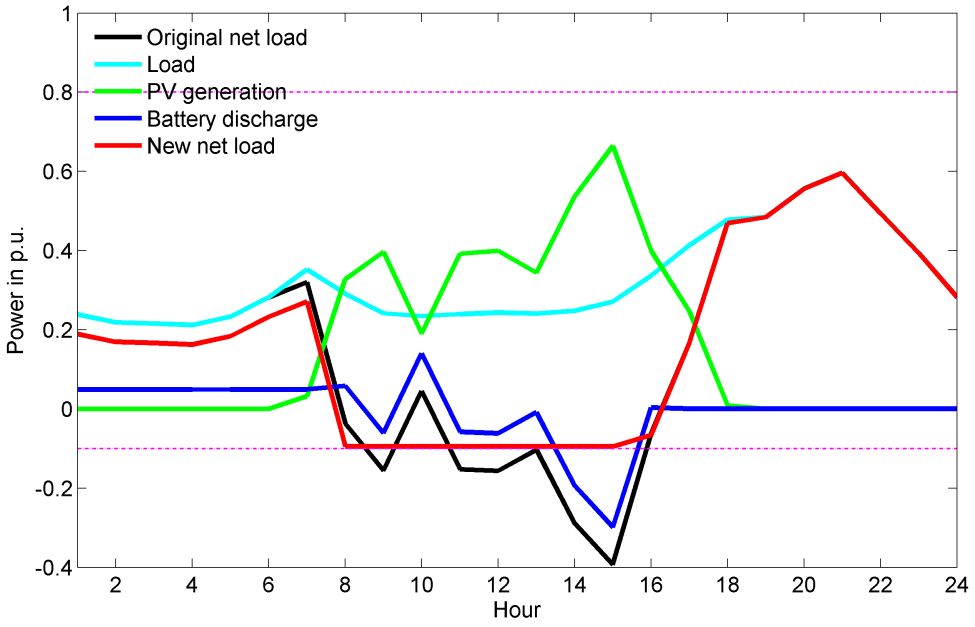

Figure 6.11: Operation of a BESS providing peak-shaving and valley-filling services for a prosumer with a variable load and a photovoltaic generator. The magenta lines correspond to the injection (-0.1) and consumption (0.8). All values are expressed as a fraction of the yearly maximum net load before the introduction of batteries.

The effect can be seen more clearly taking the weekly maximum and minimum state of charge, as shown in figure 6.13

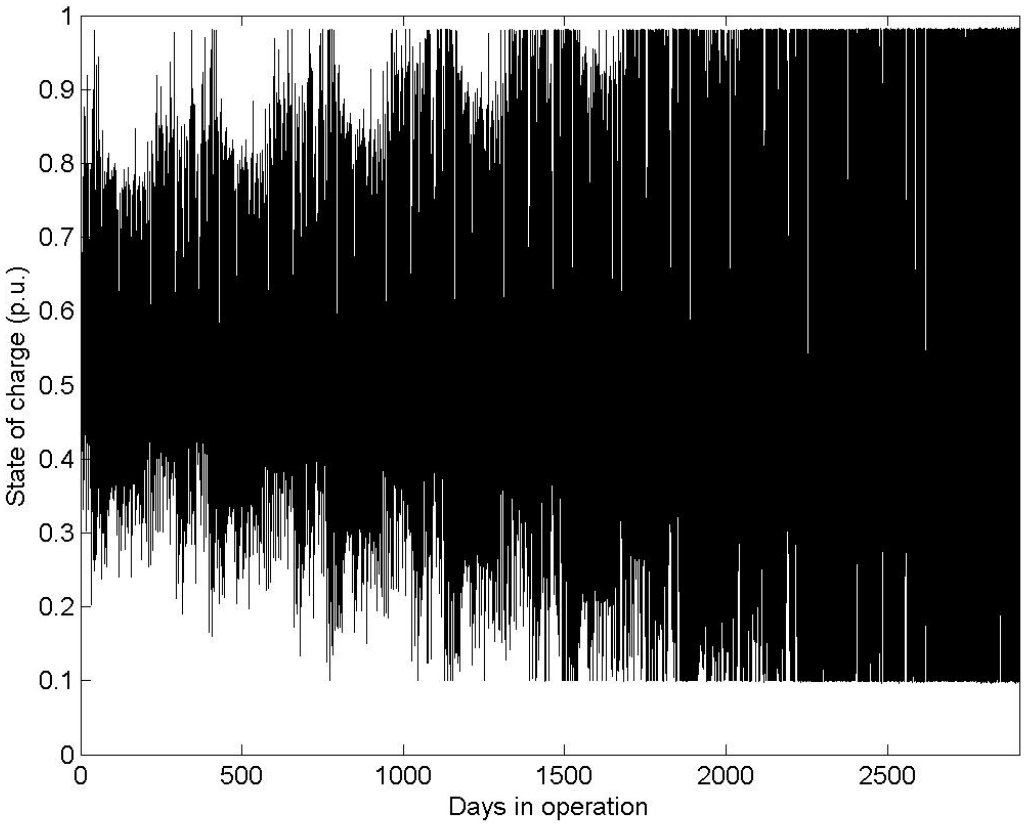

Figure 6.12: Simulated battery state of charge during its lifetime, for a system providing peak-shaving and valley-filling in California.

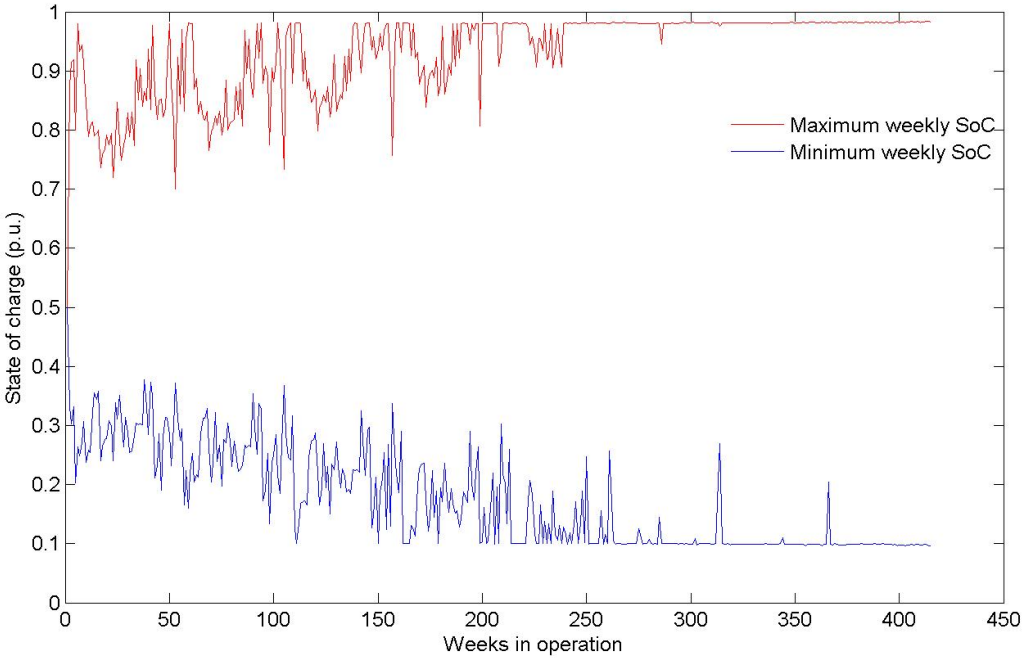

Figure 6.13: Simulated maximum and minimum state of charge, calculated weekly, for a system providing peak-shaving and valley-filling in California.

Taking advantage of the ability of the model to predict electrical variables, one can examine the convenience of hard-coded constraints. For example, figure 6.14 shows the weekly maximum and minimum cell voltage. Considering that the cell minimum and maximum voltage limits in the BMS were defined, according to the manufacturer's recommendation, at 2V and 4V respectively, it is clear that the constraint never becomes active during the lifetime of the cell, which suggests that the SOC constraint is overly conservative. The slight slope of both curves comes from the increase of cell equivalent impedance with age.

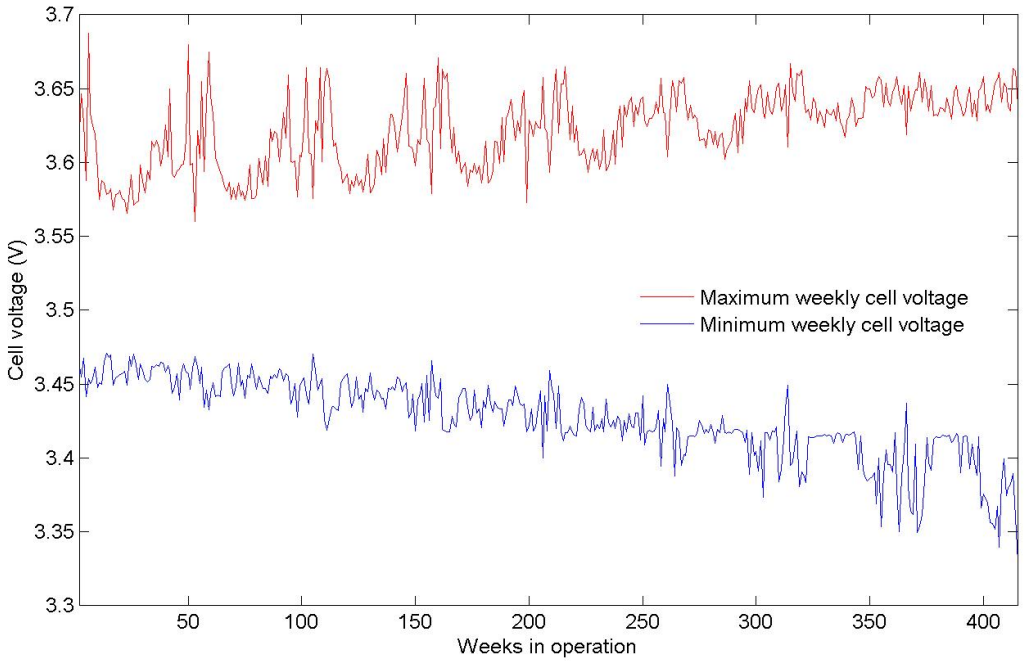

Figure 6.14: Simulated maximum and minimum cell voltage, calculated weekly, for a system providing peak-shaving and valley-filling in California.

The consequence of an active restriction is that the service will not be provided as expected, and there will be a difference between the power setpoint shown in figure 6.11 and the actual output of the BESS. As shown in figure 6.15, this error increases over time.

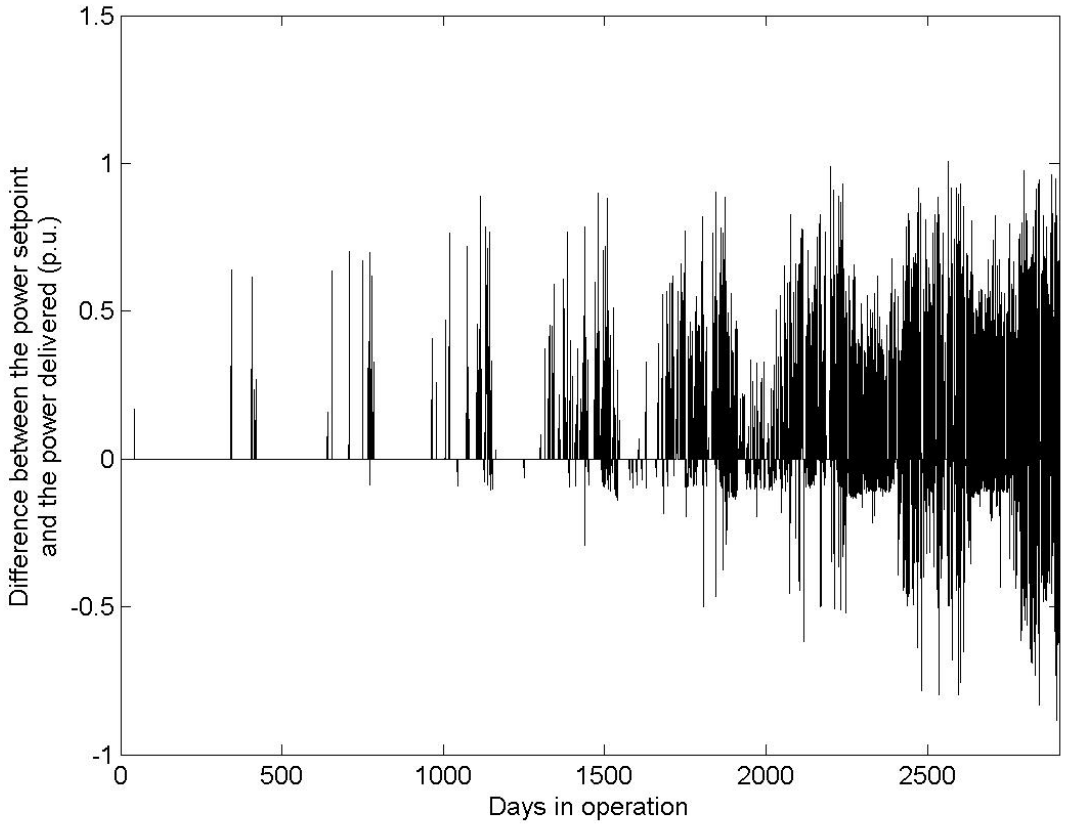

Figure 6.15: Simulated deviation from the power setpoint for a system providing peak-shaving and valley-filling in California.

Actually, the average of the absolute value of the setpoint error is 0.054 in p.u., but the figure is misleading since the number of points is in the simulation is over twelve million. Proceeding as for the other variables, one can take the average weekly positive and negative error to obtain the curves in figure 6.16, where it can be seen that year one exhibits almost perfect compliance with the peak-shaving and valley-filling function, and the quality of the service deteriorates over time.

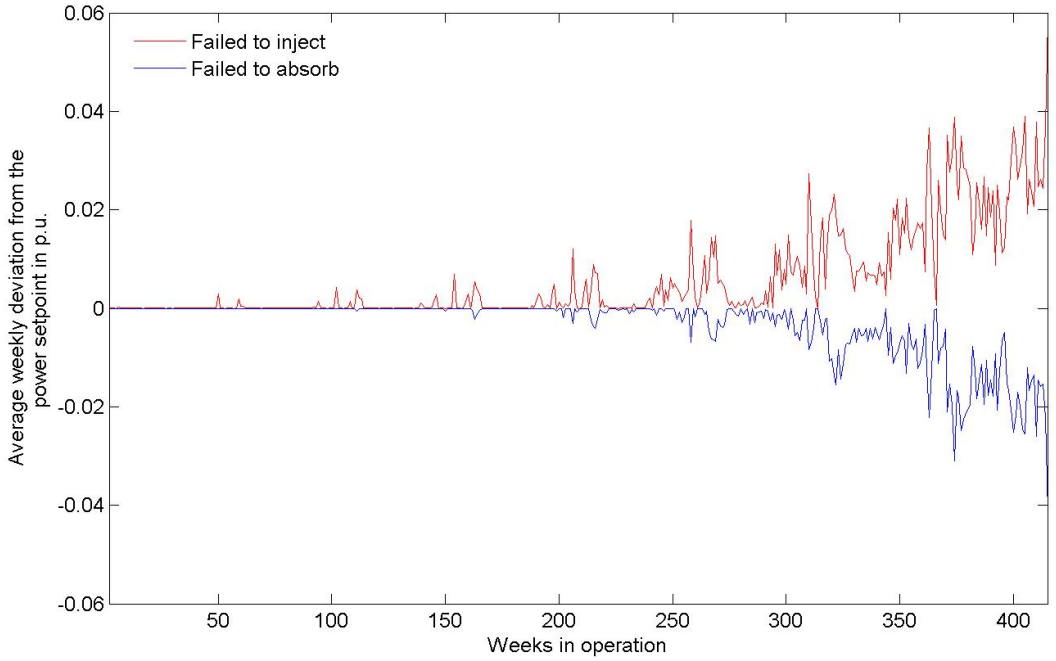

Figure 6.16: Simulated average weekly deviation from the power setpoint for a system providing peak-shaving and valley-filling in California.

The model can also be used to evaluate the choice of electrochemical cell. The A123 26650 are high-power lithium iron-phosphate cells with maximum discharge and charge power of 70 A and 10 A respectively. Figure 6.17 puts in evidence that the power capacity of the cell is significantly under-utilized, which also in part explains their long life.One can also obtain parameters that inform the sizing of power electronics and losses calculations. Let $R = \left|\frac{U-v}{i}\right|$ be the internal impedance of the cell, figure 6.18 shows the evolution of its value averaged over a week during the lifetime of the cell.

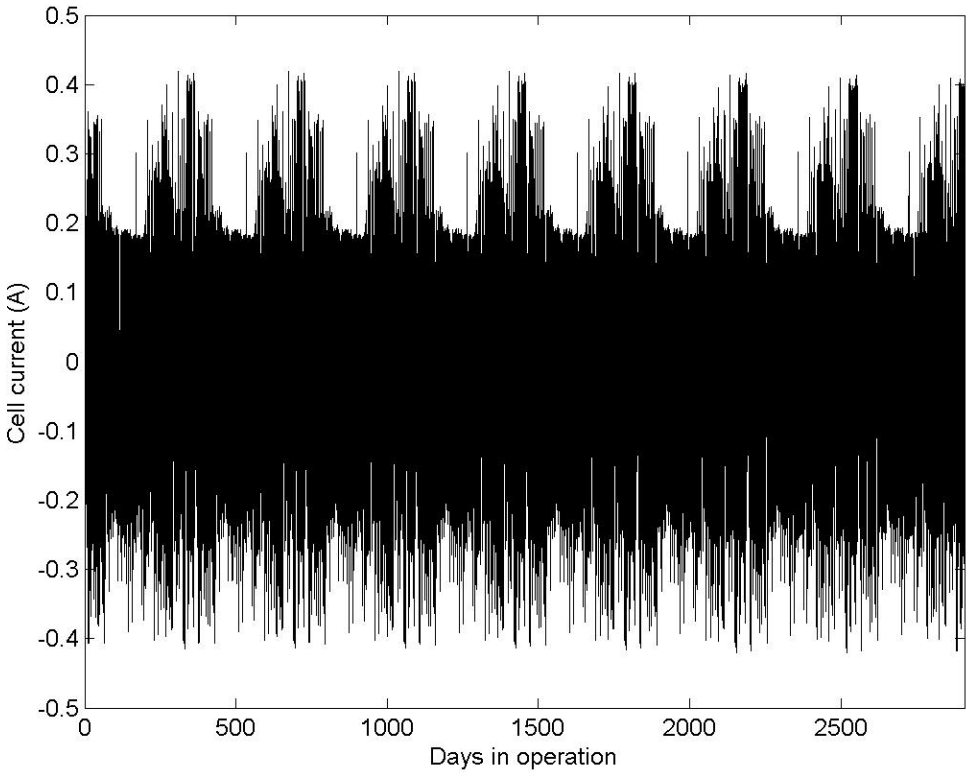

Figure 6.17: Simulated battery state of charge during its lifetime, for a system providing peak-shaving and valley-filling in California.

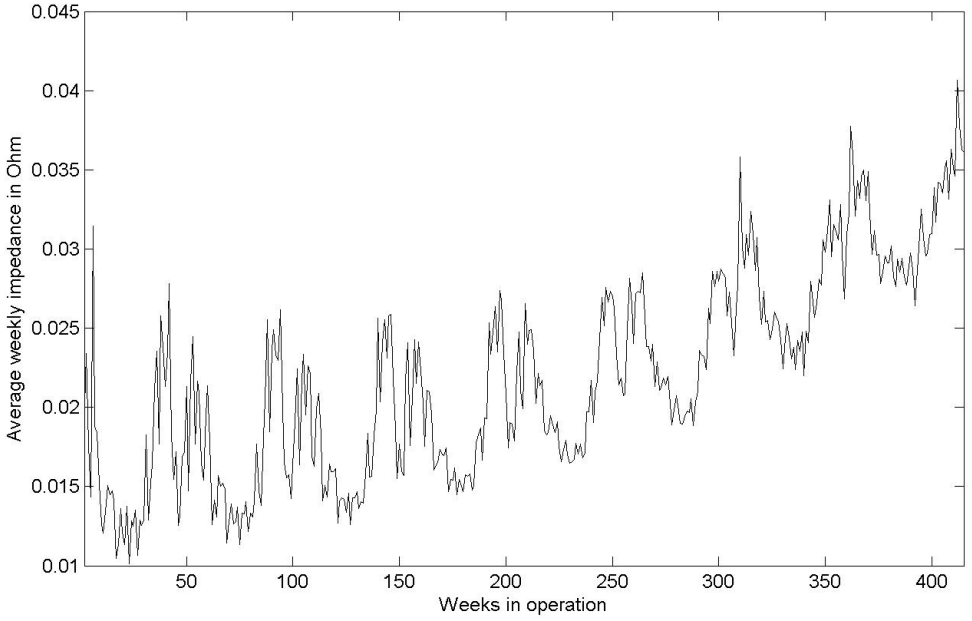

Figure 6.18: Simulated battery internal impedance averaged over a week, for a system providing peak-shaving and valley-filling in California.

The very low value for the current implies that the over-potentials, and hence the losses are very small (the process happens close to equilibrium). This is coherent with the extremely low values for the losses predicted by the model, as shown in figure 6.19. Finally, figure 6.20 shows the expected useful life for the different locations considered in the study, using as threshold to establish the end of life of the battery the time when the simulation predicts that the SOH through its proxy, the available electrode active area, reaches 0.7. Note that the locations with lower insolation (Washington (WA), Indiana (IA) and Connecticut (CT), are two to three years longer than for sunnier ones (California (CA) and Colorado(CO)). The result for Texas (TX) may be partially explained by a combination of its lower irradiation compared to Colorado and California, and also because the average daily highest temperature is 15% higher, which drives cooling loads that contribute to offset peak PV generation.

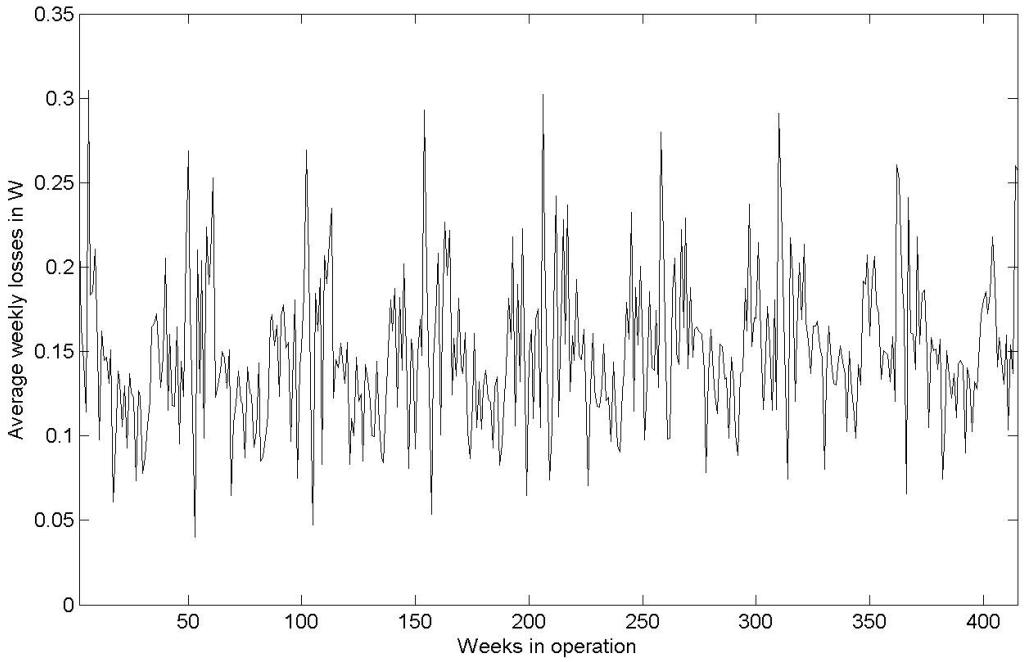

Figure 6.19: Simulated battery losses averaged over a week, for a system providing peak-shaving and valley-filling in California.

6.2.6 Conclusion

A formulation to assess the value of energy storage to support the integration of distributed grid-connected photovoltaic generators has been presented. The first part of

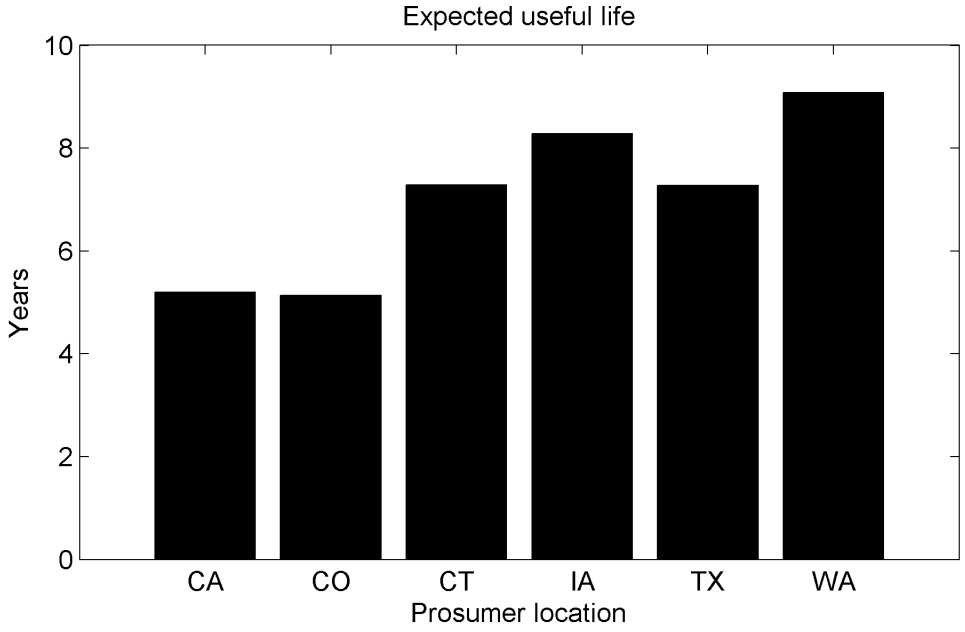

Figure 6.20: Simulated years to reach SOH=0.7 for batteries in different locations.

the analysis shows that the presence of PV generators can be a significant cost-driver in distribution network when all impacts of a PV energy share are considered, although distribution losses can be expected to decrease as the energy share increases up to very high values. The dominant impact of a significant PV energy share on a distribution network is to require new investments to maintain the quality of service. It is also found that for the same level of PV energy share, locations with higher irradiation require less extra network investments to maintain the quality of service.

The storage value analysis shows that batteries are a technically effective alternative to integrate PV generation, with potential annual infrastructure savings around 7 and as high as 35 dollars per each kWh of storage installed. For the case of the particular Lithium-Ion technology studied, the results from the degradation model show that the useful life under the same utilization policy differ in up to 50% for the locations studied. Considering upper extreme case in terms of cost v/s value , batteries placed in the state of Washington have an expected lifetime of 8.5 years and a value of 15 dollars per year per kWh for an energy share of 0.18. Considering a discount rate of 7%, this is translated in a maximum viable upfront cost of 104 dollars per kWh, which much less than the current cost, around $300 per kWh, of lithium-ion batteries.

6.3 Case 2: Frequency support

Battery Energy Storage Systems (BESS), connected to the electric grid through power electronics with digital control provide virtually unlimited response flexibility to remote set-points or to measurements made in their connection points. While this extends the possibilities to provide ancillary services, the extra degrees of freedom are accompanied by the need of an accurate description of the response that has to be meaningful from the point of view of both the battery owner and the system operator. The procedure explained here uses the battery model to take into account the coupling between the utilization of the battery and its cost of use, related to the decrease in the state of health (SOH) of the device, and the net energy purchased from the grid to maintain the state of charge and to compensate for the losses in the battery.

6.3.1 Case description

In the same way that distributed VERs create local challenges, their increasing penetration can also have major system-wide implications like an increase in the variability of the net load curve. With the prospect of capturing revenue streams derived from this situation, loads are becoming more active and flexible, and the idea of aggregating entities that offer ancillary services that can substitute traditional flexibility sources is not only compelling but presently a reality. Summarizing, four families of flexibility sources are currently over the table:

1. To ramp conventional generators up and down;
2. To reinforce the transmission and distribution infrastructure;
3. To perform demand-side energy management and load response [97] [105] [], and
4. To invest in different kinds of storage media.

This section presents a study case based on numerical simulations for a 20 MW BESS connected to the Chilean Northern Power System (SING, explained with more detail in the next sections) providing frequency regulation according to the reaction model presented in section 4.4.3. The model of the BESS follows the architecture in section

4.1[3]. The objective is to present an example of this response parametrization applied to this particular ancillary service, and discover how different parameters affect the degradation of the electrochemical cells inside the BESS. This in turn informs a cost model to determine what is the total cost of using the BESS to provide the service.

It is considered that variables that explain the evolution of the electric grid and the ambient are independent from the operation of the BESS. Therefore, ambient temperature, frequency and pricing information are included as external data-files that are read during the simulation. This implicitly assumes that the nominal power of the BESS is very small compared with the installed capacity of the power system, and that the heat released is small. Note that for indoor locations the latter assumption may not hold if the thermal model of the BESS doesn't include the building where it is placed.

A 20 MW BESS connected to the Chilean Northern Power System (SING) providing frequency regulation is considered. The objective of the study case is to explore the dependency between two frequency support parameters and the annual cost of use of the BESS, considering the degradation of the cells and operational costs. Additionally, the profit of the battery owner under a specific remuneration scheme is calculated.

6.3.2 Cost of use calculation

The cost model includes the following variables, which are calculated on every iteration:

1. The difference between the energy bought and sold to the grid when performing frequency regulation, e_f;
2. The difference between the energy bought and sold to the grid to control the SOC[4], e_s;
3. The energy bought from the grid to operate the temperature control system, e_t;
4. The decrease in the active area in the cell electrodes, dS_a.

This results in the following expression for the cost of use during an arbitrary interval:

[3]For the parameters used in the BESS model for the simulation see Appendix D.

[4]The state of charge setpoint is used as the decision variable in the case instead of the power setpoint. The latter results from the application of a proportional controller.

$$C(t) = C_{mg}(t) \cdot (e_f(t) + e_s(t) + e_t(t)) + C_b \cdot dS_a(t) \tag{6.6}$$

$C_b = \frac{cell\ cost}{nominal\ active\ area}$ is the battery specific use cost.

The A123 ANR26650 Lithium-ion cell is considered as the basic building block of the BESS, with parameters fitted to data found in the literature [146] and in the manufacturer's datasheet [147] in the mean square error (MSE) sense[5] using the evolutionary particle swarm optimization (EPSO) algorithm [148]. The parameter extraction occurs in two steps:

1. Estimation of the cell parameters for $SOH = 1$: This is done for the lumped constructive parameters a) total electrode active area b) electrolyte conductivity's temperature dependence factor, and c) electrode resistance. For these, a simulated charge-discharge curve is compared with the experimental data in [147] and the parameters are changed using EPSO in order to minimize the MSE.

2. Estimation of the cell degradation parameters: This step estimates the parameters in equations (4.26) and (4.27) that minimize the MSE between a degradation simulation over several thousand cycles and the experimental data in [146].

6.3.3 Grid

The data-set used for this purpose is obtained from operational data of the Chilean northern interconnected system shown in figure 6.21, which includes:

1. A one year long frequency log sampled every 2 seconds (Figure 6.22), corresponding to real frequency measurements during one year.

2. A one year long marginal cost log calculated every one hour (Figure 6.23).

The SING has a installed capacity of 5 GW and an average load of 2 GW. Given that the main economic activity of the region is mining, the predominating load is industrial. The

[5]This means that the objective function is to minimize the squared root of the sum of the errors, where the error is the difference between the predicted curve from the simulation and the experimental value.

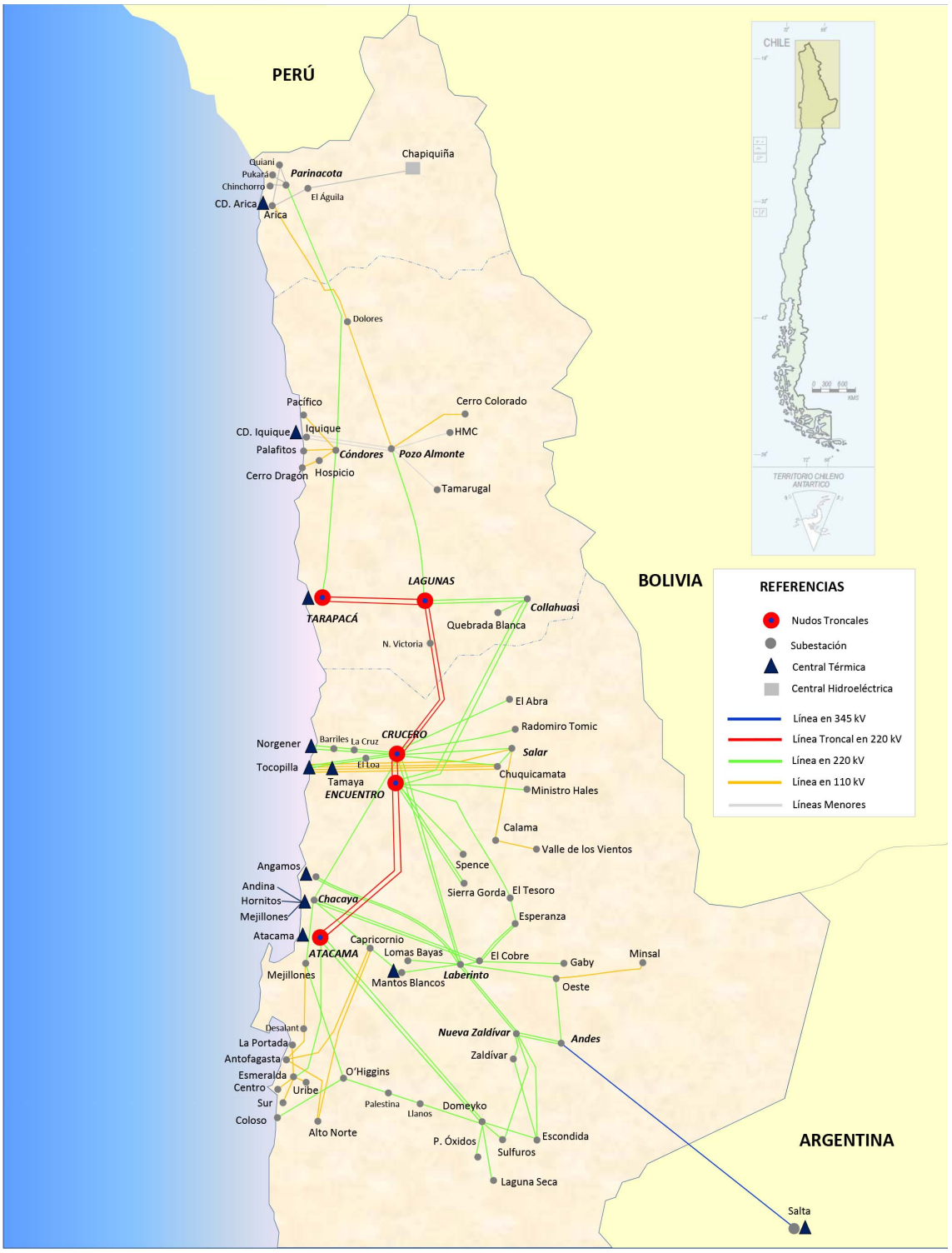

Figure 6.21: Simplified single-line diagram of the Chilean northern interconnected system down to 110 kV [21].

primary energy sources distribution is shown in Figure 6.24 [22]. All the power plants are required to provide spinning reserve,and two of them have implemented BESS to comply with this regulation and be able to operate the thermal generator closer to the

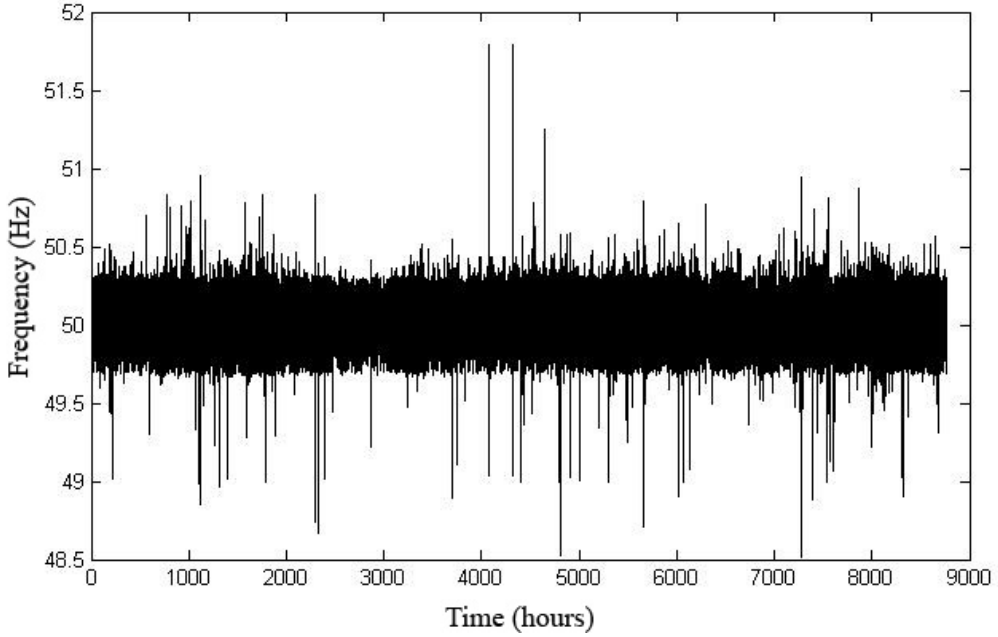

Figure 6.22: Frequency of the SING, in Hz, over a one year (8760 hours) interval. The extreme over and under-frequency events usually correspond to faults

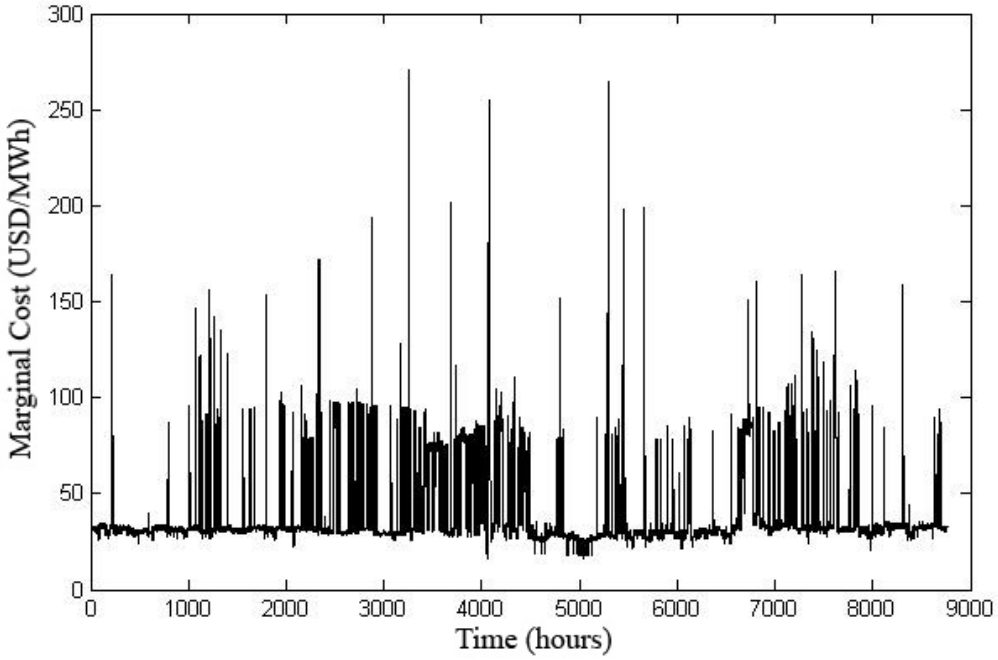

Figure 6.23: Marginal cost, in $\frac{USD}{MWh}$ in the Crucero busbar of the SING

rated power, thus maximizing energy sales.

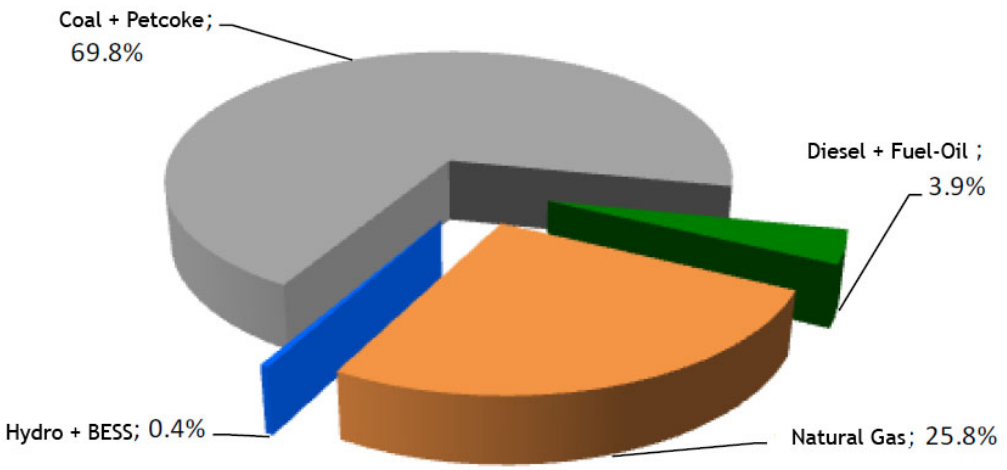

Figure 6.24: Primary energy sources in the SING [22]

6.3.4 Ambient

A one year long temperature profile for the city of Antofagasta was obtained from the EnergyPlus weather database [141] and is shown in Figure 6.25.

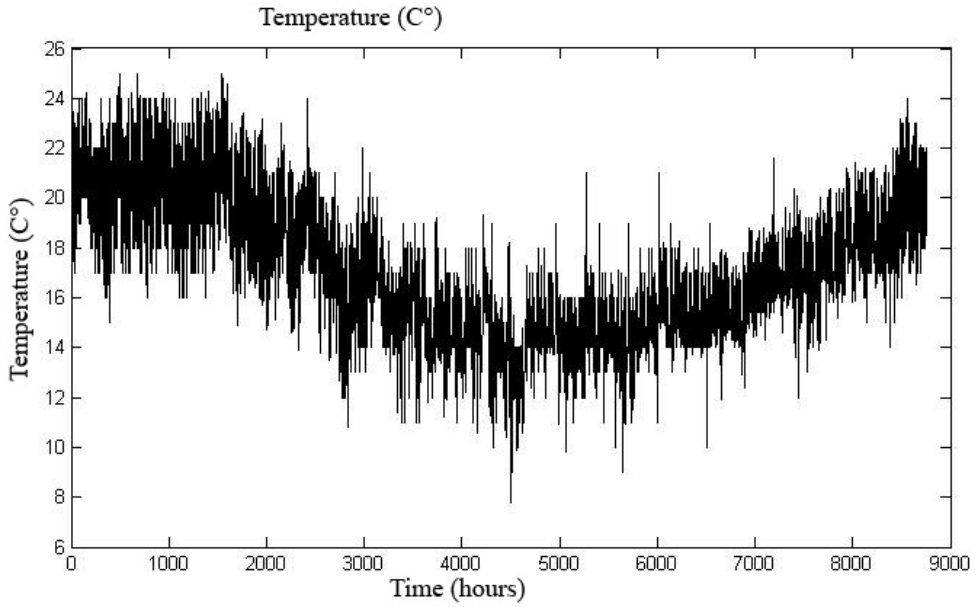

Figure 6.25: Hourly temperature in C° during one year in the city of Antofagasta

6.3.5 Results

The simulation setup described on the previous sections was used to study the operation of the BESS for different parameter sets. Three groups of results are generated:

1. Reaction parameters sweep for a 10 days operation;

2. Evolution over one year of operation for a fixed set of parameters;

3. Detailed results for one day inside the yearly operation case.

The utilization cost of the BESS, shown as a surface in figure 6.26, is calculated according to the cost model (6.6) for different values of droop and deadband reaction parameters. The income in figure 6.27 assumes that the battery owner obtains 100 US dollars for each MWh processed by the battery[6] in the opposite direction of the frequency deviation outside the deadband. Finally, figure 6.28 shows the difference between income and cost.

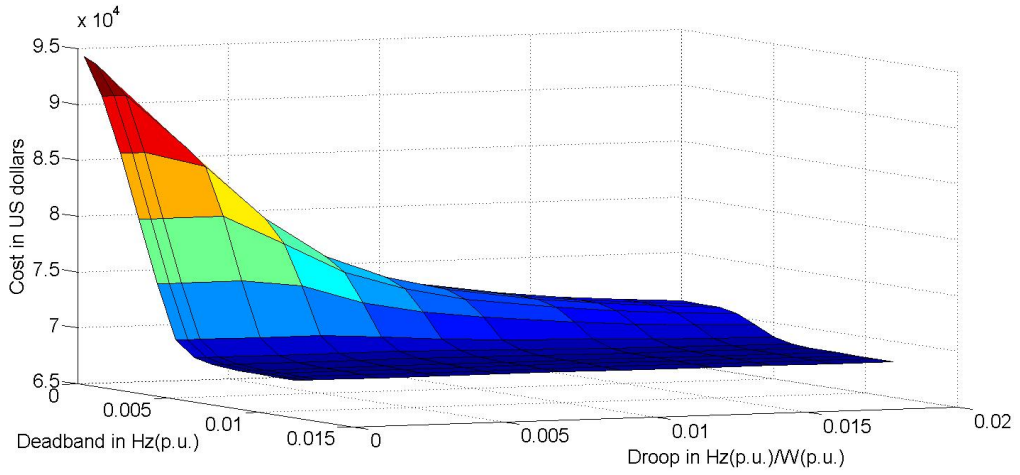

Figure 6.26: Projected cost of one year of operation of the BESS for different reaction parameters

The following results go into the operational details of the maximum profit combination of parameters. In figure 6.29 if can be appreciated that the SOH has a quasi-linear progression with some seasonal variation, being faster in summer[7]. This leads to the non-uniform degradation cost shown in figure 6.30, where it can be appreciated that the winter minimum of the degradation cost is related to the maximum profit.

It can also be inferred from figure 6.30 that the temperature control settings of the device should be tighter, as a far as that doesn't mean energy costs greater than the benefit from decreased degradation. A closer look at the operation during one day, with a 30 seconds sampling interval, helps understand the short-term cost-benefit relationships. For

[6]This is a referential value, roughly corresponding to the loss of profit of a coal power plant in the SING for adjusting the production down in 2011.

[7]The simulation begins on the first of January, and the BESS is located on the southern hemisphere.

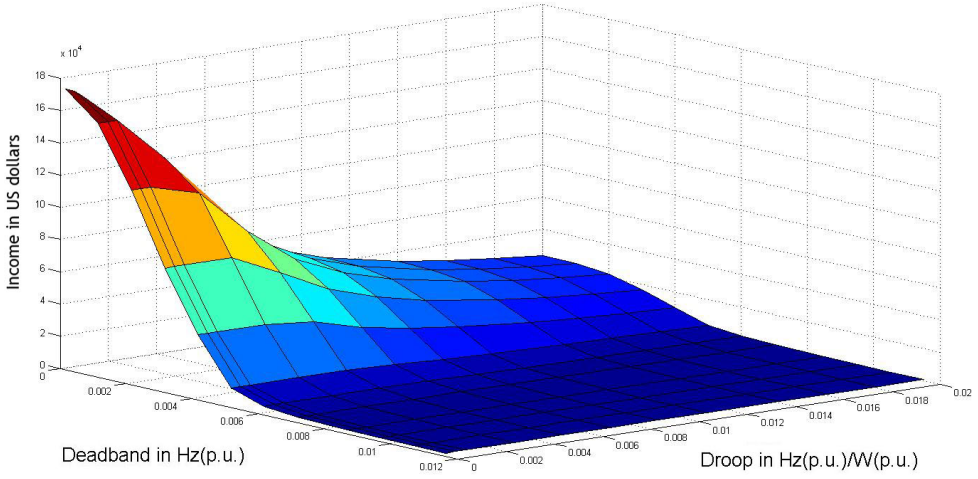

Figure 6.27: Projected income for one year of operation of the BESS for different reaction parameters

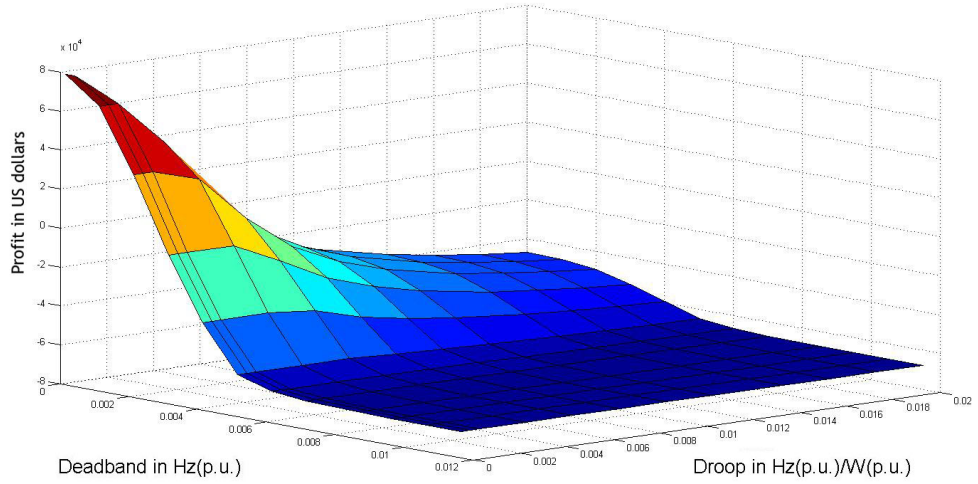

Figure 6.28: Projected profit for one year of operation of the BESS for different reaction parameters

example, comparing figure 6.31 with figure 6.30 reveals that although instantaneously[8] energy-related monetary flows[9] are an order of magnitude greater that degradation costs, sales and purchases partially cancel-out on a daily basis and degradation costs dominate.

It can be noticed from figures 6.32 and 6.33 that there is a strong dependency between the loss of electrode active area and the temperature, which is coherent with equation

[8]Here instantaneously refers to the maximum temporal resolution of the simulation, i.e., over a 30 seconds interval.

[9]Although transactions do not occur at 30 seconds intervals, the short-term balance is useful to reveal trade-offs.

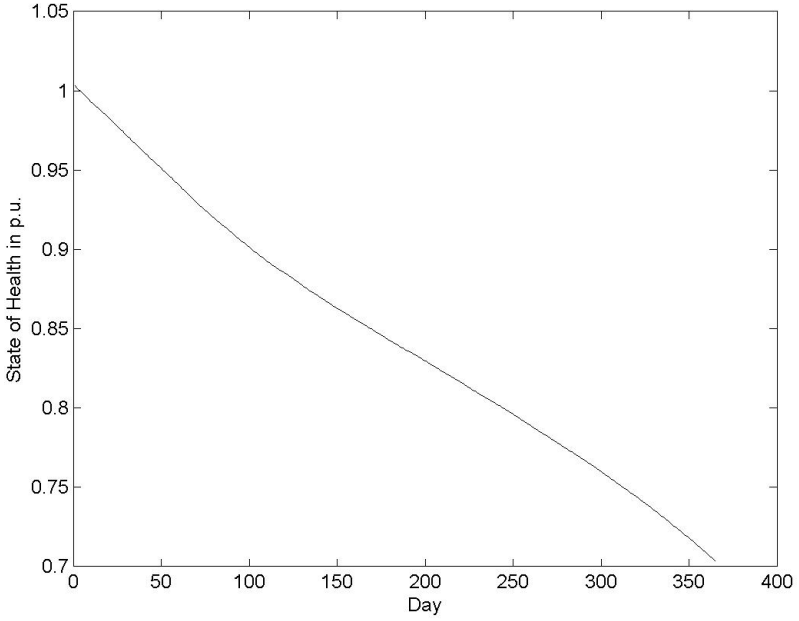

Figure 6.29: Evolution of the state of health of the batteries during one year of operation

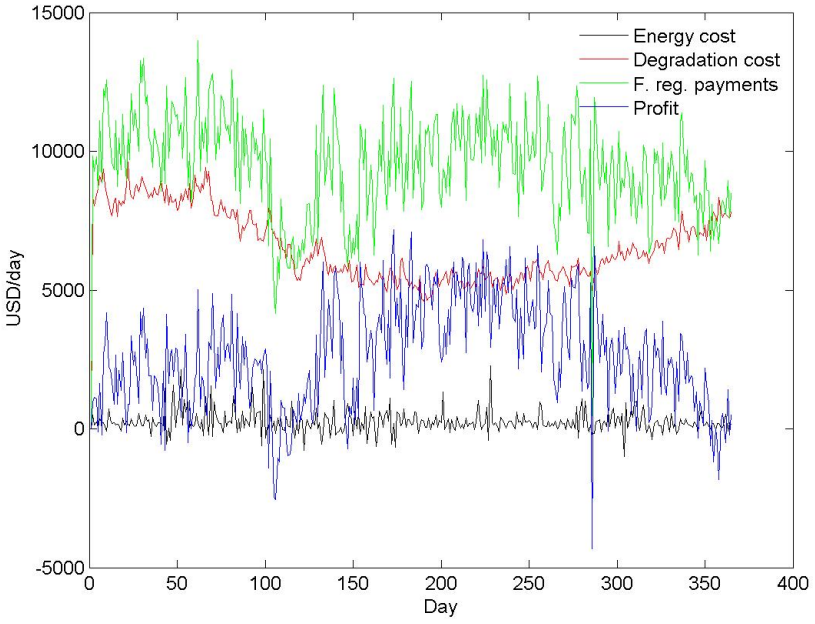

Figure 6.30: Cost and income components during one year of BESS operation.

(4.26).

Combining figures 6.31 and 6.34 yields the instantaneous profit shown in figure 6.35, where it is evident that although the daily balance is positive, in several instants the owner of the BESS looses money by providing the service. This insight could be useful if

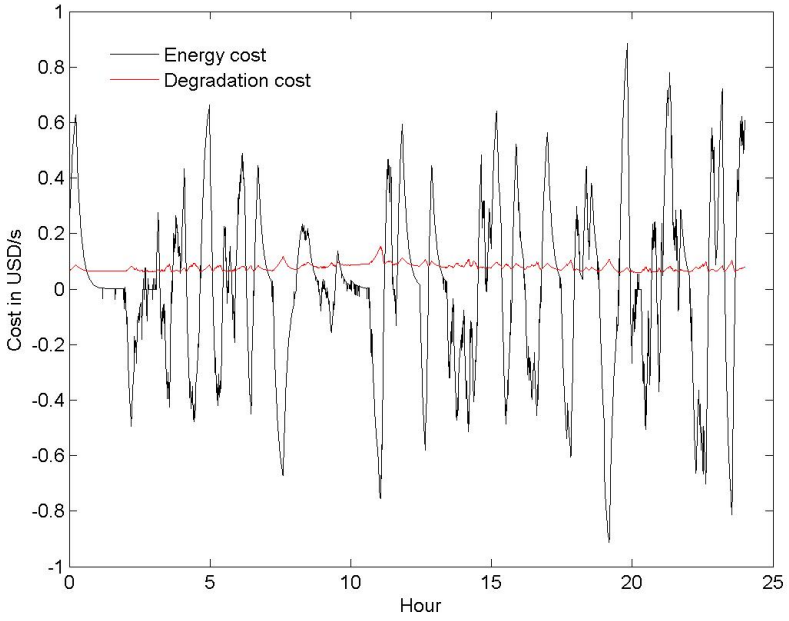

Figure 6.31: Energy and degradation instantaneous costs for one day of BESS operation (negative costs indicate revenue from energy sales)

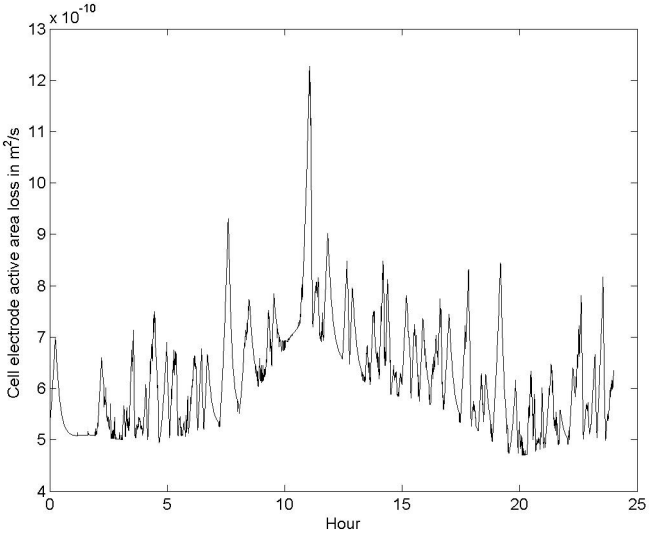

Figure 6.32: Instantaneous loss of active electrode area during one day of BESS operation.

the parameters of the BESS can be adjusted on an hourly basis or even more frequently, since the operator could decide not to offer the service when the model predicts that a combination of external (temperature, frequency) and internal (battery temperature, SOC, SOH) will result in monetary losses. Alternatively, in a competitive short-term bidding scheme, this would translate in higher bids.

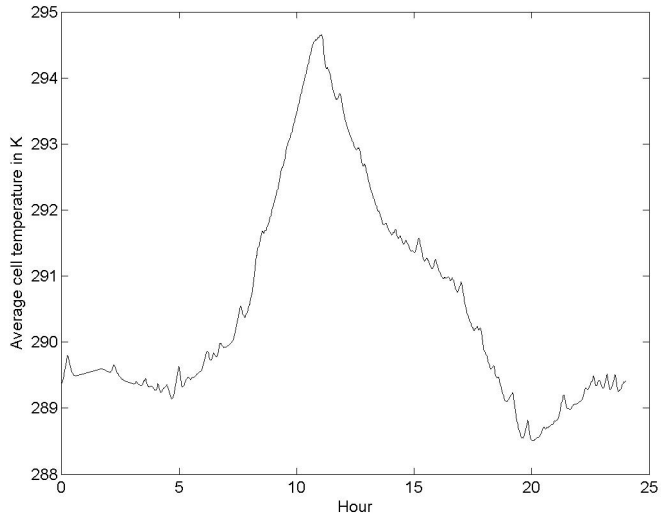

Figure 6.33: Daily evolution of the average cell temperature.

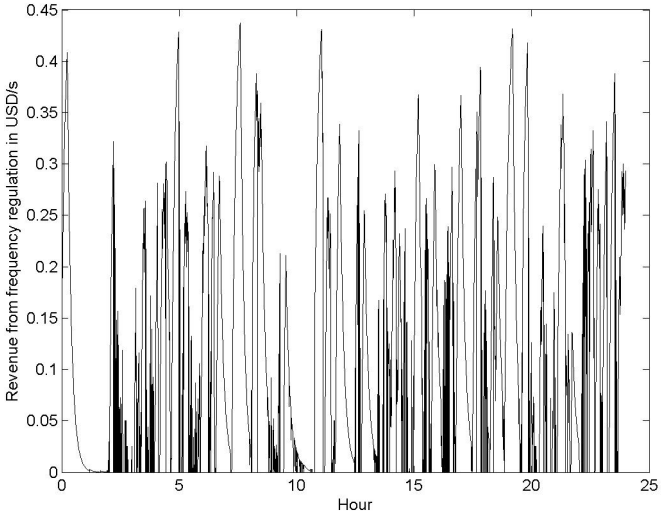

Figure 6.34: Calculated instantaneous income from frequency regulation during one day of BESS operation.

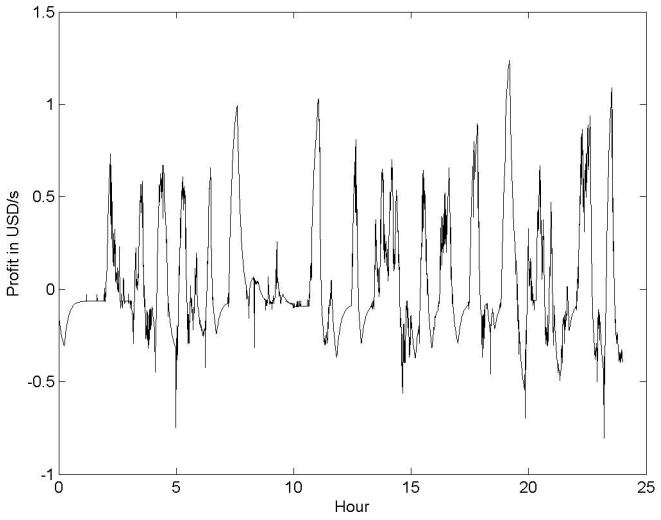

Figure 6.35: Calculated instantaneous profit during one day of BESS operation.

The intra-day analysis also sheds light on the level of utilization of the BESS. Figure 6.36 shows that power output of the device reached the rated capacity of the inverter (20 MW) several times during one day, which suggests that this component could be the limiting one. This hypothesis is supported by figures 6.37 and 6.38, where it is clear that the current and voltage of the cell remain within the safe limits (+70A and -10A for the current, 2V and 4.2V for the voltage), and also by figure 6.39, which shows that the maximum and minimum SOC do not coincide with the moments when the power limit is reached.

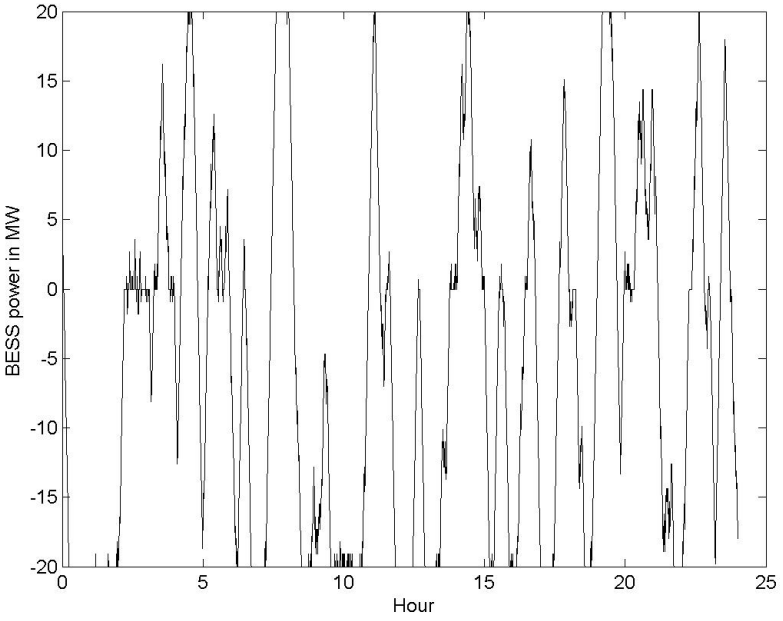

Figure 6.36: BESS power response to frequency deviations during one day of operation.

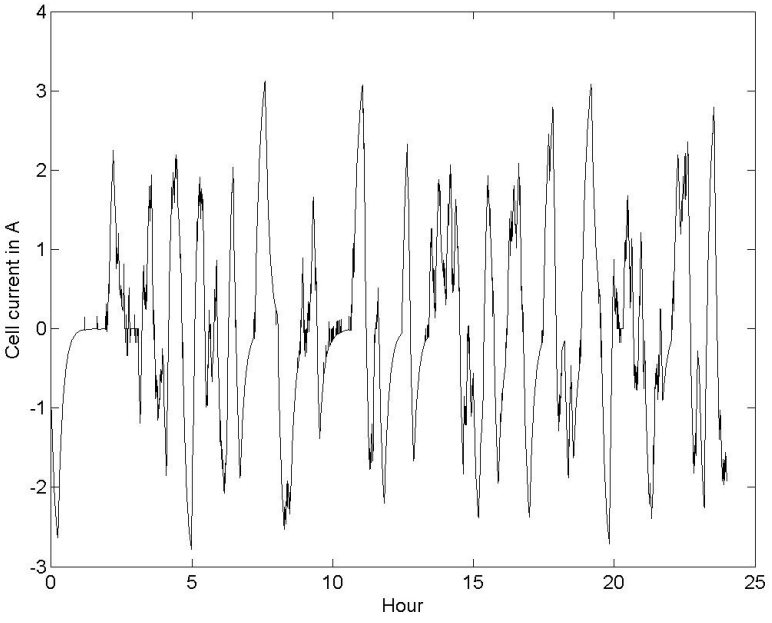

Figure 6.37: Cell current during one day of BESS operation.

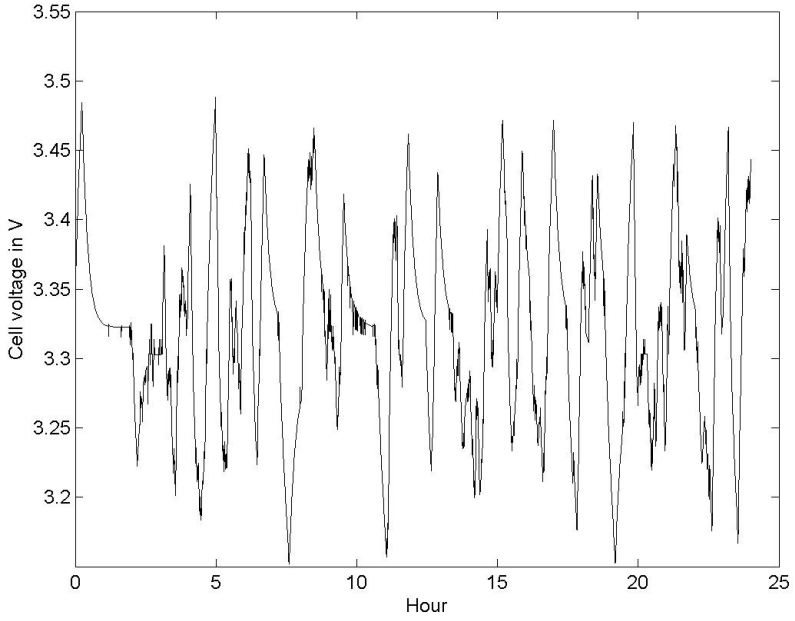

Figure 6.38: Cell terminal voltage during one day of BESS operation.

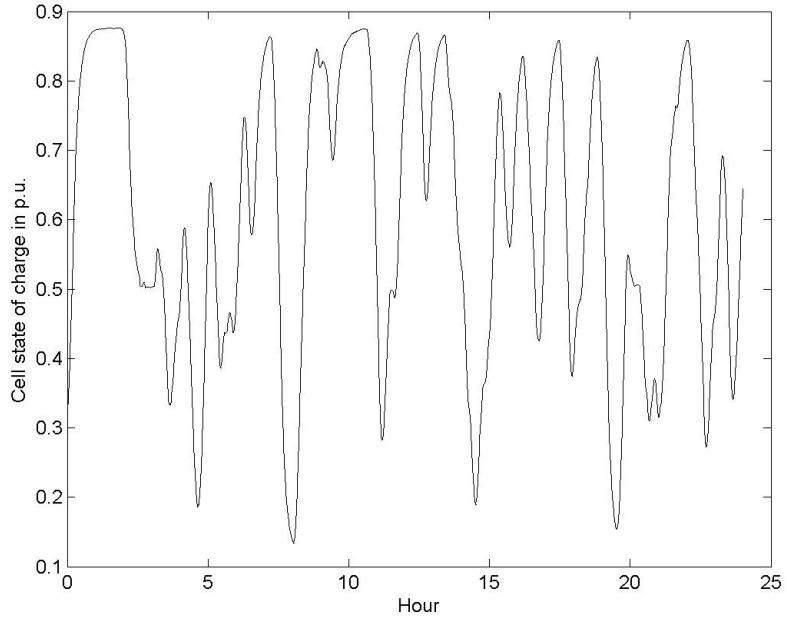

Figure 6.39: Cell state of charge trajectory during one day of BESS operation.

6.3.6 Conclusion

The analysis structure presented in this work can be applied to any scenario where a degradable device is participating in ancillary services. For the particular case modeled,

the relevant findings are:

1. A nonlinear correspondence between the level of service provided, in terms of droop and deadband, and the degradation of the device.

2. The maximum profit for the fixed frequency regulation payment coincides with the maximum utilization of the battery. This is reasonable since the battery degrades even without utilization.

3. Calculating the curve in Figure 6.28 for other frequency regulation payments and replacing the expression with an adequate one for a given regulatory framework easily informs a decision-maker about the competitiveness of the BESS for a given set of reaction parameters. Quantifying technology-specific sensitive characteristics like battery aging as presented can significantly reduce the financial risk of the stakeholder.

6.4 Case 3: Aggregating storage services

The two previous cases have shown applications of the BESS model to isolated functions defined deterministically. Although the economic balance will vary amongst different systems, it is not evident that either one can give access to sufficient revenue to pay for the existing battery technologies in general. This supports the idea that the viability of electrochemical storage in electric power systems depends on them being used for more than one thing at the same time, which is also coherent with the empirical evidence presented in chapter 3 for existing facilities. However, when the BESS is following different operational rules there's no guarantee that they are not going to conflict at a given time, because the BESS has physical constraints.

For example, consider a BESS which is providing frequency regulation according to figure 4.12 in hour 21 in figure 6.11, and suppose also that the measured frequency on a particular instant is 49.5 Hz. Hence, if the BESS follows the setpoint from the frequency response curve, the maximum injection limit would be violated. Conversely, if the injection limit is respected, the frequency regulation service will not be provided. The possibility of this scenario relates to inconvenient correlations between system-level and local-level issues, in this case local congestion v/s system-wide load imbalances.

How can trade-offs related to the utilization of BESS devices be solved? For the example above, one possibility would be to use the following constraint: always leave enough room to respond to your frequency-regulation commitment. In practice, if the service committed is 0.1 p.u. upwards frequency regulation with 10% droop, the peak in figure 6.11 should be shaved to 0.3 p.u. instead of 0.4 p.u in order to be able to adjust the power in response to an under-frequency event while at the same time respecting the injection limit. However, to comply with this for all days necessarily implies a bigger battery, even when the conflicting situation can happen only a couple of times a year.

This study case[10] shows how the proposed BESS model can help model the different trade-offs when a BESS participates in more than one service. Instead of using a hard-coded rule to assure perfect compliance with all the services being provided, an optimization algorithm is used to decide the best parameters for the multiple response characteristics, considering also the interaction between the BESS and a set of flexible residential loads.

6.4.1 Case description

A house interacting with the electric grid in an environment characterized by its ambient temperature and solar radiation profiles is considered. The components of the system are shown in figure 6.40.

In order to develop the case study, several assumptions are made, including the type of house, location, period of time, the occupants and their habits and preferences plus the appliances owned and the electricity tariffs. The location chosen is Antofagasta, Chile, the occupants of the house are a young couple, one of them working most of the time outside home and the other one staying more time at home. The tariffs analysed are flat, dual-time and three-period. The house considered is divided in six areas:

1. Main bedroom;
2. Bathroom 1;
3. Office;
4. Bathroom 2;

[10]The results of this study case have been included in [149].

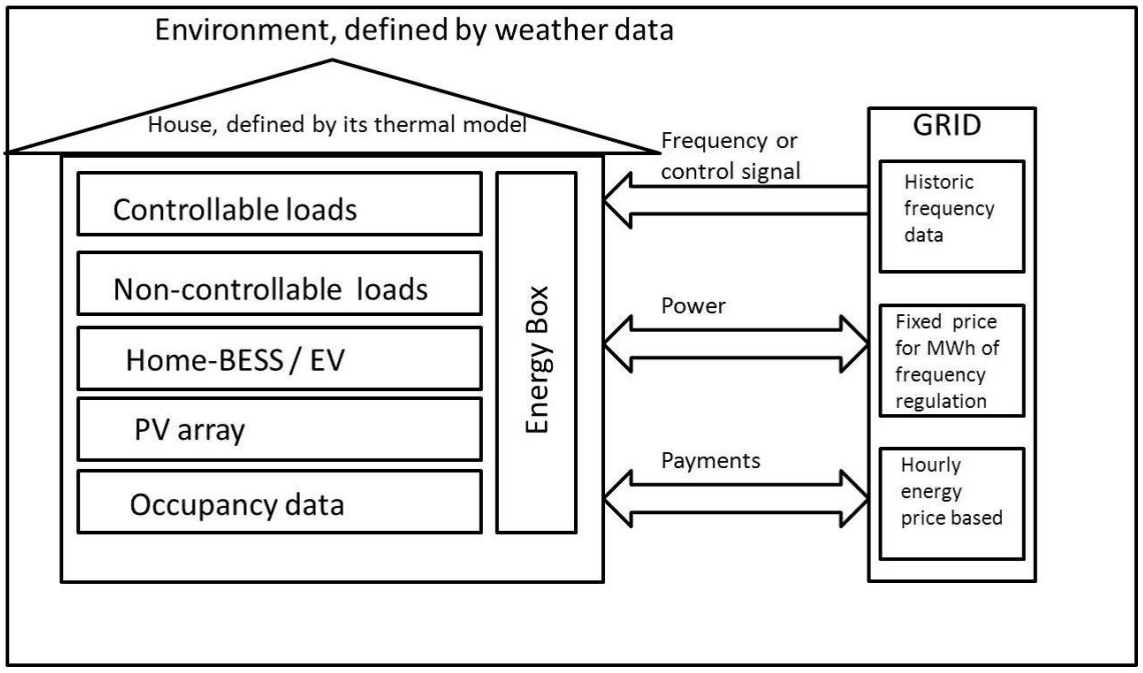

Figure 6.40: Components of the system

5. Living room, dining room and kitchen;

6. Lobby.

Besides a given set of appliances, the occupants also have a PV solar system installed and a storage system. Focusing in the loads existing in the house, they can be divided in two main categories: controllable loads and non-controllable loads. The controllable loads are those that can be the target of some kind of control. This category includes clothes washing machines, clothes dryers, dishwashers, electric water heaters, air conditioning systems and batteries. However, the type of control over these loads is not the same: while clothes washing machines, clothes dryers, dishwashers may be shifted to another period of the day, air conditioning systems and electric water heaters may have the temperature set point re-set. In turn, batteries besides helping in the optimization of the use of endogenous resources, may also contribute to frequency regulation. In order to guarantee the quality of the several energy services provided, some constraints related to users preferences have been considered, namely:

- In the case of electric water heater, it must be assured that end-users have hot water when they need;

- Concerning the clothes washing machine, the clothes dryer and the dishwasher, it has been defined when the machines were loaded and ready for operation plus when the users wanted this equipment to have completed the operation.

In turn, non-controllable loads are those that cannot be managed since their control would bring some discomfort to the user (Rosin et al. 2010). This type of loads includes televisions, laptops, lighting, oven, microwave, iron and hi-fi systems . Besides their consumption, this type of loads also have internal heat gains which are important to consider in the simulation.

The output of the PV panel is obtained using the HOMER software considering the location an optimal fixed altitude and azimuth. A simplified thermal model is considered to account for the thermal interaction between the components of the system. Each zone of the house is represented by a node with several connections representing the walls, floor and ceiling. The floor connects the zone to the ground, which is assumed to be at constant temperature, and the roof connects it to the ambient at variable temperature. The state of each zone is characterized by its temperature T_i. For notation simplicity, the ambient is modeled as six infinitely inertial zones: North, South, East, West, Up and Ground. The connections between zones are defined by the thermal conductivity $Y_{i,j}$ between them. According to this, the conductive heat flow between two zones is given by the relation:

$$Q_{i \to j} = (T_i - T_j) \cdot Y_{i,j} \tag{6.7}$$

The following effects are explicitly taken into account:

- The influence of the zone temperature in the operation of temperature sensitive devices like the electric water heater, refrigerator and HVAC system;
- The effect of ambient temperature evolution during the year;
- Internal gains from occupancy and the operation of appliances;
- Solar gains;
- Thermal inertia. The following aspects were not taken into account in this model:

- Radiant to sensitive heat conversion delays (radiant time series);
- Effect of temperature differences in the coefficient of performance (COP) of the thermal machines.

From the point of view of the electric grid the house behaves as a single entity exchanging energy, power and ancillary services. The electric system inside the house is modeled as a single power exchange model, neglecting the losses and electric variables, except in the battery model. This means that at every time step, the power consumed or injected by all the appliances is added and the resulting value plus or minus the losses in the battery is the power exchanged with the grid. The controllable appliances considered include an electric water heater[11], an HVAC system, a dishwasher, a washing machine and a clothes dryer[12].

6.4.2 Operation strategy

The objective of the control system is minimizing the electricity bill considering not only the electricity cost E_{cost}, but also the degradation of both BESS Deg_{cost} and subtracting the revenues from the participation in ancillary services, namely frequency regulation $Freg_{income}$ and spinning reserve $Spin_{income}$):

$$Bill = E_{cost} + Deg_{cost} - Freg_{income}. \tag{6.8}$$

The operation of the house is determined on the previous day under assumptions about the load, system frequency and photovoltaic energy production for the next day. It is considered that frequency regulation is paid at 15 € per MWh and that the energy can be sold and purchased at the same price. The decision variables an constraints of the optimization problem are:

Decision variables

[11] In a general sense, the electric water heater can be considered a non-reversible energy storage device. While the thermal energy stored can be used to provide sanitary water or heating services, it cannot be injected back to the grid.

[12] For the parameters of the thermal model of the house and the appliances considered, see Appendix E.

1. Hourly water temperature set-points for the electric water heater;
2. Hourly SOC set-point for the BESS;
3. Hourly temperature deviation tolerance for the HVAC system;
4. Start time for the washing machine, clothes dryer and dishwasher;
5. Droop of the BESS;
6. Spinning reserve of the BESS;

Constraints

1. The water in the boiler must be at 90°C at 6 am;
2. The state of charge of the battery in the electric vehicle must be above 0.9 at a given time of departure;
3. The washing machine, clothes dryer and dishwasher have to complete the duty cycle before a given maximum unloading time;

Due to the non-linear nature of the model and because the evaluation of the objective function corresponds to a time-domain simulation which uses this model, meta-heuristic approach has been used. The Evolutionary Particle Swarm Optimization (EPSO) [148] algorithm combines characteristics from evolutionary and particle swarm algorithms to efficiently search the optimal solution within the feasible space. This algorithm is implemented in Matlab and used in the following way:

1. In the first iteration, a swarm of particles representing solutions within the search space is randomly generated. In this study 16 particles have been used;
2. Using Matlab parallel computing toolbox, the swarm is split and sent to Matlab workers [13]. In this case 4 threads have been used;

[13]A *Matlab worker* refers to an instance of matlab which is automatically activated when a parallel pool of work is created. Each instance solves a problem independently and returns results to the main algorithm.

3. Each Matlab worker runs a time-domain simulation with 30 seconds time step and Euler solution for differential equations. If the solutions are prematurely found to violate any of the constraints, the simulation is stopped and a very high value for the objective function is returned[14];

4. The objective function values are returned to the EPSO algorithm;

5. A new swarm is generated and the next iteration begins;

6. The algorithm is run until the value of the objective function shows small changes between iterations. Typically this happened before 100 iterations.

The benefit from optimizing the operation of the house is assessed for three tariff schemes: flat rate, dual tariff and three-periods tariff. For each one of them the net-metering case is compared with the consumer-only contract. While in the consumer-only contract case the end-user consumes electricity without implementing any demand side management programs and no payment is received for reacting to external signals or for injecting energy to the grid, in the net metering case the energy injected to the system is paid at the same price than the energy consumed and the electricity consumption is optimized. In all cases, and in addition to the appliances described before, an EV with a 10 kWh battery pack plus a stationary 5 kWh BESS and a 5 kW PV system are considered.

6.4.3 Results

The results achieved for the reference case and the optimized case are presented in table 6.4. For each type of tariff and for both types of contracts, the value represents the electricity bill at the end of the month in euros. While the positive value represents a bill that must be paid by the end-user, negative values represent the economic benefit attained.

Considering the energy price in figure **??** and the PV production profile on figure 6.42, a close-up to two days (48 hours) of operation is presented in figures 6.43 to 6.45. While in the reference case (figure 6.42) the EV batteries is charged till the full SOC and

[14] this is found to be an effective way to speed-up the convergence of the algorithm, although it can be objected that it eliminates relevant gradient information.

	Tariff	A - Consumer-only Contract	B - Net Metering
Reference Case	1 - Flat	55.5	7.62
	2 - Two-periods	64.5	3.87
	3 - Three-periods	64.03	4.98
Optimized case	1 - Flat	34.8	-28.5
	2 - Two-periods	48	-75.12
	3 - Three-periods	50.2	-60.3

Table 6.4: Monthly electricity bill balance for different contracts and energy rates.

the stationary battery is kept at a constant 0.5 SOC, in the optimized consumer-only contract case (figure 6.44) the stationary battery is mainly recharged when there is a higher PV production of electricity. In contrast, in the optimized net metering case (figure 6.45), the SOC of the stationary battery is changed in a completely different way: since the value paid by the grid for buying electricity is attractive, the optimized scheme chooses to sell energy instead of storing it for later use.

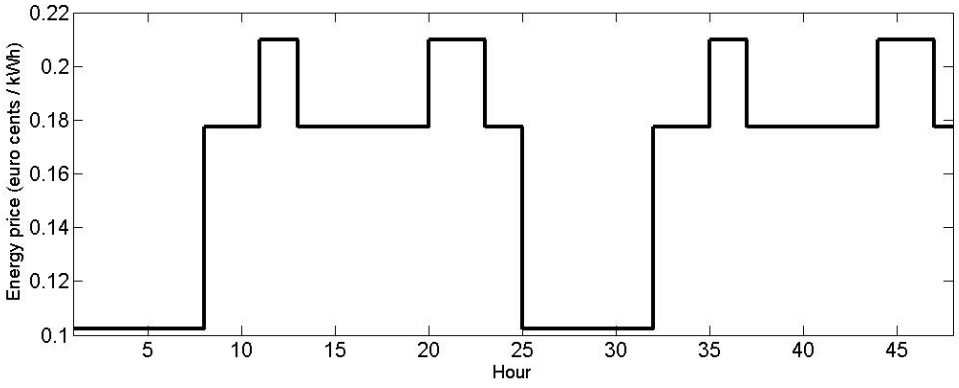

Figure 6.41: Energy cost perceived by the customer.

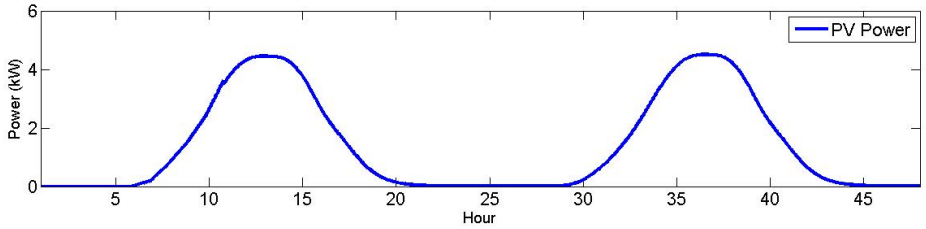

Figure 6.42: Solar power production profile for two clear days).

6.4.4 Conclusion

This study focused on the determination of the optimal utilization of the devices inside a house from the end-user point of view for 6 different schemes. In all the 6 cases, the

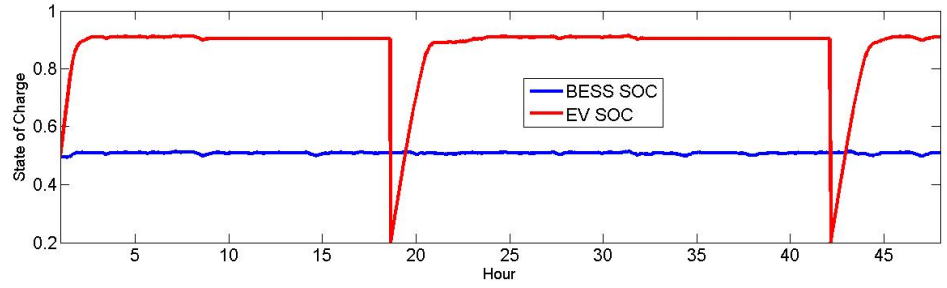

Figure 6.43: Operation of both BESSs without optimization.

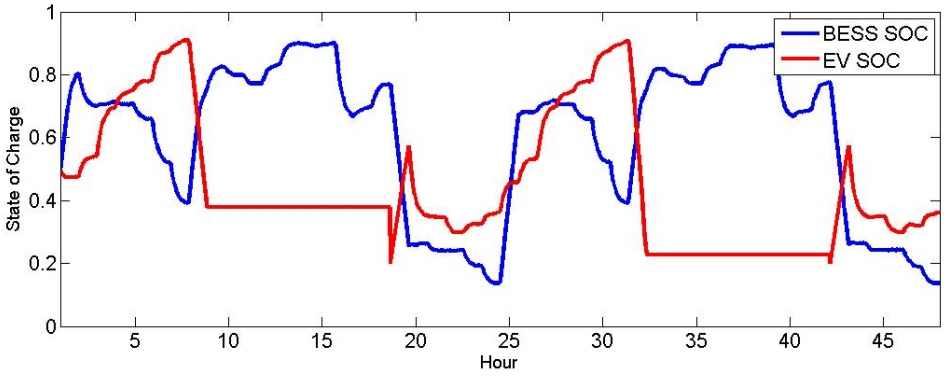

Figure 6.44: Optimized operation of both BESS under a consumer-only energy contract.

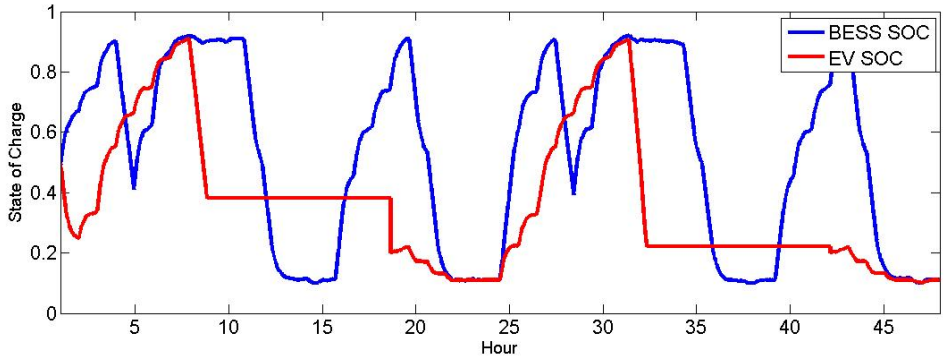

Figure 6.45: Optimized operation of both BESS under a net-metering energy contract.

optimization process generates a significant reduction in the operation cost, ranging from 25 % (three periods tariff, consumer-only contract) to 142 % euros (two-periods, net-metering contract) of benefit per month [15]. The results indicate that the tariff structure has a dramatic influence on how the domestic energy resources need to be operated in

[15] In both cases, as a percentage of the consumer-only flat tariff monthly expenditure. A factor that influences these results is that the customer has an unusually high electricity load compared to average residential customers in Europe. This results from a) all thermal loads are met with electricity and b) the presence of an electric vehicle. Also, the size of the PV panel is not rational if the customer had a consumer-only contract, but the size is kept the same in both cases for consistency.

order to maximize the benefit. For example, under net-metering there is little incentive to store solar power in the battery, contrasting with the consumer-only case. From the point of view of the grid, this means that a storage asset is not being used and therefore the overall operation of the power system could be improved. This could be done by increasing the incentives to provide ancillary services. Based on these results, we conclude that model-based simulation approaches should be taken into account for designing strategies that could contribute to the overall optimal operation of the system, namely in the design of tariffs structures.

Chapter 7

Conclusions and future work

This chapter examines the outcome of the Thesis with respect to the formulated objectives, identifying original contributions and proposing promising research directions. In general terms, the models and methodologies developed are deemed relevant to address the main research question: *How Should Electrochemical Accumulators be Exploited to Support the Operation of Electric Power Systems?*, in multiple contexts within and beyond electric power systems. It has been shown through case studies that a comprehensive and detailed description of battery energy storage can reveal opportunities to improve the design of BESSs for particular applications and to guide the development of regulation to encourage a more efficient use of them from a social perspective.

7.1 Revision of objectives

As stated in section 1.3, the guiding objective of the research is to help answer the research question through the development of *models and methodologies that can assess the technical and economical performance of electrochemical accumulators connected to electric power systems*. This is achieved in chapter 4 through a complete model for battery energy storage systems comprising the most relevant physical and control characteristics, and in chapter 5 through methodologies to incorporate models into power systems studies. The methodological part is further developed through case studies in chapter 6, involving:

1. The evaluation of battery energy storage as a resource to integrate photovoltaic generation in distribution networks;
2. Simulation of the lifecycle performance of a BESS providing frequency regulation;
3. Optimized operation of a BESS and a set of domestic appliances at the residential level engaged in energy arbitrage and frequency regulation;

The level of achievement of each group of specific objectives declared in section 1.3 is explained below:

1. **Electrochemical cell models:** The model described in section 4.3.3 complies with the proposed features.
2. **Power conversion system (PCS):** The model described in section 4.2 complies with the proposed features. However, emulated inertia was not implemented in a case study.
3. **Monitoring and control unit (MCU):** All the features are contained in the model described in section 4.4. Only the voltage regulation functionality was not implemented in a case study.
4. **Distribution network expansion planning:** The methodologies explained in section 6.2 and section 5.2, together with the battery model described in section 5.1 are sufficient to meet this objective, as is shown in the case study of section 6.2.
5. **Bulk energy arbitrage:** The model described in section 5.1 together with the heuristic optimization methodology described in section 6.4 meet this objective, as demonstrated in the case study in that same section.
6. **Bulk frequency regulation:** The battery model described in section 5.1 is adequate to meet this objective. However, electrochemical ramping limitations were not implemented explicitly in the case study of section 6.3.
7. **Microgrid design** The model explained in section 5.1.4 is intended to be adequate for this purpose, although is was not implemented in a case study.

8. **Microgrid operation** The models explained in sections 5.1 and 5.1.4 are adequate for this purpose. Although an specific microgrid operation case was not studied, most of the relevant features are contained in the one described in section 6.4.

In summary, it is considered that the declared objectives were fulfilled by the Thesis.

7.2 Contributions of the thesis

The models developed in the Thesis are a contribution towards the creation of standard models to represent battery energy storage in power systems studies, and also in methodologies to use these models to support specific planning and operation decisions. In summary, the relevant contributions to the current state of the art are:

1. **A detailed and generic model for battery energy storage systems:** The continuous-time model described in chapter 4 provides a uniform and detailed representation of a BESS for power systems studies. The model of the electrochemical cell is taken from the literature and a discrete-time state-space formulation is developed in section 5.1 to make it compatible with this kind of studies. The representation of the BMS, MCU and power electronics are also included in the model with a parametrical representation. The benefits of this modeling approach for power systems studies are:

   (a) The cell model allows to represent most electrochemical storage technologies, with the exception of flow batteries;

   (b) Physical variables like current, voltage and temperature are explicitly included in the output of the model, which enables the extraction of the model's parameters from electrical tests. This is an advantage with respect to models that reduce the operation of the cell to energy flows;

   (c) Parameter changes due to degradation can be simulated with arbitrary time resolution, which allows for cost-balance calculation on each simulation time step. This is an advantage compared with models which use a cycle as the fundamental unit of degradation;

(d) The different levels of control can be defined parametrically. A model containing quasi-steady-state reaction parameters was implemented in Matlab version 2013, and the transient response ones in DigSILENT Power Factory version 14.

2. **A methodology to assess the economic and technical performance of battery energy storage as a means to integrate variable energy resources:** This allows to estimate the aggregate economic benefit of battery energy storage taking into account its lifecycle performance. The benefits of this approach are:

   (a) Allows for a quantification of the value of storage devices in general when compared to other network assets;

   (b) Gives an estimation of the performance of a BESS during its lifetime providing a distribution-support service, including the compliance with service terms as the cells age;

   (c) Extends the applicability of the Reference Network Model developed by IIT-Comillas to include storage devices. Although the storage sizing and operation rule described in section 5.2 is most likely sub-optimal, it allows to compare energy storage and network reinforcements by running the RNM several times for different control parameters like injection and consumption limits.

3. **A detailed optimization model to incorporate a BESS in day-ahead scheduling problems:** The method explicitly takes into account the time-varying battery use and losses costs in combination with other decision variables.

   (a) The representation of the control system and power electronics allows to simulate autonomous, supervised, and optimized operation. Optimization and simulation can be used in tandem with different levels of detail. Also, agent-like behavior can be incorporated easily through rules or optimization algorithms.

   (b) Offers a tool to evaluate the influence of different regulations (e.g., network tariffs) over the expected behavior of "intelligent" energy management systems containing energy storage.

7.3 Future work

Throughout the development of the main contributions, progress was made in promising directions which could not be followed because of time and/or scope considerations. This section comments these with the purpose of motivating future research or applications.

1. **Optimization of BESS parameters for real applications:** The application of the model developed here is able to reveal, for example, the under-utilization of some BESS components. It can be used as an evaluation sub-routine to obtain the optimal design of a BESS for a given application. Examples of this are the optimal sizing of BESSs connected to the distribution network providing voltage and net load control, and also the same for a residential BESS for a given context (regulation, grid, weather, appliances and users' behavior).

2. **Implementation of a real-time MCU:** The model has been used from a simulation perspective, and it has been assumed that the state variables are available to make decisions. In real operation, the challenge is to be able to estimate the state variables from measurable data (voltage, current, temperature, pressure, etc.) and use them to inform decisions. A necessary step in this direction is the observability analysis of the model of chapter 4, were it is likely to be found that not all the parameters can be observed, which would require to develop a reduced-order model which is still able to lead to the right decisions. The full model can be used to benchmark candidate observable representations, and periodic tests can be done to correct for parameters drift.

3. **Transient stability in small isolated systems:** The short-term electrochemical dynamics described in chapter 4 were not implemented in a case study. It would be interesting to do so in order to compare the lifecycle performance of a BESS with other devices (for example, a flywheel) in contexts where fast dynamics are relevant, such as inertial response or dynamic security assessment in isolated systems.

4. **Technology comparison:** Although it is possible to adjust the parameters of the model to represent a range of different battery chemistries, the study cases only used a specific lithium-ion cell. It is reasonable to expect that different contexts will favor different chemistries, for example regarding their power/energy ratio.

Regulation, through its influence over market rules and business models, will likely play an important role in this analysis[1].

5. **Impact of tariffs on optimal operation:** The case study in section 6.4 showed that the structure of the tariff has a big influence over the operation decisions of a BESS. Combining this methodology with, for example, the centralized operation rule used in 6.2, one can find the tariff structure that drives social behavior towards the social optimum. A candidate methodology to allocate network costs in a way that would send appropriate economic signal for energy storage is included in Appendix F.

[1] See for example the case of payment for performance on FERC rule 755.

Appendix A

Motivation case details

End buses	Length (km)	Resistance (Ω)	Reactance (Ω)
1 - 2	1	1.5	0
2 - 3	0.5	0.75	0

Table A.1: Characteristics of the lines considered in the motivation case in chapter one.

Voltage regulator		
Parameter	Value	Unit
Minimum voltage	190	V
Maximum voltage	250	V
Nominal voltage	220	V
Tap step	0.05	p.u.
Taps	5	
Nominal ratio	1	p.u.
Time constant	15	minutes
Hysteresis	5	V

Table A.2: Characteristics of the voltage regulator considered in the motivation case in chapter one.

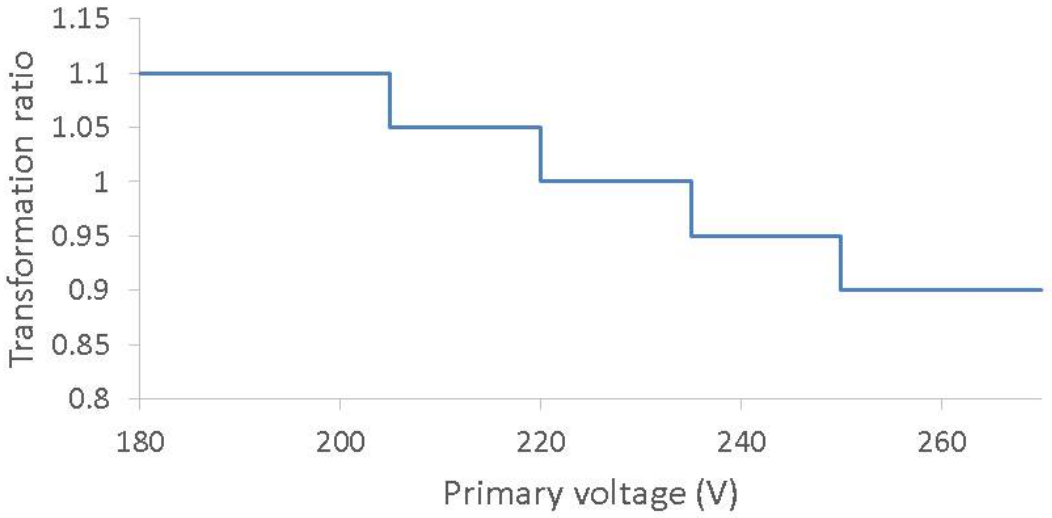

Figure A.1: Voltage ratio between the primary and secondary connections of the voltage regulator as a function of the primary voltage.

Appendix B

Cell model parameters

The cell model used to represent the electrochemical cell in the case studies is an improved version of the one presented by the author in [150], where mass and charge transport short-term dynamics and spatial variability are neglected, which is considered acceptable given the time step of the simulation. The state evolution equations are hence simplified from the equations in section 5.1.3 to:

$$q(p+1) = q(p) - I_{ion}(p) \cdot \delta_t, \tag{B.1}$$

where $\frac{I_{ion}}{A_{cell}} = j_s = j_e$, with j_s and j_e as defined in equations 5.6. For the temperature evolution, considering that the internal gains IG correspond to the resistive losses in the battery:

$$H(p+1) = H(p) + IG(p) + h_{a,b} \cdot (T_a - T_b) \tag{B.2}$$

Also, the overpotentials from equations (5.8), (5.6) and (5.10) are represented through equivalent conductivities, which are dependent on the state of charge and the direction of the current.

$$\begin{aligned} \sigma_r =& \sigma_{max} \cdot \frac{\zeta s}{\zeta^{\max_S \max}} \\ \sigma_d =& \sigma_{max} \cdot \left(1 - \frac{\zeta s}{\zeta^{\max_S}}\right) \end{aligned} \tag{B.3}$$

The degradation of the electrodes is represented with equation 5.16. The A123 ANR26650 Lithium-ion cell is considered as the basic building block of the BESS in the three study cases. The cell parameters were fitted to data found in the literature [146] and in the manufacturer's datasheet [147].

Parameter	Symbol	Value	Unit
Nominal temperature	T_0	298	K
Nominal electrochemical potential	U_0^{cell}	3.2769	V
Electrode planar area	A_{cell}	4.987	m^2
Electrode thickness	δ_e	$5.042 \cdot 10^{-}5$	m
Separation between electrodes	δ_s	$3.71 \cdot 10^{-}5$	m
Electrode active area per unit volume	a_s	1023	$\frac{1}{m}$
Specific heat of the battery pack	C_v	207	$\frac{J}{K}$
Ambient-Cell thermal resistance	h_0	1	$\frac{K}{W}$
Conductivity of the electrodes	σ_{e0}	$3.143 \cdot 10^{-3}$	$\frac{1}{\Omega \cdot m}$
Equivalent conductivity	σ_{max}	218	$\frac{1}{\Omega \cdot m}$
Degradation coefficient	β_1	$2.92 \cdot 10^{-22}$	
Degradation coefficient	β_2	$3.41 \cdot 10^{-24}$	
Degradation coefficient	β_3	$3.41 \cdot 10^{-24}$	

Table B.2: Model coefficients fitted to the ANR26650 data

Appendix C

Study case 1 details

The robust study of the impact of photovoltaic generators over the costs of distribution networks required to take into account a diversity of scenarios. Two main assumptions which were not developed in the main body of the Thesis are the composition of the load and the distribution of photovoltaic generation across voltage levels. This section also shows the section of each geographic location that was considered, and the locations identified as viable for large PV generators.

C.1 Densely populated areas

C.1.1 Los Angeles, California

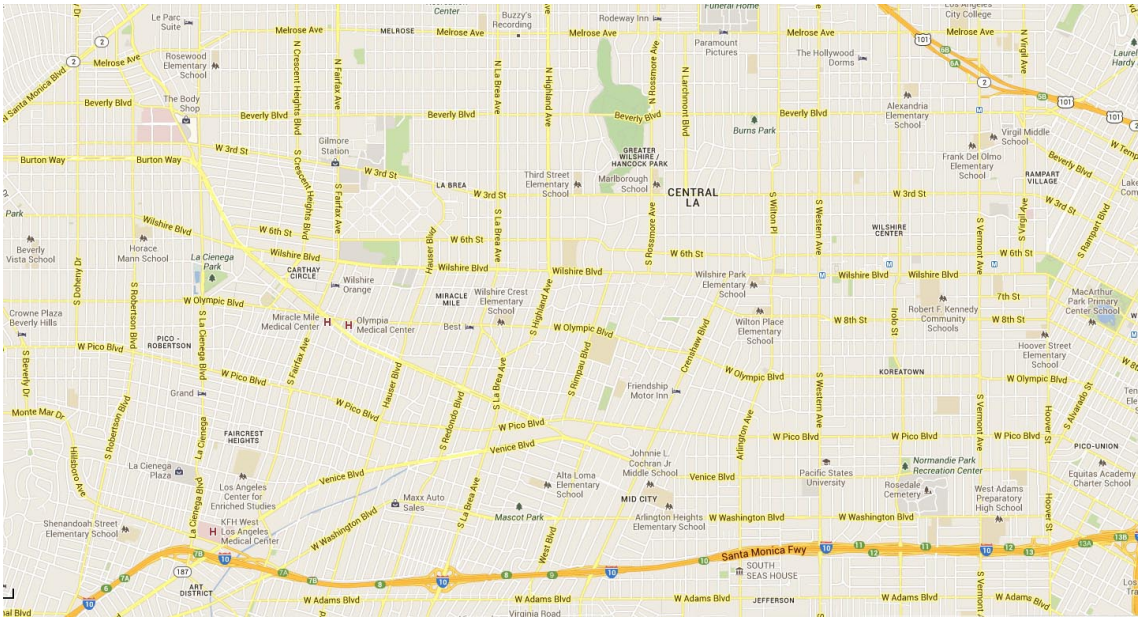

Figure C.1: 11 x 5 km section of the Los Angeles area considered in the study.

	Unit	LV	MV	HV						
Load power density	kW/km^2	**3500**	**2500**	**2000**	1			LV	MV	HV
Aprox. load energy density	kWh/(km^2*yr)	12264000	13140000	14016000	2		Points/km^2	233	12	0
Load point average power	kW	**15**	**200**	**5000**	3		PV capacity factor	**0.12**	**0.15**	**0.2**
Load average energy	kWh/yr	12264000	13140000	14016000	4		PV penetration (p.u.)	**0**	**0**	**0**
Load average PF	p.u.	**1**	**1**	**1**	5		PV power (kW)	-	-	-
Load StDev power	p.u.	**0.2**	**0.2**	**0.2**	6					
Load StDev energy	p.u.	**0.3**	**0.3**	**0.3**	7		Simultaneity factors			
Load StDev PF	p.u.	**0**	**0**	**0**	8		LV	0.3		
Industrial profile share	p.u.	**0.8**	**0.8**	**0.8**	9		MV	0.6		
Commercial profile share	p.u.	**0.15**	**0.15**	**0.15**	10		HV	0.9		
Residential profile share	p.u.	0.05	0.05	0.05	11					
Initial PV power density	kW/km^2	0	0	0	12					
Intial PV energy density	kWh/(km^2*yr)	0	0	0	13					
PV average power	kW	**15**	**200**	**5000**	14		**Data for Los Angeles, CA**			
PV average capacity factor	p.u.	**0.22**	**0.23**	**0.24**	15					
PV average PF	p.u.	**1**	**1**	**1**	16					
PV StDev power	p.u.	**0.2**	**0.2**	**0.2**	17					
PV StDev capacity factor	p.u.	**0.1**	**0.1**	**0.1**	18					
PV StDev PF	p.u.	**0**	**0**	**0**	19					
Voltage	kV	**0.24**	**12**	**33**	20					

Table C.1: Parameters of the Los Angeles network before the introduction of PV generation.

C.1.2 Denver, Colorado

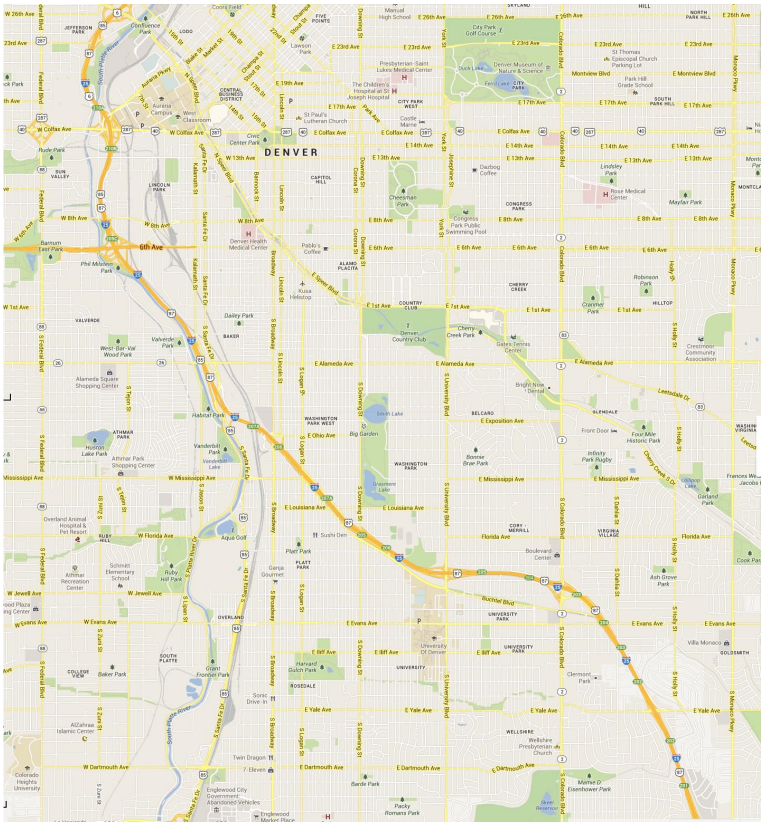

Figure C.2: 11 x 11 km section of the Denver area considered in the study.

	Unit	LV	MV	HV						
Load power density	kW/km^2	**900**	**600**	**100**	1					
Aprox. load energy density	kWh/(km^2*yr)	3153600	3153600	700800	2		Points/km^2	60	3	0
Load point average power	kW	**15**	**200**	**5000**	3		PV capacity factor	**0.12**	**0.15**	**0.2**
Load average energy	kWh/yr	3153600	3153600	700800	4		PV penetration (p.u.)	**0**	**0**	**0**
Load average PF	p.u.	**1**	**1**	**1**	5		PV power (kW)	-	-	-
Load StDev power	p.u.	**0.2**	**0.2**	**0.2**	6					
Load StDev energy	p.u.	**0.3**	**0.3**	**0.3**	7		Simultaneity factors			
Load StDev PF	p.u.	**0**	**0**	**0**	8		LV	0.3		
Industrial profile share	p.u.	**0.8**	**0.8**	**0.8**	9		MV	0.6		
Commercial profile share	p.u.	**0.15**	**0.15**	**0.15**	10		HV	0.9		
Residential profile share	p.u.	0.05	0.05	0.05	11					
Initial PV power density	kW/km^2	0	0	0	12					
Intial PV energy density	kWh/(km^2*yr)	0	0	0	13					
PV average power	kW	**15**	**200**	**5000**	14		**Data for Denver, CO**			
PV average capacity factor	p.u.	**0.24**	**0.25**	**0.26**	15					
PV average PF	p.u.	**1**	**1**	**1**	16					
PV StDev power	p.u.	**0.2**	**0.2**	**0.2**	17					
PV StDev capacity factor	p.u.	**0.1**	**0.1**	**0.1**	18					
PV StDev PF	p.u.	**0**	**0**	**0**	19					

Table C.2: Parameters of the Denver network before the introduction of PV generation.

C.1.3 Hartford Connecticut

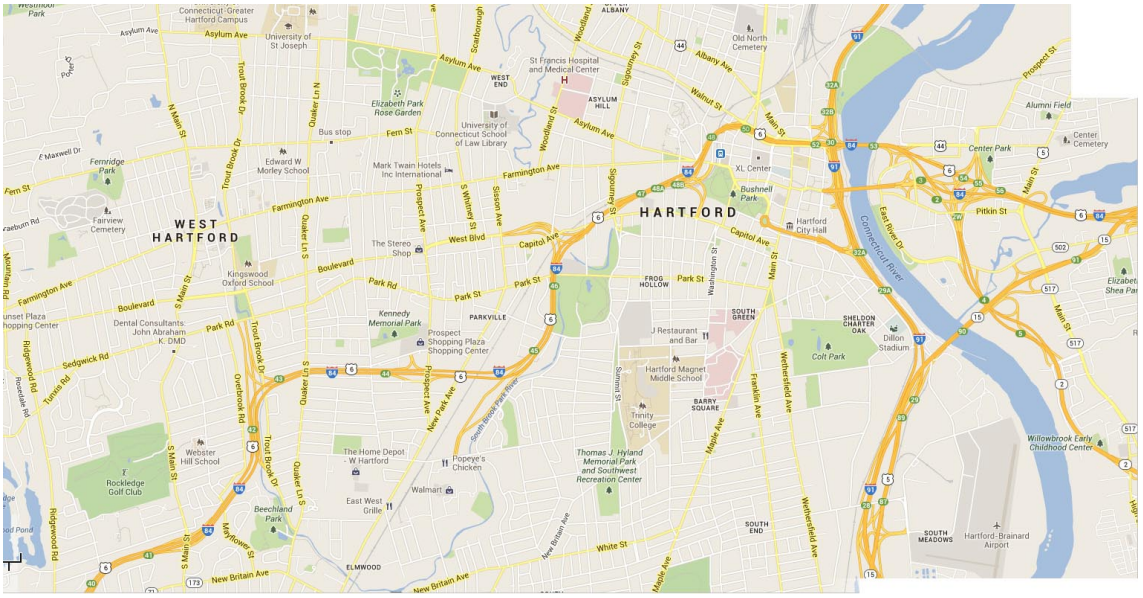

Figure C.3: 11 x 6 km section of the Hartford area considered in the study.

	Unit	LV	MV	HV
Load power density	kW/km^2	**2000**	**1000**	**500**
Aprox. load energy density	kWh/(km^2*yr)	7008000	5256000	3504000
Load point average power	kW	**15**	**200**	**5000**
Load average energy	kWh/yr	7008000	5256000	3504000
Load average PF	p.u.	**1**	**1**	**1**
Load StDev power	p.u.	**0.2**	**0.2**	**0.2**
Load StDev energy	p.u.	**0.3**	**0.3**	**0.3**
Load StDev PF	p.u.	**0**	**0**	**0**
Industrial profile share	p.u.	**0.8**	**0.8**	**0.8**
Commercial profile share	p.u.	**0.15**	**0.15**	**0.15**
Residential profile share	p.u.	0.05	0.05	0.05
Initial PV power density	kW/km^2	0	0	0
Intial PV energy density	kWh/(km^2*yr)	0	0	0
PV average power	kW	**15**	**200**	**5000**
PV average capacity factor	p.u.	**0.17**	**0.18**	**0.19**
PV average PF	p.u.	**1**	**1**	**1**
PV StDev power	p.u.	**0.2**	**0.2**	**0.2**
PV StDev capacity factor	p.u.	**0.1**	**0.1**	**0.1**
PV StDev PF	p.u.	**0**	**0**	**0**

	LV	MV	HV
Points/km^2	133	5	0
PV capacity factor	**0.12**	**0.15**	**0.2**
PV penetration (p.u.)	**0**	**0**	**0**
PV power (kW)	-	-	-

Simultaneity factors	
LV	0.3
MV	0.6
HV	0.9

Data for Hartford, CT

Table C.3: Parameters of the Hartford network before the introduction of PV generation.

C.1.4 Des Moines, Indiana

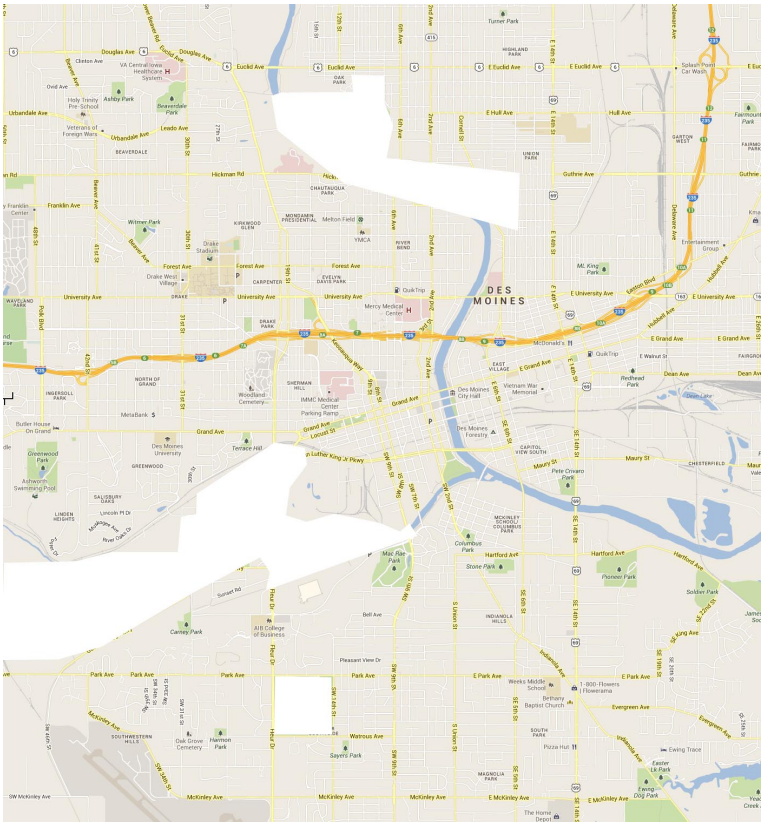

Figure C.4: 10 x 11 km section of the Des Moines area considered in the study.

	Unit	LV	MV	HV
Load power density	kW/km^2	**700**	**200**	**100**
Aprox. load energy density	kWh/(km^2*yr)	2452800	1051200	700800
Load point average power	kW	**15**	**200**	**5000**
Load average energy	kWh/yr	2452800	1051200	700800
Load average PF	p.u.	**1**	**1**	**1**
Load StDev power	p.u.	**0.2**	**0.2**	**0.2**
Load StDev energy	p.u.	**0.3**	**0.3**	**0.3**
Load StDev PF	p.u.	**0**	**0**	**0**
Industrial profile share	p.u.	**0.8**	**0.8**	**0.8**
Commercial profile share	p.u.	**0.15**	**0.15**	**0.15**
Residential profile share	p.u.	0.05	0.05	0.05
Initial PV power density	kW/km^2	0	0	0
Intial PV energy density	kWh/(km^2*yr)	0	0	0
PV average power	kW	**15**	**200**	**5000**
PV average capacity factor	p.u.	**0.18**	**0.19**	**0.2**
PV average PF	p.u.	**1**	**1**	**1**
PV StDev power	p.u.	**0.2**	**0.2**	**0.2**
PV StDev capacity factor	p.u.	**0.1**	**0.1**	**0.1**
PV StDev PF	p.u.	**0**	**0**	**0**

		LV	MV	HV
Points/km^2		46	1	0
PV capacity factor		**0.12**	**0.15**	**0.2**
PV penetration (p.u.)		**0**	**0**	**0**
PV power (kW)		-	-	-
Simultaneity factors				
LV	0.3			
MV	0.6			
HV	0.9			

Data for Des Moines, IA

Table C.4: Parameters of the Des Moines network before the introduction of PV generation.

C.1.5 Austin, Texas

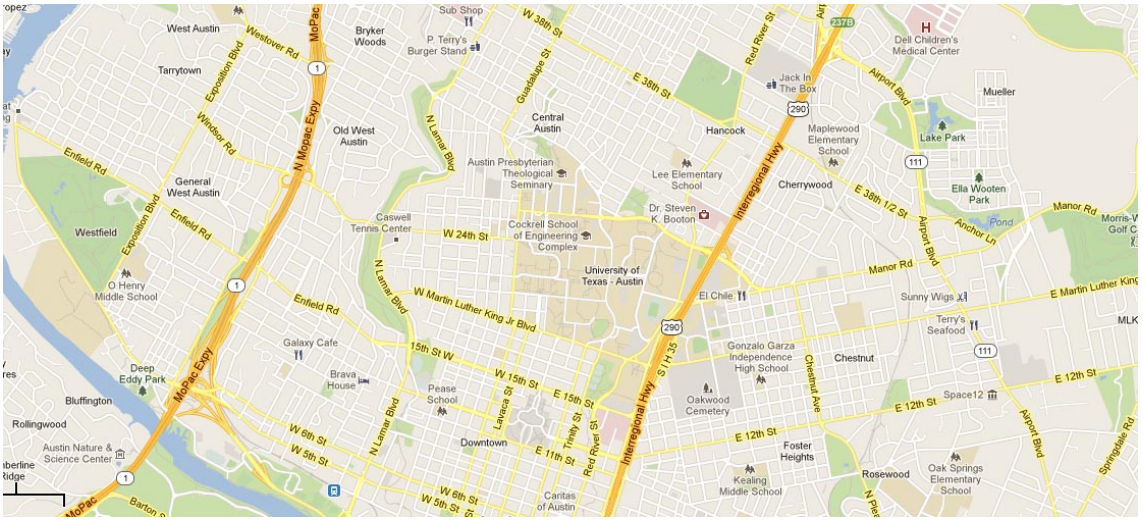

Figure C.5: 9 x 4 km section of the Austin area considered in the study.

	Unit	LV	MV	HV						
Load power density	kW/km^2	**1800**	**700**	**500**	1			LV	MV	HV
Aprox. load energy density	kWh/(km^2*yr)	6307200	3679200	3504000	2	Points/km^2		120	7	0
Load point average power	kW	**15**	**100**	**5000**	3	PV capacity factor		**0.12**	**0.15**	**0.2**
Load average energy	kWh/yr	6307200	3679200	3504000	4	PV penetration (p.u.)		**0**	**0**	**0**
Load average PF	p.u.	**1**	**1**	**1**	5	PV power (kW)		-	-	-
Load StDev power	p.u.	**0.2**	**0.2**	**0.2**	6					
Load StDev energy	p.u.	**0.3**	**0.3**	**0.3**	7	Simultaneity factors				
Load StDev PF	p.u.	**0**	**0**	**0**	8	LV		0.3		
Industrial profile share	p.u.	**0.8**	**0.8**	**0.8**	9	MV		0.6		
Commercial profile share	p.u.	**0.15**	**0.15**	**0.15**	10	HV		0.9		
Residential profile share	p.u.	0.05	0.05	0.05	11					
Initial PV power density	kW/km^2	0	0	0	12					
Intial PV energy density	kWh/(km^2*yr)	0	0	0	13					
PV average power	kW	**15**	**200**	**5000**	14	**Data for Austin, TX**				
PV average capacity factor	p.u.	**0.21**	**0.22**	**0.23**	15					
PV average PF	p.u.	**1**	**1**	**1**	16					
PV StDev power	p.u.	**0.2**	**0.2**	**0.2**	17					
PV StDev capacity factor	p.u.	**0.1**	**0.1**	**0.1**	18					
PV StDev PF	p.u.	**0**	**0**	**0**	19					

Table C.5: Parameters of the Austin network before the introduction of PV generation.

C.1.6 Seattle, Washington

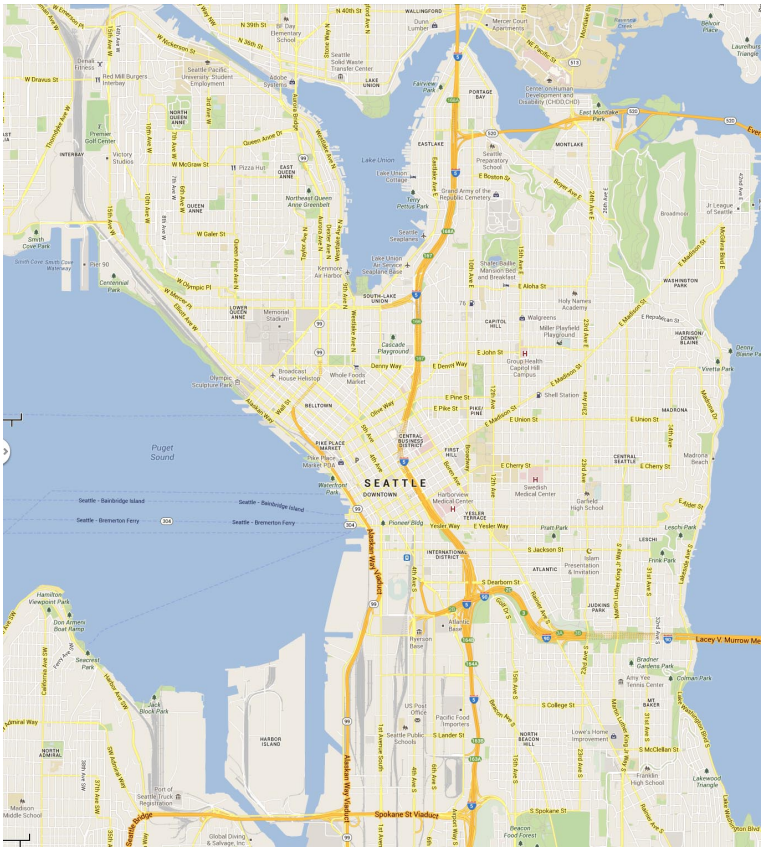

Figure C.6: 9 x 10 km section of the Seattle area considered in the study.

	Unit	LV	MV	HV
Load power density	kW/km^2	**1,800**	**1,000**	**500**
Aprox. load energy density	kWh/(km^2*yr)	6307200	5256000	3504000
Load point average power	kW	**15**	**100**	**5000**
Load average energy	kWh/yr	6307200	5256000	3504000
Load average PF	p.u.	**1**	**1**	**1**
Load StDev power	p.u.	**0.2**	**0.2**	**0.2**
Load StDev energy	p.u.	**0.3**	**0.3**	**0.3**
Load StDev PF	p.u.	**0**	**0**	**0**
Industrial profile share	p.u.	**0.8**	**0.8**	**0.8**
Commercial profile share	p.u.	**0.15**	**0.15**	**0.15**
Residential profile share	p.u.	0.05	0.05	0.05
Initial PV power density	kW/km^2	0	0	0
Intial PV energy density	kWh/(km^2*yr)	0	0	0
PV average power	kW	**15**	**200**	**5000**
PV average capacity factor	p.u.	**0.14**	**0.15**	**0.16**
PV average PF	p.u.	**1**	**1**	**1**
PV StDev power	p.u.	**0.2**	**0.2**	**0.2**
PV StDev capacity factor	p.u.	**0.1**	**0.1**	**0.1**
PV StDev PF	p.u.	**0**	**0**	**0**

	LV	MV	HV
Points/km^2	120	10	0
PV capacity factor	**0.12**	**0.15**	**0.2**
PV penetration (p.u.)	**0**	**0**	**0**
PV power (kW)	-	-	-

Simultaneity factors	
LV	0.3
MV	0.6
HV	0.9

Data for Seattle, WA

Table C.6: Parameters of the Seattle network before the introduction of PV generation.

C.2 Sparsely populated areas

C.2.1 Lancaster, California

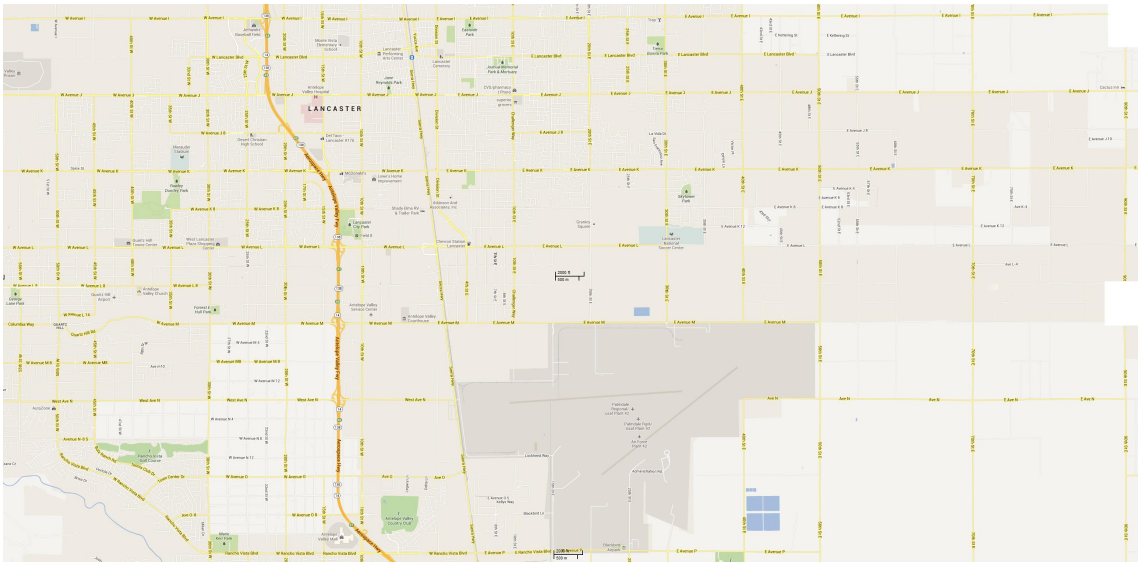

Figure C.7: 29 x 13 km section of the Lancaster area considered in the study.

	Unit	LV	MV	HV
Load power density	kW/km^2	**200**	**100**	**80**
Aprox. load energy density	kWh/(km^2*yr)	700800	525600	560640
Load point average power	kW	**5**	**100**	**5000**
Load average energy	kWh/yr	700800	525600	560640
Load average PF	p.u.	**1**	**1**	**1**
Load StDev power	p.u.	**0.2**	**0.2**	**0.2**
Load StDev energy	p.u.	**0.3**	**0.3**	**0.3**
Load StDev PF	p.u.	**0**	**0**	**0**
Industrial profile share	p.u.	**0.8**	**0.8**	**0.8**
Commercial profile share	p.u.	**0.15**	**0.15**	**0.15**
Residential profile share	p.u.	0.05	0.05	0.05
Initial PV power density	kW/km^2	0	0	0
Intial PV energy density	kWh/(km^2*yr)	0	0	0
PV average power	kW	**15**	**200**	**5000**
PV average capacity factor	p.u.	**0.23**	**0.24**	**0.25**
PV average PF	p.u.	**1**	**1**	**1**
PV StDev power	p.u.	**0.2**	**0.2**	**0.2**
PV StDev capacity factor	p.u.	**0.1**	**0.1**	**0.1**
PV StDev PF	p.u.	**0**	**0**	**0**
Voltage	kV	**0.24**	**12**	**33**

	LV	MV	HV	Total
Points/km^2	40	1	0	41
PV capacity factor	**0.12**	**0.15**	**0.2**	
PV penetration (p.u.)	**0**	**0**	**0**	
PV power (kW)	-	-	-	

Simultaneity factors	
LV	0.3
MV	0.6
HV	0.9

Data for Lancaster, CA

Table C.7: Parameters of the Lancaster network before the introduction of PV generation.

C.2.2 Eaton, Colorado

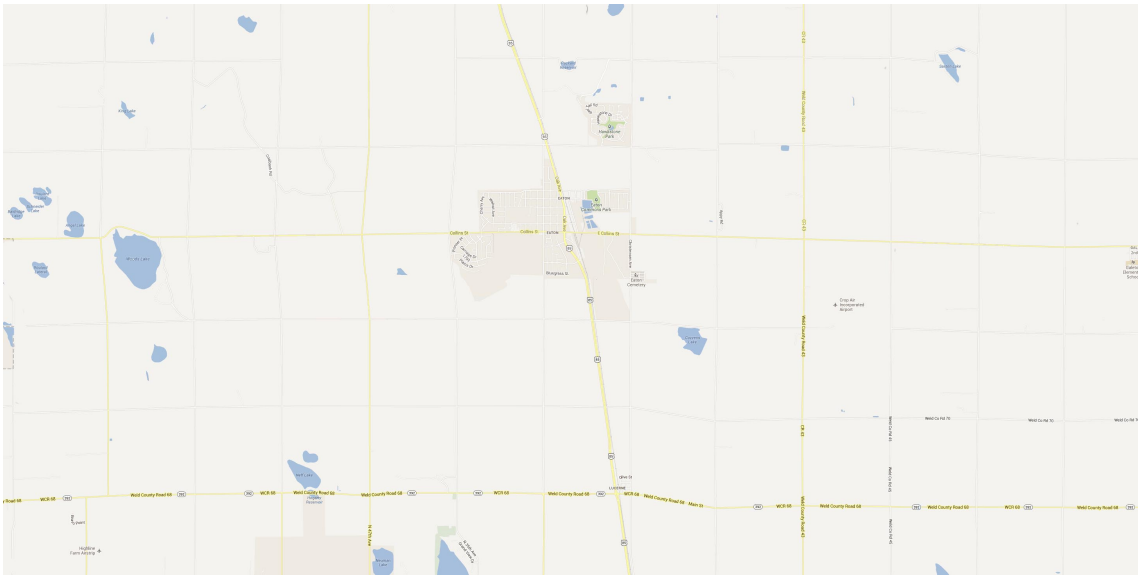

Figure C.8: 23 x 12 km section of the Eaton area considered in the study.

	Unit	LV	MV	HV					
Load power density	kW/km^2	**10**	**2**	**2**	1				
Aprox. load energy density	kWh/(km^2*yr)	35040	10512	14016	2	Points/km^2	2	0	0
Load point average power	kW	**5**	**50**	**1000**	3	PV capacity factor	**0.12**	**0.15**	**0.2**
Load average energy	kWh/yr	17520	350400	3504000	4	PV penetration (p.u.)	**0**	**0**	**0**
Load average PF	p.u.	**1**	**1**	**1**	5	PV power (kW)	-	-	-
Load StDev power	p.u.	**0.2**	**0.2**	**0.2**	6				
Load StDev energy	p.u.	**0.3**	**0.3**	**0.3**	7	Simultaneity factors			
Load StDev PF	p.u.	**0**	**0**	**0**	8	LV	0.3		
Industrial profile share	p.u.	**0.8**	**0.8**	**0.8**	9	MV	0.6		
Commercial profile share	p.u.	**0.15**	**0.15**	**0.15**	10	HV	0.9		
Residential profile share	p.u.	0.05	0.05	0.05	11				
Initial PV power density	kW/km^2	0	0	0	12				
Intial PV energy density	kWh/(km^2*yr)	0	0	0	13				
PV average power	kW	**10**	**100**	**500**	14	**Data for Eaton, CO**			
PV average capacity factor	p.u.	**0.25**	**0.26**	**0.27**	15				
PV average PF	p.u.	**1**	**1**	**1**	16				
PV StDev power	p.u.	**0.2**	**0.2**	**0.2**	17				
PV StDev capacity factor	p.u.	**0.1**	**0.1**	**0.1**	18				
PV StDev PF	p.u.	**0**	**0**	**0**	19				

Table C.8: Parameters of the Eaton network before the introduction of PV generation.

C.2.3 Torrington Connecticut

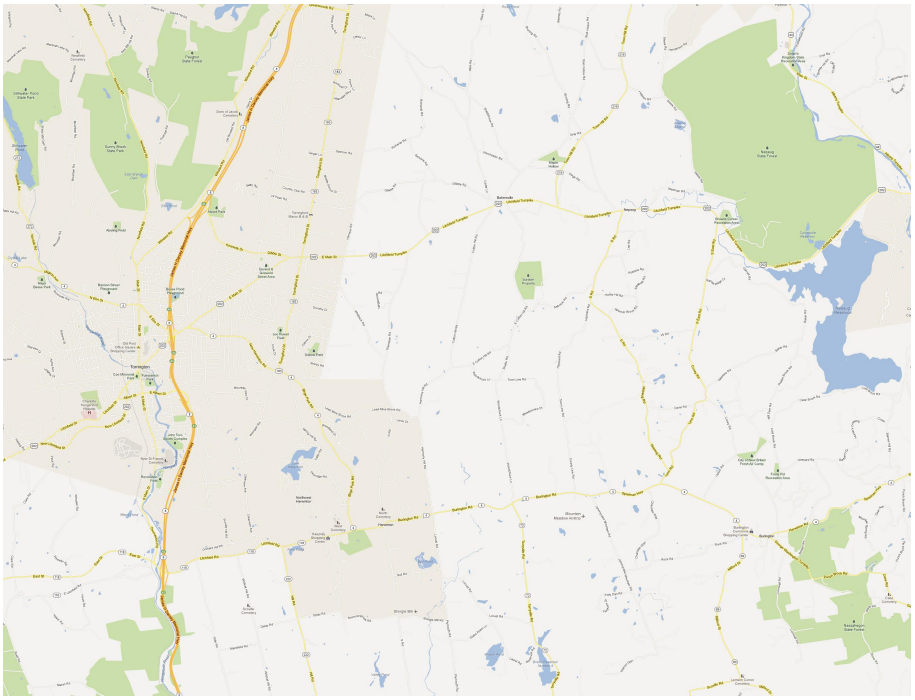

Figure C.9: 19 x 14 km section of the Torrington area considered in the study.

	Unit	LV	MV	HV						
Load power density	kW/km^2	**100**	**30**	**5**	1					
Aprox. load energy density	kWh/(km^2*yr)	350400	157680	35040	2		Points/km^2	20	0	0
Load point average power	kW	**5**	**100**	**5000**	3		PV capacity factor	**0.12**	**0.15**	**0.2**
Load average energy	kWh/yr	350400	157680	35040	4		PV penetration (p.u.)	**0**	**0**	**0**
Load average PF	p.u.	**1**	**1**	**1**	5		PV power (kW)	-	-	-
Load StDev power	p.u.	**0.2**	**0.2**	**0.2**	6					
Load StDev energy	p.u.	**0.3**	**0.3**	**0.3**	7		Simultaneity factors			
Load StDev PF	p.u.	**0**	**0**	**0**	8		LV	0.3		
Industrial profile share	p.u.	**0.8**	**0.8**	**0.8**	9		MV	0.6		
Commercial profile share	p.u.	**0.15**	**0.15**	**0.15**	10		HV	0.9		
Residential profile share	p.u.	0.05	0.05	0.05	11					
Initial PV power density	kW/km^2	0	0	0	12					
Intial PV energy density	kWh/(km^2*yr)	0	0	0	13					
PV average power	kW	**15**	**200**	**5000**	14		**Data for Torrington, CT**			
PV average capacity factor	p.u.	**0.16**	**0.17**	**0.18**	15					
PV average PF	p.u.	**1**	**1**	**1**	16					
PV StDev power	p.u.	**0.2**	**0.2**	**0.2**	17					
PV StDev capacity factor	p.u.	**0.1**	**0.1**	**0.1**	18					
PV StDev PF	p.u.	**0**	**0**	**0**	19					

Table C.9: Parameters of the Torrington network before the introduction of PV generation.

C.2.4 Altoona, Indiana

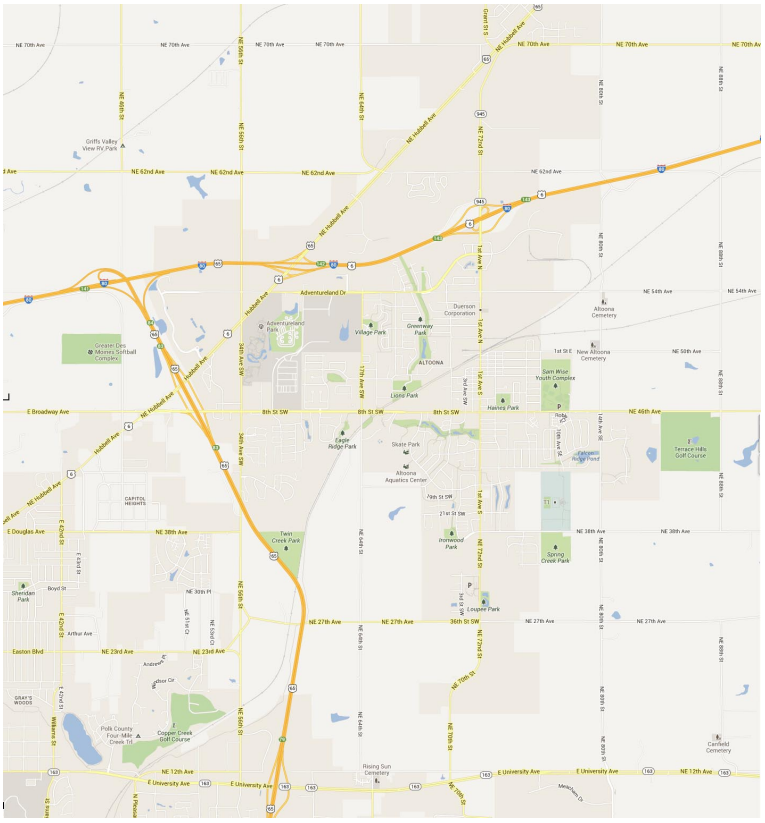

Figure C.10: 10 x 11 km section of the Altoona area considered in the study.

	Unit	LV	MV	HV						
Load power density	kW/km^2	**200**	**100**	**80**	1			LV	MV	HV
Aprox. load energy density	kWh/(km^2*yr)	700800	525600	560640	2		Points/km^2	40	1	0
Load point average power	kW	**5**	**100**	**5000**	3		PV capacity factor	**0.12**	**0.15**	**0.2**
Load average energy	kWh/yr	700800	525600	560640	4		PV penetration (p.u.)	**0**	**0**	**0**
Load average PF	p.u.	**1**	**1**	**1**	5		PV power (kW)	-	-	-
Load StDev power	p.u.	**0.2**	**0.2**	**0.2**	6					
Load StDev energy	p.u.	**0.3**	**0.3**	**0.3**	7		Simultaneity factors			
Load StDev PF	p.u.	**0**	**0**	**0**	8		LV	0.3		
Industrial profile share	p.u.	**0.8**	**0.8**	**0.8**	9		MV	0.6		
Commercial profile share	p.u.	**0.15**	**0.15**	**0.15**	10		HV	0.9		
Residential profile share	p.u.	0.05	0.05	0.05	11					
Initial PV power density	kW/km^2	0	0	0	12					
Intial PV energy density	kWh/(km^2*yr)	0	0	0	13					
PV average power	kW	**15**	**200**	**5000**	14		**Data for Altoona, IA**			
PV average capacity factor	p.u.	**0.18**	**0.19**	**0.2**	15					
PV average PF	p.u.	**1**	**1**	**1**	16					
PV StDev power	p.u.	**0.2**	**0.2**	**0.2**	17					
PV StDev capacity factor	p.u.	**0.1**	**0.1**	**0.1**	18					
PV StDev PF	p.u.	**0**	**0**	**0**	19					

Table C.10: Parameters of the Altoona network before the introduction of PV generation.

C.2.5 San Marcos, Texas

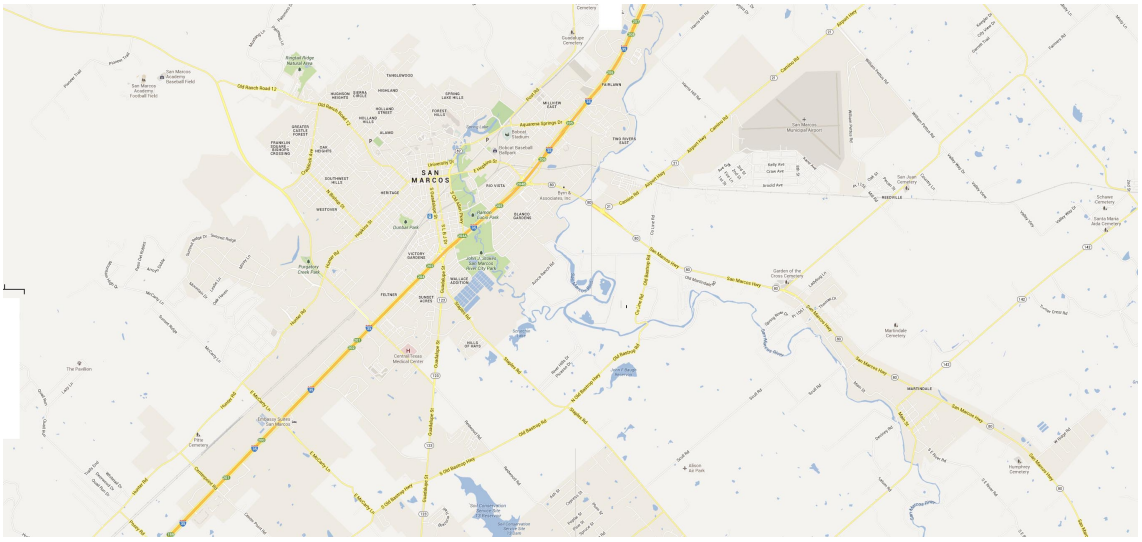

Figure C.11: 22 x 10 km section of the San Marcos area considered in the study.

	Unit	LV	MV	HV
Load power density	kW/km^2	**150**	**80**	**30**
Aprox. load energy density	kWh/(km^2*yr)	525600	420480	210240
Load point average power	kW	**5**	**100**	**5000**
Load average energy	kWh/yr	525600	420480	210240
Load average PF	p.u.	**1**	**1**	**1**
Load StDev power	p.u.	**0.2**	**0.2**	**0.2**
Load StDev energy	p.u.	**0.3**	**0.3**	**0.3**
Load StDev PF	p.u.	**0**	**0**	**0**
Industrial profile share	p.u.	**0.8**	**0.8**	**0.8**
Commercial profile share	p.u.	**0.15**	**0.15**	**0.15**
Residential profile share	p.u.	0.05	0.05	0.05
Initial PV power density	kW/km^2	0	0	0
Intial PV energy density	kWh/(km^2*yr)	0	0	0
PV average power	kW	**15**	**200**	**5000**
PV average capacity factor	p.u.	**0.22**	**0.23**	**0.24**
PV average PF	p.u.	**1**	**1**	**1**
PV StDev power	p.u.	**0.2**	**0.2**	**0.2**
PV StDev capacity factor	p.u.	**0.1**	**0.1**	**0.1**
PV StDev PF	p.u.	**0**	**0**	**0**

	LV	MV	HV
Points/km^2	30	0	0
PV capacity factor	**0.12**	**0.15**	**0.2**
PV penetration (p.u.)	**0**	**0**	**0**
PV power (kW)	-	-	-

Simultaneity factors	
LV	0.3
MV	0.6
HV	0.9

Data for San Marcos, TX

Table C.11: Parameters of the San Marcos network before the introduction of PV generation.

C.2.6 Covington, Washington

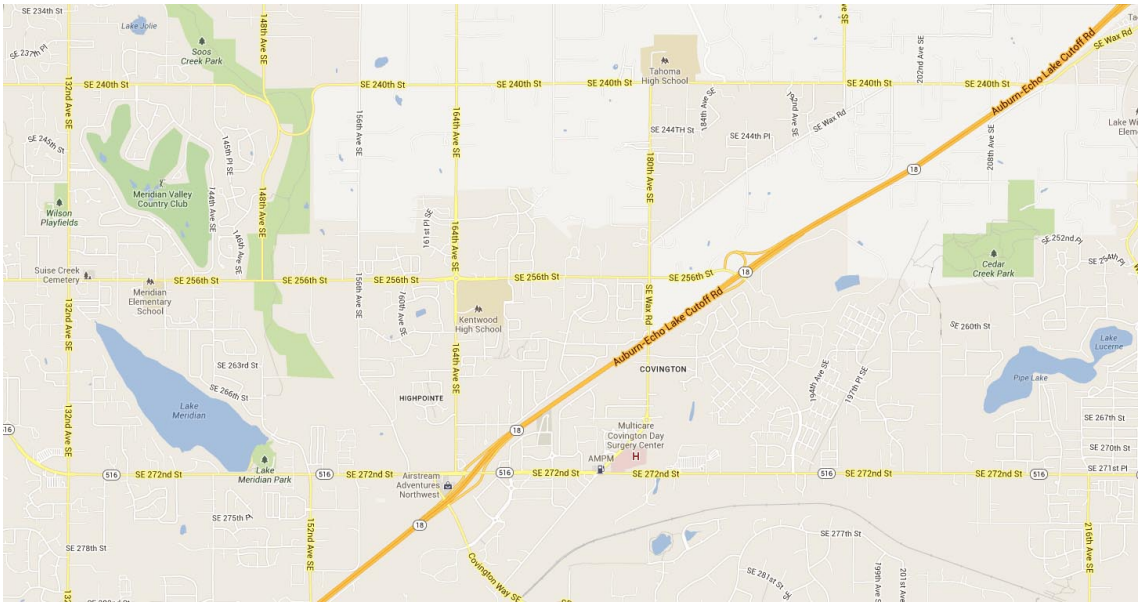

Figure C.12: 9 x 10 km section of the Covington area considered in the study.

	Unit	LV	MV	HV						
Load power density	kW/km^2	**300**	**100**	**50**	1			LV	MV	HV
Aprox. load energy density	kWh/(km^2*yr)	1051200	525600	350400	2		Points/km^2	60	1	0
Load point average power	kW	**5**	**100**	**5000**	3		PV capacity factor	**0.12**	**0.15**	**0.2**
Load average energy	kWh/yr	1051200	525600	350400	4		PV penetration (p.u.)	**0**	**0**	**0**
Load average PF	p.u.	**1**	**1**	**1**	5		PV power (kW)	-	-	-
Load StDev power	p.u.	**0.2**	**0.2**	**0.2**	6					
Load StDev energy	p.u.	**0.3**	**0.3**	**0.3**	7		Simultaneity factors			
Load StDev PF	p.u.	**0**	**0**	**0**	8		LV	0.3		
Industrial profile share	p.u.	**0.8**	**0.8**	**0.8**	9		MV	0.6		
Commercial profile share	p.u.	**0.15**	**0.15**	**0.15**	10		HV	0.9		
Residential profile share	p.u.	0.05	0.05	0.05	11					
Initial PV power density	kW/km^2	0	0	0	12					
Intial PV energy density	kWh/(km^2*yr)	0	0	0	13					
PV average power	kW	**15**	**200**	**5000**	14		**Data for Covington, WA**			
PV average capacity factor	p.u.	**0.14**	**0.15**	**0.16**	15					
PV average PF	p.u.	**1**	**1**	**1**	16					
PV StDev power	p.u.	**0.2**	**0.2**	**0.2**	17					
PV StDev capacity factor	p.u.	**0.1**	**0.1**	**0.1**	18					
PV StDev PF	p.u.	**0**	**0**	**0**	19					

Table C.12: Parameters of the Covington network before the introduction of PV generation.

Appendix D

Study case 2 details

The power conversion system is represented as in section 4.2 with the addition of a state of charge controller. The evolution of the state of charge is given by the series of frequency responses over time and the losses, and since the net result will not by itself maintain the state of charge within safe limits, a proportional SOC controller is necessary. The response of this controller is slow enough to not interfere with the frequency regulation service.

Parameter	Symbol	Value	Unit
Rated interface power	P_{inv}	20	MW
Droop	kD	$\in (0, 0.02)$	$\frac{Hz(p.u.)}{W(p.u.)}$
Maximum ramp	R_{max}	0.03	$\frac{W(p.u.)}{s}$
Deadband	DB	$\in (0, 0.015)$	$Hz(p.u.)$
Cells in series per string		40000	
Strings in parallel		400	
Maximum SOC		9.50E-01	
Minimum SOC		1.00E-01	
SOC setpoint		5.00E-01	
SOC control deadband		1.00E-02	
SOC control gain		1.00E+01	
Average ambient-cell thermal resistance		1	$\frac{K}{W}$
Maximum HVAC electric power		1000	W
HVAC COP		0.4	
Temperature setpoint		298	K°
HVAC Proportional gain		10	
HVAC dead band		5	K

Table D.1: Construction and configuration parameters of the BESS

Appendix E

Study case 3 details

E.1 Building model

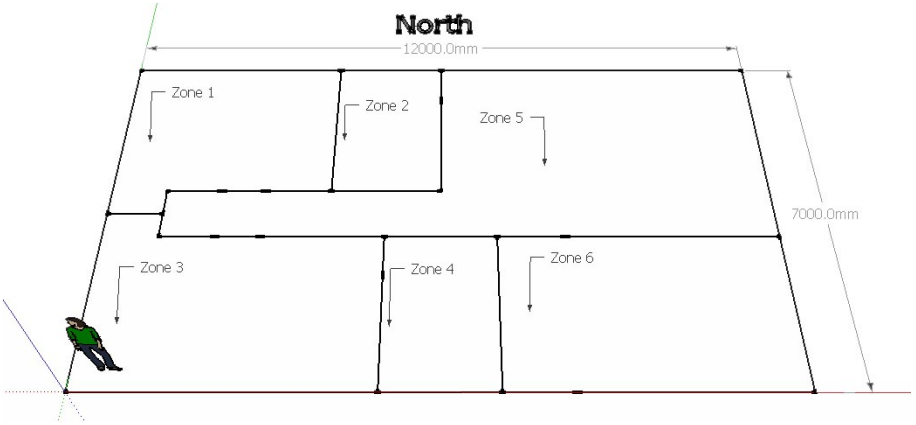

Figure E.1: Distribution of zones in the house considered in study case 2.

Area (m^2)	Heat capacity $\left(\frac{J}{K}\right)$
12.5	1.25E+05
6	6.00E+04
15.5	1.55E+05
6	6.00E+04
15	1.50E+05
18	1.80E+05

Table E.1: Heat capacity by zone for the house considered in study case 2.

Surface	Thermal conductivity $\left(\frac{\mathrm{W}}{\mathrm{K}\cdot\mathrm{m}^2}\right)$
Internal walls	5
External walls	0.5
Roof	0.1
Floor	0.2

Table E.2: Thermal conductivities of the surface of house considered in study case 2.

Contact area in m^2

	Z1	Z2	Z3	Z4	Z5	Z6	N	S	E	W	C	G
Z1	0	9	0	0	9	0	12	0	0	10.5	12.5	12.5
Z2	9	0	0	0	6	0	6	0	0	0	6	6
Z3	0	0	0	9	12	0	0	15	0	10.5	15.5	15.5
Z4	0	0	9	0	6	9	0	6	0	0	6	6
Z5	9	6	12	6	0	15	18	0	13.5	0	15	15
Z6	0	0	0	9	15	0	0	15	9	0	18	18

Table E.3: Contact area between the zones, and with the environment, of the house considered in study case 2. The environment is divided in the walls facing North, South, East and West, plus Ceiling and Ground.

Thermal conductivity in $\frac{\mathrm{W}}{\mathrm{K}}$

	Z1	Z2	Z3	Z4	Z5	Z6	N	S	E	W	C	G
Z1	0	45	0	0	45	0	6	0	0	5.25	1.25	2.5
Z2	45	0	0	0	30	0	3	0	0	0	0.6	1.2
Z3	0	0	0	45	60	0	0	7.5	0	5.25	1.55	3.1
Z4	0	0	45	0	30	45	0	3	0	0	0.6	1.2
Z5	45	30	60	30	0	75	9	0	6.75	0	1.5	3
Z6	0	0	0	45	75	0	0	7.5	4.5	0	1.8	3.6

Table E.4: Thermal conductivity between the zones, and with the environment, of the house considered in study case 2. The environment is divided in the walls facing North, South, East and West, plus Ceiling and Ground.

E.2 Appliances

Clothes dryer		
Parameter	Value	Unit
Nominal power	2200	W
Job duration	3600	s
Loading day 1	3	day
Loading hour on day 1	16	hour
Unloading hour on 1	22	hour
Start hour on day 1	17	hour
Loading day 2	7	day
Loading hour on 2	16	hour
Unloading hour on 2	22	hour
Start hour on day 2	17	hour

Table E.5: Parameters of the clothes dryer in case study 3.

Dishwasher		
Parameter	Value	Unit
Nominal power	2500	W
Water volume	0.05	m^3
Job duration	3600	s
Water consumption interval	300	s
Maximum heating power	1000	W
Required water temperature	303	K
Loading hour	14	
Unloading hour	20	
Start hour	15	

Table E.6: Parameters of the dishwasher in case study 3.

Water cylinder

Parameter	Value	Unit
Thermal resistance	1	$\frac{K}{W}$
Water volume	0.1	m^3
Heating power available	1300	W
Zone	2	
Water volume- specific heat	4.19E+06	$\frac{J}{K \cdot m^3}$
Temperature setpoint	363	K
Temperature hysteresis	1	K

Table E.7: Parameters of the water cylinder in case study 3.

Electric vehicle

Parameter	Value	Unit	Day type
Arrival time	19	hour	Weekdays
Required SOC at departure	0.9	p.u.	
SOC at arrival	0.2	p.u.	
Temperature at arrival	313	K	
Daily driving degradation	0.001	p.u.	
Arrival hour	19		Weekend
Required SOC at departure	0.9	p.u.	
SOC at arrival	0.2	p.u.	
Temperature at arrival	313	K	
Daily driving degradation	0.0002	p.u.	

Table E.8: Parameters of the electric vehicle in case study 3.

Washing machine		
Parameter	Value	Unit
Nominal power	2150	W
Water volume	0.05	m^3
Job duration	3600	s
Water consumption interval	300	s
Maximum heating power	500	W
Required water temperature	303	K
Loading day 1	3	day
Loading hour on day 1	8	hour
Unloading hour on day 1	16	hour
Start hour on day 1	9	hour
Loading day 2	7	day
Loading hour on day 2	8	hour
Unloading hour on day 2	16	hour
Start hour on day 2	9	hour

Table E.9: Parameters of the washing machine in case study 3.

BESS		
Parameter	Value	Unit
Nominal power	10	kWh
Type of cell	ANR26650	
Nominal capacity	5.58	kWh
Maximum SOC	0.95	p.u.
Minimum SOC	0.1	p.u.

Table E.10: Parameters of both BESS in case study 3 (stationary and on-board the EV).

Refrigerator		
Parameter	Value	Unit
Thermal resistance	0.1	K/W
Total heat capacity	83200	J/K
Maximum electric power	500	W
Coefficient of Performance	3	
Zone number	5	
Temperature setpoint	278	K
Temperature hysteresis	1	K

Table E.11: Parameters of the refrigerator in case study 3.

Appendix F

Distribution network costs allocation

F.1 Introduction

The electricity distribution activity is of often a regulated monopoly under cost of service remuneration. In most systems the users of the electric network pay a network tariff that is calculated taking into account not the cost of particular feeder where they are connected but a wider collection of infrastructure, making the allocation of the cost among the users of the network a non-trivial task. The objectives of the methodology presented here are to a) Show how a dominant allocation methodology induces cross-subsidization and does not encourage the use of energy storage; and b) propose a new methodology that solves this problems. The discussion is guided by the author's belief in that the attributes a properly designed tariff should have are the ones described below.

F.1.1 Desirable tariff structure attributes

Cost-causality coherence Except for the connection charge, direct causality is impossible to establish in general because of the existence of shared infrastructure of lumpy nature. However, it is expected that the types of customers which, on aggregate, more significantly explain the need for investments, bear a greater share of the cost.

Not arbitrarily discriminatory Consumers with similar electricity consumption characteristics should be allocated similar shares of the total cost, regardless of situations out of their control like their electrical location in the network.

Provide incentives to exploit sources of flexibility The users of the distribution network should be able, in principle,to modify their consumption behavior against the network tariff to reduce their network charges. The tariff structure should be such that the desired behavior positively impacts the long-term distribution cost.

Transparency The procedure to calculate individual payments should be easy to understand and reproducible by the customers.

Robust to technological and behavioral changes The chosen structure should be able to correctly allocate costs for any network utilization regime.

F.1.2 Types of network users

Many kinds of individuals and organizations benefit from the existence of the distribution network (DN). Traditionally, the dominant use of the infrastructure was to deliver electricity to be used in the production of energy, hence network users were referred in general as consumers. Currently, it is common to find electricity generation equipment connected the DN, both as stand-alone facilities or combined with consumption points. A network user is defined here as a collection of infrastructure behind a point of common coupling (PCC) that defines its boundary with the DN. Three types of network users are considered according to the sign of active power P withdrawn from the DN:

1. If P is always positive or zero, the user is a consumer;
2. If P is always negative or zero, the user is a producer;
3. If P is sometimes positive and sometimes negative, the user is a prosumer.

It is also useful to differentiate between the power profile of consumers and producers. Consumers can be categorized in residential, commercial and industrial depending on the

predominant energy services mix together with their temporal utilization pattern. Producers are conveniently grouped in the categories of dispatchable and non-dispatchable, depending on the nature of the characteristics of the primary energy resource used to generate electricity. While the power output of the former can be controlled within some constraints, the latter can only be curtailed, in which case the primary energy resource involved is spilled. A relevant subset of these last are variable energy resources (VER) like wind and solar radiation. Note that combining different combinations of generation technologies and load types behind the PCC can cause a network user to be categorized in any of the three types described above.

F.2 Revealing the shortcomings of a dominant allocation methodology

The intention is to expose a pathology that can happen - and in some networks is happening now - when a particular regulatory approach exists. For this we use the data generated from the simulations described in Case Study 1. In the context of this section, we will consider that:

- A volumetric allocation of network cost is used, distributing the total network cost in proportion to the volume of electricity that is consumed by each customer;
- Net-metering is employed to determine the volume of electricity consumed by a customer. It consists in using a single meter that increases or decreases measured consumption in proportion to the magnitude and according to the direction of the power flowing through it. After a pre-defined period of time(one or two months, typically, when conventional meters are checked), the value in the meter is read, and the customer pays the corresponding tariff times the net volume consumed.

Here we exemplify what can happen in a particular network when both of the above elements are applied, as they often are. The first effect of this combination is shown in Figure F.1a. As the penetration of distributed generation goes up, customers (or, now, *prosumers*) that own PV systems will lower their net volume of energy consumed. Since network costs don't decrease (even increase, as we have seen) with penetration, the amount that has to be allocated to each kWh consumed to recover network costs has to

increase. The prosumers with PV systems, responsible both for the decrease in volume and for the increase in network cost, avoid a big portion of the cost, as Figure F.1b shows. On the other end, customers without distributed generation systems will fully perceive the tariff increase, which is likely to be perceived as unfair[1]. Moreover, they will have an incentive to get a PV system, resulting in a positive feedback mechanism that can render the distribution business non viable.

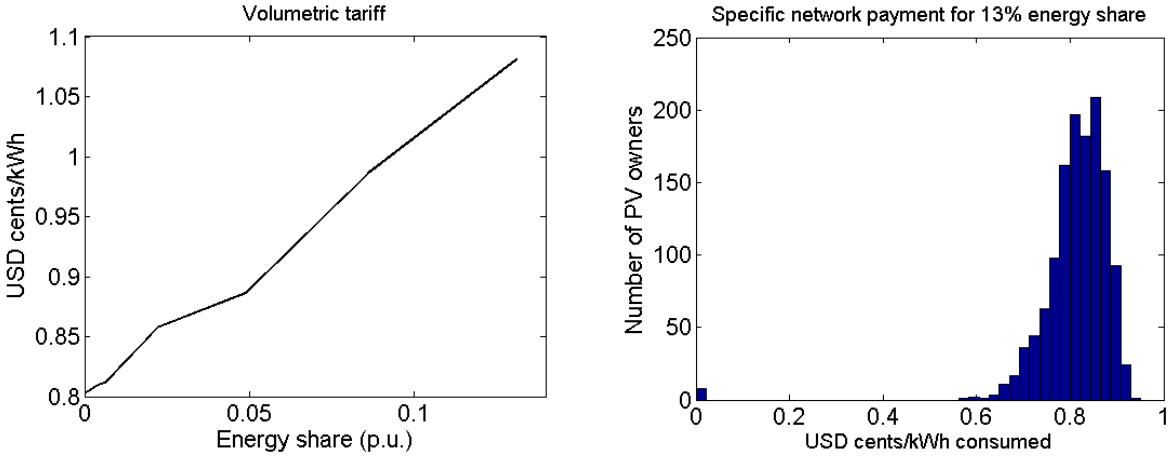

(a) Specific network cost. **(b) Perceived network charge.**

Figure F.1: Effect of volumetric tariff under net-metering for the Des Moines base network. The figure on the right shows the network charge perceived by prosumers. The variability exists because different prosumers will have different shares of their total consumption being offset by their PV generators. The rest of the users of the network (about 6 thousand) will pay the network charge shown on the left hand figure for each kWh that their loads consume.

F.2.1 Implications for distributed energy storage

As it has been discussed previously in this Thesis, network costs are primarily driven by local peak load and peak generation scenarios, in other words they are *locally profile-driven*. Hence, the design of the tariff should aim to send incentives to locally reduce both peaks, for example through load management and/or storage devices. This doesn't happen at all when volumetric allocation is used together with long net-metering periods, preventing energy storage to have access to an otherwise valid revenue stream. The

[1]The results shown here assume a standard meter that is read once a year. When a shorter reading period is used, the asymmetry will be reduced because there will be periods in which the PV production is going to smaller than others. For example: if monthly metering is available, the avoided network charge in winter months will be smaller; if the readings are done hourly, there would be no avoidance during the night.

utilization of advanced metering infrastructure would allow the implementation of time-location sensitive network charges that can correct this problem [2].

F.3 Proposed methodology

This methodology assumes hourly information about the power exchange profile of all network users. It involves two stages: (a) the total cost is allocated to four cost-drivers; (b) individual payments are calculated based on the participation of the individual customer on each cost driver.

F.3.0.1 Allocation to cost-drivers

It is proposed that four components explain the cost of the network:

1. *Topological cost* C_T, related to the existence and dispersion of the customers. This can be understood as the cost of a network with the smallest conductors and transformers available.
2. *Demand capacity cost* C_D, related to the increase in size of conductors and equipment to be able to cope with worst-case load scenarios.
3. *Generation capacity cost* C_G, related to the increase in size of conductors and equipment to be able to cope with worst-case distributed generation scenarios.
4. *Losses-driven cost* C_L, which occur when the cost of the losses is considered in the design of the network.

$C_N = C_T + C_D + C_G + C_L$ is the total cost of the network. To calculate each component, we use a reference network model (RNM) in the following way:

1. Solve a case in which the nominal power of each customer is a small positive number (e.g., 1kW), the consumption profile is flat and the cost of losses is 0. Let's call the result of this run C_1.

[2] When the metering interval is small (hours or minutes) the distinction between power and energy is less relevant and a time-varying net volumetric rate provides the right incentives to modify the net power exchange profile. A spatial dependency can also be justified on cost-causality grounds, but could also be seen as discriminatory.

2. Solve a case in which the nominal power and consumption profile of each customer are the actual ones but always positive and the cost of losses is 0. Let's call the result of this run C_2.

3. Solve a case in which the nominal power and consumption profile of each customer are the actual and the cost of losses is 0. Let's call the result of this run C_3.

4. Solve a case in which the nominal power and consumption profile of each customer are the actual and the cost of losses is the actual value. Let's call the result of this run C_4.

Then, $C_T = C_1$, $C_D = C_2 - C1$, $C_G = C_3 - C2 - C1$ and $C_L = C_4$. All the cost calculations include the low , medium and high voltage parts of the distribution network.

F.3.0.2 Calculation of payments

1. *Allocation of the topological cost.* For a network with n customers where customer $1 : m$ are more than d_{max} meters from the nearest-neighbor, make $C_T^* = C_T - \sum_{i=1}^{m} Cl_i$, where Cl_i is the cost of the line that connects customer i. Them, the topology-related payment of customer i is

$$P_i^T = \begin{cases} C_T^*/n + Cl_i & \text{if } i \in [1, m] \\ C_T^*/n & \text{if } i \in [m+1, n]. \end{cases} \tag{F.1}$$

2. *Allocation of the demand capacity cost.*

   (a) Determine, ex-post, a set $\boldsymbol{D}$ with the k days with highest total net demand in the network[3];

   (b) Calculate the contribution to the peak $SD_{i,d}$ of each of the n customers on each day in $\boldsymbol{D}$ in per-unit, where $\forall d \in \boldsymbol{D}, \sum_{i=1}^{n} SD_{i,d} = 1$

   (c) The demand-capacity related payment of customer i corresponds to its average contribution to the peak:

$$P_i^D = C_D \frac{\sum_{d \in \boldsymbol{D}} SD_{i,d}}{k} \tag{F.2}$$

[3]The system's peak could also consider a subset of the network. The individual payments in this case need to be calculated with respect to the contribution of the subset to the total costs.

3. *Allocation of the generation capacity cost.*

   (a) Determine, ex-post, a set $\boldsymbol{G}$ with the q days with highest total net generation in the network;

   (b) Calculate the contribution to the peak $SG_{i,d}$ of each of the n customers for each day $d \in \boldsymbol{G}$ in per-unit, where $\forall d \in \boldsymbol{G}, \sum_{i=1}^{n} SG_{i,d} = 1$

   (c) The demand-capacity related payment of customer i corresponds to its average contribution to the peak:

$$P_i^G = C_G \frac{\sum_{d \in \boldsymbol{G}} SG_{i,d}}{q} \tag{F.3}$$

4. *Allocation of the losses-driven cost*

   (a) Calculate the sum of the absolute value of all the hourly injections and withdrawals for all the customers $E_{total} = \sum_{h=1}^{8760} \sum_{i=1}^{n} |E_{h,i}|$, where $E_{h,i}$ is the energy exchanged in hour h by the PCC of customer i.

   (b) Calculate the individual payments in proportion to the contribution to E_{total}[4]:

$$P_i^L = C_L \frac{\sum_{h=1}^{8760} |E_{h,i}|}{E_{total}} \tag{F.4}$$

5. The total payment of customer i is then:

$$P_i^{total} = P_i^T + P_i^D + P_i^G + P_i^L \tag{F.5}$$

F.3.1 Implications for energy storage

From the private point of view, it is evident that energy storage can generate value streams by reducing the user's participation in payment components 2 and 3, and possibly also in component 4 by maximizing self-consumption. It can also be claimed that a BESS controlled by a rational agent optimizing the customer's energy utilization profile as in case study 2 will take actions in the direction of reducing the total network and losses cost, and hence benefiting the other users of the network.

[4]This formulation does not consider the quadratic nature of losses. This could be introduced through a correction factor for each hour.

Bibliography

[1] Antonio Gomez-Exposito, Antonio J. Conejo, and Claudio Canizares. *Electric Energy Systems: Analysis and Operation (Electric Power Engineering Series)*. CRC Press, 2008.

[2] E.H. Watanabe, M. Aredes, P.G. Barbosa, F.K. de Araújo Lima, R.F. da Silva Dias, and G. Santos. *Power Electronics Hand*, chapter Flexible AC Transmission Systems. Elsevier, 2007.

[3] ENTSO-E. *Continental Europe Operation Handbook, Policy 1: Load-Frequency Control*, 2009.

[4] Abbas A. Akhil, Georgianne Huff, Aileen B. Currier, Benjamin C. Kaun, Dan M. Rastler, Stella Bingqing Chen, Andrew L. Cotter, Dale T. Bradshaw, and William D. Gauntlett. Doe/epri 2013 electricity storage handbook in collaboration with nreca. Technical report, Sandia National Laboratories, 2013.

[5] Robert Huggins. *Advanced Batteries: Materials Science Aspects*. Springer, 12 2008.

[6] David J. Bradwell, Hojong Kim, Aislinn H. C. Sirk, and Donald R. Sadoway. Magnesium-antimony liquid metal battery for stationary energy storage. *Journal of the American Chemical Society*, 134(4):1895–1897, 2012. doi: 10.1021/ja209759s. URL http://pubs.acs.org/doi/abs/10.1021/ja209759s.

[7] Ralph J. Brodd, editor. *Batteries for Sustainability: Selected Entries from the Encyclopedia of Sustainability Science and Technology*. Springer, 2013 edition, 12 2012.

[8] S. Rael and M. Hinaje. Using electrical analogy to describe mass and charge transport in lithium-ion batteries. *Journal of Power Sources*, 222(0):112 – 122, 2013.

ISSN 0378-7753. doi: http://dx.doi.org/10.1016/j.jpowsour.2012.08.071. URL http://www.sciencedirect.com/science/article/pii/S0378775312013699.

[9] N. Legrand, S. Ral, B. Knosp, M. Hinaje, P. Desprez, and F. Lapicque. Including double-layer capacitance in lithium-ion battery mathematical models. *Journal of Power Sources*, 251(0):370 – 378, 2014. ISSN 0378-7753. doi: http://dx.doi.org/10.1016/j.jpowsour.2013.11.044. URL http://www.sciencedirect.com/science/article/pii/S0378775313018715.

[10] M.R. Jongerden and B.R. Haverkort. Which battery model to use? *Software, IET*, 3(6):445–457, December 2009. ISSN 1751-8806. doi: 10.1049/iet-sen.2009.0001.

[11] James F. Manwell and Jon G. McGowan. Lead acid battery storage model for hybrid energy systems. *Solar Energy*, 50(5):399 – 405, 1993. ISSN 0038-092X. doi: http://dx.doi.org/10.1016/0038-092X(93)90060-2. URL http://www.sciencedirect.com/science/article/pii/0038092X93900602.

[12] J.W. Beck, D.P. Carroll, G. E. Gareis, P.C. Krause, and C. M. Ong. A computer study of battery energy storage and power conversion equipment operation. *Power Apparatus and Systems, IEEE Transactions on*, 95(4):1064–1072, July 1976. ISSN 0018-9510. doi: 10.1109/T-PAS.1976.32198.

[13] Xiangjun Li, Dong Hui, and Xiaokang Lai. Battery energy storage station (bess)-based smoothing control of photovoltaic (pv) and wind power generation fluctuations. *Sustainable Energy, IEEE Transactions on*, 4(2):464–473, April 2013. ISSN 1949-3029. doi: 10.1109/TSTE.2013.2247428.

[14] S. Teleke, M.E. Baran, A.Q. Huang, S. Bhattacharya, and L. Anderson. Control strategies for battery energy storage for wind farm dispatching. *Energy Conversion, IEEE Transactions on*, 24(3):725–732, Sept 2009. ISSN 0885-8969. doi: 10.1109/TEC.2009.2016000.

[15] Min Chen and G.A. Rincon-Mora. Accurate electrical battery model capable of predicting runtime and i-v performance. *Energy Conversion, IEEE Transactions on*, 21(2):504–511, June 2006. ISSN 0885-8969. doi: 10.1109/TEC.2006.874229.

[16] T. Kim and Wei Qiao. A hybrid battery model capable of capturing dynamic circuit characteristics and nonlinear capacity effects. In *Power and Energy Society*

General Meeting, 2012 IEEE, pages 1–1, July 2012. doi: 10.1109/PESGM.2012.6345454.

[17] Sophia Ruester, Jorge Vasconcelos, Xiang He, Eshien Chong, and Jean-Michel Glachant. Electricity storage: How to facilitate its deployment and operation in the EU. Technical report, Florence School of Regulation, European University Institute, 2012.

[18] A123 Systems. Grid storage solution, 2012. URL http://www.a123systems.com.

[19] Jose R. Espinoza. *Power electronics handbook*, chapter 15, pages 357–406. Elsevier, 2010.

[20] Kandler Smith and Chao-Yang Wang. Power and thermal characterization of a lithium-ion battery pack for hybrid-electric vehicles. *Journal of Power Sources*, 160(1):662–673, 2006.

[21] CDEC-SING. Diagrama unilineal simplificado del sing, . URL http://cdec2.cdec-sing.cl. Accessed in July 2014.

[22] CDEC-SING. Informe semestral del cdec-sing, julio-diciembre de 2011, . URL http://cdec2.cdec-sing.cl. Accessed in June 2012.

[23] Organisation for Economic Co-Operation and Development and International Energy Agency (OECD). *World Energy Outlook 2013*. OECD, 2013.

[24] U.S. Department of Energy. Grid energy storage. Technical report, U.S. Department of Energy, December 2013.

[25] Raymond Harry Byrne, Verne William Loose, Matthew K Donnelly, and Daniel J Trudnowski. Methodology to determine the technical performance and value proposition for grid-scale energy storage systems: a study for the doe energy storage systems program. Technical report, Montana Tech of The University of Montana, Butte, MT; Sandia National Laboratories (SNL-NM), Albuquerque, NM (United States), 2012.

[26] Public Utilities Commission of the State of California. Decision adopting energy storage procurement framework and design program. Technical report, 2013.

[27] Steven Pinker. *The better angels of our nature: The decline of violence in history and its causes*. Penguin UK, 2011.

[28] Jon Norberg and Graeme S Cumming. *Complexity theory for a sustainable future*. Columbia University Press, 2013.

[29] Dilip Kondepudi. *Introduction to Modern Thermodynamics*. Wiley, Chichester, 2008.

[30] Richard P. Feynman, Robert B. Leighton, and Matthew Sands. *The Feynman Lectures on Physics*, volume I. Addison-Wesley Publishing Company, the deffinitive edition edition, 2011.

[31] *Glossary of Statistical Terms*. Organisation for Economic Co-operation and Development, 2007. URL http://stats.oecd.org/glossary.

[32] IPCC. 2013: Summary for policimakers. in: *Climate Change 2013: The Physical Science Basis. Contribution of Working I to the Fifth Assessment Report of the Intergovernmental Panel on Climate Change* [stocker, t.f., d. qin, g.-k. plattner, m.tignor, s.k. allen, j. boschung, a. nauels, y. xia, v. bex and p.m. midgley (eds.)]. cambridge university press, cambridge, united kingdom and new york, ny, usa. Technical report, IPCC, 2013.

[33] UN Secretary-Generals Advisory Group on Energy and Climate Change. *Energy for a Sustainable Future*. Sustainable Energy For All, United Nations and World Bank, 2010.

[34] K. Moon and Ganesh R. Kale. Energy analysis in combined reforming of propane. *Journal of Engineering*, 2013:10, 2013. doi: 10.1155/2013/301265. URL http://dx.doi.org/10.1155/2013/301265.

[35] Nicolas Leonard Saidi Carnot. *Reflections on the Motive Power of Heat, and on Machines Fitted to Develop that Power*. John Wiley and Sons, 1897.

[36] Richard P. Feynman, Robert B. Leighton, and Matthew Sands. *The Feynman Lectures on Physics*, volume II. Addison-Wesley Publishing Company, the deffinitive edition edition, 2011.

[37] Prabha Kundur. *Power System Stability and Control*. McGraw-Hill, 1994. ISBN 9780070359581.

[38] Graham Rogers. *Power System Oscillations*. Springer, 2000. doi: 10.1007/978-1-4615-4561-3.

[39] E.L. Owen. The origins of 60-hz as a power frequency. *Industry Applications Magazine, IEEE*, 3(6):8, 10, 12–14, Nov 1997. ISSN 1077-2618. doi: 10.1109/2943.628099.

[40] W.W. Price, K.A. Wirgau, A. Murdoch, and F.Nozari. *Load Modeling for Power Flow and Transient Stability Computer Studies*. Electric Power Research Institute, 1987.

[41] Luis Morán and Juan Dixon. *Power Electronics Handbook*, chapter Active Filters. Elsevier, 2007.

[42] I. Papic. Power quality improvement using distribution static compensator with energy storage system. In *Harmonics and Quality of Power, 2000. Proceedings. Ninth International Conference on*, volume 3, pages 916–920 vol.3, 2000. doi: 10.1109/ICHQP.2000.896851.

[43] R.K. Varma, V. Khadkikar, and R. Seethapathy. Nighttime application of pv solar farm as statcom to regulate grid voltage. *Energy Conversion, IEEE Transactions on*, 24(4):983–985, Dec 2009. ISSN 0885-8969. doi: 10.1109/TEC.2009.2031814.

[44] John Newman and Karen E. Thomas-Alyea. *Electrochemical Systems, 3rd Edition*. Wiley-Interscience, 3 edition, 2004. ISBN 9780471477563.

[45] David Linden and Thomas Reddy. *Handbook of Batteries*. McGraw-Hill Professional, 4 edition, 10 2010.

[46] Gerardine G. Botte and Madhivanan Muthuvel. *Handbook of Industrial Chemistry and Biotechnology, Chapter 38*. Springer, 12 edition, 2013.

[47] Ghada Merei, Sophie Adler, Dirk Magnor, Matthias Leuthold, and Dirk Uwe Sauer. Multi-physics model for a vanadium redox flow battery. *Energy Procedia*, 46(0):194 – 203, 2014. ISSN 1876-6102. doi: http://dx.doi.org/10.1016/j.egypro.2014.01.173. URL http://www.sciencedirect.com/science/article/pii/S1876610214001891. 8th International Renewable Energy Storage Conference and Exhibition (IRES 2013).

[48] Richard Baxter. *Energy storage: a nontechnical guide*. PennWell Books, 2006.

[49] Kurt E. Sickafus and John M. Wills. Structure of spinel. *Journal of the American Ceramics Society*, 82:3279–3292, 1999.

[50] A123 Systems. Nanophosphate basics: An overview of the structure, properties and benefits of a123 systems proprietary lithium ion battery technology, 2008.

[51] Allan J. Jacobson and Linda F. Nazar. Intercalation chemistry. *Encyclopedia of Inorganic and Bioinorganic Chemistry*, 1:1–37, 2006.

[52] Gianfranco Pistoia, editor. *Lithium-Ion Batteries: Advances and Applications*. Elsevier, 1 edition, 2014.

[53] Aden Seaman, Thanh-Son Dao, and John McPhee. A survey of mathematics-based equivalent-circuit and electrochemical battery models for hybrid and electric vehicle simulation. *Journal of Power Sources*, 256(0):410 – 423, 2014. ISSN 0378-7753. doi: http://dx.doi.org/10.1016/j.jpowsour.2014.01.057. URL http://www.sciencedirect.com/science/article/pii/S0378775314000810.

[54] M. Swierczynski, D.I. Stroe, A.-I. Stan, R. Teodorescu, and D.U. Sauer. Selection and performance-degradation modeling of $limo_2/li_4\ ti_5o_{12}$ and $lifepo_4/c$ battery cells as suitable energy storage systems for grid integration with wind power plants: An example for the primary frequency regulation service. *Sustainable Energy, IEEE Transactions on*, 5(1):90–101, Jan 2014. ISSN 1949-3029. doi: 10.1109/TSTE.2013.2273989.

[55] Wladislaw Waag, Christian Fleischer, and Dirk Uwe Sauer. Critical review of the methods for monitoring of lithium-ion batteries in electric and hybrid vehicles. *Journal of Power Sources*, 258(0):321 – 339, 2014. ISSN 0378-7753. doi: http://dx.doi.org/10.1016/j.jpowsour.2014.02.064. URL http://www.sciencedirect.com/science/article/pii/S0378775314002572.

[56] Anthony Barr, Benjamin Deguilhem, Sbastien Grolleau, Mathias Grard, Frdric Suard, and Delphine Riu. A review on lithium-ion battery ageing mechanisms and estimations for automotive applications. *Journal of Power Sources*, 241(0):680 – 689, 2013. ISSN 0378-7753. doi: http://dx.doi.org/10.1016/j.jpowsour.2013.05.040. URL http://www.sciencedirect.com/science/article/pii/S0378775313008185.

[57] Marc Doyle, Thomas F Fuller, and John Newman. Modeling of galvanostatic charge and discharge of the lithium/polymer/insertion cell. *Journal of the Electrochemical Society*, 140(6):1526–1533, 1993.

[58] Thomas F Fuller, Marc Doyle, and John Newman. Simulation and optimization of the dual lithium ion insertion cell. *Journal of the Electrochemical Society*, 141 (1):1–10, 1994.

[59] Kandler Smith and Chao-Yang Wang. Solid-state diffusion limitations on pulse operation of a lithium ion cell for hybrid electric vehicles. *Journal of Power Sources*, 161(1):628–639, 2006.

[60] Irene J Ong and John Newman. Double-layer capacitance in a dual lithium ion insertion cell. *Journal of The Electrochemical Society*, 146(12):4360–4365, 1999.

[61] Yuanyuan Xie, Jianyang Li, and Chris Yuan. Multiphysics modeling of lithium ion battery capacity fading process with solid-electrolyte interphase growth by elementary reaction kinetics. *Journal of Power Sources*, 248(0):172 – 179, 2014. ISSN 0378-7753. doi: http://dx.doi.org/10.1016/j.jpowsour.2013.09.059. URL http://www.sciencedirect.com/science/article/pii/S0378775313015553.

[62] Alexander P. Schmidt, Matthias Bitzer, Arpad W. Imre, and Lino Guzzella. Model-based distinction and quantification of capacity loss and rate capability fade in li-ion batteries. *Journal of Power Sources*, 195(22):7634 – 7638, 2010. ISSN 0378-7753. doi: http://dx.doi.org/10.1016/j.jpowsour.2010.06.011. URL http://www.sciencedirect.com/science/article/pii/S0378775310009948.

[63] Yonghuang Ye, Yixiang Shi, and Andrew A.O. Tay. Electro-thermal cycle life model for lithium iron phosphate battery. *Journal of Power Sources*, 217(0): 509 – 518, 2012. ISSN 0378-7753. doi: http://dx.doi.org/10.1016/j.jpowsour.2012.06.055. URL http://www.sciencedirect.com/science/article/pii/S0378775312010555.

[64] Harry J Ploehn, Premanand Ramadass, and Ralph E White. Solvent diffusion model for aging of lithium-ion battery cells. *Journal of The Electrochemical Society*, 151(3):A456–A462, 2004.

[65] A. Khatamianfar, M. Khalid, A.V. Savkin, and V.G. Agelidis. Improving wind farm dispatch in the australian electricity market with battery energy storage

using model predictive control. *Sustainable Energy, IEEE Transactions on*, 4(3): 745–755, July 2013. ISSN 1949-3029. doi: 10.1109/TSTE.2013.2245427.

[66] J.M. Gantz, S.M. Amin, and A.M. Giacomoni. Optimal capacity partitioning of multi-use customer-premise energy storage systems. *Smart Grid, IEEE Transactions on*, 5(3):1292–1299, May 2014. ISSN 1949-3053. doi: 10.1109/TSG.2014.2312182.

[67] S.X. Chen, H.B. Gooi, and M. Q. Wang. Sizing of energy storage for microgrids. *Smart Grid, IEEE Transactions on*, 3(1):142–151, March 2012. ISSN 1949-3053. doi: 10.1109/TSG.2011.2160745.

[68] M. Stadler, M. Kloess, M. Groissbck, G. Cardoso, R. Sharma, M.C. Bozchalui, and C. Marnay. Electric storage in californias commercial buildings. *Applied Energy*, 104(0):711 – 722, 2013. ISSN 0306-2619. doi: http://dx.doi.org/10.1016/j.apenergy.2012.11.033. URL http://www.sciencedirect.com/science/article/pii/S0306261912008264.

[69] R. Palma-Behnke, C. Benavides, F. Lanas, B. Severino, L. Reyes, J. Llanos, and D. Saez. A microgrid energy management system based on the rolling horizon strategy. *Smart Grid, IEEE Transactions on*, 4(2):996–1006, June 2013. ISSN 1949-3053. doi: 10.1109/TSG.2012.2231440.

[70] E.I. Vrettos and S.A. Papathanassiou. Operating policy and optimal sizing of a high penetration res-bess system for small isolated grids. *Energy Conversion, IEEE Transactions on*, 26(3):744–756, Sept 2011. ISSN 0885-8969. doi: 10.1109/TEC.2011.2129571.

[71] J.F. Manwell, A.Rogers, G. Hayman, C.T. Avelar, J.G. McGowan, U. Abdulwahid, and K. Wu. *HYBRID2- A HYBRID SYSTEM SIMULATION MODEL : THEORY MANUAL*. National Renewable Energy Laboratory, 2006.

[72] D. Guasch and S. Silvestre. Dynamic battery model for photovoltaic applications. *Progress in Photovoltaics: Research and Applications*, 11(3):193–206, 2003. ISSN 1099-159X. doi: 10.1002/pip.480. URL http://dx.doi.org/10.1002/pip.480.

[73] Daler N Rakhmatov and Sarma BK Vrudhula. An analytical high-level battery model for use in energy management of portable electronic systems. In *Proceedings*

of the 2001 IEEE/ACM international conference on Computer-aided design, pages 488–493. IEEE Press, 2001.

[74] Dong-Jing Lee and Li Wang. Small-signal stability analysis of an autonomous hybrid renewable energy power generation/energy storage system part i: Time-domain simulations. *Energy Conversion, IEEE Transactions on*, 23(1):311–320, March 2008. ISSN 0885-8969. doi: 10.1109/TEC.2007.914309.

[75] I. Serban, R. Teodorescu, and C. Marinescu. Energy storage systems impact on the short-term frequency stability of distributed autonomous microgrids, an analysis using aggregate models. *Renewable Power Generation, IET*, 7(5):531–539, Sept 2013. ISSN 1752-1416. doi: 10.1049/iet-rpg.2011.0283.

[76] S.S.G. Jayasinghe, D.M. Vilathgamuwa, and U.K. Madawala. Direct integration of battery energy storage systems in distributed power generation. *Energy Conversion, IEEE Transactions on*, 26(2):677–685, June 2011. ISSN 0885-8969. doi: 10.1109/TEC.2011.2122262.

[77] C.-F. Lu, C. C Liu, and C.J. Wu. Dynamic modelling of battery energy storage system and application to power system stability. *Generation, Transmission and Distribution, IEE Proceedings-*, 142(4):429–435, Jul 1995. ISSN 1350-2360. doi: 10.1049/ip-gtd:19951858.

[78] P.K. Goel, B. Singh, S.S. Murthy, and N. Kishore. Isolated windhydro hybrid system using cage generators and battery storage. *Industrial Electronics, IEEE Transactions on*, 58(4):1141–1153, April 2011. ISSN 0278-0046. doi: 10.1109/TIE.2009.2037646.

[79] V.C. Ganti, B. Singh, S.K. Aggarwal, and T.C. Kandpal. Dfig-based wind power conversion with grid power leveling for reduced gusts. *Sustainable Energy, IEEE Transactions on*, 3(1):12–20, Jan 2012. ISSN 1949-3029. doi: 10.1109/TSTE.2011.2170862.

[80] N. Eghtedarpour and E. Farjah. Distributed charge/discharge control of energy storages in a renewable-energy-based dc micro-grid. *Renewable Power Generation, IET*, 8(1):45–57, January 2014. ISSN 1752-1416. doi: 10.1049/iet-rpg.2012.0112.

[81] X. Li. Fuzzy adaptive kalman filter for wind power output smoothing with battery energy storage system. *Renewable Power Generation, IET*, 6(5):340–347, Sept 2012. ISSN 1752-1416. doi: 10.1049/iet-rpg.2011.0177.

[82] Xiao Luo, Shiwei Xia, and Ka Wing Chan. A decentralized charging control strategy for plug-in electric vehicles to mitigate wind farm intermittency and enhance frequency regulation. *Journal of Power Sources*, 248(0):604 – 614, 2014. ISSN 0378-7753. doi: http://dx.doi.org/10.1016/j.jpowsour.2013.09.116. URL http://www.sciencedirect.com/science/article/pii/S0378775313016236.

[83] Tomihisa Kamada and Satoru Kawai. An algorithm for drawing general undirected graphs. *Information processing letters*, 31(1):7–15, 1989.

[84] Sikai Huang and David Infield. The potential of domestic electric vehicles to contribute to power system operation through vehicle to grid technology. In *Universities Power Engineering Conference (UPEC), 2009 Proceedings of the 44th International*, pages 1–5. IEEE, 2009.

[85] John D Kueck, Aaron F Snyder, Fangxing Li, and Isabelle B Snyder. Use of responsive load to supply ancillary services in the smart grid: Challenges and approach. In *Smart Grid Communications (SmartGridComm), 2010 First IEEE International Conference on*, pages 507–512. IEEE, 2010.

[86] Alex Q Huang, Mariesa L Crow, Gerald Thomas Heydt, Jim P Zheng, and Steiner J Dale. The future renewable electric energy delivery and management (freedm) system: the energy internet. *Proceedings of the IEEE*, 99(1):133–148, 2011.

[87] João A Peças Lopes, Filipe Joel Soares, and Pedro Miguel Rocha Almeida. Integration of electric vehicles in the electric power system. *Proceedings of the IEEE*, 99(1):168–183, 2011.

[88] B.B. McKeon, J. Furukawa, and S. Fenstermacher. Advanced lead-acid batteries and the development of grid-scale energy storage systems. *Proceedings of the IEEE*, 102(6):951–963, June 2014. ISSN 0018-9219. doi: 10.1109/JPROC.2014.2316823.

[89] M.T. Lawder, B. Suthar, P.W.C. Northrop, S. De, C.M. Hoff, O. Leitermann, M.L. Crow, S. Santhanagopalan, and V.R. Subramanian. Battery energy storage

system (bess) and battery management system (bms) for grid-scale applications. *Proceedings of the IEEE*, 102(6):1014–1030, June 2014. ISSN 0018-9219. doi: 10.1109/JPROC.2014.2317451.

[90] B.M. Grainger, G.F. Reed, A.R. Sparacino, and P.T. Lewis. Power electronics for grid-scale energy storage. *Proceedings of the IEEE*, 102(6):1000–1013, June 2014. ISSN 0018-9219. doi: 10.1109/JPROC.2014.2319819.

[91] Seth Fletcher. *Bottled lightning: superbatteries, electric cars, and the new lithium economy*. Macmillan, 2011.

[92] Avi M Gopstein. Energy storage & the grid-from characteristics to impact [point of view]. *Proceedings of the IEEE*, 100(2):311–316, 2012.

[93] Kristina Hamachi LaCommare and Joseph H Eto. Understanding the cost of power interruptions to us electricity consumers. 2004. URL http://certs.lbl.gov/pdf/55718.pdf.

[94] Rogerio G R. G. de Almeida and J.A. Peças-Lópes. Participation of doubly fed induction wind generators in system frequency regulation. *Power Systems, IEEE Transactions on*, 22(3):944–950, 2007.

[95] H. Nikkhajoei and R.H. Lasseter. Distributed generation interface to the certs microgrid. *Power Delivery, IEEE Transactions on*, 24(3):1598–1608, July 2009. ISSN 0885-8977. doi: 10.1109/TPWRD.2009.2021040.

[96] J A Peças-Lópes, Silvan A Polenz, C L Moreira, and Rachid Cherkaoui. Identification of control and management strategies for lv unbalanced microgrids with plugged-in electric vehicles. *Electric Power Systems Research*, 80(8):898–906, 2010.

[97] Ning Lu and Donald J Hammerstrom. Design considerations for frequency responsive grid friendly tm appliances. In *Transmission and Distribution Conference and Exhibition, 2005/2006 IEEE PES*, pages 647–652. IEEE, 2006.

[98] Edgardo D Castronuovo and JA Peças-Lópes. On the optimization of the daily operation of a wind-hydro power plant. *Power Systems, IEEE Transactions on*, 19(3):1599–1606, 2004.

[99] German Solar Industry Association (BSW). Information on support measures for solar power storage systems. 2013. Accessed from http://www.solarwirtschaft.de/ on July 28, 2014.

[100] *PowerFactory Technical Reference Documentation*. DIg SILENT.

[101] A. Millner. Modeling lithium ion battery degradation in electric vehicles. In *Innovative Technologies for an Efficient and Reliable Electricity Supply (CITRES), 2010 IEEE Conference on*, pages 349–356, Sept 2010. doi: 10.1109/CITRES.2010.5619782.

[102] Fengchun Sun, Rui Xiong, and Hongwen He. Estimation of state-of-charge and state-of-power capability of lithium-ion battery considering varying health conditions. *Journal of Power Sources*, 259(0):166 – 176, 2014. ISSN 0378-7753. doi: http://dx.doi.org/10.1016/j.jpowsour.2014.02.095. URL http://www.sciencedirect.com/science/article/pii/S0378775314002882.

[103] Rui Xiong, Hongwen He, Fengchun Sun, Xinlei Liu, and Zhentong Liu. Model-based state of charge and peak power capability joint estimation of lithium-ion battery in plug-in hybrid electric vehicles. *Journal of Power Sources*, 229(0): 159 – 169, 2013. ISSN 0378-7753. doi: http://dx.doi.org/10.1016/j.jpowsour.2012.12.003. URL http://www.sciencedirect.com/science/article/pii/S0378775312018253.

[104] R.H. Lasseter and P. Paigi. Microgrid: a conceptual solution. In *Power Electronics Specialists Conference, 2004. PESC 04. 2004 IEEE 35th Annual*, volume 6, pages 4285–4290 Vol.6, June 2004. doi: 10.1109/PESC.2004.1354758.

[105] Yanyan Li, M.M. Olama, and J.J. Nutaro. Frequency waves, grid friendly appliances and geographic limits in a smart grid. In *Innovative Technologies for an Efficient and Reliable Electricity Supply (CITRES), 2010 IEEE Conference on*, pages 220–224, Sept 2010. doi: 10.1109/CITRES.2010.5619807.

[106] IJ Fernández, CF Calvillo, A Sánchez-Miralles, and J Boal. Capacity fade and aging models for electric batteries and optimal charging strategy for electric vehicles. *Energy*, 60:35–43, 2013.

[107] Sung-Yoon Chung, Jason T Bloking, and Yet-Ming Chiang. Electronically conductive phospho-olivines as lithium storage electrodes. *Nature materials*, 1(2): 123–128, 2002.

[108] Gerbrand Ceder, Geoffroy Hautier, Anubhav Jain, and Shyue Ping Ong. Recharging lithium battery research with first-principles methods. *Mrs Bulletin*, 36(03): 185–191, 2011.

[109] Irene George Wadie Barsoum. Electrification of rural areas: optimal microgrid energy management. Master's thesis, ICAI, Universidad Pontificia Comillas, 2014.

[110] G. Celli, F. Pilo, G.G. Soma, R. Cicoria, G. Mauri, E. Fasciolo, and G. Fogliata. A comparison of distribution network planning solutions: Traditional reinforcement versus integration of distributed energy storage. In *PowerTech (POWERTECH), 2013 IEEE Grenoble*, pages 1–6, June 2013. doi: 10.1109/PTC.2013.6652338.

[111] P.S. Moura and A.T. de Almeida. The role of demand-side management in the grid integration of wind power. *Applied energy*, 87(8):2581–2588, 2010.

[112] A. Gomes, C.H. Antunes, and A.G. Martins. A multiple objective approach to direct load control using an interactive evolutionary algorithm. *IEEE Transactions on Power Systems,*, 22(3):10041011, 2007.

[113] J. Torriti, M.G. Hassan, and M. Leach. Demand response experience in europe: Policies, programmes and implementation. *Energy*, 35(4):1575–7188, 2010.

[114] A.H. Mohsenian-Rad. Autonomous demand-side management based on game-theoretic energy consumption scheduling for the future smart grid. *IEEE Transactions on Smart Grid*, 1(3):320–331, 2010.

[115] N. Pruggler, W. Pruggler, and F. Wirl. Storage and demand side management as power generators strategic instruments to influence demand and prices. *Energy*, 36(11):63086317, 2011.

[116] N.S. Wade. Evaluating the benefits of an electrical energy storage system in a future smart grid. *Energy Policy*, 38(11):7180–7188, 2010.

[117] T. Miller and M. Edmonds. Energy storage can enable wider deployment of distributed generation. In *Electricity Distribution (CIRED 2013), 22nd International Conference and Exhibition on*, pages 1–4, June 2013. doi: 10.1049/cp.2013.0995.

[118] I. Atzeni, L.G. Ordonez, G. Scutari, D.P. Palomar, and J.R. Fonollosa. Noncooperative and cooperative optimization of distributed energy generation and storage in the demand-side of the smart grid. *Signal Processing, IEEE Transactions on*, 61(10):2454–2472, May 2013. ISSN 1053-587X. doi: 10.1109/TSP.2013.2248002.

[119] Xiao Zhang, Feng Gao, Xinjie Lv, Hairong Lv, Qiming Tian, Junhua Ma, Wenjun Yin, and Jin Dong. Line loss reduction with distributed energy storage systems. In *Innovative Smart Grid Technologies - Asia (ISGT Asia), 2012 IEEE*, pages 1–4, May 2012. doi: 10.1109/ISGT-Asia.2012.6303333.

[120] G. Celli, F. Pilo, G. Pisano, and G. G. Soma. Optimal operation of active distribution networks with distributed energy storage. In *Energy Conference and Exhibition (ENERGYCON), 2012 IEEE International*, pages 557–562, Sept 2012. doi: 10.1109/EnergyCon.2012.6348215.

[121] M.J.E. Alam, K.M. Muttaqi, and D. Sutanto. Mitigation of rooftop solar pv impacts and evening peak support by managing available capacity of distributed energy storage systems. *Power Systems, IEEE Transactions on*, 28(4):3874–3884, Nov 2013. ISSN 0885-8950. doi: 10.1109/TPWRS.2013.2259269.

[122] G. Carpinelli, G. Celli, S. Mocci, F. Mottola, F. Pilo, and D. Proto. Optimal integration of distributed energy storage devices in smart grids. *Smart Grid, IEEE Transactions on*, 4(2):985–995, June 2013. ISSN 1949-3053. doi: 10.1109/TSG.2012.2231100.

[123] O. Moraes Toledo, D. Oliveira Filho, A.S.A.C. Diniz, J. Helvecio Martins, and M.H. Murta Vale. Methodology for evaluation of grid-tie connection of distributed energy resources - case study with photovoltaic and energy storage. *Power Systems, IEEE Transactions on*, 28(2):1132–1139, May 2013. ISSN 0885-8950. doi: 10.1109/TPWRS.2012.2207971.

[124] A.A. Thatte and Le Xie. Towards a unified operational value index of energy storage in smart grid environment. *Smart Grid, IEEE Transactions on*, 3(3): 1418–1426, Sept 2012. ISSN 1949-3053. doi: 10.1109/TSG.2012.2190114.

[125] Erin Baker, Meredith Fowlie, Derek Lemoine, and Stanley S Reynolds. The economics of solar electricity. *resource*, 5, 2013.

[126] Michael Vanderberg, Diana Cracium, Vincent Helmbrecht, Roland Hermes, Riccardo Lama, Paolo Michele Sonvilla, Manoel Rekinger, and Giorgia Concas. Prioritisation of technical solutions available for the integration of pv into the distribution grid. Technical report, PV-GRID, 2013.

[127] A Soares, A Gomes, and CH Antunes. Domestic load characterization for demand-responsive energy management systems. In *Sustainable Systems and Technology (ISSST), 2012 IEEE International Symposium on*, pages 1–6. IEEE, 2012.

[128] M. Begovic, A. Pregelj, A. Rohatgi, and D. Novosel. Impact of renewable distributed generation on power systems. In *System Sciences, 2001. Proceedings of the 34th Annual Hawaii International Conference on*, pages 654–663, 2001. doi: 10.1109/HICSS.2001.926265.

[129] P. Mitra, G.T. Heydt, and V. Vittal. The impact of distributed photovoltaic generation on residential distribution systems. In *North American Power Symposium (NAPS), 2012*, pages 1–6, 2012. doi: 10.1109/NAPS.2012.6336330.

[130] R.A. Shayani and M.A.G. de Oliveira. Photovoltaic generation penetration limits in radial distribution systems. *Power Systems, IEEE Transactions on*, 26(3):1625–1631, 2011. ISSN 0885-8950. doi: 10.1109/TPWRS.2010.2077656.

[131] Po-Chen Chen, R. Salcedo, Qingcheng Zhu, F. de Leon, D. Czarkowski, Zhong-Ping Jiang, V. Spitsa, Z. Zabar, and R.E. Uosef. Analysis of voltage profile problems due to the penetration of distributed generation in low-voltage secondary distribution networks. *Power Delivery, IEEE Transactions on*, 27(4):2020–2028, 2012. ISSN 0885-8977. doi: 10.1109/TPWRD.2012.2209684.

[132] The impact of localized energy resources on southern california edisons transmission and distribution system. Technical report, Southern California Edison, 2012.

[133] Johannes Brantl. New challenges for dso. In *Task 14 High Penetration PV Workshop, SMA, Kassel, Germany.* IEA Photovoltaic Power Systems Programme, 2012.

[134] J. Bebic. Power system planning: Emerging practices suitable for evaluating the impact of high-penetration photovoltaics. Technical report, National Renewable Energy Laboratory, 2008.

[135] Tim Lindl and Kevin Fox. Integrated distribution planning concept paper. Technical report, Interstate Renewable Energy Council, Inc., 2013.

[136] Jeff Smith. Alternative screening methods pv hosting capacity in distribution systems. In *Solar Forum*. Electric Power Research Institute, 2013.

[137] Sebastian Schwenen Carlos Batlle Sophia Ruester, Ignacio Prez-Arriaga and Jean-Michel Glachant. From distribution networks to smart distribution systems: Rethinking the regulation of european electricity dsos. Technical report, Florence School of Regulation, European University Institute, 2013.

[138] Rate design matters, the impact of tariff structure on solar project economics in the u.s. Technical report, Green Tech Media, 2013.

[139] Network tariff structure for a smart energy system. Technical report, Eurelectric, 2013.

[140] United States Department of Energy. database of standard residential and commercial buildings. URL http://energy.gov/eere/buildings/building-technologies-office.

[141] Energyplus energy simulation software. URL http://apps1.eere.energy.gov/buildings/energyplus/.

[142] Typical meteorological year 3, . URL http://rredc.nrel.gov/solar/old_data/nsrdb/1991-2005/tmy3/.

[143] Openei website. URL http://en.openei.org.

[144] C.M. Domingo, T.G.S. Romn, A. Snchez-Miralles, J.P.P. Gonzlez, and A.C. Martnez. A reference network model for large-scale distribution planning with automatic street map generation. *Power Systems, IEEE Transactions on*, 26(1): 190–197, 2011. ISSN 0885-8950. doi: 10.1109/TPWRS.2010.2052077.

[145] Pv watts photovoltaic production calculator, . URL http://www.nrel.gov/rredc/pvwatts/.

[146] Scott B Peterson, Jay Apt, and JF Whitacre. Lithium-ion battery cell degradation resulting from realistic vehicle and vehicle-to-grid utilization. *Journal of Power Sources*, 195(8):2385–2392, 2010.

[147] A123 Systems. data sheet md100001-02 for high power lithium ion battery cell anr26650m1a. *http://www.a123systems.com*, 2012.

[148] Vladimiro Miranda and Nuno Fonseca. Epso-evolutionary particle swarm optimization, a new algorithm with applications in power systems. In *Proc. of the Asia Pacific IEEE/PES Transmission and Distribution Conference and Exhibition*, volume 2, pages 745–750. Citeseer, 2002.

[149] Claudio Vergara, Ana Soares, Alvaro Gomes, Carlos Hengeller Antunes, and J A Peças-Lópes. In-house energy consumption and storage optimization. In *International Workshop on Energy Efficiency for a More Sustainable World*, 2012.

[150] Claudio R Vergara. Parametric interface for battery energy storage systems providing ancillary services. In *Innovative Smart Grid Technologies (ISGT Europe), 2012 3rd IEEE PES International Conference and Exhibition on*, pages 1–7. IEEE, 2012.